CRANFIELD UNIVERSITY

UCHE OSOKOGWU

INVESTIGATION OF THE EFFECT OF SAND ON ANNULAR FLOW BEHAVIOUR IN HORIZONTAL PIPES

SCHOOL OF WATER, ENERGY & ENVIRONMENT,
ENERGY AND POWER,
OIL & GAS ENGINEERING CENTRE.

PhD Thesis

Academic Year: 2016- 2017

Supervisor: Prof. Gioia Falcone
October, 2017

CRANFIELD UNIVERSITY

SCHOOL OF WATER, ENERGY AND ENVIRONMENT,
ENERGY AND POWER

PhD Thesis

Academic Year 2016 - 2017

UCHE OSOKOGWU

Investigation of the Effect of Sand on Annular Flow Behaviour in Horizontal Pipes

Supervisor: Prof. Gioia Falcone
October, 2017

This thesis is submitted in partial fulfilment of the requirements for the degree of PhD

© Cranfield University 2017. All rights reserved. No part of this publication may be reproduced without the written permission of the copyright owner.

ABSTRACT

Annular flow is encountered in petroleum production systems, where reservoir fluids are conveyed to surface via wells and transport lines and also nuclear power plants, chemical and refining processes (e.g. reactors, heat exchangers). In this type of flow regime, the gas, together with the entrained liquid droplets, flows within the core of the pipe at high velocities, while the liquid flows as a film along the pipe walls.

Experimental investigations on annular flow behaviour, sand transport and its effect on annular flow in horizontal pipe are presented, with the aim of progressing the understanding of such flow and facilitate the optimum design of hydrocarbon production systems.

The experiments were conducted using a closed-loop horizontal pipe with an internal diameter of 2-inch (0.0504m). The experiments could be categorized into: water/air flow, water/sand flow, water/air/sand annular flow and sand sampling. The water/air flow experiments could be subdivided into water/air flow (Plug, Slug, Stratified-smooth and stratified-wavy flows) and water/air annular flow. The results of water/air flow were plotted on flow regime map to aid the recognition of the different flow regimes. For the water/air annular flow experiments, key flow features are presented, with discussion on liquid hold up, film thickness, wave frequency and pressure gradient.

The water/sand flow experiments investigated sand saltation, sand streaks, moving dunes and sand beds. Also, sand particles of 212microns and 500microns for water/air/sand annular flow were investigated. Similarly, sand sampling experiments were also carried out.

The OLGA dynamic multiphase flow simulator was run against the experimental results. The OLGA simulations of the water/air annular flow shows a better liquid hold-up match at lower superficial liquid velocities. For sand transport, OLGA also identified sand flow in annular flow as no bed.

The main contributions of this study are: presenting the minimum transport velocities for water/sand flow in horizontal pipe. For water/air annular flow, the

contributions are: detailed annular flow behaviours in horizontal pipes with annular-wavy slug flow at low superficial liquid and gas velocities, and full symmetrical annular flow from superficial gas velocity of 12m/s at low Vsl. The study proves that superficial liquid velocity has impact and significance on wave frequency: This has refuted Setyawan *et al*., (2014), whose report presented superficial liquid velocity to be insignificant in wave frequency. The study also identified that the higher the Vsl, the higher the interfacial shear stress but the lower the wave velocity. Also, the higher the Vsl, the higher interfacial friction factor/shear stress, but the lower the wave frequency.

For water/air/sand annular flow, this study identifies saltation and suspension as the two main sand distribution in annular flow, with small-size particles being transported at the gas core and the bigger particles at the bottom (i.e. in the liquid film) along in the horizontal pipes. Finally, sand particles' size does not appear to have an impact on wave velocity and wall shear stress, while sand concentration affects wall shear stress, but not wave velocity. Lastly, presence of sand particles in the liquid film is associated with increase in wave amplitude in annular flow, as more energy is being dissipated from the gas phase to keep the waves in motion.

Key words: Annular flow, Regime, Wave frequency, Sand flow, Sand concentration, Sand distribution.

ACKNOWLEDGEMENTS

I thank and acknowledge God, the most beneficent, the most merciful and the great provider. I thank you Lord, for the good health, provision, wisdom and knowledge to achieve this fit. It can only be you that made this to be possible.

I wish to express my gratitude to Prof. Gioia Falcone, the Head, Oil & Gas Engineering Centre and also Process Systems & Engineering Laboratory for being a good supervisor to me. I sincerely thank you for your technical guidance and contributions in making this research a success. Once again, thank you.

To Dr Liyun Lao, I say a big thank you for your care, contributions and advices throughout my research time. You often paid attention to me with much enthusiasms without minding if I booked for such meeting or not.

Special thanks to my mentor/academic father Prof. Joseph.A. Ajienka, the 7th Vice Chancellor of University of Port Harcourt. Your mentorship, indeed paid me. Special thanks also to TETFUND for the scholarship. To my friends, Dr Olawale Taye Fajemidupe, Dr and Mrs Ebi Saturday, Dr Joseph Amieibibama, Engr Kazeem Salem, Engr Opara Ignatius, Engr Lessor Ikeh, IPR Ltd Staff etc.

I sincerely thank my parents, Mr and Mrs .O. Osokogwu, Madam Ndego Egwuenu for their care, prayers and love. Also to Barr. & Mrs C.I Egwuenu, Mr and Mrs George Nzei, Mrs Hellen Iyom, Mr Azuka S. Okom, Mr and Mrs Friday Orjieh, Mr and Mrs Anthony Osokogwu for their care all through these periods. Also to Mr and Mrs Monday Olise, Pastor and Mrs Joel Omessah, Mr and Mrs. L.E. Eze, Pastor Emmanuel Prince, Pastor and Mrs Olufemi Awoleye and the entire RCCG (Newgate Parish), Bedford, UK and finally to Prof. Adewale Dosunmu for advising me to choose Cranfield University against other school's I was offered admission.

A big thank you to my lovely and most beautiful wife Mrs. C.N Osokogwu. Even when admission and scholarship were not at sight, God showed it to you that I should start preparing for UK. To my kids Ashinedu Marvellous Boluwatife, Chidinma Merit, Koliseyenum Ozioma Success and Chidiebube Ifeakachukwu Joshua. Without your understanding and co-operations, I wouldn't have achieved this fit. To my in-law, Mrs Mary Ebele Obinne, I say thank you for all your calls.

TABLE OF CONTENTS

ABSTRACT i
ACKNOWLEDGEMENTS iii
LIST OF FIGURES ix
LIST OF TABLES xiv
NOMENCLATURE xvi
LIST OF ABBREVIATIONS xxiii
1 INTRODUCTION 1
1.1 Background 1
1.2 Sand in Petroleum Production Systems 1
1.2.1 Sand Migration from the Reservoir 2
1.2.1.1 Drilling 2
1.2.1.2 Water Production 2
1.2.1.3 Pore Pressure Reduction 2
1.2.1.4 Unconsolidated Reservoir Formations 3
1.2.1.5 High Drawdown/High Production Rate 3
1.2.2 Sand Particle Sizes 3
1.2.3 Sand Control, Monitoring and Management Strategy 5
1.3 Why this Research? 5
1.4 Significance of Work 6
1.5 Aims and Objectives 6
1.6 Structure of Thesis 7
2 LITERATURE REVIEW 10
2.1 Background 10
2.2 Annular Flow 11
2.2.1 Flow Regime Map 11
2.3 Pressure Gradient 12
2.3.1 Beggs and Brill (1973) 12
2.3.2 Dukler *et al.,* (1964) 13
2.3.3 Shear Stress 14
2.4 Film Thickness 14
2.4.1 Methods of Determining Film Thickness 15
2.4.2 Triangular Relationship 15
2.5 Some Parameters used for Annular Flow Analysis. 16
2.5.1.1 Probability Density Function 16
2.5.1.2 Power Spectral Density 16
2.5.1.3 Wavelet 17
2.6 Liquid Entrainment 17
2.6.1 Entrainment Correlations for Vertical Flow 17
2.6.1.1 Wallis (1968) 17
2.6.1.2 Oliemans *et al.,* (1986) 18

2.6.1.3 Ishii and Mishima (1989) 18
2.6.1.4 Pan and Hanratty (2002a) 19
2.6.1.5 Sawant *et al.,* (2008) 19
2.6.2 Entrainment Correlations for Horizontal Flow 20
2.6.2.1 Wicks and Dukler (1960) 20
2.6.2.2 Paleev and filipovich (1966) 21
2.6.2.3 Dallman *et al.,* (1979) 21
2.6.2.4 Pan and Hanratty (2002b) 22
2.6.2.5 Mantilla *et al.,* (2009) 22
2.7 Wave Characteristics in Annular flow 23
2.7.1 Wave Velocity 24
2.7.1.1 How to Determine Wave Velocity. 24
2.7.2 Wave Velocity Correlation. 25
2.7.2.1 Ousaka *et al.,* (1992) 25
2.7.2.2 Schubring and Shedd (2008) 25
2.7.2.3 Setyawan *et al.,* (2014) 25
2.7.3 Wave Frequency Correlation 26
2.7.3.1 Ousaka *et al.*, (1992) 26
2.7.3.2 Schubring and Shedd (2008) 26
2.7.3.3 Setyawan *et al.,* (2014) 27
2.8 Sand Transport in Horizontal Water/Sand Flow 27
2.8.1 Durand (1952) 27
2.8.2 Newit *et al.,* (1955) 28
2.8.3 Wicks (1971) 29
2.8.4 Oroskar and Turian (1980) 30
2.8.5 Takahashi *et al.*, (1989) 32
2.8.6 Salama (1998) 32
2.8.7 Ravelet *et al.,* (2013) 33
2.8.8 Soepyan *et al.,* (2013) 34
2.9 Sand Transports in Horizontal Gas Flow in Pipes 35
2.9.1 Tsuji and Morikawa (1982) 35
2.9.2 Sommerfeld and Huber (1999) 36
2.9.3 Akilli *et al.*, (2001) 36
2.9.4 Sommerfeld (2003) 36
2.9.5 Jiang *et al.,* (2017) 37
2.10 Sand Transports in Horizontal Sand-Gas-Liquid (Slug, Stratified-Annular) Flows 37
2.10.1 Scott and Rao (1971) 38
2.10.2 Angelson *et al.*, (1989) 39
2.10.3 Oudeman (1993) 41
2.10.4 Gillies et al., (1997) 43
2.10.5 Stevenson and Thorpe (2002) 44

2.10.6 Ramadan *et al.*, (2005) 45
2.10.7 Bello *et al*., (2011) 46
2.10.8 Kesana *et al*., (2012) 47
2.10.9 Franklin (2013) 48
2.10.10 Ibarra *et al*., (2014) 49
2.10.11 Kamyar Najmi *et al.*, (2015) 52
2.11 Factors affecting Solid Transport in Multiphase flow in Pipes. 53
2.11.1 Pressure Drop 53
2.11.1.1 Durand (1952) 53
2.11.1.2 Worster (1952) 54
2.11.1.3 Zandi and Govatos (1967) 54
2.11.1.4 Turian and Yuan (1977) 55
2.11.1.5 Weber (1986) 55
2.11.2 Solid Concentrations 56
2.11.3 Fluid Viscosity 57
2.11.4 Particle Diameters (Sizes) 57
2.12 Multi-Fluid Simulator (OLGA) 58
2.12.1 Bendlksen *et al*., (1991) 58
2.12.2 Ellul *et al.,* (2004) 61
2.12.3 Helgeland Sannæs and Johnson (2010) 61
2.12.4 Staff *et al*., (2015) 62
2.13 Summary of Literature Review 64
3 EXPERIMENTAL INVESTIGATION 67
3.1 Experimental Approach 67
3.1.1 Experimental Set-Up 69
3.1.2 Why Horizontal and Sand Injection Location Important. 72
3.1.3 Facility Instrumentation and Equipment 72
3.1.3.1 Sand Supply 72
3.1.3.2 Water/Sand Mixer 73
3.1.3.3 Water Supply 74
3.1.3.4 Gas (Air) Supply 75
3.1.4 Instrumentation and Calibration Procedure 75
3.1.4.1 Liquid Flow Meter 76
3.1.4.2 Sand/water Flow Meter 76
3.1.4.3 Gas (Air) Flow Meter 76
3.1.4.4 Thermocouple 77
3.1.4.5 Pressure Transducer 77
3.1.4.6 Conductivity Ring Sensors 80
3.1.4.7 Sand Probe Sensors 81
3.1.4.8 Film Thickness Probes 83
3.1.4.9 Re-Calibration Conducted on Annular Flow 84

3.1.4.10 Comparing the Previous Calibration and New Calibration Results 85
3.1.5 Data Processing 86
3.1.6 Cross-Correlation 86
3.1.7 Sand Sampling Procedure 87
3.1.7.1 Experimental Set-Up 87
3.1.7.2 Experimental Procedures 89
3.2 Limitations of this Study 90
3.3 Experimental Error and Uncertainty Analysis 91
3.4 Error and Uncertainty 92
3.5 Error Propagation (Propagation of Uncertainty) 93
3.5.1 Superficial Liquid Velocity 93
3.5.2 Superficial Gas Velocity 94
3.5.3 Water/Air in Annular Flow 95
3.5.3.1 Superficial Liquid Velocity 95
3.5.3.2 Superficial Gas Velocity 96
3.5.3.3 Liquid Hold-Up 97
3.5.4 Water/Air/Sand in Annular Flow 97
3.5.4.1 Superficial Liquid Velocity 98
4 Water/Air Flow Test Results 99
4.1 Water/Air Annular Flow Test Results 101
4.1.1 Annular Flow Regime 102
4.1.2 Annular flow behaviour in 2-inch horizontal pipe. 103
4.1.3 Annular wavy-flow at upper walls of horizontal pipes 104
4.2 Liquid Hold-Up Results. 105
4.3 Determining the Film Thickness 106
4.3.1 Film Thickness using Conductance Probe 106
4.3.2 Wave Velocity of the Film Thickness (Probe) 107
4.3.3 Film Thickness using Conductivity Ring Sensors 110
4.3.4 Wave Frequency Analysis on Ring Sensors 110
4.3.4.1 Comparing Wave Frequency from Experiments with Correlations 111
4.3.5 Film Thickness using Triangular Relationship 116
4.3.6 Comparing Liquid Film Thickness from different Methods 117
4.3.7 Interfacial friction factor/interfacial shear stress analysis 120
4.4 Probability Density Function/Void Fraction in Annular Flow 125
4.5 Power Spectral Density Analysis on Film Thickness 126
4.6 Wavelet Analysis on Film Thickness 127
4.7 Film thickness with time series analysis 130
4.7.1 Pressure Gradient and Superficial Gas Velocity 131
4.8 Chapter Summary 135
5 Sand Transport Flow Results 137

5.1 Water/Sand Flow Test (Visual Observation) 137
5.2 Water/Sand Flow Test (Instrumentation) 140
5.3 Water/Air/Sand Annular Flow (instrumentation) 147
5.3.1 Sand Flow Regime/Behaviour in Annular Flow 147
5.3.2 Power Spectral Density (PSD) of Sand in Annular Flow. 151
5.3.3 Effect of Sand Particle's Sizes/Concentration on Wave Velocity.... 154
5.3.4 Effect of Sand Particles' Sizes/Sand Concentration on Wall Shear Stress. 156
5.4 Physical Modes of Sand Distribution in Annular flow (Sampling Method) 158
5.5 Chapter Summary 160
6 OLGA Simulations 163
6.1 OLGA Flow Geometry Setup 164
6.1.1 OLGA Flow Model 164
6.1.2 OLGA Liquid Hold up Model. 165
6.1.3 OLGA Sand Transport Model. 165
6.2 Liquid Hold –Up (OLGA). 167
6.3 Sand Simulation (OLGA) 170
7 Conclusions 177
7.1 Recommendations for Future Work. 179
REFERENCES 181
APPENDICES 197
A-1: Calibration Using New sets of Blocks for Annular Flow 197
B-2: Liquid Hold-Up in Annular Flow 203
B-2.1: Liquid Hold-Up Proposed Model/Beggs & Brill (1973) vs Measured 207
C-1.Calculation on Solid Concentration by Volume 209
D-1: Uncertainty of Pump Efficiency 210
E-1.1: Water/Air in Annular Flow - Error and Uncertainty Analysis. 213
Differential Pressure Measurement (Pressure Transducer) 213
Flow Meter (Gas Flow Rate) 214
Flow Meter (Liquid Flow Rate) 214
E-1.2: Water/Sand Flow 215
Differential Pressure Measurement (Pressure Transducer) 215
Flow Meter (Liquid Flow Rate) 215
Flow Meter (Water/Sand Mixture Flow Rate) from Sand Hopper 216
E-1.3:Water/Air/Sand in Annular Flow (Multiphase Flow) 216
Differential Pressure Measurement (Pressure Transducer) 216
Flow Meter (Liquid Flow Rate) 217
Flow Meter (Gas Flow Rate) 217
Flow Meter (Water/Sand Mixture Flow Rate) from Sand Hopper 218
F-1.1: Statistical Error Analysis Used 219
F-1.2: OLGA plotted for Water/Air/Sand Annular Flow. 220

LIST OF FIGURES

Figure 2.1 Horizontal Two-Phase Flow Pattern in Pipes (Balasubramaniam *et al.,* 2006). 10

Figure 2.2: Horizontal Flow Map showing different Flow Pattern (Lawrence & Steven, 2003) 12

Figure 2.3: Entrainment Fraction against Weber Number (Sawant *et al.,* 2008) 20

Figure 2.4: Horizontal Sand-Gas-Liquid Flow (Yan *et al.,* 2011) 40

Figure 2.5: Sand Particles in Annular Flow (Kesana *et al*., 2012) 48

Figure 2.6: Distinct Sand Flow Regime in Horizontal Pipelines (Peysson, 2004) 51

Figure 3.1: Sketch of the 2-inch Flow Loop Design used in Experiments..... 70

Figure 3.2: A 2-inch Pipeline Test Facility used in the Experiments 71

Figure 3.3: Sand Hopper for the 2-inch Pipeline Test Facility..... 73

Figure 3.4: Water/Sand Mixer used for slurry mixing..... 74

Figure 3.5: The Plastic Fibre Water Storage Tank used in Experiments 75

Figure 3.6: Sand/water Flow Meter connected to Pipeline from Sand Hopper . 76

Figure 3.7: Gas (Air) Flowmeter (Vortex) 76

Figure 3.8: A Thermocouple Installed on 2-inch Pipeline Test Facility 77

Figure 3.9: Pressure Calibration in the Lab 78

Figure 3.10: Calibration Plot of Pressure against Voltage (V) (P1) Upstream. . 79

Figure 3.11: Calibration Plot of Pressure against Voltage (V) (P2) Downstream 79

Figure 3.12: Conductivity Ring Sensors used in Experiment..... 80

Figure 3.13: Normalized Volt against Reference liquid Fraction Calibration..... 81

Figure 3.14: A Sketch of the Sand Probe Sensors used 82

Figure 3.15: Normalized Voltage against Reference Film Thickness (mm)..... 84

Figure 3.16: A Horizontal Calibration Pipe used for Annular Film Thickness ... 84

Figure 3.17: Cross-Correlation of Probe (S1 and S2) for Vsl=0.0502m/s, Vsg=14.0307m/s..... 87

Figure 3.18: Sand Sampling Point on the Flow Loop 88

Figure 3.19: Container/Storage used for Sand Sample Experiments 89

Figure 3.20: Hot Air Dry Tool Figure 3.21: Beaker (Fishbrand) 600ml 90

Figure 3.22: Error Propagation on Superficial Liquid Velocity 96

Figure 3.23: Error Propagation on Superficial Gas Velocity 97

Figure 4.1: Stratified-Smooth Flow from 2-inch flow Pipe (Side View) 99

Figure 4.2: Plug Flow from the 2-inch Flow test rig 100

Figure 4.3: Slug Flow from the Experiment using 2-inch Pipe..... 100

Figure 4.4: Stratified-Wavy Flow from the Experiment using 2-inch Pipe..... 100

Figure 4.5: Experimental Result of Flow Regime with Taitel & Dukler (1976) 101

Figure 4.6: Annular Flow Regime of 2-inch Horizontal Pipe (Taitel & Dukkler, 1976) 103

Figure 4.7:(a)Vsl =0.0501m/s, Vsg=23.2796m/s,(b) Vsl=0.0501m/s, Vsg =23.2796m/s..... 104

Figure 4.8:(a)Vsl=0.0901m/s, Vsg=23.5707m/s, (b) Vsl=0.0901m/s, Vsg =23.5707m/s..... 105

Figure 4.9: Liquid hold-up against superficial gas velocity. 106

Figure 4.10: Film thickness (probe at bottom) against superficial gas velocity107

Figure 4.11: Wave velocity against superficial gas velocity..... 108

Figure 4.12: Film thickness (probe at bottom) against wave velocity 109

Figure 4.13: Film thickness (probe at bottom) against pressure gradient..... 109

Figure 4.14: Film thickness from ring sensor against superficial gas velocity. 110

Figure 4.15: Wave frequency against superficial gas velocity 111

Figure 4.16: Wave frequency Vs Superficial gas Velocity (Vsl~0.0505m/s) ... 112

Figure 4.17: Wave frequency Vs Superficial gas velocity (Vsl~0.0714m/s).... 112

Figure 4.18: Wave frequency Vs Superficial gas velocity (Vsl~0.0903m/s).... 113

Figure 4.19: Wave frequency Vs Superficial gas velocity (Vsl~0.1355m/s).... 113

Figure 4.20: Wave frequency Vs Superficial gas velocity (Vsl~0.1851m/s).... 114

Figure 4.21: Plots of Performance to identify Correlation that matched the Experimental (Measured) Wave Frequency 115

Figure 4.22: Film thickness Vs Vsg using Triangular Relationship..... 117

Figure 4.23: Comparing film thickness from three methods (Vsl ~ 0.0505m/s) 118

Figure 4.24: Comparing film thickness from three methods (Vsl ~ 0.0714m/s) 118

Figure 4.25 [a], [b]: Plot of Predicted against Measured Liquid Film Thickness 119

Figure 4.26: Interfacial friction factor against superficial gas velocity 121

Figure 4.27: Interfacial friction factor against pressure gradient 122

Figure 4.28: Interfacial shear stress against superficial gas velocity 123

Figure 4.29: Film thickness against interfacial shear stress 123

Figure 4.30: Interfacial shear stress against wave frequency 124

Figure 4.31: Interfacial shear stress against interfacial friction factor 124

Figure 4.32: Interfacial friction factor against wave frequency 125

Figure 4.33: Vsl 0.0508m/s, Vsg 10.0773m/s Vsl = 0.0501m/s, Vsg = 23.2796m/s 126

Figure 4.34: Vsl 0.1892m/s, Vsg 10.3927m/s Vsl = 0.1805m/s, Vsg = 23.7259m/s 126

Figure 4.35: (a). Vsl = 0.0508m/s Vsg = 10.0773m/s (b). Vsl = 0.0501m/s, Vsg = 23.2796m/s 127

Figure4.36: (a). Vsl = 0.1892m/s Vsg = 10.3927m/s (b). Vsl = 0.1805m/s, Vsg = 23.7259m/s 127

Figure 4.37: (a). Vsl=0.0508m/s, Vsg=10.0773m/s, (b). Vsl=0.0501m/s, Vsg = 23.2796m/s 129

Figure 4.38: (a). Vsl=0.1892m/s, Vsg=10.3927m/s (b).Vsl=0.1805m/s, Vsg=23.7259m/s 129

Figure 4.39: (a). Vsl = 0.0508m/s vsg =10.0773m/s (b). Vsl = 0.0501m/s Vsg = 23.2796m/s 130

Figure 4.40: (a). Vsl=0.1892m/s, Vsg=10.3927m/s (b). Vsl=0.1805m/s, Vsg=23.7259m/s 131

Figure 4.41: Pressure gradient Vs Superficial gas velocity (Vsl ~0.0505m/s) 131

Figure 4.42: Pressure gradient Vs Superficial gas velocity (Vsl ~ 0.0714m/s) 132

Figure 4.43: Pressure gradient Vs Superficial gas velocity (Vsl ~ 0.0903m/s) 132

Figure 4.44: Pressure gradient Vs Superficial gas velocity (0.1355m/s) 133

Figure 4.45: Pressure gradient Vs Superficial gas velocity (Vsl~0.1851m/s) . 133

Figure 4.46: A Plot of Predicted against the Experimental Pressure Gradient 134

Figure 4.47: A Plot of Slip against Pressure Gradient, [kPa/m] 134

Figure 4.48: A Plot of Slip Ratio against Superficial Gas Velocity. 135

Figure 5.1: Sand bed for 200microns at bottom of pipe (Vsl =0.1208m/s)..... 138

Figure 5.2: Moving dune at bottom of pipe (Vsl = 0.1910m/s) 138

Figure 5.3: Sand scoring for 200microns at bottom of pipe (Vsl = 0.3241m/s)138

Figure 5.4: Comparing sand flow regime (200microns) with Angelson et al., (1989) 139

Figure 5.5: Sand dune, Vsl = 0.1504m/s (212microns, 200lb/1000bbl) - both are same..... 141

Figure 5.6: Saltation, Vsl = 0.1775m/s (212microns, 200lb/1000bbl) - both are same..... 142

Figure 5.7: Streaks, Vsl =0.1967m/s (212microns, 200lb/1000bbl)..... 142

Figure 5.8: Suspension, Vsl 0.2427m/s (212microns, 200lb/1000bbl) 143

Figure 5.9: Sand dune, Vsl = 0.1527m/s (500microns, 200lb/000bbl) - both are same..... 143

Figure 5.10: Saltation, Vsl = 0.1783m/s (500micron, 200lb/1000bbl)..... 144

Figure 5.11: Sand Streak, Vsl = 0.1949m/s (500microns, 200lb/1000bbl) 144

Figure 5.12: Suspension, Vsl = 0.2486m/s (500microns, 200lb/1000bbl). 144

Figure 5.13: Sand dune/saltation, Vsl = 0.1481m/s (500microns, 500lb/1000bbl) 145

Figure 5.14: Sand Saltation, Vsl = 0.1772m/s (500microns, 500lb/1000bbl).. 145

Figure 5.15: Sand Streaks, Vsl = 0.1931m/s (500microns, 500lb/1000bbl).... 146

Figure 5.16: Sand Suspension, Vsl = 0.2466m/s (500microns, 500lb/1000bbl) 146

Figure 5.17: (a) Sand Saltation (212microns, 200lb/1000bbl) (b) Water/air-no sand..... 148

Figure 5.18: (a) Sand saltation (212microns, 200lb/1000bbl) (b) Water/air-no sand..... 149

Figure 5.19: (a) Sand Saltation (212microns, 500lb/1000bbl) (b) Water/air-no sand..... 149

Figure 5.20: (a) Sand saltation (212microns, 500lb/1000bbl) (b) Water/air-no sand..... 150

Figure 5.21: (a) Sand Saltation (500microns, 500lb/1000bbl) (b) Water/air-no sand..... 150

Figure 5.22: (a) Sand saltation (500microns, 500lb/1000bbl) (b) Water/air-no sand..... 150

Figure 5.23: Wave Velocity vs Vsl on Sand Particle Sizes/Sand Concentrations 155

Figure 5.24: Wave Velocity vs Vsl on Sand Particle sizes/Sand Concentration 156

Figure 5.25: Wall Shear Stress against Film Thickness- Effect of Gas velocity felt. 157

Figure 5.26: Wall Shear Stress against Film Thickness- Effect of Particle Sizes. 157

Figure 5.27: Wall Shear Stress against Film Thickness- Effect of Concentration felt..... 158

Figure 5.28: Sand Distribution in the Pipe for Vsl=0.0732m/s, 212microns.... 159

Figure 5.29: Sand Distribution in the Pipe for Vsl=0.1042m/s, 500microns.... 160

Figure 6.1: OLGA flow geometry for the simulations**Error! Bookmark not defined.**

Figure 6.2: OLGA/Experiment (Measured) Liquid Hold-Up for Vsl=0.0505m/s 167

Figure 6.3: OLGA/Experiment(Measured)Liquid Hold Up for Vsl=0.0714m/s. 168

Figure 6.4: OLGA/Experiment(Measured)Liquid Hold-Up for Vsl=0.0903m/s. 168

Figure 6.5: OLGA/Experiment(Measured)Liquid Hold-Up for Vsl=0.1355m/s. 169

Figure 6.6: OLGA against Experiment (Measured) Liquid Hold-Up..... 169

Figure 6.7*:* Sand Flow Regime in Sand Transport in Annular Flow (Vsl=0.1145m/s and Vsg = 14.9179m/s, 212microns, 200lb) 171

Figure 6.8: Particle Mass flow in water in Annular Flow (Vsl=0.1145m/s and Vsg = 14.9179m/s, 212microns, 200lb) 171

Figure 6.9: Particle Mass flow in Suspension in Annular Flow (Vsl=0.1145m/s and Vsg = 14.9179m/s, 212microns, 200lb)..... 172

Figure 6.10: Particle Volume Flow both in Water + Suspension (Vsl=0.1145m/s and Vsg = 14.9179m/s, 212microns, 200lb) 173

Figure 6.11: Comparison of Total Sand Particle Mass Used in Experiment and OLGA Simulated Results..... 173

Figure 6.12: Comparison of Sand Concentration by Volume in Experiment and OLGA Simulated Results 174

LIST OF TABLES

Table 1.1: Sand Particle Sizes (Durand (1952) 4

Table 2.1: Beggs & Brill (1973) Equations for Liquid Hold-Up 13

Table 2.2: Solid beads used in the experiment, (Ravelet et al., 2013). 33

Table 2.3: Gas fraction input *m* and *n* for sand transport rate in flow 42

Table 2.4: Constants for values of A, B and C (Bello *et al.,* 2012)..... 46

Table 2.5: Suspension and Rolling Equation Constants (Bello *et al*, 2012)..... 47

Table 2.6: Summary of Most Sand Transport, Phases, Flow Pattern and Model developed in Multiphase Flow Experiment over the Years 65

Table 3.1: Water/Air Flow Properties used in the Experiments 67

Table 3.2: Water/Air Annular Flow Properties used in the Experiments 67

Table 3.3: Water/Sand Flow Properties used in the Experiments 67

Table 3.4: Water/Air/Sand Annular Flow Properties Used for second Experiments 68

Table 3.5: Sand Sampling Properties used in the Experiments..... 68

Table 3.6: Calibration data for Pressure Transducer (P1) Upstream..... 78

Table 3.7: Calibration data for Pressure Transducer (P2) Downstream 79

Table 3.8: Porosity obtained..... 83

Table 3.9: Summary of Error of new Liquid Holdup from previous Liquid Hold-up Calibrated. 85

Table 3.10: Summary of Statistical Error for new Film Thickness from previous ones..... 85

Table 3.11: Instrumentation for Experimental Measurements 91

Table 3.12: Error Propagation for Superficial Liquid Velocity 95

Table 3.13: Error Propagation for Superficial Gas Velocity 96

Table 3.14: Error Propagation (Vsl) for Water/Air/Sand in Annular Flow. 98

Table 4.1: Experimental Result of Flow Patterns in 2-inch Pipe. 99

Table 4.2: Experiment data for Annular Flow 102

Table 4.3: Annular flow showing flow behaviour in 2-inch horizontal pipe..... 103

Table 5.1: Water/Sand Test with Flow Regimes..... 137

Table 5.2: Study Results compared with Angelson et al., (1989) Results 139

Table 5.3: Water/Sand Flow Experimental results (MTC) 140

Table 5.4: PSD of Sand in Annular Flow compared with Annular Flow without Sand. 152

Table 5.5: Effect of Sand Particles on Wave Velocity in Annular Flow 155

Table 6.1: Summary of Statistical Error for OLGA Hold-up variance from Measured Hold-up. 170

Table 6.2: Summary of Statistical Error Margin of OLGA from Experiment. ... 175

Table A-1.0.1: Summary of Statistical Error for new Liquid Hold-up from previous Liquid Hold-up Calibrated. 201

Table A-1.0.2: Summary of Statistical Error for new Film Thickness from previous ones..... 201

NOMENCLATURE

Symbol	Description	Units
A	Cross-Sectional Area of Pipe	m^2
A_b	Cross-Sectional Area of Bed Layer	m^2
A_f	Cross-Sectional Area of Liquid Film in the Pipe	m^2
A_G	Cross-Sectional Area of Gas Zone in the Pipe	m^2
A_h	Cross-Sectional Area of Heterogeneous Slug in the Pipe	m^2
A_0	Cross-Sectional Area of Empty Pipe	m^2
A_S	Flow Area of Segmental Region above the Bed	m^2
B_o	Oil Formation Volume Factor	bbl/stb
C	Solid Concentration by Volume	*(-)*
C_b	Solid Volume Fraction of Bed Layer	*(-)*
C_D	Drag Coefficient	*(-)*
C_h	Solid Volume Fraction of Upper Layer in Heterogeneous Flow	*(-)*
C_L	Lift Coefficient	*(-)*
C_o	Discharge Concentration of Solids	*(-)*
C_r	In-Situ Concentration	*(-)*
C_v	Sand Concentration	v/v
C^*	Bed Deposit Concentration	*(-)*
D	Inside Pipe Diameter	m
D_{EQ}	Diameter of Fluid Section above Sand Bed	m

D_f	Hydraulic Diameter of the Liquid-Phase	m
D_{hh}	Hydraulic Diameter of Heterogeneous Slug	m
d_p	Particle Diameter	m
E	Liquid Hold-Up Fraction	*(-)*
E_l	Slug Frequency	s^{-1}
Es	Solid/Liquid Density Ratio	*(-)*
f	Fanning Friction Factor	*(-)*
F_B	Buoyancy Force	N
F_{bm}	Dry Friction Force in moving Bed with respect to length	N/m
F_{Durand}	Durand Coefficient for Ratio of Solid Density to Liquid Density	*(-)*
F_D	Drag Force on a Particle	N
F_G	Gravity Force	N
f_i	Friction Coefficient	*(-)*
f_{ib}	Interfacial Friction Factor	*(-)*
F_L	Lift Force	N
Fr_f	Froude Number based on Superficial Liquid Velocity	*(-)*
f_s	Pseudo-Average Friction Factor	*(-)*
f_w	Wave Frequency Correlation	*(-)*
g	Acceleration due to Gravity	$m.s^{-2}$
h	Bed height of Deposited Solids	m
h_d	Thickness of the Dispersed Layer	m

H_g	Gas Hold-Up	*(-)*
H_L	Liquid Hold-Up	*(-)*
H_o	Bed Height of Liquid Layer	m
i	Frictional Head Loss for Flow of Slurry	$kg/m^2/s^2$
i_w	Frictional Head Loss for Flow of Water	$kg/m^2/s^2$
j_f	Superficial Liquid Velocity	m/s
j_{fC}	Critical Superficial Liquid Velocity	m/s
j_g	Superficial Gas Velocity	m/s
k	Dimensionless Group	*(-)*
K	Constant (≈ 0.23)	*(-)*
L	Pipe Length	m
M	Mass	kg
n	Gas Fraction Input for Sand Transport Rate (Constant)	*(-)*
P	Pressure	$Barg$
P_D	Rate of Dissipation of Energy for Suspended Particles	J/m^3s
q_g	Gas Flow Rate	m^3/s
q_L	Liquid Flow Rate	m^3/s
q_o	Oil Flow Rate	m^3/s
q_w	Water Flow Rate	m^3/s
R	Pipe Radius	m
R_{e_f}	Reynold's Number	*(-)*

S	Transport Rate per unit Bed	m^3/s
S_b	Wetted Region by Bed Layer	*(-)*
$S_{f,}$	Wetted Region by Liquid Film	*(-)*
S_G	Wetted Region by Gas	*(-)*
S_h	Wetted Region by heterogeneous Slug	*(-)*
S_{ib}	Wetted Region by interfacial bed layer	*(-)*
S_L	Wetted Region by Liquid	*(-)*
S_S	Ratio of Solid/Liquid Densities	*(-)*
T	Time	s
U_H	Homogeneous Suspension Flow Velocity	m/s
U^o	Fraction Velocity	m/s
U_s	Standard Velocity	m/s
U_t	Terminal Settling Velocity	m/s
V	Velocity of Fluid in Pipe	m/s
Vc	Critical Velocity	m/s
V_g	Actual Gas Velocity	m/s
V_L	Actual Liquid Velocity	m/s
$V_{L,C}$	Critical Sand Deposition Liquid Velocity	m/s
V_m	Mixture Velocity	m/s
$V_{M,C}$	Critical Sand Deposition Mixture Velocity for Stratified Flow	m/s
$V_{M,D}$	Minimum Mixture Velocity void of Sand Particle Deposition	m/s

V_P	Average Particle Flow Velocity in Pipe if no Bed Deposit	m/s
V_{sg}	Superficial Gas Velocity	m/s
V_{sL}	Superficial Liquid Velocity	m/s
V_S	Slippage Velocity	m/s
V_{Sv}	Average Flow Velocity in Flow Region above Solid Bed	m/s
V_R	Minimum Transport Velocity Profile	m/s
w	Average Velocity of the Liquid Stratum	m/s
w_c	Critical Velocity of the Liquid Stratum	m/s
X	Lockhart-Martinelli Parameter	*(-)*
y	Denote Position in the Pipe	*(-)*
Z	Gas Compressibility Factor	*(-)*

Greek Symbol	Description	Units
α	Angle of Inclination	*Dimensionless*
ξ	Dimensionless Liquid Rate	*Dimensionless*
ε_s	Particle Diffusion Coefficient	m^2/s
π	Pie constant (3.1415926)	*(-)*
ϕ	Dimensionless Transport Rate	*Dimensionless*
Φ	Critical Velocity	m/s
θ_b	Angle, Angle of Bed Layer, Angle Liquid Film respectively	*Dimensionless*
φ_L	Parameter in Lockhart-Martinelli Correlation	*Dimensionless*
ρ	Density of Fluid	kg/m^3
ρ_g	Density of Gas	kg/m^3
ρ_L	Density of Liquid	kg/m^3
ρ_n	No-Slip Mixture Density	kg/m^3
ρ_o	Density of Oil	kg/m^3
ρ_p	Density of Solid or Sand Particles in Fluid Flow	kg/m^3
ρ_s	Slip Mixture Density	kg/m^3
ρ_w	Density of Water	kg/m^3
η	Dry Friction Coefficient	*Dimensionless*
τ_o	Shear Stress	Pa
μ_g	Gas Viscosity	$kg/m.s$
μ_L	Liquid Viscosity	$kg/m.s$
μ_n	No-Slip Mixture Viscosity	$kg/m.s$

μ_s	Slip Mixture Viscosity	$kg/m.s$
λ_g	No-Slip Gas Hold-Up	*(-)*
λ_l	No-Slip Liquid Hold-Up	*(-)*
υ_c	Critical Velocity of Slurry	m/s
υ_s	Hindered Settling Velocity of Solid	m/s
υ_∞	Settling Velocity of Solid in Unbounded Quiescent Fluid	m/s
ω_∞	Particle Terminal Velocity	m/s
ψ	Dimensionless Shear Stress	*Dimensionless*
γ_g	Specific gravity of Gas	*(-)*
γ_o	Specific gravity of Oil	*(-)*

LIST OF ABBREVIATIONS

API	American Petroleum Institute
BP	British Petroleum
CMC	Carboxyl Methyl Cellulose
CV	Critical Velocity
IMV	Incipient Motion Velocity
MTV	Minimum Transport Velocity
MTC	Minimum Transport Condition
MMFV	Maximum Mixture Flow Velocity
OPEX	Operating Expenditure
PAC	Poly-Anionic Cellulose
PCP	Progressive Cavity Pump
PSE	Process System & Engineering
RP	Recommended Practices
SINTEF	*Stiftelsen for Industriell og teknisk forskning*
TSV	Terminal Settling Velocity

1 INTRODUCTION

1.1 Background

Multiphase flow in pipes involve different phases flowing together, either at the same or different velocity. As the flow develops along vertical or horizontal pipes, different flow patterns or flow regimes can be observed, depending on the phase that is dominant in the system, the properties of each phase present in the flow (e.g. viscosity, density) its velocity and pipe geometry. The main flow regimes are: bubble flow, plug flow, slug flow, stratified flow, annular flow and mist flow. In oil and gas production systems, these flow patterns often carry sand particles as well, which originate from the reservoir. Sand particles pose operational, safety and cost issues, depending on where in the production system they are encountered, the sand control mechanism in place and the amount of sand dislodged from the reservoir. One particular flow regime of high relevance to oil and gas industry is horizontal annular flow with sand.

Gas-liquid annular flow is often encountered in petroleum production systems, where reservoir fluids are conveyed to surface via wells and transport lines, but also in nuclear power plants, as well as chemical and refining processes (e.g. reactors, heat exchangers). In annular flow, the liquid flows as a film along the pipe walls under gravity, induced by the high velocity gas stream in the pipe core, (Sergey *et al.,* 2014). The gas, together with entrained liquid droplets, flows within the core of the pipe; at high velocities, the entrained droplets travel at a velocity close to that of the gas, (Kesana *et al.,* 2012). When sand is present, particles that tend to be entrained in the gas phase may impact on the walls of the pipes, blind tees, the elbow joints, etc. Over time, the sand particles impinging on the pipe walls may lead to serious erosion problems.

1.2 Sand in Petroleum Production Systems

In petroleum production systems, sand particles originate from the reservoir formation, where they can be dislodged and be carried along with the fluids in the wells and flowlines/pipelines. According to Sunday and Andrew (2010), sand production is a process that develops progressively in three stages: failure of the

rocks surrounding an open hole or perforation from which free sand grains are generated, disaggregation of sand particles from weak formation and transport of those free grains by effluents into the wellbore; and up to the surface.

1.2.1 Sand Migration from the Reservoir

Sand migration from the reservoir to the surface may be triggered by fines being mobilised from the porous space by the drag action of the fluids flowing through formation. There are several factors that may facilitate the dislodgement of sand particles from the reservoir: drilling, water production, reduction of pore pressure, unconsolidated formations and high drawdown/high production rate.

1.2.1.1 Drilling

During drilling the bits causes mechanical stress on the near-wellbore rock structure, which leads to a localised crushed zone from which solid particles may start being produced once the system is brought online.

1.2.1.2 Water Production

Several hydrocarbon reservoirs produce under strong water aquifer drive. As aquifer water advances into the reservoir and reaches the wells (by either raising from the bottom, or via fingering through high permeability layers), it has a tendency to carry sand particles with it.

The reasons why sand production increases with increase in water production as noted by Kuncoro *et al.,* (2001) are;

- Water contains compounds/elements which weaken or dissolve the natural bonds (by compactions) between sand grains.
- Water saturation affects the capillary pressure that holds the sand grains together.

1.2.1.3 Pore Pressure Reduction

As depletion takes place, the reservoir pressure reduction combined with the action of the overburden, increases stress on the solid formation, (Kuncoro *et al.,* 2001). If the latter is poorly consolidated, solid production is enhanced.

1.2.1.4 Unconsolidated Reservoir Formations

Unconsolidated reservoir formations typically occur in younger geological sediments. They are poorly compacted with high porosity, high permeability and a compressive pressure strength which is less than 1000psi (Kuncoro *et al.,* 2001). They also tend to be shallower (depths 3000ft to 9000ft) than the more consolidated formations (>10,000ft). In an unconsolidated reservoir, the sand tends to be transported more easily by the flowing hydrocarbons and/or water.

1.2.1.5 High Drawdown/High Production Rate

When the production rate from a well is increased (by manipulating the wellhead choke valve, for example) this may result in an excessive drawdown (i.e. the difference between reservoir pressure and flowing bottom-hole pressure) across the near-wellbore region. This can not only accelerate water encroachment, but also promote sand production. In similar situations, a short-term increase in hydrocarbons throughout can have a long-term negative impact on the overall system performance.

1.2.2 Sand Particle Sizes

Sand particle size, diameter, shape and concentration have an impact on the characteristics of multiphase flow in pipes depending on fluid velocity and on the forces acting on the sand (e.g. gravity, lift, buoyancy and drag). In horizontal flow, small sized sand particles are easily suspended in fluid flow under high velocity, while the larger, heavier sizes are often scoured along the bottom of the pipes due to gravity, depending on the fluid flow velocity.

Ravelet *et al.,* (2012) also noted that grains size and specific mass have strong effects on flow regimes, mostly between a stationary bed and suspended flow.

Table 1.1: Sand Particle Sizes (Durand (1952)

Classification	Size	Fraction
Very Fine Sand	0.0625mm-0.125mm	$\left(\frac{1}{16} - \frac{1}{8}\right)$
Fine Sand	0.125mm-0.25mm	$\left(\frac{1}{8} - \frac{1}{4}\right)$
Medium Sand	0.25mm-0.5mm	$\left(\frac{1}{4} - \frac{1}{2}\right)$
Coarse Sand	0.5mm-1mm	$\left(\frac{1}{2} - 1\right)$
Very Coarse Sand	1mm-2mm and above	-

In his work, Durand (1952) was able to associate sand particles sizes having a specific gravity of 2.65 to flow regimes, as follows: sand particles sizes $< 40\mu m$ are transported as homogenous suspension, sizes between $40\mu m$ and $0.15\mu m$ move in suspension under turbulence, sizes between $0.15mm\ and\ 1.5mm$ are transported by suspension and saltation, while sizes greater than $1.5mm$ are transported by saltation.

Based on sand concentrations, Wicks (1971) also classified sand in relation to two distinct flow regimes to show its impact and importance in fluid flow in pipes:

- If solid concentrations across the flow area are distinctly non-uniform, the flow regime is heterogeneous provided particles are in motion with the fluid.
- When solid concentrations and distributions are practically uniform across the flow area, a near-homogeneous flow condition is exhibited.

Stevenson *et al.,* (1999) observed that sand concentrations in the oil and gas industry are within 5lb/1000bbl to 50lb/1000bbl, or approximately 0.0005% to 0.005% by volume fraction.

With respect to sand particles shape Wicks (1971) observed that; rounded sand particles roll provided the pipe's surface is smooth, long and thin sand particles slide or tumble along depending on whether the pipe's wall is smooth or rough

respectively. Rough or irregularly shaped sand particles jump or bounce in a manner that is called saltation.

1.2.3 Sand Control, Monitoring and Management Strategy

Sand control is the act of preventing or minimising the influx of sand in oil and gas wells. Sand control can be grouped into; mechanical, chemical and combination methods. Mechanical methods, involve selective perforation on wells where screens/gravels are used. The screens are designed to prevent or minimise sand influx into the wellbore and examples are; slotted liners (large holes), wire-wrapped screens (small holes), pre-packed screens (offers finest filtering), expandable screens and gravel pack.

Chemical methods, involve the use of chemical techniques in preventing or minimising sand influx into the wells. Chemicals are injected directly into the targeted sand layers through the perforations, to hold the sand particles together. Examples of chemical for sand consolidations are phenolic, furan and epoxy resins, Talaghat *et al.,* (2009).

Combination methods, involve the joint use of mechanical and chemical methods in binding the sand grains together. A typical example in the oil and gas industry, is the used of resin-coated gravel pack. Sand monitoring and management strategy will continue to be of paramount importance in the oil and gas industry with wells and pipelines integrity continuing to remain priority, particularly in mature fields.

1.3 Why this Research?

Several researchers to date have investigated the complex nature of annular flow in pipes and provided experimental analyses for liquid hold-up, wave velocity, wave frequency, liquid film thickness and liquid entrainment. The literature also offers experimental analyses of sand behaviours in several flow regimes, both in horizontal and vertical pipes. However, there is no reported experimental research on sand transport in annular flow in pipes, as summarized in Table 2.2.

Sand transport in slug flows were more researched because of the paradigm shift from onshore to deep-water exploration and production, where slug flows were dominant and as such represented the more imminent need.

Therefore, there is a need to present a detailed experimental investigation on sand behaviour in horizontal annular flow to progress the knowledge of the industries that are directly involved in such flow in their systems.

1.4 Significance of Work

The significance of this research is to present sand transport in horizontal-annular flow with basic information like: mode of sand transport, sand flow regimes and effects of sand available, which will assist in well planning/pipeline design; by providing insight into sand behaviour in annular flow.

1.5 Aims and Objectives

Aims

The aim of this research is to investigate the effect of sand on annular flow behaviour in horizontal pipes through a dedicated experimental campaign. This will progress the fundamental understanding of this type of flow occurrence and hence facilitate optimum design of oil and gas production system where it is often encountered.

Objectives

The objectives of this research are:

- To conduct a comprehensive literature review of sand (transport) in multiphase flow in horizontal pipes.
- To experimentally analyse annular flow behaviours, liquid film thickness, interfacial friction and shear stress and wave characteristics in water/air annular flow.
- To experimentally analyse how sand impacts on single-phase horizontal flow and on two-phase horizontal annular flow.

- To investigate physical modes of sand distribution in annular flow to assess where sand particles are transported.
- To analyse the effects of sand concentration and sand particle sizes on annular flow characteristics.
- To test commercial software package broadly used across the oil and gas industry against the obtained experimental data to identify potential areas where further advances in multiphase flow modelling are needed towards improvement.

1.6 Structure of Thesis

1: Introduction

This chapter presented an introduction to annular flow in horizontal pipes. It included a brief discussion on what can be expected when sand is also present and on the root causes of it becoming dislodged from the reservoir in the first place. The potential impact of sand particles size and concentration was presented vis-à-vis how the sand can be transported along with the fluid. This chapter also highlighted the importance of being able to understand sand transport in annular flow in order to better plan sand management strategies.

2: Literature Review

This chapter covers the fundamental concepts of annular flow in horizontal pipes such as, film thickness, liquid entrainment and wave characteristics. Also, reviewed previous experimental studies on sand transport in multiphase flow, with emphasis on water/sand, air/sand and water/air/sand under different flow regimes in horizontal pipes, with a discussion on their key findings and limitations.

3: Experimental Investigations (Methodology/Approach)

This chapter covers the flow loop design, the experimental set-up, the experimental procedures adopted, experimental error and uncertainty analysis, and the re-calibration (annular) conducted in this study. The experiment was conducted using a 2-inch (0.0504m) flow loop of 28.68m long. A 2-inch air injection pipe was connected to the flow loop immediately after the bend at 15.81m while the sand sampling point was at a distance of 9.24m away from the

air injection point. More so, the distance of the sand injection point to the sand sampling point was 5.27m. The sand sampling pipe has an internal diameter of 2.92mm (0.00292m) which was adjustable for sampling purposes at different levels in the internal diameter of the pipe. More so, the re-calibration of annular flow tests which were conducted with the aid of five different acryl rods (blocks) of 49mm, 48mm, 47mm, 46mm and 45mm.

The chapter also provides detailed explanations of the experimental error and uncertainty analysis. In particular, the propagation of the measurement error in superficial liquid velocity, superficial gas velocity, film thickness and liquid hold up is discussed to permit a full assessment of the overall accuracy of the results obtained.

4: Water/Air Flow Test Results

This chapter presents the results for stratified-smooth, plug, slug and stratified-wavy flows. The water/ air annular flow results are presented with emphasis on liquid hold-up and film thickness, comparing three methods for obtaining film thickness and discussing wave characteristics, pressure gradient and interfacial shear stress. Also, discussed are the results of wavelet, power spectral density and time series analysis of the film thickness. The water/air annular flow case represented the base case scenario prior to the introduction of sand, to be able to quantify its impact on this type of flow regime.

5: Sand Transport Flow Test

This chapter covers water/sand experiments to illustrate the different sand flow regimes in horizontal pipe using both instrumentation and visual inspections. Also, discussed are sand minimum transport conditions (MTC) from the experiments. Again, the water/sand experiments presented the major sand flow regimes e.g. sand dune, saltation, sand streaks and suspension in horizontal in pipes.

Also in chapter five were the results of water/air/sand annular flow and the sand sampling experiments conducted in the horizontal pipe. The two sand flow regimes detected were also presented with the mode of sand distributions from

the sand sampling experiments, presented. The power spectral density of water/air/sand annular flow is compared with that of water/air annular flow to further buttress the sand transport in annular flow. The effects of sand particles size and concentration on the experimental results were discussed.

6: OLGA Simulations

This chapter presents the OLGA simulations that were run and compared with the experimental results for the water/air and water/air/sand annular flow cases.

7: Conclusions and Recommendations

This chapter draws the conclusion on the overall results obtained during this study and recommends future research on sand transport in annular flow in horizontal pipes.

2 LITERATURE REVIEW

2.1 Background

Multiphase flow is the act of conveying different fluids and solids together in a system (e.g. pipe) to its destination either for processing or sales. The flow of different fluids in pipes are characterised with changes as the fluid is being transported from the reservoirs to the delivery point.

Multiphase flow exhibits various flow characteristics depending on the fluid temperature, gas velocity, gas pressure, liquid volume, pipe geometry (e.g. horizontal, vertical, uphill and down-hill) and orientation. In most cases, the liquid flows along the bottom of the pipe due to gravity, or dispersed as droplets in the gas core. And this flow behaviour because of liquid and gas interaction in the pipes when transported from the reservoirs to the separation units, is what is referred to as flow regime or patterns.

Flow regimes or patterns could be categorized in horizontal pipes as: bubble, plug, stratified-smooth, stratified-wavy, slug, annular and annular-mist flows as shown in Figure 2.1. In this study, the focus is on annular flow in horizontal pipes.

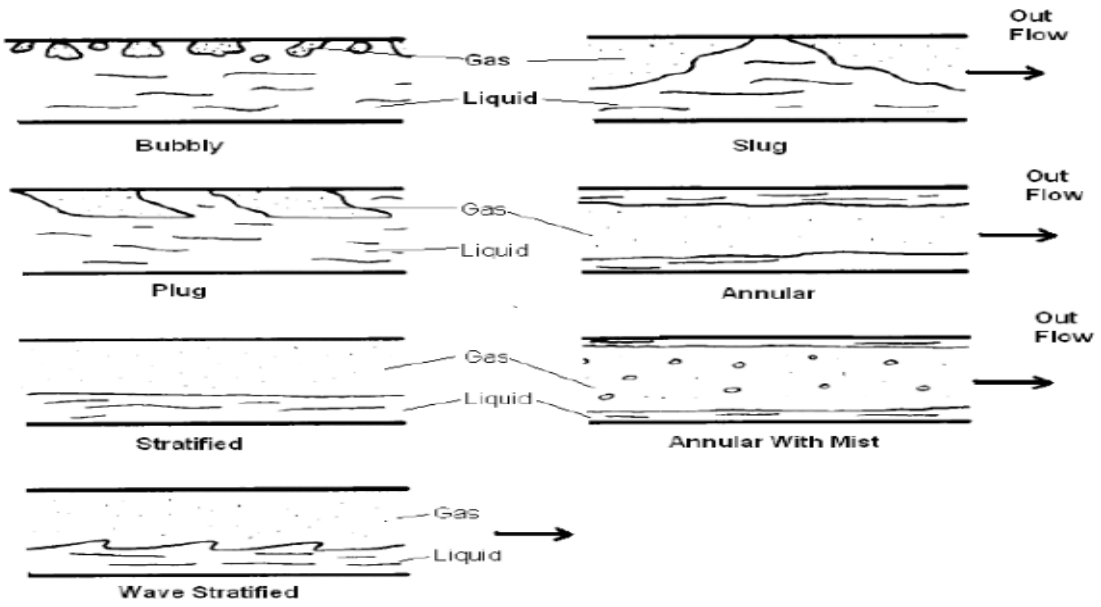

Figure 2.1 Horizontal Two-Phase Flow Pattern in Pipes (Balasubramaniam *et al.,* 2006).

2.2 Annular Flow

Annular flow is a complex flow regime, experienced in vertical and horizontal pipe in the oil and gas industry. Annular flow in horizontal pipes flow with high gas velocity at the core centre of the pipe with much impact of gravity leaving the circumferential liquid film on the internal walls of the pipe which drains down to the bottom of the pipe. Annular flow, represents a thick liquid film at the bottom that moves slowly on the internal pipe walls than the gas phase, Kesana *et al.*, (2012). The combined slow flow of the liquid at the bottom with the fast gas phase at the interface aids to increase the pressure gradient and wall shear stress in annular flow. However, a thin liquid film exists at the curved surfaces and the upper walls of the internal diameter of the horizontal pipes.

There are also special characteristics associated with annular flow in pipes e.g. wave characteristics, circumferential liquid film thickness, mechanism of liquid entrainments and shear characteristics. With the above characteristics of annular flow in pipes, experimental investigation on sand transport becomes more challenging.

2.2.1 Flow Regime Map

The horizontal flow pattern in Figure 2.1 could be represented in a flow map of liquid superficial velocity against gas superficial velocity with respect to gas void fraction as shown in Figure 2.2.

The superficial liquid and gas velocities obtained from the experiments, could be presented in a flow map to determine the flow regimes. The essence is to justify how oil, gas and water flows in pipes. The flow map are useful in determining pressure gradient and to account for possible production problems like sand particle depositions and erosion in the pipes.

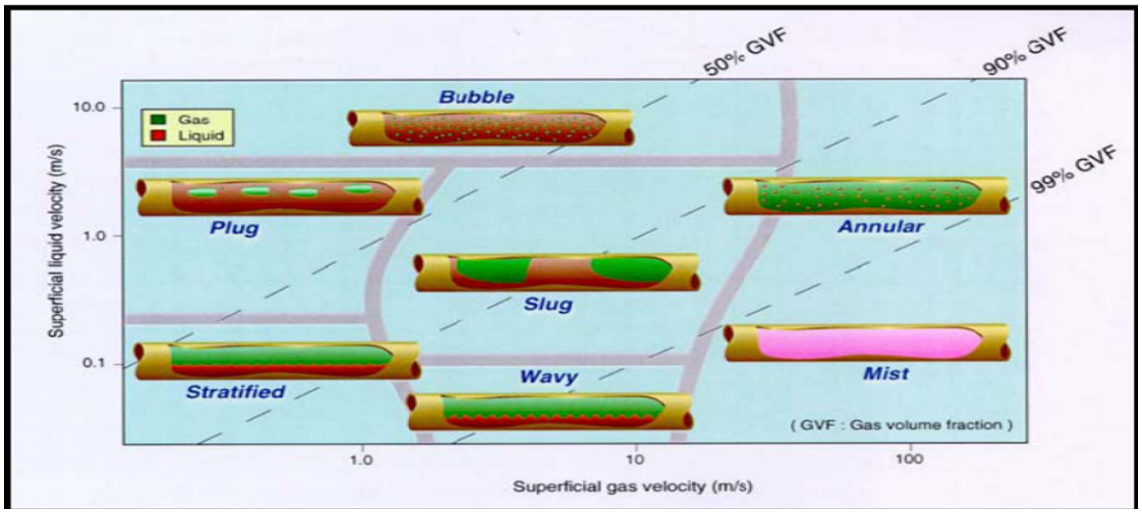

Figure 2.2: Horizontal Flow Map showing different Flow Pattern (Lawrence & Steven, 2003)

2.3 Pressure Gradient

Multiphase flow in pipes are also complicated with slippage between the different phases (oil, gas, water) and sand particles as flow regime changes, with mass and energy transfer between the phases which often results to pressure losses. Pressure gradient is used to account for pressure losses per unit distance transported by these fluids in the pipes. The effect of pressure losses could also propagate shear stress in the pipe with respect to liquid film thickness at the internal walls of the pipe in multiphase flow.

Pressure gradient could be obtained from several empirical correlations and mechanistic models. Among the correlations, Beggs and Brill (1973) and Dukler *et al.,* (1963) are more prominent in horizontal flow in pipes.

2.3.1 Beggs and Brill (1973)

Beggs and Brill (1973) on pressure gradient conducted experiment on two-phase using transparent acrylic pipe (1 and 1.5-inch) of 90ft long, with liquid and gas flow rates ranging from 0-30gal/min and 0-300Mscf/D respectively. From their experimental studies, pressure gradient correlation to predict flow at different pipe geometry was developed based on energy balance for fluid flowing between two end points as follows:

$$\frac{-dp}{dz} = \frac{\frac{g}{g_c}\sin\theta\left[\rho_L H_L + \rho_g\left(1 - H_L\right)\right] + \frac{f_{tp} G_m v_m}{2 g_c d}}{1 - \frac{\left[\rho_L H_L + \rho_g\left(1 - H_L\right)\right] v_m v_{sg}}{g_c p}} \quad \textbf{(2-1)}$$

where,

$$\rho_g = \frac{pM}{z_g RT} \quad \textbf{(2-2)}$$

$$f_{tp} = \left[\frac{dp}{dz}\left(1 - \frac{\rho_{tp} v_m v_{sg}}{g_c p}\right) - \frac{g}{g_c}\sin\theta\rho_{tp}\right]\frac{2 g_c d}{G_m v_m} \quad \textbf{(2-3)}$$

$$\rho_{tp} = \rho_L H_L + \rho_g\left(1 - H_L\right) \quad \textbf{(2-4)}$$

Where the H_L which is, the liquid hold up from Beggs and Brill (1973) could be obtained from Table 2.1 depending on the flow regime.

Table 2.1: Beggs & Brill (1973) Equations for Liquid Hold-Up

Horizontal Flow	***Horizontal Hold-Up***
Segregated *(Stratified, Wavy, Annular)*	$H_L(0) = \frac{0.98\,\lambda^{0.4846}}{(N_{FR})^{0.0868}}$
Intermittent *(Plug, Slug)*	$H_L(0) = \frac{0.845\,\lambda^{0.5351}}{(N_{FR})^{0.0173}}$
Distributed *(Bubble, Mist)*	$H_L(0) = \frac{1.065\,\lambda^{0.5824}}{(N_{FR})^{0.0609}}$

2.3.2 Dukler *et al.,* (1964)

Dukler *et al.,* (1964) developed a correlation for pressure gradient in horizontal two-phase flow, based on frictional energy losses having studied and compared certain correlations of pressure drops and holdup in horizontal flow. The pressure gradient could be mathematically expressed from the general equation in a simplified manner as:

$$\left(\frac{\Delta P}{\Delta L}\right)_T = \left(\frac{\Delta P}{\Delta L}\right)_{friction} + \left(\frac{\Delta P}{\Delta L}\right)_{accelerati\ on} + \left(\frac{\Delta P}{\Delta L}\right)_{elevation} \quad \textbf{(2-5)}$$

Where the acceleration term is dependent on the flow pattern and the distribution of gas/liquid across the pipes. For stratified-smooth, stratified-wavy and annular flow, it is:

$$(\Delta P)_A = (\Delta P)_{AL} + (\Delta P)_{AG} \quad \textbf{(2-6)}$$

where,

$$(\Delta P)_{AL} = \frac{W_L}{g_c A_P}(V_{L2} - V_{L1}) \quad \textbf{(2-7)}$$

$$(\Delta P)_{AG} = \frac{W_G}{g_c A_P}(V_{G2} - V_{G1}) \quad \textbf{(2-8)}$$

2.3.3 Shear Stress

Shear stress in two-phase flow in pipes could be categorized into wall shear stress and interfacial shear stress. Wall shear stress is attributed to the frictional effects impacted on the walls of the pipe, because of the phases and solid in most cases being transported in the pipe. While interfacial shear stress occurs at the interface between the liquid and gas phases in the pipe as they flow together. The stress created at the interface on both phases, is called interfacial shear stress in multiphase flow in pipes.

2.4 Film Thickness

In annular flow in horizontal pipe, the liquid film is thin. This is because in annular flow, the superficial gas velocity is high and much of the liquids are entrained as droplets in the gas core. More so, the liquid is non-uniform and flows circumferentially around the pipe walls. Again, the liquid film in annular flow is characterized by asymmetry distributions, depending on the mass flow rate of the liquid and gas (Setyawan *et al.*, 2016).

Liquid film thickness is observed to be higher at the bottom of the pipe compared to the curved surface area and the upper walls of the pipe internally. This is because of the effects of gravity-induced drainage, which increases the liquid film

thickness at the bottom of the pipe, Setyawan *et al.*, (2016), Shedd, (2001). On film thickness, McManus (1961) investigation was based on circumferential water film thickness, while Anderson & Russel (1970) presented film thickness at the upper part of the walls of the pipe and Butterworth (1973, 1972) conducted experiments on film thickness with respect to axial flow. Others who researched on film thickness were: Chien and Ibele (1964), Telles and Dukler (1970), Lin *et al.*, (1985), Pearce and Fisher (1979).

2.4.1 Methods of Determining Film Thickness

There are different experimental methods used in determining liquid film thickness in the pipes. These methods, could be classified majorly into:

- ***Optical method:*** e.g. pin, high speed cameras/Laser for detecting interface, etc.
- ***Electrical method***: capacitance, conductance method (flush-mounted, parallel-wire)
- ***Acoustic method:*** e.g. ultrasonic in which the reflected signals of time interval emitted from gas-liquid interface are converted to film thickness.
- ***Radiological method***: e.g. X-ray, neutrons and gamma-ray. The different attenuations are used to measure liquid film thickness.

These methods for determining liquid film thickness differs in measurement principles, ease of use, frequency response, calibration techniques, accuracy and method of installation (intrusive or non-intrusively mounted). Apart from the experimental measurement, film thickness also could be obtained from correlations like triangular relationship and Tso and Sugawara (1990) equation (3-4).

2.4.2 Triangular Relationship

Triangular relationship signifies three important variables that are dependent on one another: pressure gradient, liquid film rate and liquid film thickness. It is a correlation that is based on pressure gradient and liquid film flow rate as a function of film thickness. The liquid film flow rate, could be obtained by measuring the liquid film thickness and pressure gradient on a straight pipe

segment, Falcone *et al.,* (2003). Hewitt and Hall-Taylor (1970), clearly simplified it for flow in round tubes with assumptions that gravitational and acceleration effects are ignored. Therefore, all flow in pipes, and flows in in the film including shear stress equals that of wall shear stress. Triangular relationship for film thickness, is often used for upward or vertical pipes.

$$\dot{M}_{LF} = f\left(\delta, \frac{dp}{dz}\right) \quad \textbf{(2-9)}$$

In this study, equation (2.9) was used to make comparison with the experimental results.

The limitations of the correlations are: all liquid flow in the pipe do not flow in the film as noted in the assumptions for the correlation, as liquid droplets and circumferential liquid flow across pipes in annular flow are observed. Shear stress in liquid is not and also not equal the wall shear stress as presented in the assumptions. More so, triangular relationship is preferably used for multiphase flow in vertical pipes.

2.5 Some Parameters used for Annular Flow Analysis.

In annular flow in pipes, signals are further analysed using: probability density function (PDF), power spectral density, (PSD) and wavelet to present wave characteristics in pipes

2.5.1.1 Probability Density Function

This is a probability time series functions that describes the statistical distribution of the instantaneous film thickness. It is a statistical function that gives a random variable on a range of values. Mathematically, PDF could be expressed as:

$$fX(x) = \underset{\Delta \to 0^+}{Lim} \frac{P\{x < X \leq x + \Delta\}}{\Delta} \quad \textbf{(2-10)}$$

2.5.1.2 Power Spectral Density

Power spectral density is an autocorrelation signal analysis functions, which measures the power intensity signals with respect to frequency domain. It illustrates how energy strength of the output signals on time series, are distributed

with respect to frequency of that signal. The power spectral density is used to determine wave frequency in multiphase flow in pipes.

2.5.1.3 Wavelet

The continuous wavelet transform (cwt), is a short time Fourier transform that is used to analysis signals at multiple scales. In extracting output signals from experimental data, the continuous wavelet transform (cwt) uses an analysis window which is referred to as wavelet.

Wavelet is a signal analysis that exhibits time-varying statistics in both time scales, and in frequency domain with a plot of output signals and the scale wavelet called scalogram, (Shoeb and Clifford, 2005).

Continuous wavelet transform could be expressed as:

$$C_{(a,\tau)} = \int \frac{1}{\sqrt{a}} \Psi\left(\frac{t-\tau}{a}\right) x(t) dt \qquad \textbf{(2-11)}$$

2.6 Liquid Entrainment

Entrainment is simply the fraction of liquid droplets dispersed in the gas core. It involves a droplet-breakup from the liquid film due to wave actions of the high gas velocity flow in the pipes. Entrainments in gas core have been investigated with wide publications. Among the experimental investigations on entrainment in pipes are: Cousins and Hewitt (1968) for vertical flow, keeys *et al.,* (1970), Laurinat (1982), Williams (1990), Paras and Karabelas (1991b), Tayebi *et al.*, (2000) and Ousaka and Kariyasaki (1992) for horizontal flow.

2.6.1 Entrainment Correlations for Vertical Flow

There are several correlations for liquid entrainment, among them are:

2.6.1.1 Wallis (1968)

Wallis studied the work of Paleev and Flipovich (1966) and improved on it by substituting the liquid viscosity with gas viscosity in his correlation as:

$$F_E = 1 - \exp\left\{-0.125 \times \left(\frac{10^4 V_{sg}\,\mu_g}{\sigma\sqrt{\rho_g / \rho_L - 1.5}}\right)\right\} \quad \textbf{(2-12)}$$

In terms of observations, liquid viscosity and velocity were not considered. Again, for low Reynolds number and entrainment fraction > 0.5, the correlation will fail.

2.6.1.2 Oliemans *et al.,* (1986)

Entrainment correlation was developed based on a wide range of flow conditions (Harwell databank) with pipe diameters of 6-32mm. The correlation covers a range of surface tension of 0.012-0.0173 N/m and gas Froude number 1-10. They considered both laminar/turbulent conditions in their correlation as shown below:

$$\frac{F_E}{(1 - F_E)} = 10^{-2.52}\,\rho_L^{1.08}\,\rho_g^{0.18}\,\mu_L^{0.27}\,\mu_g^{0.28}\,\sigma^{-1.8}\,d^{1.72}\,V_{SL}^{0.7}\,V_{Sg}^{1.44}\,g^{0.46} \quad \textbf{(2-13)}$$

It behoves to note, that gas Froude number > 10 is not covered and hence the correlation will fail if large gas Froude numbers above 10 are involved.

2.6.1.3 Ishii and Mishima (1989)

Their scholarly works on entrainment were based on emphasis on Reynolds number (liquid) and Weber number of gas. The proposed correlation is:

$$F_E = \tanh\left(7.25 \times 10^{-7} W_{eg}^{1.25} R_{el}^{0.25}\right) \quad \textbf{(2-14)}$$

where,

$$W_{eg} = \frac{\rho_g V_{sg}^2 d}{\sigma}\left[\frac{\rho_L - \rho_g}{\rho_g}\right]^{\frac{1}{3}} \quad \textbf{(2-15)}$$

and,

$$R_{eL} = \frac{\rho_L V_{SL} D}{\mu_L} \quad \textbf{(2-16)}$$

The limitation of the correlation, is that a correction factor for a high Weber number of gas phase is required. The correlation also performs better on low viscosity liquids only.

2.6.1.4 Pan and Hanratty (2002a)

Their correlation was based on atomization and rate of deposition of droplets from experimental data with pipe diameters ranging from 10.6-57.2mm, superficial liquid and gas velocities 0.012 -1.35m/s and 20 -119m/s respectively. The correlation is presented below:

$$\frac{F_E / F_{E,\max}}{1 - F_E / F_{E,\max}} = 6 \times 10^{-5} \left[(v_G - v_{Gcr})^2 d \sqrt{\rho_L \rho_g} / \sigma \right] \quad \textbf{(2-17)}$$

Where critical gas velocity at onset entrainment is;

$$v_{G,cr} = 40 \sqrt{\sigma / \left(d \sqrt{\rho_L \rho_g} \right)} \quad \textbf{(2-18)}$$

Limitation of the correlation is on pipe diameter. The pipe diameters considered during the developed correlation are in a range of 10.6mm to 57.2mm only. Therefore, correlation will not fit in for 4-inch pipes and above.

2.6.1.5 Sawant *et al.,* (2008)

From their experiments, entrainment fraction correlation was developed with emphasis on Weber number and liquid Reynolds number in line with Ishii and Mishima (1989). The correlation was validated with data from flow conditions of pipe diameter (9.4mm), superficial liquid and gas velocities of 0.05-0.75m/s and 15-100m/s respectively. The correlation is mathematically expressed as:

$$F_E = F_{E,\max} \tanh\left(\alpha N_{We}^{1.25} \right) \quad \textbf{(2-19)}$$

Where maximum entrainment fraction is:

$$F_{E,\max} = 1 - N_{\mathrm{Re}\,f,\lim} / N_{\mathrm{Re}\,sL} \quad \textbf{(2-20)}$$

and

$$\alpha = 2.31 \times 10^{-4} N_{\mathrm{Re}sL}^{-0.35} \quad \textbf{(2-21)}$$

While limiting liquid-film Reynolds number is:

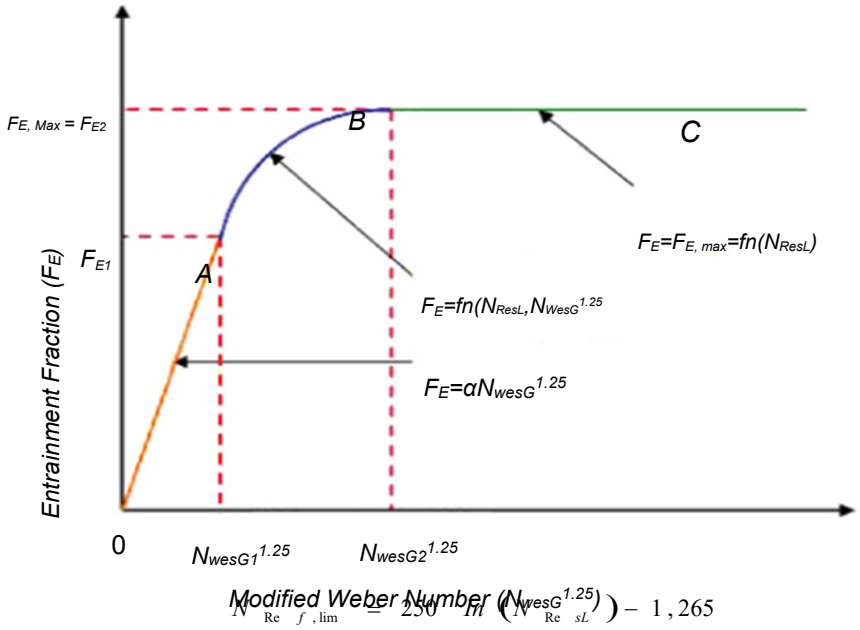

$$N_{\mathrm{Re}_{f,\lim}} = 250 \ln\left(N_{\mathrm{Re}_{sL}}\right) - 1,265$$

Figure 2.3: Entrainment Fraction against Weber Number (Sawant *et al.,* 2008)

Sawant *et al.,* (2008) grouped their correlations into three as shown in Figure 2.3

- ***Group (O-A*)**: a thick liquid film exists here

- ***Group (A-B):*** liquid film decreases with increase in gas superficial velocity
- ***Group (B-C):*** liquid film is entrained almost totally into gas core where increase in gas superficial velocity has no effect again. However, in the development of the correlation, only internal pipe diameter of 9.4mm was considered.

2.6.2 Entrainment Correlations for Horizontal Flow

The following liquid entrainment correlations below, are preferably used in horizontal pipes:

2.6.2.1 Wicks and Dukler (1960)

An entrainment correlation group ***R*** (lbmft^3/lbf-hr) was developed based on pipe internal diameters of 25.4mm and 76.2mm with superficial liquid velocities of 0.12-0.77m/s and superficial gas velocities of 12-62m/s. Again, critical Weber number ranging from 13 to 22 and pressure gradient, were considered in the correlation expressed as:

$$R = \left(\frac{q_L}{q_g}\right)\left(\frac{N_{We,cr} W_{LE}}{(dp/d_L)_G}\right) \quad \textbf{(2-22)}$$

The above equation (2.22) of the entrainment correlation group ***R*** could be re-written with Lockhart-Martinelli parameter X, if the correlation group ***R*** is within the ranges of 0.5 to 200.

$$R = 168\, X^{2.05} \quad \textbf{(2-23)}$$

while,

$$X = \sqrt{\frac{(dp/d_L)_L}{(dp/d_L)_G}} \quad \textbf{(2-24)}$$

2.6.2.2 Paleev and filipovich (1966)

Their correlation was based on gas velocity, viscosity, droplet concentration, surface tension and liquid density. The correlation is expressed as:

$$F_E = 0.015 + 0.44 \log\left[\frac{\rho_m}{\rho_L}\left(\frac{\mu_L V_g^2}{\sigma}\right)10^4\right] \quad \textbf{(2-25)}$$

In the correlation, pipe diameter was not considered.

2.6.2.3 Dallman *et al.,* (1979)

Correlation developed was based on air/water flow using a 0.0231m pipe diameter. The flow conditions considered in their correlation were based on Vsg of 15-88m/s, Vsl of 0.0072-0.9m/s, gas density (between 1.6 to 2.75kg/m^3), liquid density of 1000kg/m3 with liquid viscosity of 1mPas and surface tension of 73mN/m. The developed correlation is:

$$\overset{*}{\varepsilon} = k_A\left(\frac{W_{LF} - W_{LFc}}{p}\right)V_g^2 \rho_g^{0.5} \rho_f^{0.5} \quad \textbf{(2-26)}$$

where,

$$k_A = 3.5 \times 10^{-6}\ Sec^2 / kg \quad \textbf{(2-27)}$$

and;

$$\frac{W_{LFc}}{p} = 0.046\ , kg\ /\ m.s \quad \textbf{(2-28)}$$

The correlation considered only a pipe with an internal diameter of 0.0231m. It will present a wrong result if a larger pipe diameter is involved.

2.6.2.4 Pan and Hanratty (2002b)

This is an explicit correlation that considers critical liquid film rate. The correlation considers deposition coefficient, droplet size, entrainment fraction, maximum entrainment as noted by Mantilla *et al.*, (2009) and Magrini *et al.,* (2012). Below is the correlation:

$$\frac{f_E / f_{Em}}{1 - f_E / f_{Em}} = 9 \times 10^{-8}\left(\frac{DV_g^{\ 3}\sqrt{\rho_L - \rho_g}}{\sigma V d}\right) \quad \textbf{(2-29)}$$

where,

$$f_{Em} = 1 - \frac{W_{Fcr}}{W_L} \quad \textbf{(2-30)}$$

Where critical liquid-film-flow rate could be calculated using:

$$W_{Fcr} = 0.25\ \mu_L \pi D R_{eFcr} \quad \textbf{(2-31)}$$

While the Reynolds number for liquid-film-flow rate is:

$$R_{eFcr} = 7.3(\log\ \omega)^3 + 44.2(\log\ \omega)^2 - 263\ \log\ \omega + 439 \quad \textbf{(2-32)}$$

and,

$$\omega = \left(\frac{\mu_L}{\mu_g}\right)\sqrt{\frac{\rho_g}{\rho_L}} \quad \textbf{(2-33)}$$

The limitation of this correlation is that, critical-film-flow rate gives a negative result on maximum fraction of entrainment for low liquid flow rates.

2.6.2.5 Mantilla *et al.,* (2009)

They developed correlations for entrainment fraction and maximum entrainment based on pipe diameters of 50.8mm and 152.4mm (ID). In the developed

correlations, superficial liquid and gas velocities, pipe diameter, liquid wave, deposition coefficient and wave fraction were considered. The entrainment fraction correlation is as follows:

$$f_E = \frac{1 - \frac{4}{v_{SL}\pi D^2}\int_0^{A(h_{Lb})} \bar{u}\, dA}{1 + \frac{k_D}{v_{sG}}\frac{4 S_I L_w}{\phi\pi D^2}} \quad \textbf{(2-34)}$$

while the maximum entrainment correlation is here below:

$$f_{Em} = 1 - \frac{q_{Fcr}}{q_L} \quad \textbf{(2-35)}$$

where the critical liquid film flow rate is given as:

$$q_{Fcr} = \pi D v \left(12.514 + 5 h_{Lm}^{+} Inh_{Lm}^{+} - 8.05 h_{Lm}^{+}\right) \quad \textbf{(2-36)}$$

Where the dimensionless liquid film thickness at maximum entrainment condition is:

$$h_{Lm}^{+} = 0.6 R_{eSL}^{0.45} \quad \textbf{(2-37)}$$

The correlations could be improved by introducing frequency, wave celerity, amplitude and spacing, (Mantilla *et al.,* 2009).

2.7 Wave Characteristics in Annular flow

Wave characteristics could be grouped into: wave behaviour, wave velocity and wave frequency in annular flow.

Wave is an oscillation with a transfer of energy that travels through a medium while frequency is the time-dependent for wave transfer. In annular flow, a non-uniform thin liquid-film thickness exists circumferentially across the pipes. This liquid film thickness, exhibits an interfacial wave behaviour due to high superficial gas velocities and low liquid velocities attributed to annular flow in pipes.

More so, interfacial wave behaviour reveals, a wavy structure that could be grouped into: ripple and disturbance waves.

Ripple waves

They are low amplitude and high frequency waves that contribute to the interfacial shear stress in the pipes, (Kumar *et al.,* 2002). Also, they are characterized by low velocity, short-life time and non-coherent wave that creates interfacial roughness and promote pressure drop in annular flow, (Setyawan *et al.,* 2016).

Disturbance waves

The wave travels with higher velocities, higher film thickness, higher amplitude, and longer-life time, which are responsible for liquid entrainment in the gas core, (Setyawan *et al.*, 2016). The disturbance wave forms a complete ring structures in the pipe.

For wave frequency in annular flow, several investigations have been carried out and also correlated to justify their behaviours. Among the investigations are the works of: Wilkes *et al.,*(1983), Azzopardi (1986), Jayanti *et al.,* (1990), Paras and Karabelas (1991), Ousaka *et al.*, (1992), Fukano (1998), Mori *et al.*, (1999), Weidong *et al.*, (1999), Ousaka *et al.*, (2006), Kumar *et al.*, (2002), Han *et al.*, (2006), Schubring & Shedd (2008), Sawant *et al.,* (2008), Mantilla (2008), Alamu and Azzopardi (2011), Al-Sarkhi *et al.,* (2012), Gawas *et al.,* (2014), Zhao *et al.,* (2013), Setyawan *et al.,* (2015), Setyawan *et al.,* (2016).

2.7.1 Wave Velocity

Wave velocity could be defined as wave displacement per time delay as wave travels through space or medium. If the sensors' distance apart and time delay are known, the wave velocity could be presented as a ratio of distance per time delay from cross-correlations.

2.7.1.1 How to Determine Wave Velocity.

Wave velocity could be obtained from the signals of the conductivity ring sensors or conductance probes in annular flow using Matlab. If the sensors' distance apart and time delay are known, the wave velocity could be presented as a ratio of distance per time delay from cross-correlations. The downstream sensor (sensor 2) is delayed by several milliseconds compared to sensor 1 (Setyawan *et al.,*

2016). Wave velocity in annular flow could be obtained from the signals of the upstream and downstream sensors.

2.7.2 Wave Velocity Correlation.

There are considerable wave velocity correlations that exist, notable among them are:

2.7.2.1 Ousaka *et al.,* (1992)

They developed a wave velocity correlation in horizontal flow which is expressed as:

$$C_{W,Ousaka} = 3.0V_{SL}\left(\frac{R_{eG}}{R_{eL}}\right)^{0.78} \quad \textbf{(2-38)}$$

2.7.2.2 Schubring and Shedd (2008)

Their correlation was developed based on pipe internal diameters of 8.8mm, 15.1mm and 26.3mm. The first experiment was carried out with 2.4m/s to 6m/s of wave velocity under the superficial gas and liquid velocities of 32m/s to 91m/s and 0.04m/s to 0.39m/s respectively. The subsequent experiment, with pipe internal diameters of 8.8mm to 15.1m/s, yielded a range of wave velocities of 1.9m/s to 8.37m/s on liquid superficial velocities of 0.05m/s to 0.2m/s. These experiments were used to develop a correlation as follows:

$$C_{w,ss} = 0.42\,\frac{V_{Sg}}{\sqrt{x}}R_{eG}^{-0.25} \quad \textbf{(2-39)}$$

2.7.2.3 Setyawan *et al.,* (2014)

Their correlation was based on smaller pipe diameters of 16mm to 26mm. The superficial water velocities were 0.05m/s to 0.2m/s and superficial air velocities of 12m/s to 40m/s. Wave velocity, means displacement of wave per time as it travels through a medium. The correlation developed is expressed as:

$$C_{W,Corr} = 0.34\,\frac{V_{Sg}}{\sqrt{x}}R_{eG}^{-0.2} \quad \textbf{(2-40)}$$

2.7.3 Wave Frequency Correlation

Wave frequency in multiphase flow, is obtained from a corresponding frequency of the largest peak of the "***power spectral density***" ***(PSD)*** function. In annular flow, several investigations exist to show the effects of superficial liquid and gas velocities on wave frequency. Among these are: Fukano *et al.,* (1983), Jayanti *et al.,* (1990), Paras and Karabelas (1991), Ousaka *et al*, (1992), Schubring and Shedd (2008) and Setyawan *et al.,* (2014) who reported that increase in superficial gas velocity, increases wave frequency in annular flow in horizontal pipes.

Setyawan *et al.,* (2014) further reported that wave frequency decreases with increase in the pipe internal diameter and lastly, that superficial liquid velocity has negligible effect on wave frequency.

Apart from using power spectral density to determine wave frequency, there are correlations such as:

2.7.3.1 Ousaka *et al.*, (1992)

Ousaka *et al.*, (1992) correlation, was also part of the experimental works carried out while developing the wave frequency correlation. However, the same flow conditions and pipe internal diameters used in wave velocity correlation exists in the wave frequency correlation which is expressed as:

$$f_W = 0.066 \frac{V_{SL}}{D} \left(\frac{R_{eG}}{R_{eL}} \right)^{1.18} \quad \textbf{(2-41)}$$

2.7.3.2 Schubring and Shedd (2008)

The developed correlation for wave frequency was based on the experiments conducted with pipe internal diameters of 8.8mm and 15.1mm.

$$f_W = 0.005 \left(\frac{V_{sg}}{D\sqrt{x}} \right) \quad \textbf{(2-42)}$$

Also, a second wave frequency correlation was developed based on the subsequent experiments, conducted with a pipe internal diameter of 26.3mm.

$$f_W = 0.035\left(\frac{V_{sg}\sqrt{Fr_{\text{mod}}}}{D}\right) \quad \textbf{(2-43)}$$

2.7.3.3 Setyawan *et al.,* (2014)

They conducted experiments on wave characteristics using air-water in annular horizontal flow in pipes with internal diameters of 16mm and 26mm. The superficial air velocities were 12m/s to 40m/s with the superficial water velocities of 0.05m/s to 0.2m/s respectively. The correlation is as follows:

$$f = 0.035\left(\frac{V_{sL}^{0.02} V_{sg}^{0.9} Fr_{\text{mod}}^{0.25}}{D^{0.8} x^{0.25}}\right) \quad \textbf{(2-44)}$$

From the experimental results, Setyawan *et al.*, (2014) reported that the superficial liquid velocity has less significant effect on wave frequency compared to superficial gas velocity.

In conclusion, they considered only 16mm and 26mm pipes in the experiments, meaning the wave frequency correlation developed will match better with such pipe range than in larger pipe diameters which may be a limitation on such correlation.

2.8 Sand Transport in Horizontal Water/Sand Flow

Several experimental investigations on sand transport in water/sand flow in horizontal pipes exist, notable among them are:

2.8.1 Durand (1952)

Durand was one of the early investigators that carried out experiment on solid transportations in pipelines. His experiments were carried out on horizontal pipes ranging from 1.5inch (0.0381m) to 28-inch (0.7112m) with different solids like sand, coal and gravels ranging from 1/10-inch (0.05mm) to 4-inch (25mm).

From his investigations, a clear distinction was made on solid particles and flow regimes. The particles were grouped into homogeneous and heterogeneous flow regimes, in accordance with their sizes. And for the fine particles, they were

separated from those suspended in water/sand flow as saltation e.g. gravel. Below, are the grouping of his results:

Homogeneous: Solid Particles' size ranging from (20 to 30 μ m) were observed to be in the homogeneous flow mixture. And these solids are clay, fine ash and very smooth powered coal.

Intermediates: These were sand particles whose sizes were bigger than those in homogeneous flow mixture, e.g. silt and on the range of (25 to 50 μ m)

Heterogeneous Flow: The heterogeneous flow was sub-divided into solid suspension and saltation.

- Solid Suspension; are solids transported by suspension in the fluid flow. Their diameters are within the ranges of (50 μ to 0.2mm).
- Saltation is referred to those that were much heavier in the flow like gravel and lumps of coal with size diameters above 2mm.

At the end of Durand (1953) experiments, equation (2.45) which is the critical velocity correlation was developed based on the following considerations: pipe diameters, particle sizes, solid concentrations and densities of both the liquid and solid phases in the flow.

$$V_C = F_{Durand} \left[2gD\ (s-1)\right]^{1/2} \quad \textbf{(2-45)}$$

Where V_C is the critical velocity, F_{Durand} represents Durand coefficient for the ratio of solid density to liquid density.

2.8.2 Newit *et al.,* (1955)

They conducted an experiment on solid transport in horizontal pipes. Their investigation was based on flow regime and solid behaviours in horizontal pipes. This was done with solid particles' size ranging from 0.0625 to 6.0mm in 1-inch and 6-inch pipes. For sand behaviours, they observed that sand transport in the liquid flow could behave as follows:

- Homogenous suspension: solid concentrations that are suspended and uniform across the flow area
- Heterogeneous suspension: signifies that the solid concentrations are suspended but not uniform across the flow area.
- Saltation: where pick-up particles are deposited at the pipe walls
- Sliding bed: Solids moves in motion along the bottom of the pipe walls

The above explanations were the sand behaviours observed with regards to solid transport in water/sand flow. Though, the solid particles' range (size) that could be found in each of the four distinct sand flow regimes were not mentioned in their report because solid particle size of 4.00mm will not be homogenously suspended in the flow owing to its weight and the gravitational forces that would be acting on it. Also, fine particles of 0.0625mm will be difficult to be found sliding.

2.8.3 Wicks (1971)

He investigated solids transport at low concentration in horizontal pipes. The experiments were based on solid-liquid flow that were conducted separately on 1" and 6" pipes with sand been pushed constantly at about 1% by volume. Wicks observed that solid particles in motion are under four forces namely; gravity, buoyancy, lift and drag. Gravity and buoyancy forces being constant while lift and drag forces depends on fluid viscosity and flow condition. For solid behaviour in his work, solid particles' flow regimes were categorized into four:

I. Migration: solid particles migrating to the pipe walls and at stationary state under very low velocities with the aid of gravity and buoyancy forces.
II. The solid particles move at three distinct ways at moderate velocities, viscos and gravity forces as follows:
    - Rolling: assuming smooth boundary, solid particles that are round rolls
    - Slide: the solid particles that are thin and long, slides on smooth surface and somersault when surface is rough.
    - Saltation: Bounces/Jumping were observed when particles are irregular in shape.

III. Heterogeneous: where solid particles concentration across flow area were not uniform at high velocities.

IV. Homogenous: where solid particles concentration across flow area were uniform at extremely high velocities.

In his work, average flow velocity was developed with the assumption that liquid flowing with sand bed, is insignificant.

$$V_S = V_P \frac{\pi R_P^2}{A_S(h, R_P)} \quad \textbf{(2-46)}$$

The relationship between the flow area above the sand bed and pipe radius was established as:

$$\frac{A_S}{R_P^2} = \cos^{-1}\phi - \phi\sqrt{(1-\phi^2)} \quad \textbf{(2-47)}$$

The pipe radius could be calculated for sand bed height that is less than one, using the equation (2.48) below:

$$\cos^{-1}(-\phi) = \pi - \cos^{-1}\phi \quad \textbf{(2-48)}$$

Where,

$$\phi = \frac{h}{R_p} - 1 \quad \textbf{(2-49)}$$

For the fluid flowing above the sand bed, Wicks gave an equation as:

$$D_{EQ} = D_P \frac{\cos^{-1}\phi - \phi\sqrt{(1-\phi^2)}}{\cos^{-1}\phi + \sqrt{(1-\phi^2)}} \quad \textbf{(2-50)}$$

In summary, Wicks (1971) models were compared with Durand (1952), Cairns *et al.,* (1960), Hughmark (1961) and Condolios *et al.,* (1963) models in his work. His models were in total variance with others models' results.

2.8.4 Oroskar and Turian (1980)

Oroskar and Turian (1980) carried out investigations, based on descriptive analysis of energy required for solid particles' suspension and dissipation of

energy fraction of the turbulent eddies, to develop a predictive model for critical velocity for slurry transport in pipes. Critical velocity is the minimum velocity demarcating flows in which solid particles form a bed at the bottom of the pipe from fully suspended flows, Oroskar and Turian (1980). Meaning, the velocity at which fully suspended solid particles in the flow could fall to form solid beds at the bottom of the pipes.

To derive the equation of critical velocity, particles settling or terminal velocity in an unbounded flow conditions were considered. Assumption was made that, for particles to be kept stationary and suspended, velocity will be high and in the presence of drag forces that acts on such solid particles. So, the rate of dissipation of energy for the solid particles to be suspended due to drag forces was given as:

$$P_D = F_D \upsilon_\infty = C_D \left(\frac{1}{2} \rho_l \upsilon_\infty^2 \right) \frac{\pi d^2}{4} \upsilon_\infty \qquad \textbf{(2-51)}$$

But, if the energy dissipation required for the solid particles to be suspended is from turbulent eddies, the drag forces could differ. Hence, the drag forces could be accounted for using:

$$F_D = C_D \left(\frac{1}{2} \rho_l \upsilon_s^2 \right) \frac{\pi d^2}{4} \qquad \textbf{(2-52)}$$

And the Vs which is the settling velocity of the particle or hindered settling velocity that depend on concentration of particles in the slurry is given by:

$$\upsilon_s = \upsilon_\infty (1 - C)^n \qquad \textbf{(2-53)}$$

Oroskar and Turian (1980), further developed a critical velocity model with the assumption that, only eddies whose instantaneous velocities that are greater or equal to terminal settling velocities of particles are needed for the solid particles to be in suspension. Therefore, critical velocity becomes:

$$\frac{\upsilon_c}{\sqrt{gd\ (s-1)}} = \left\{ 5C\ (s-1)^{2n-1} \left(\frac{D}{d} \right) \left(\frac{D \rho_l \sqrt{gd\ (s-1)}}{\mu} \right)^{1/8} / x \right\}^{8/15} \qquad \textbf{(2-54)}$$

Where x is given as:

$$x = \frac{2}{\sqrt{\pi}}\left\{\frac{2}{\sqrt{\pi}}\gamma \exp(-\frac{4\gamma^2}{\pi}) + \int_{\gamma}^{\infty} \exp(-\frac{4\gamma^2}{\pi}) d\gamma\right\} \quad \textbf{(2-55)}$$

The critical velocity equation of (2.56) was based on 357 critical velocity data of improved regression fittings:

$$\frac{\upsilon_c}{\sqrt{gd\ (s-1)}} = 1.85\ C^{0.1536}\ (1-C)^{0.3564}\left(\frac{d}{D}\right)^{-0.378}(N_{\mathrm{Re}})^{0.09}\ x^{0.30} \quad \textbf{(2-56)}$$

Where,

$$N_{\mathrm{Re}} = \frac{D\rho_l\sqrt{gd\ (s-1)}}{\mu} \quad \textbf{(2-57)}$$

In summary, the critical velocity models were derived from mere perspective rather than experiments. But having judged their models from extensive slurry flow data from several experimental works on critical velocity, gives one confidence in recommending their models.

2.8.5 Takahashi *et al.*, (1989)

Critical velocity for lifting sand particles from a stationary bed was predicted in their work. They observed that at low flow rates below the critical velocity, the sand bed is stationary with no sand particles in motion. At this point, accumulation occurs at the bottom of the pipeline with a specific sand bed height.

2.8.6 Salama (1998)

He worked extensively on sand settling, where a sand settling velocity model was developed based on two approaches: rolling a solid particle by investigating forces acting on a single particle like (gravity, buoyancy, lift and drag forces) and on turbulence theory. The model is expressed as:

$$V_m = \left[1.3\left(\frac{V_{sl}}{V_m}\right)^{0.53}\right] d^{0.17}\,\vartheta^{-0.09}\left(\frac{\Delta\rho}{\rho_f}\right)^{0.55} D^{0.47} \quad \textbf{(2-58)}$$

Where;

$\frac{V_{sl}}{V_m}$ = Ratio between liquid superficial velocity and mixture velocity at the sand settling condition (for single phase, this ratio is 1)

The settling velocity model is standard but was based on only liquid (single) flow mainly in the pipes. Sand particle concentration was not considered in the above model. Again, superficial gas velocity was not considered hence it was water/sand flow only.

2.8.7 Ravelet *et al.,* (2013)

Ravelet *et al.*, (2013) presented an experimental investigation of hydraulic transport of large particles above (5mm) in horizontal solid-liquid flow in pipes. Effects of specific mass, solid particle size on velocity and pressure drop were investigated using a glass pipe with an internal diameter of 100mm and 10m long.

Although, pressure drops observed were less in the case of large particles in the horizontal flow than vertical pipes, but solid particles' size and specific mass were recognised to have strong effects on the transition between flow regimes with dispersed flow and stationary bed. To measure the pressure drops in solid-liquid flow as a function of solid concentration and velocity, solid particles sizes (beads) ranging from 5% to 18% in diameters were used as shown on Table 2.2 in the study.

Table 2.2: Solid beads used in the experiment, (Ravelet *et al.,* 2013).

Type	**Glass beads**	**Alumina beads**	**Mixture 1(Alumina)**	**Mixture 2 (Alumina)**	**Mixture 3 (Alumina/Glass)**	**Stones**
size	5mm 10mm 16mm	6mm 15mm	50% 6mm 50% 15mm D_{50}:10.5mm	75% 6mm 25%15mm D_{50}: 8:25mm	50%6mm Alumina 50%5mm Glass D_{50}:5.5mm	8-18mm D_{50}:10mm
Specific mass	2500	3650	3650	3650	3075	2700

D means mean diameter and the attached 50% stands for the mixture where one solid is greater than the other.

In summary, three flow regimes were observed in their work as a function of critical velocity (V_{crit}) and mixture velocity (V_{mix}). The flow regimes are:

Stationary bed

Stationary bed was observed with a layer of beads flowing above when mixture velocity is less than critical velocity ($V_{mix} < V_{crit}$). And the solid which tend to settle as mixture velocity decreases more in the system.

Moving bed

In this case, a moving bed on the bottom of the pipe was noted with few solid mixture velocities that increased slightly above the critical velocity ($V_{mix} \geq V_{crit}$).

Fully dispersed flow/solid beds suspension

In terms of this, the bed disappeared with flow been fully dispersed while the solid beads were transported in the flow by suspension when the mixture velocity was higher than the critical velocity ($V_{mix} > V_{crit}$).

More so, models were developed to account for the mixture velocity and critical velocity as follows:

For mixture velocity equation (2.79) was introduced as:

$$V_{mix} = \frac{Q_l + Q_s}{A} \quad \textbf{(2-59)}$$

For the critical velocity, the correlation of Durand and Condolios (1952) was used.

$$V_{crit} = F_l \{2Dg(s-1)\}^{1/2} \quad \textbf{(2-60)}$$

For terminal velocity:

$$V_0 = \sqrt{\frac{4 d_p g (s-1)}{3 c_d}}, \quad \Phi = 121\, C \left(\frac{V_{mix}^2}{gD(s-1)} \sqrt{\frac{3}{4}} C_d \right)^{-1.5} \quad \textbf{(2-61)}$$

2.8.8 Soepyan *et al.,* (2013)

The work was to improve the accuracy of threshold velocity prediction for solid particle transport. They did a validation using a 164-experimental data of

horizontal solid-liquid flow at low sand concentration. This was to justify and improve on the accuracy of the threshold velocity prediction model.

In conclusions, if the sand concentration of less than 1% as Hill (2011) noted or less than 0.02% as noted by Yan *et al.,* (2011), were found to be predominant in the oil and gas industry, whereas sand concentration above 1% are usually in conventional hydraulic slurry systems, then the 164-experimental data were not justifiable unless the data were grouped in the above stated conditions. Therefore, the result presented might need more clarifications on sand concentration to know if results presented could be used in the oil and gas industry.

2.9 Sand Transports in Horizontal Gas Flow in Pipes

The characteristics of sand particles transported in gas flow is important, and necessary in investigating sand behaviour in annular flow in pipes. Although, there are limited experiments on sand-gas flow in pipes, but several simulations using computational fluid dynamic approach (CFD) and numerical modelling approach exists. Among the few experimental and simulated investigations are:

2.9.1 Tsuji and Morikawa (1982)

Tsuji and Morikawa (1982), presented detailed experimental investigations on air-solid flow in horizontal pipe, using a pipe with an internal diameter of 30.5mm. The plastic particle diameters used were 0.2mm and 3.4mm with a density of 1000kg/m^3 respectively. The experiments were focused on air and solid velocity measurements using Laser Doppler Velocimeter (LDV), with gas flow matrix ranging from 6m/s to 20m/s, and a frequency tracker for analysing and processing the obtained signals from the photomultipliers.

In conclusion, solid particle's sizes were discovered to have impact on air flow turbulence with 3.4mm solid particles, presenting a great increase in the turbulence tendency of the gas flow while 0.2mm decreased it. The probability density function (PDF) with the presence of solids in the gas flow deviated from the normal distribution trend, while the frequency from the PSD increases with an increase in loading ratio or solid concentration.

2.9.2 Sommerfeld and Huber (1999)

They had an experimental investigation on particle-wall collision which was also modelled in the study. The experimental measurement was conducted using a horizontal particle laden channel flow with a width of 300mm, 3m long and a height of 30mm. The glass bead-particles' sizes used were 100microns, 500microns with quartz particles of 100microns. The experiments were conducted to validate their wall collision model which was developed based on Lagrangian approach.

In conclusion, they observed that wall roughness and irregular shape of solid particles have much influence on wall collision. Also reported that particles hit a roughness structure with impact angles below 10^0.

2.9.3 Akilli *et al.*, (2001)

Experimental investigations were conducted on gas-solid flow behaviours in horizontal pipes with configuration of 90^0 vertical elbow pipes on it. Their experimental facility was a horizontal closed-loop pipe system with internal diameter of 0.154m and 6.1m long with two vertical elbow sections of 90^0 each. The experiments were conducted using air velocities ranging from 15m/s to 30m/s, and a pulverized coal as solid particles with mean diameter of 50microns.

To measure the particles' concentration and particle velocities, fibre-optic probes were used with the aid of cross-correlation to analyse the results.

Akilli *et al.,* (2001) presented in their experiments that solid particles spread entirely across the internal diameter of the horizontal pipes with the larger solid particles moving at the walls of the bottom of the horizontal pipe due to gravity effect. Their results at the elbow sections were validated using a CFD.

2.9.4 Sommerfeld (2003)

Sommerfeld (2003) developed a numerical correlation based on Lagrangian method, using spherical solid particles in a horizontal channel. In the numerical analysis, the solid particle sizes of 30, 60, 110, 195, 300, 500 and 700 microns with a gas velocity of 18m/s were used respectively. The essence was to

investigate the inter-particle collisions and distribution in turbulent horizontal flow. The study was validated using a phase-Doppler anemometry in measuring of solid particle behaviours.

In conclusion, he discovered that high solid particles were more at the bottom of the horizontal channel with inter-particle collision causing particles dispersion and promoting an increase in solid particles' dispersion at the upper walls of the horizontal channel. For small particles' size, he observed that the wall collision frequency decreases with increase in mass loading, but increases at higher particles' sizes.

2.9.5 Jiang *et al.,* (2017)

Their experimental studies were on particle collision in a pseudo two-dimensional gas-solid fluidized bed using an optimized particle tracking velocimetry (PTV).

The experiments were conducted using: alumina 1.8mm with a density of 945kg/m^3, minimum fluidization velocity of 0.56m/s, 3.0m/s, 2.5m/s and 2.0m/s. The particles' temperature, impact velocity and particle collision frequency were the focus of the study.

In summary, particle-particle collision was presented from the experimental studies with further observations that particles' temperature increases with increase in superficial gas velocities.

2.10 Sand Transports in Horizontal Sand-Gas-Liquid (Slug, Stratified-Annular) Flows

It is pertinent, to acknowledge that a lot has been done experimentally on gas-liquid flow and liquid-solid flow behaviours in pipes. There are several experiments on solid-gas-liquid flow in slug, bubble and stratified flow but such has not being extended to sand flow behaviour in annular flow in pipes. However, presented below are some of the experimental investigations in slug and stratified flow:

2.10.1 Scott and Rao (1971)

Scott and Rao (1971) investigated solid transports on sand-gas-liquid flow in horizontal pipes within bubble and slug flows only. The experiments were carried out using 1-inch and 2-inch horizontal flow loop with slurry concentrations up 14% by volume and solid particles' sizes of 500microns and 100microns to measure saltation velocities and account for pressure drops. In their work, they observed three operating flow conditions as:

- Settling Flow: this they noted that liquid velocities low enough for this to occur are found in bubble and plug flow.
- Not-fully Suspended: here the solid-liquid slurry was not homogeneous. It was also noted that this condition exists in bubble and plug flow regions with little occurrence in slug for dense particles.
- Fully Suspended: in this case, it was observed in slug and annular flow regions with high velocity. The fully suspended was referred as homogeneous flow in their work.

For pressure drop which is one of the aims of the investigations, Scott and Rao (1971) assumed that most solid transports in the pipes are conveyed with fully suspended flow (homogeneous flow), therefore modified Lockhart-Martinelli flow parameters X^2 and φ where used as:

$$X^2 = \frac{\Delta P_L}{\Delta P_G} \quad \textbf{(2-62)}$$

$$\varphi_L^2 = \frac{\Delta P_{MP}}{\Delta P_L} \quad \textbf{(2-63)}$$

Where ΔP_L is for pressure drop of liquid phase flowing alone in the pipe and ΔP_G is for the gas flow alone, while ΔP_{MP} is the pressure drop (solid-gas-liquid multiphase flow) and X^2, φ_L are parameters in Lockhart-Martinelli correlation.

Saltation velocity, which was defined in their work as slurry velocity at which a few solid particles among those that had settled at the bottom of the pipe remained stationary for a short time interval of few seconds, Scott and Rao

(1971). To account for it mathematically, Durand (1952) correlation was considered with the true mean slurry velocity V adopted as saltation velocity:

$$\frac{i - iw}{iw} = 121\ C \left\{ \frac{gD\ (S-1)}{V^2} \cdot \frac{V_t}{\sqrt{gdp\ (S-1)}} \right\}^{1.5} \quad \textbf{(2-64)}$$

Where C is fractional solids concentration by volume, D is diameter of pipe, d is bubble diameter, d_p as diameter of particles, g is gravitational constant, i as frictional head loss of slurry flow (in feet of water), i_w as frictional head loss for water flow (in feet of water), S, is the specific gravity of solid particles (dimensionless), V, is the mean flow velocity while V_t is terminal settling velocity of a single particle in water.

However, average saltation velocities were given as 2.7ft/sec for 500microns in a 1-inch pipe, 4.7ft/sec for 500microns in a 2-inch pipe and a range of 2.3 - 2.5ft/sec for 100microns in a 1-inch pipe.

2.10.2 Angelson *et al.*, (1989)

Angelson *et al.,* (1989) carried out experiments on sand transport and its characterization in horizontal and near horizontal 1-inch and 4-inch pipes. On characterization, sand settling characteristics in stratified and single phase flows were also investigated with sand particles' sizes of 200microns in a pipe diameter of 0.025m. The stratified flow regimes observed in horizontal sand-gas-liquid flow were:

Sand bed

With a liquid velocity of 0.15m/s in the experiment, a stationary bed of particles was settled at the bottom of the pipe as a stable sand bed. At a stable height, the upper part of the particles were then rolled downstream, thereby stretching out the length of sand bed at the bottom of the pipe. As the flow rate then increases, the upper part of the sand bed became wavy and reduces in height as more movement occurred.

Moving bed dunes

As the liquid velocity was increased from 0.15m/s to 0.3m/s and flow rate with the same sand particles' size of 200microns, the stationary sand bed breaks up into a slow-moving sand dunes.

Scouring: As the liquid velocity was increased further to 0.35m/s with increase in the flow rate, most of the sand particles came in close range with the walls of the pipe thereby scouring along the bottom of the pipe.

Scouring/Dispersed

In this case, the liquid velocity was increased to 0.4m/s with more increase in the liquid flow rate. However, the sand became fully dispersed in the liquid flow and in the gas phase leaving a very little sand scouring at the bottom of the pipe.

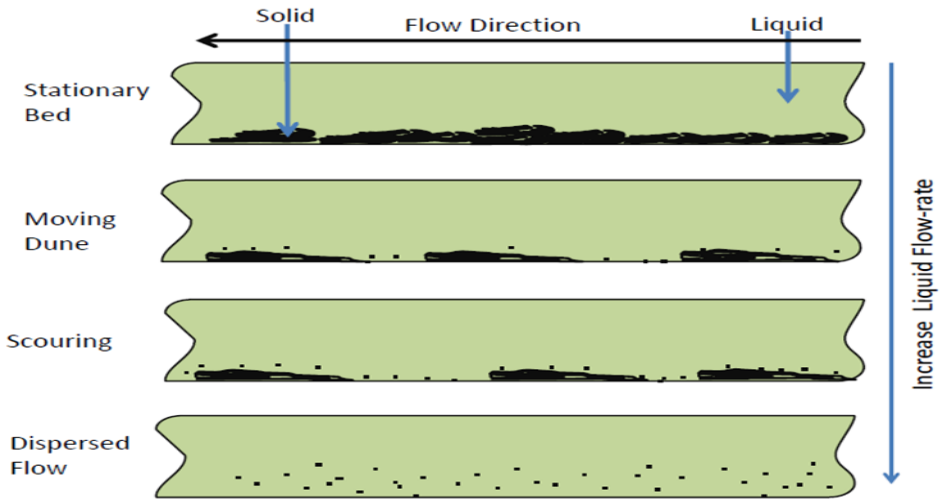

Figure 2.4: Horizontal Sand-Gas-Liquid Flow (Yan *et al.*, 2011)

From their investigations on flow regimes, the following equations were developed as:

Mean liquid velocity V_L was given as:

$$V_L = \frac{V_L^S}{E} \qquad \textbf{(2-65)}$$

Hydraulic equivalent diameter was given as:

$$D_{EQ} = \frac{4 A_L}{S_L} \quad \textbf{(2-66)}$$

Liquid hold-up as:

$$A_L = \frac{E \pi D^2}{4} \quad \textbf{(2-67)}$$

Wetted perimeter was given as:

$$S_L = \frac{1}{2 \gamma D} \quad \textbf{(2-68)}$$

Where V_L^S is the liquid superficial velocity, E, is the liquid hold-up fraction, V_L is the mean liquid velocity, A_L as liquid hold up and γ is the liquid hold-up angle.

In conclusion, sand particles' concentration, not taken into considerations in the models.

2.10.3 Oudeman (1993)

His experiments were on sand transportation and deposition in subsea horizontal pipes on stratified and slug flows only. Experiments were conducted on sand-air-water flow using a pipe with an internal diameter of 0.007m and with sand particle's sizes of 0.15-0.30mm. With the aid of sampling probe, acoustic sand detector and visual observations, investigations were carried out. In summary, sand transportation in horizontal pipe were analysed in these areas: stationary bed, sand moving bed and suspension. In the magnitude of sand transportation in the study, two main conclusions were drawn: that liquid velocity aids sand transportation strongly, secondly, that sand transport increases with gas fraction strongly and much more than liquid velocity.

Other important issues noted in his research are:

- There are limited differences between sand transport in pure water and in viscosified water. Reason was that the viscosified water is less able to erode the sand beds even if it has an increased sand carrying capacity.

- That gas fraction has minor influence on transition from stationary to sand moving beds under stratified wavy flow.
- Gas fraction has considerable influence on transition from sand moving beds to suspension because of the increase in velocity.

Therefore, for each gas fraction, one could calculate the actual sand transport using a relation between a dimensionless sand transport rate and dimensionless flow rate as:

$$\phi = m\,\psi^{n} \qquad \textbf{(2-69)}$$

Where ***m*** and ***n*** are from the gas fraction input is shown on **Table 2.3**

Table 2.3: Gas fraction input *m* and *n* for sand transport rate in flow

Gas Fraction (%)	m	n
0	220	3.6
10	75	2.8
20	67	2.5
Average values of 10 & 20	70	2.7

Based on his observations, conclusion was made that comparing field conditions with results experimentally, there should be a general relation between sand transport and mechanical fluid parameters that could be used to design sand-tolerant completions or facilities to allow effective precautionary measures to be taken.

Meanwhile, these two-general sand transport equations of (2.70) and (2.71) (dimensionless), were used in his work as:

$$\phi = \frac{S}{\sqrt{d^{3} g\,(F-1)}} \qquad \textbf{(2-70)}$$

$$\psi = \frac{V_{b}^{2}}{gd\,(F-1)} \qquad \textbf{(2-71)}$$

In conclusion, hence the experimental work was only based on 0.070m I.D, several other pipe diameters should have been considered to replicate the true scenario in the field as conducting experiments with different pipe diameters will aid in validated conclusions drawn in his work. Again, prediction of a critical velocity for incipient in an early stage of existence in sand deposition, will not be possible with his method.

2.10.4 Gillies et al., (1997)

Gillies *et al.,* (1997) conducted experiments to investigate sand transport in a horizontal pipe with an internal diameter of 52.5mm and 47m long using a gas-liquid flow at low velocities to examine laminar and turbulent conditions. The experiments, involved the use of sand at high concentrations of 7-28% by volume in an intermittent flow where the sand settled at the bottom of the pipe as sand beds. The liquid parameters used in the experiments were oil with density of 872kg/m^3, viscosity of 78cp and water with viscosity of 1.0cp and 998k/m^3 of density. Sand parameter used, has the density of 2650kg/m^3 with median diameters of 0.2mm, 0.1mm and 0.01mm in size.

In the research, transport rates for sand within the range diameters of 0.2mm to 0.1mm were predicted using empirical Meyer-Peter (1949) equation below:

$$\phi = \left[\left(\frac{4}{\psi}\right) - 0.188\right]^{1.5} \quad \textbf{(2-72)}$$

Where,

$$\xi = \frac{\rho_L g d\ (S_S - 1)}{\tau_o} \quad \textbf{(2-73)}$$

and,

$$\tau_o = \frac{f V^2 \rho_m}{2} \quad \textbf{(2-74)}$$

For in-situ solid concentration, the following was used:

$$C_r = \frac{(A - A_o)C^*}{A} \quad \textbf{(2-75)}$$

Where S_s is the density ratio (solids/fluid), d as the particle diameter, g is the acceleration due to gravity, ψ is the dimensionless shear stress, τ_o is the stress for flow in closed conduit, V is the mean velocity, f is for fanning friction factor, ρ_m is the mean mixture density, ρ_L is the liquid density, A_o is for area available for flow, A is the total cross-sectional area, C_r is the in-situ solids concentration and C* is bed deposit concentration.

In summary, it was discovered that gas injection has little effect on laminar flow to transport sand at low superficial liquid velocity of 0.23m/s with oil viscosity of 78cp. This is simply because the gas and the sand were observed to be moving separately in the pipe with gas at top. Therefore, on laminar flow, gas has less effect on sand transport, Gillies *et al.,* (1997).

In turbulent flow conditions, increase in gas yields much influence on sand transportations which also increases, the axial pressure gradient. Above all, Meyer-Peter (1949) equation (2.72) was proven to estimate sand transport rate at low velocities under turbulent flow with sand particle diameters greater than 0.1mm.

In conclusion, the work could be judged as detailed with good results even as pipe diameter of 50mm was the only pipe diameter used. But, it could be possible that results may appear different when a larger pipe diameter is involved.

2.10.5 Stevenson and Thorpe (2002)

They conducted experiments on sand particle transports in horizontal pipe with internal diameters of 40mm and 70mm and with a length of 12m in a stratified flow. Also considered in the experiments, were stratified-smooth flows at 1° and 2° in horizontal pipes with sand particles' diameters ranging from 150microns to 1180microns.

At the end of the experiments, correlations for critical velocity with isolated particles in a stratified- smooth flow, was developed as:

$$\frac{V_p}{w} = 1.03\left[1 - 3.43\left(\frac{wd}{v}\right)^{-0.34}\left(\frac{g(s-1)D_f}{w^2}\right)^{0.33}\right] \quad \textbf{(2-76)}$$

For critical velocity of liquid stratum (m/s), the equation was given as:

$$w_C = 3.43\, d^{-0.34} v^{0.34} \left[g(s-1)D_f\right]^{0.33} \quad \textbf{(2-77)}$$

Where, d is sieving diameter (m), D is internal diameter (m), v is for kinematic viscosity (m^2/s), V_p is for average particle velocity (m/s) and s is the ratio of particles to liquid density.

2.10.6 Ramadan *et al.*, (2005)

Ramadan *et al., (2005),* worked on three-layer modelling for solids transport in horizontal/inclined pipes under stratified flow conditions using a pipe with an internal diameter of 70mm. The work involved, an experiment and modelling to mimic the transportations of cuttings (solids) during drilling in both horizontal and inclined wells with one of the polymer-viscosified fluids which is commonly used in the field as poly-anionic cellulose, (PAC).

The predictive models developed were aimed to improve on the limitations of existing models, hence the dispersed layer thickness was modelled based on pueudo-hydrostatic pressure gradient. While the mean velocity of the dispersed layer was based on Wilson (1987) equations which was modified as:

$$U_d = \frac{4\sqrt{2}}{3k}\sqrt{\frac{\tau_i}{\rho_p}} + U_b \quad \textbf{(2-78)}$$

Where Darcy-Weibach equation of interfacial shear stress is used as:

$$\tau_i = \frac{1}{8}\rho_s f_i (U_s - U_d)^2 \quad \textbf{(2-79)}$$

Where k which is Von Karman's constant is 0.4, τ_i is interfacial shear stress between the suspended layer and dispersed layer, ρ_p is the density of solid particles while U_b is the mean flow velocity of the sand bed.

The dispersed layer thickness was given as:

$$h_d = \frac{2.67\tau_{dis}}{g \sin \alpha (\rho_p - \rho_L)} \quad \textbf{(2-80)}$$

In conclusion, the three-layer models were developed to predict transport rate of stationary sand beds for Newtonian and power-law fluids using Reynolds numbers within the range of 15 and 400.

2.10.7 Bello *et al*., (2011)

Bello *et al*., (2011) investigated and developed, predictive minimum transport velocity (MTV) models for suspended sand particles in multiphase flow in pipes. In developing their models, the concept of sand particle velocity profile was used on the following flow regimes (annular flow, bubble flow, slug flow, and stratified flow) to establish the models in highly deviated and horizontal pipes.

However, sand particle velocity profiles were considered based on the different flow regimes (annular flow, bubble flow, slug flow, and stratified flow) in developing minimum transport velocity models for rolling and suspension of particles in the flow, using the general equation as:

$$V_R = AfR_e^B V_{\max} \left[1 - \left(\frac{r}{R}\right)^2\right]^C \quad \textbf{(2-81)}$$

Where A, B and C values are in **Table 2.4.**

Table 2.4: Constants for values of A, B and C (Bello *et al.,* 2012)

Flow Pattern	A	B	C
Dispersed Bubble	3-4	0.2-0.5	0.1-0.5
Annular	1-2	0.2-1	0.1-0.5
Slug Flow	2.5-3.5	0.3-0.5	1-1.5
Single Phase	0.001-0.003	1-2	0.1-1

In conclusion, Bello *et al*., (2012) presented that, sand particles' settling could be equally avoided, if the flow velocities are above the minimum transport velocity (MTV). Therefore, the minimum transport velocities developed were given as:

For suspension:

$$V_m = A \times \left[\frac{g d_p}{C_L \rho_L} (\rho_p - \rho_L) \sin \theta \right]^B \left[\frac{D \rho_L}{\mu_L} \right]^C \quad \textbf{(2-82)}$$

For rolling:

$$V_m = \left[\frac{A \times d_p \left[\frac{\rho_p}{\rho_f} - 1 \right] g (\cos \theta + f_S \sin \theta)}{(C_D + f_s C_L)} \right]^B \quad \textbf{(2-83)}$$

Where, $C_D = \left[\frac{a}{\mathrm{Re}_p^b} \right]; C_L = \left[\frac{c}{\mathrm{Re}_p^d} \right]$, and the Re given as

$$\mathrm{Re}_p = \left[\frac{\rho_f v_p d_p}{\mu_f} \right] \quad \textbf{(2-84)}$$

Where Cd and CL are drag and lift coefficients respectively while A, B and C are constants show in **Table 2.5**,

Table 2.5: **Suspension and Rolling Equation Constants (Bello *et al*, 2012).**

MTV	A	B	C
Suspension	0.01-0.03	0.5-1	0.5-1
Vertical Pipes	4-6	0.1-1	-

2.10.8 Kesana *et al*., (2012)

They conducted experiments to find out particles' size effect on erosion with respect to slug and annular flow in horizontal pipes. The experiments were achieved using a pipe internal diameter of 3-inches with flow matrix ranging from superficial gas velocities of 25.2m/s to 45.7m/s and superficial liquid velocities of 0.45m/s to 0.76m/s. The sand particle sizes were 20microns, 150microns and 300microns with CMC of 1cp and 10cp for liquid viscosities.

Their key interest, was the impact of the sand particles' sizes on erosion. In conclusion, they found that in annular flow, sand particles which were discovered to be transported in the gas core created erosion more, than the sand particles in

the slug flow. This is because in slug flow, the sand particles are transported in the water phase and not in the gas phase whereas in annular flow, the sand particles were discovered to be transported majorly in the gas core as illustrated in Figure 2.5.

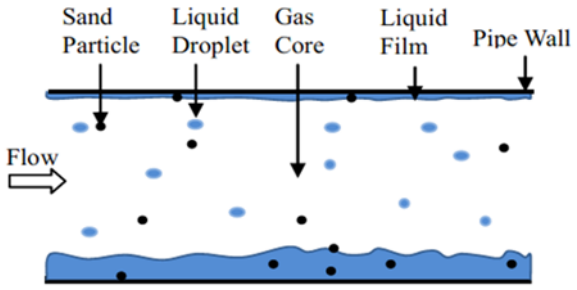

Figure 2.5: Sand Particles in Annular Flow (Kesana *et al.*, 2012)

2.10.9 Franklin (2013)

Prediction of solid particles' transport in a gas-liquid stratified flow was done by Franklin (2013). Though, it was a mathematical modelling without an experiment conducted, he was able to model solid particles' (bed-load) transport in a stratified gas-liquid flow. The special emphasis and considerations were on mean thickness of the granular layer and mean thickness of the liquid layer. The focus was to establish a bed-load flow rate model in line with pressure-driven gas-liquid fluid flow that could be categorized into: basic or saturated state where bed-load flow rate and fluid flow are equal with undulated perturbations.

For the basic or saturated state, the following equation of Meyer-Peter and Mueller (1948) was used as:

$$\frac{Q_0}{\sqrt{(s-1)gd^3}} = 8(\theta_0 - \theta_{th})^{3/2} \quad \textbf{(2-85)}$$

where,

$$\theta = \frac{\tau}{(\rho_S - \rho_l)gd} \quad \textbf{(2-86)}$$

And where Q_o is the bed-load flow rate, s is the ratio of solid density to liquid density, θ, is the dimensionless shields number in the basic state. For perturbation, the shear stress for the perturbation was given as:

$$\tau = \tau_0 (1 + \tau_{Pert}) \quad \textbf{(2-87)}$$

Thus,

$$\tau_{pert} = f(Fr) A \left(\frac{h}{H_o} + B \partial_X h \right) \quad \textbf{(2-88)}$$

And where A=0(1) and B=0(0.1), and:

$$f(Fr) = \frac{-1}{Fr^2 - 1} \quad \textbf{(2-89)}$$

With,

$$Fr = \frac{U_0}{\sqrt{gH_0}} \quad \textbf{(2-90)}$$

Where Fr is the Froude number taken in the work to be ratio of mean flow velocity and celerity of surface gravity waves, U_0 is the mean flow velocity, τ_{pert} is the shear stress perturbation by undulation and θ_{th} is the shields parameter at the bed-load threshold. Also, bed-load occurs when $0.01 \leq \theta \leq 1$.

In conclusion, the predictive equation (2.85) was purely an analytical model that was based on Meyer-Peter and Mueller (1948) works. Though, Franklin (2013) only extended it to accommodate his thought on bed-load in a stratified horizontal flow in pipes. But the observation is this, the predictive model was not validated with any work nor experimental data, hence could not be adjudged good until proven by validations.

2.10.10 Ibarra *et al.*, (2014)

Experimental studies were conducted on hydrodynamic sand transport in a sand-gas-liquid stratified flow in horizontal pipes at low concentrations. The experiments were carried out using a 4-inch horizontal pipe with an average liquid

density of 2475kg/m^3 and particles' diameters ranging from 211 to 297microns on stratified flow to develop a critical sand deposition velocity model.

Observed in the experiments, were sand flow behaviours in three distinct manners, in line with the investigations of sand flow regime by Doron and Barnea (1996) as:

Suspension: On high velocity, the sand was always dispersed or suspended in the liquid phase. And this flow regime could be grouped into:

- ***Pseudo-Homogeneous Suspension:*** For such flow, Angelson *et al.,* (1989) reported that there is a uniform particles' distribution in the entire liquid phase with the aid of a very high rate where some solid particles are suspended.
- ***Heterogeneous Suspension:*** This involves much particles in the flow moving along the bottom of the pipe as the fluid velocities reduces.

Moving Bed: heterogeneous suspension flow, occurs above the moving bed flow conditions. In this case, the sand particles move along the bottom of the pipe walls continuously at lower fluid velocities.

Stationary bed/Dunes: This condition occurs when both the liquid rates and the gas velocities are very low. In their work, it was observed at superficial liquid velocity ranging from 0.10m/s-0.14m/s and superficial gas velocities of 6.53m/s-8.08m/s. At these conditions, the sand particles where found moving slowly as sand dunes under low sand concentrations. With more reduction in the velocity, sand stationary bed was created. At very low velocities, Ibarra *et al.,* (2014) noted that, top surface of the sand beds were smooth and as more reduction in fluid velocities were created, the upper part became wavy in nature.

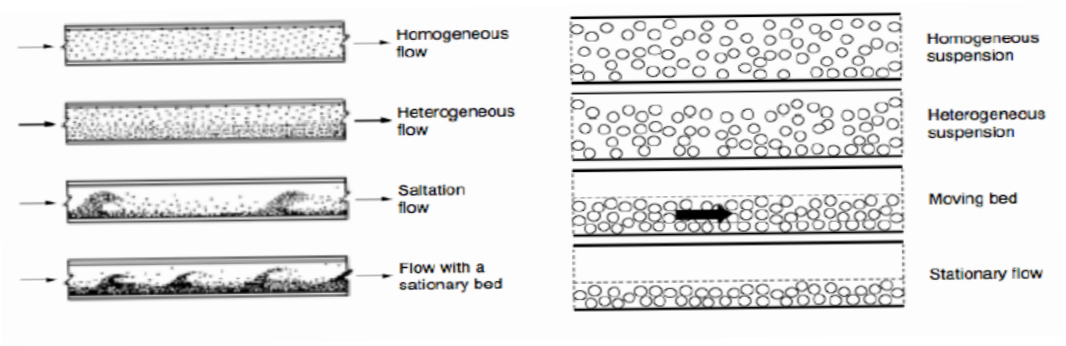

Figure 2.6: Distinct Sand Flow Regime in Horizontal Pipelines (Peysson, 2004)

To develop the critical sand deposition velocity model for horizontal stratified flow in pipes, the critical velocity model of Oroskar and Turian (1980) and Salama (2000) critical velocity model of two-phase flow in pipes were extended and modified as:

$$\frac{V_{M,C}}{\sqrt{gd_P\left(\frac{\rho_P}{\rho_L}-1\right)}} = 1.3277 \left(\frac{V_{SL}}{V_{M,C}}\right)^{-0.285} (1-C_V)^{-35.490} \left(\frac{d_P}{D}\right)^{-0.378} N_{\mathrm{Re},c}^{0.09} \quad \textbf{(2-91)}$$

Where the minimum mixture velocity void of sand particle deposition was given as:

$$V_{M,D} = \left(\frac{V_{SL}}{V_M}\right)^{0.53} d_P^{0.17} \left(\frac{\mu_L}{\rho_L}\right)^{-0.09} \left(\frac{\rho_P}{\rho_L}-1\right)^{0.55} D^{0.47} \quad \textbf{(2-92)}$$

Modified Reynolds number as:

$$N_{\mathrm{Re},c} = \frac{D\rho_L\sqrt{gd_P\left(\frac{\rho_L}{\rho_G}-1\right)}}{\mu_L} \quad \textbf{(2-93)}$$

A modified liquid hold-up correlation of Chisholm (1967) with the Lockhart-Martinelli parameter (X) was used as:

$$H_L = 1-\left(1+X^{1.06}\right)^{-0.573} \quad \textbf{(2-94)}$$

While the critical sand deposition liquid velocity model was also given as:

$$V_{L,C} = \frac{V_{SL}}{H_L} \quad \textbf{(2-95)}$$

Where D is inside pipe diameter, dp is the particle diameter, g is for acceleration due gravity.

In conclusion, the correlations or models were only compared to the experimental data of the same work, though with relative errors of $< 5\%$ and $\pm 2.5\%$ for liquid velocity and critical sand deposition mixture velocity models respectively. The models should be validated with much experimental data works of other scholars, to be proven reliable not just on only personal experimental data.

2.10.11 Kamyar Najmi *et al.*, (2015)

Their researches were on experimental investigations of the effects of physical parameters on sand transport in gas-liquid flow in horizontal pipes. The experiments were carried out using pipes with internal diameters of 0.1m and 0.05m and with special considerations on physical parameters like; sand sizes, sand shapes and sand concentration.

For sand concentration, it was observed in the work when sand concentration volume of 0.01% and 0.1% were used, that critical velocity increases with increase in sand concentration. This is because, higher concentration of sand gives higher particle-particle interactions in the systems.

For particle shapes in the experiments, silica sands that has rough shapes and glass beads of spherical shapes were used. The critical velocity observed on silica sand was a little higher than that of glass beads. This is because the silica sand which is irregular in shape creates more frictions between itself and the walls of the pipes.

And for the particles' sizes, the effects were much. In the experiments, sand sizes of silica ranging from 20, 150 and 300microns were used. They observed that the critical velocity increases as sand particles' sizes increases. This is because, the larger particles create more frictions and as such its drag forces, increases with increase in sand particles' sizes.

2.11 Factors affecting Solid Transport in Multiphase flow in Pipes.

2.11.1 Pressure Drop

In multiphase flow in pipes, there is also a pressure difference in the systems as the fluids flow from the high-pressure reservoirs to a low-pressure end being the facilities e.g. flow stations. This pressure difference could be of: hydrostatic, frictional and kinetic pressures. The kinetic pressure losses are minimal and neglected or ignored while the other two pressure losses are seen prominent in transportation of fluids from the reservoirs through the pipes to the flow stations.

The hydrostatic pressure losses, are dependent on the density of the fluid flow in the pipes while the frictional losses are functions of the flowing conditions as well as the fluid properties of the fluid in the pipes. In multiphase flow in pipes, pressure drop increases with increase in liquid and gas flow rates in the systems. Though, the effect of gas rate is less on pressure drop compared to liquid flow rates. Also, increase in sand concentrations in pipe, promotes increase in pressure losses in the systems as the fluids flow from the reservoir to the facilities. Some of the investigations and correlations to account for pressure losses are:

2.11.1.1 Durand (1952)

Durand (1952) conducted experiments on hydraulic transport of coal and solid in horizontal pipes. The experiments were conducted in horizontal pipe diameter sizes of 3.8 to 58cm with solid particles ranging from 0.2mm to 25mm in a solid-water flow conditions.

At the end of the work, empirical correlation on pressure losses in horizontal pipes was developed and presented by Durand as:

$$\frac{i - i_w}{i_w C_o} = k\left[\frac{v^2}{gD}\sqrt{C_D}\right]^{-1.5} \quad \textbf{(2-96)}$$

Where the drag coefficient was give as:

$$C_D = \frac{4gd_s\left[s-1\right]}{3v_\infty^2} \quad \textbf{(2-97)}$$

Where v is the mean mixture velocity (m/s), k is a constant (3.18, for sand slurry), C_D, is the drag coefficient, D, is the internal diameter of a pipe, *i* and i_w are frictional losses or drop of slurry and water respectively.

The above equations of (2.96) and (2.97), did not account for fluid or particle density, therefore hydrostatic pressure losses as earlier noted were not taken into cognizance.

In summary, the same Durand (1952) correlation was improved upon to account for the effect of density to yield:

$$\frac{i - i_w}{i_w C_o} = k\left[\frac{v^2}{gD\ (s-1)}\sqrt{C_D}\right]^{-1.5} \quad \textbf{(2-98)}$$

2.11.1.2 Worster (1952)

In his quest on hydraulic transport of coal in pipes, Worster (1952) developed an empirical correlation for pressure drop or losses in pipes. His investigation was based on large coal particles which he used in developing a similar correlation of Durand (1952) pressure loss correlation as shown below:

$$\frac{i - i_w}{i_w C_o} = 120\left[\frac{\sqrt{gD}}{v}\sqrt{\frac{\rho_{s-P}}{\rho}}\right]^3 \quad \textbf{(2-99)}$$

2.11.1.3 Zandi and Govatos (1967)

Zandi and Govatos (1967) from their experiments on heterogeneous flow of solids in pipes, developed pressure drop models of slurry flow for fully suspended flow regime as:

$$\frac{i - i_w}{i_w C} = 280\,\psi^{-1.93} \quad \text{provided, } \psi < 10 \quad \textbf{(2-100)}$$

$$\frac{i - i_w}{i_w C} = 6.30\,\psi^{-0.354} \quad \text{provided, } \psi > 10 \quad \textbf{(2-101)}$$

Where,

$$\psi = \frac{v^2}{gD\ (s-1)}\sqrt{C_D} \quad \textbf{(2-102)}$$

2.11.1.4 Turian and Yuan (1977)

They conducted experimental investigations to develop pressure drop correlations, using a total number of 2,848 data. The pressure drop correlations presented, could be used to account for four different flow regimes as the slurry velocity increases from stationary beds, saltation, homogeneous to heterogeneous flow in pipes as shown:

For stationary bed flow regime, the pressure drop was given as:

$$i - i_w = 0.4036 \; C^{0.7389} \; f_w^{0.7717} \; C_D^{-0.4054} \left[\frac{v^2}{Dg\ (s-1)} \right]^{-1.096} \quad \textbf{(2-103)}$$

Where i is represents frictional head loss for slurry and i_w is frictional head loss for water.

For saltation flow regime, the developed pressure drop was given as:

$$i - i_w = 0.9857 \; C^{1.013} \; f_w^{1.048} \; C_D^{-0.4213} \left[\frac{v^2}{Dg\ (s-1)} \right]^{-1.334} \quad \textbf{(2-104)}$$

For homogeneous flow regime:

$$i - i_w = 0.8444 \; C^{0.5024} \; f_w^{1.428} \; C_D^{0.1316} \left[\frac{v^2}{Dg\ (s-1)} \right]^{-0.3531} \quad \textbf{(2-105)}$$

And for the heterogeneous flow regime condition, it was given as:

$$i - i_w = 0.5513 \; C^{0.8687} \; f_w^{1.200} \; C_D^{-0.1677} \left[\frac{v^2}{Dg\ (s-1)} \right]^{-0.6938} \quad \textbf{(2-106)}$$

Where *i* and i_w are frictional head losses of slurry and water respectively, C is solid concentration by volume, fw is water fraction, C_D is drag coefficient, g is acceleration, D is diameter, v is velocity and s is transport rate per bed.

2.11.1.5 Weber (1986)

His investigation work was to improve on Durand (1952) experiments on pressure losses which was limited to only slurry flow in pipes. The improvement from Weber (1986) considered the transition between the heterogeneous and pseudo-

homogeneous transport of solids in fluid flow in pipes. The improved Durand (1952) correlation on pressure losses by Weber (1986) was then given as:

$$\Delta P = \left[83^{\frac{1}{m}} \left[\frac{gD}{v_m^2} (\rho_s - \rho_{fs}) \rho_f \sqrt{C_D} \right]^{\frac{1.5}{m^3}} (1 - F) C_o + 1 \right] . \lambda_f \rho_{fs} 2 v_m^2 \frac{L}{D} \quad \textbf{(2-107)}$$

Where ρ_s, and ρ_f are solid and fluid densities, C_o is total solid concentration, λ_f is pipe friction factor, F is solid/liquid density ratio, g is acceleration, D is diameter, L is length, and C_D is drag coefficient. And m which is the poly-disperse mixture of grain size distribution was taken from the correlation of Wagner (1982) as:

$$m = 2 - \left(\frac{d_{s90}}{d_{s10}} \right)^{-0.4} \quad \textbf{(2-108)}$$

Where d_{s90} and d_{s10} represents particle diameters at 90% and 10% sieve respectively.

2.11.2 Solid Concentrations

Based on sand particles' concentration, Wicks (1971) in his work presented his observation into two distinct flow regimes to show their importance in fluid flow in pipes as follows:

- If solid concentrations across the flow area are distinctly non-uniform, the flow regime is heterogeneous provided particles are in motion within the fluid.
- When solid concentrations and distributions are practically uniform across the flow area, a near-homogeneous flow condition is exhibited.

In summary, increase in solid or sand concentration, increases the hydrostatic pressure losses in multiphase flow in pipes, Wicks (1971).

Kamyar *et al.*, (2015) who also investigated the effect of sand concentration using two volume of 0.01% and 0.1% with sand size of $300\mu m$ in a pipe diameter of 0.05m, presented that the critical velocity of 0.1% volume concentration was higher compared than the 0.01% volume. The critical velocity as reported increases, with increase in sand concentration. This simply means that, the

higher the sand concentration, the more room for particle-particle interactions in the systems. Again, the more the particles are in contact or proximity to one another, the more exposed to lower drag forces in the systems.

In conclusion, higher particles' concentration dampens the turbulent eddies of liquid flow in pipes, (Kamyar *et al.,* 2015).

2.11.3 Fluid Viscosity

Effect of fluid viscosity on solid or sand transport has not been given much attentions. Viscosity does affect sand transportation in multiphase flow of fluid in pipes. This is because an increase in viscosity promotes increase in shear rate of the fluid in the pipe which also will affect the sand flow behaviours.

King *et al.*, (2000) in their study, investigated the effect of viscosity using carboxyl-methyl cellulose (CMC) of 3cp, 150cp and 300cp in a 6-inch pipeline on sand behaviour and transportation in the systems. While the superficial gas velocity was increasing, they found that the threshold velocity for solid transport was higher for a light liquid compared to more viscous liquid.

Gillies *et al.,* (1997) in their work also investigated the effect of viscosity in a liquid flow using oil viscosity of 78cp and oil density of 872kg/m^3 with water viscosity of 0.1cp and 998kg/m^3 for density. The threshold velocity was noted from the experiment to be 0.3m/s with sand sizes of 100microns transported while that of 200microns was found to be 1m/s. This is simply to show that the effect of viscosity will be higher when we have more solids or sand concentrations in the systems which will permit more resistance to solid transport compare to when less sand concentrations are involved.

2.11.4 Particle Diameters (Sizes)

Wilson (1979) in his experiments, reported that particle diameters or sizes can affect sand transport in multiphase flow in pipes. Fine sand particles between the ranges of 0.15mm to 0.50mm (less than 500microns) increases in concentration with increase in superficial velocity from 1.45m/s to 1.85m/s respectively, Wilson (1979). This is because such particles are lighter and could be easily transported

or suspended in the flow. As the sand particles diameter becomes larger (0.50mm-30mm), the velocity decreases, Wilson (1979). This is in line with Angelsen *et al.,* (1989) investigations where $100\mu m, 200\mu m, 400\mu m$ were used in a 4-inch pipeline experiments. As the sand particles became larger in sizes, more energy were needed to transport them in the pipeline. Again, the larger the sizes the more tendency of deposition at the bottom of the pipe, if such energy to keep them suspended in the flow is not dissipated or provided.

2.12 Multi-Fluid Simulator (OLGA)

OLGA is a dynamic multiphase flow simulator developed by Schlumberger. OLGA simulator, comprises of three separate continuity equations for (gas phase, liquid film phase and liquid droplets), two momentum equations for (combined gas/droplets and liquid film) and mixture energy conservation equations with more like thermal equations etc.

OLGA as a dynamic multi-fluid simulator is used to model gas-water flow, water/oil/gas and liquid/oil/sand or water/gas/sand flow in pipes. It has two distinct approaches, namely: steady state and transient. The steady state defines a state where the fluid flow or process do not change with time, while transient defines a state where the fluid flow, process or system changes with time.

2.12.1 Bendlksen *et al*., (1991)

Bendlksen *et a.,l* (1991) evaluated and presented in details, the application and theory of OLGA simulations. The basic equations like conservation of mass, conservation of momentum, pressure, energy, thermal, interfacial mass transfer and many correlations for flow regimes, friction factors and entrainments were elaborated. Also noted, was OLGA flow regime which is divided into; separated (annular-mist and stratified) and distributed (slug and bubble) flows.

For the separated flow, the liquid flow was assumed to be in the form of wall layer with droplets in the gas core in OLGA, (Bendlksen et al (1991). In accounting for separated flow (annular) liquid droplets/entrainment in OLGA, the conservation of mass and momentum were used. For the gas phase, conservation of mass were expressed as:

$$\frac{\partial}{\partial_t}\left(V_{gf}\,\rho_{gp}\right)=\frac{1}{A_P}\frac{\partial}{\partial_L}\left(V_{gf}\,V_{gp}\,\rho_{gp}\,A_p\right)+M_g+\psi_g \qquad \textbf{(2-109)}$$

Where V_{gf} is gas volume fraction, V_{gp} is the velocity of the gas phase (m/s), A_p is the area of the pipe (m^2), ρ_{gp} is the density of the gas phase (kg/m^3) , M_g is the mass source of gas phase and ψ_g is the gas mass transfer term ($kg/m^3.s$)

For liquid phase it was given as:

$$\frac{\partial}{\partial_t}\left(V_{lf}\,\rho_{lp}\right)=\frac{1}{A_P}\frac{\partial}{\partial_L}\left(V_{lf}\,V_{lp}\,\rho_{lp}\,A_p\right)-\psi_g\left(\frac{V_{lp}}{V_{lp}+V_d}\right)-\left(\psi_\varepsilon+\psi_\gamma+M_l\right) \qquad \textbf{(2-110)}$$

Where V_{lf} is liquid volume fraction, V_{lp} is the velocity of the liquid phase (m/s), A_p is the area of the pipe (m^2), ρ_{lp} is the density of the liquid phase (kg/m^3), M_L is the mass source of liquid phase and ψ_l is the liquid mass transfer term ($kg/m^3.s$).

For liquid droplets, it was given as:

$$\frac{\partial}{\partial_t}\left(V_{dlf}\,\rho_{lp}\right)=\frac{1}{A_P}\frac{\partial}{\partial_L}\left(V_{dlf}\,V_{dlp}\,\rho_{lp}\,A_p\right)-\psi_g\left(\frac{V_{dlp}}{V_{lp}+V_d}\right)+\left(\psi_\varepsilon-\psi_\gamma+M_d\right) \qquad \textbf{(2-111)}$$

Where V_{dlf} is liquid droplet volume fraction, V_{dlp} is the liquid droplet velocity (m/s), A_p is the area of the pipe(m^2), ρ_{lp} is the density of the liquid phase (kg/m^3), M_d is the mass source of droplet phase, $\psi_{(g,\varepsilon,\gamma)}$ is the mass transfer term of (gas, entrainment, droplet deposition) respectively in ($Kg/m^3.s$).

For momentum, the conservation equations are:

The gas phase equation is:

$$\frac{\partial}{\partial_t}\left(V_{gf}\,\rho_{gp}\,V_{gp}\right)=-A-B+C+D \qquad \textbf{(2-112)}$$

Where,

$$A=V_{gf}\left(\frac{\partial p}{\partial_L}\right)-\frac{1}{A_p}\frac{\partial}{\partial_L}\left(V_{gf}V_{gp}^2\,\rho_{gp}\,A_p\right) \qquad \textbf{(2-113)}$$

Where;

$$B = \lambda_{gp} \frac{1}{2} \rho_{gp} \left(\frac{1}{4} \frac{x_{gp}}{A_p} \right) \quad \textbf{(2-114)}$$

$$C = \lambda_{if} \rho_{gp} \left(\frac{1}{4} \frac{x}{A_p} \right) \quad \textbf{(2-115)}$$

and

$$D = V_{gp} \rho_{gp} g.\cos\theta + \psi_g V_{ac} - f_d \quad \textbf{(2-116)}$$

Where V_{gf} is gas droplet volume fraction, V_{gp} is the gas droplet velocity (m/s), A_p is the area of the pipe (m^2), ρ_{gp} is the density of the gas phase (kg/m^3), V_{ac} is the velocity due to acceleration (kg/m^3), x_{gp} is the wetted perimeter of gas (m), θ is the inclination angle, V_L is the liquid velocity (m/s), V_{dd} is velocity of droplet (m/s), f_d is drag force (N/m^3), M_d is the mass source of droplet phase ($kg/m^3.s$), λ_{gp} is the friction coefficient of the gas phase, λ_{if} is the friction coefficient at the interface and $\psi_{(g,\varepsilon,\gamma,d)}$ is the mass transfer term of (gas, entrainment, droplet deposition) respectively in ($Kg/m^3.s$).

That of liquid droplets is given as:

$$\frac{\partial}{\partial_t}\left(V_{dlf}\ \rho_{lp} V_d\right) = -V_d\left(\frac{\partial p}{\partial L}\right) - \frac{1}{A_P}\frac{\partial}{\partial L}\left(V_{dlf}\ V_{dlp}^2\ \rho_{lp} A_p\right) + E - F + G \quad \textbf{(2-117)}$$

Where;

$$E = (V_d \rho_{lp} g)\cos\theta \quad \textbf{(2-118)}$$

$$F = \psi_g \left(\frac{V_{dlf}}{V_{lp} + V_{dlf}}\right) V_{ac} \quad \textbf{(2-119)}$$

$$G = \psi_\varepsilon V_{if} - \psi_d V_{dd} + f_d \quad \textbf{(2-120)}$$

Where V_{dlf} is liquid droplet volume fraction, V_{dlp} is the liquid droplet velocity (m/s), A_p is the area of the pipe (m^2), ρ_{lp} is the density of the liquid phase (kg/m^3), V_d is

the droplet velocity (m/s), V_L is the liquid velocity (m/s), V_{dd} is velocity of droplet (m/s), f_d is drag force (N/m^3), M_d is the mass source of droplet phase (kg/m^3.s), and $\psi_{(g,\varepsilon,\gamma,d)}$ is the mass transfer term of (gas, entrainment, droplet deposition) respectively in (Kg/m^3.s).

More so, experimental data of SINTEF and field data were simulated and compared. In their work, the pressure drop from OLGA presented 15% lower while the liquid hold-up matched closely with the compared field data. Though, it was a riser case with low superficial gas velocities. In conclusion, Bendlksen et al (1991), further noted that OLGA is a unified model hence liquid hold-up used were not separate user-correlations.

2.12.2 Ellul *et al.,* (2004)

They presented a tutorial on steady and transient states for multiphase conditions both in Pipesim and OLGA. OLGA as a dynamic multi-fluid simulator was emphasised on the mechanism of operations and the governing equations also expatiated in line with Bendlksen *et al.,* (1991). At the end, field examples were simulated using both steady state and transient approach.

2.12.3 Helgeland Sannæs and Johnson (2010)

OLGA simulator was used to compare experimental flow regimes and liquid hold up from horizontal pie flow experiments of two (oil/gas) and three phase (gas/oil/water) flow. The experiments were conducted using a pipe diameter of 3-inch with a length of 200m at high pressure of 110bar and temperature of 140^{o}C. The superficial liquid and gas velocities used are (0.5m/s and 1.7m/s) and (0.5m/s and 5m/s) respectively. Low and high water cut of 31% and 35% and 71% and 75% were also applied respectively. Experimentally, stratified-wavy, annular slug and bubble flow regimes were determined in the study.

The experiments were achieved by using natural gas with a density of 65.4kg/m3, viscosity of 0.00001(Pa.s), and surface tension of 0.01 (N/m). The crude was a North Sea with density of 785(kg/m3), viscosity of 0.00174 (Pa.s) and surface

tension of 0.01(N/m). More so, a brine with density of 1028 (kg/m3), viscosity of 0.000510 (Pa.s) and surface tension of 0.0476 was also used.

In conclusion from their report, OLGA model predicted flow regime favourably in fifty-seven percent cases, while for gas/oil and gas/oil/water at low water cut, the simulator's prediction was unfavourable. This was attributed to the simulator being developed from low pressure air and nitrogen with water and oil.

2.12.4 Staff *et al*., (2015)

Staff *et al.,* (2015) carried out extensive experiments on large pipe diameter using SINTEF flow loop, which were analysed with the results compared with the OLGA HD stratified flow simulation results. The experiments were based on pseudo-transient and transient investigations to determine the boundary from low liquid up and high liquid up in two-phase flow in large diameter pipes during ramp-up.

The choice of OLGA HD stratified flow model was based on the necessary improvement, which made it more reliable for high gas, gas condensate and long distance predictions. OLGA HD stratified flow model was improved for more reliable predictions in gas pipelines by resolving the inconsistency of the 1D models, combining 3D consistency with the speed of 1D (axial) and accounting for 2D velocity distribution over the pipe cross sections in the system, Staff *et al.,* (2010), Biberg *et al.,* (2015).

In comparing the OLGA two-phase flow model with the SINTEF experimental results, OLGA liquid hold up was further proven from mass and momentum conservation equations as follows:

For mass conservation for the gas phase:

$$\frac{\partial}{\partial t}\left(\rho_{gp} h_{gp}\right)+\frac{\partial}{\partial z}\left(\rho_{gp} h_{gp} V_{gp}\right)=0 \qquad \textbf{(2-121)}$$

Mass conservation for the liquid phase

$$\frac{\partial}{\partial t}\left(\rho_{lp} h_{lp}\right)+\frac{\partial}{\partial z}\left(\rho_{lp} h_{lp} V_{lp}\right)=0 \qquad \textbf{(2-122)}$$

For momentum conservation for gas and liquid phases are further expressed as:

$$\frac{\partial}{\partial t}\left(\rho_{gp} h_{gp} V_{gp}\right)+\frac{\partial}{\partial z}\left(\rho_{gp} h_{gp} V_{gp}^{2}\right)=-h_{gp}\frac{\partial p}{\partial z}-\tau_{gp}\frac{x_{gp}}{A_p}-\tau_i\frac{x_i}{A_p}-\beta \quad \textbf{(2-123)}$$

Where;

$$\beta=-\rho_{gp} h_{gp} g\sin\theta-\rho_{gp} h_{gp} g\cos\theta\frac{\partial \Re_g}{\partial z} \quad \textbf{(2-124)}$$

Momentum conservation for liquid phase;

$$\frac{\partial}{\partial t}\left(\rho_{lp} h_{lp} V_{lp}\right)+\frac{\partial}{\partial z}\left(\rho_{lp} h_{lp} V_{lp}^{2}\right)=-h_{lp}\frac{\partial p}{\partial z}-\tau_{lp}\frac{x_{lp}}{A_p}-\tau_i\frac{x_i}{A_p}-\vartheta \quad \textbf{(2-125)}$$

Where,

$$\vartheta=-\rho_{lp} h_{lp} g\sin\theta-\rho_{lp} h_{lp} g\cos\theta\frac{\partial \Re_l}{\partial z} \quad \textbf{(2-126)}$$

Staff *et al.,* (2015) further noted that for gas and liquid phases at steady state conditions, the equations (0) and () will yield

For gas phase

$$-h_{gp}\frac{\partial p}{\partial z}-\tau_{gp}\frac{x_{gp}}{A_p}-\tau_i\frac{x_i}{A_p}-\rho_{gp} h_{gp} g\sin\theta \quad \textbf{(2-127)}$$

While the liquid phase from momentum conservation becomes:

$$-h_{lp}\frac{\partial p}{\partial z}-\tau_{lp}\frac{x_{lp}}{A_p}-\tau_i\frac{x_i}{A_p}-\rho_{lp} h_{lp} g\sin\theta \quad \textbf{(2-128)}$$

From equations () and () without the pressure terms and as friction force is equal to the gravity term, the liquid hold up was presented by Staff *et al.,* (2015).as:

$$h_{lp}\left(1-h_{lp}\right)A_p\left(\rho_{lp}-\rho_{gp}\right)g\sin\theta=h_{lp}\tau_{gp}x_{gp}-\left(1-h_{lp}\right)\tau_i x_i+\tau_i x_i \quad \textbf{(2-129)}$$

Where h_{lp} is the liquid hold up for liquid phase, h_{gp} is gas hold up for gas phase, g is acceleration, x_i, x_{lp}, x_{gp} stands for gas-liquid, liquid-wall, gas-wall interface wtted lengths respectively, A_p is cross of the pipe, P is pressure, ρ_{lp},ρ_{gp} represents liquid phase and gas phase densities, V_{lp},V_{gp} represents liquid and

gas phases velocities, τ_{gp}, τ_{lp} are for gas-wall, liquid-wall interfacial shear stress and $\Re_{lp}$ is for gas-liquid interface height.

In conclusion, both OLGA HD stratified flow mode and the SINTEF were compared with OLGA replicating the results favourably. The limitation is that ramp-up pressure changes with time likewise hold up in the system, therefore using steady state simulation will not represent the true situation of transient flow conditions in the pipeline.

2.13 Summary of Literature Review

From the several experimental studies reviewed on sand transport in multiphase flow in pipes, we could rightly conclude that there are detailed experimental analysis of sand flow behaviour in virtually all the flow regimes in horizontal pipes except sand transport on annular flow in pipes where there are no experimental reports or publications as shown in the summarised Table 2.6.

However, several experimental studies have been published in multiphase flow in pipes, mostly on the dynamics of two-phase flow, e.g. liquid/gas, liquid/solid flow. Also on simultaneous transport of two-phase flow containing solid/gas/liquid flow in horizontal pipes as noted by Afshin *et al.,* (2008). Among the studies are: Thomas (1964), Scott and Rao (1971),Turian *et al.*, (1987), Angelson *et al.*, (1989), Oudeman (1993), Gillies *et al.,* (1997), Stevenson *et al.*, (1999, 2001), Steveson and Thorpe (2002), Orell (2007), Bello *et al.,* (2005), Ravelet et al., (2013), Franklin, (2013), Ibarra *et al.,* (2014) and kamyar *et al.,* (2015). But all these studies were mainly on slug flow with only the last three mentioned, on stratified flow with none on annular flow. Annular flow conditions with respect to wave velocity, wave frequency, wave severity, liquid film and entrainment have been extensively investigated. But, experimental studies on sand transport and its effect on annular flow behaviour in horizontal pipes are yet to be harnessed, to enhance the knowledge base of the oil and gas industry, the nuclear power plants, the chemical and refining industries. Summarised literature review is presented in Table 2.6.

Table 2.6: Summary of Most Sand Transport, Phases, Flow Pattern and Model developed in Multiphase Flow Experiment over the Years

Author	Phase	Model	Model Type	Flow Pattern	Particle Sizes	Pipe Size
Durand (1952)	Solid/Liquid	Critical Velocity	Empirical	-	0.05mm-25mm	1.5inch-28inch
Newitt *et at.,* (1955)	Solid/Liquid	Critical Velocity	Empirical	-	0.0625mm-6.0mm	1inch & 6inch
Scott & Rao (1971)	Solid/gas/liquid	Saltation Velocity	Empirical	Bubble, Slug	(100,500)microns	1inch & 2inch
Wicks (1971)	Solid/Liquid	Measured	Semi-empirical	-	Not mentioned	1inch & 6inch
Oroskar & Turian (1980)	Solid/Liquid	Critical Velocity	Semi-mechanistic	Used SRC (1973) Report data of (V, IV, II, VI, VII)	And also Wasp et al (1970) experimental data	-
Tsuji and Morikawa (1982)	Air/Solid	-	-	-	0.2mm, 3.4mm	30.5mm
Angelson *et al.,* (1989)	Sand/Air/Water	Based on Wicks (1970) model	Semi-empirical based on Wicks	Slug, Elongated Bubble, Stratified	(30, 100, 200, 550) microns	1inch & 4inch
Oudeman (1993)	Sand/Air/Water	Sand Transport Rate	Empirical	Stratified, Slug	0.15-0.30mm	0.007m
Gillies *et al.,* (1997)	Solid/gas/liquid	Sand Transport Rate	Based on Meyer-Peter (1949) Meyer-Peter & Muller-(1949) equation adapted	Intermittent Flow	0.2mm, 0.1mm	52.5mm
Salama (1998)	Solid/Liquid	MMFV	Empirical	-	$< 400microns$	-

Sommerfeld and Hubber (1999)	Solid/Gas	Particle-Wall Collision	Wall Collision Model	Gas Flow	(100 & 500)microns	(300)mm Laden Channel Flow
Akilli *et al.,* (2001)	Solid/Gas	Particle Velocity	-	Gas Flow	50microns	0.154m
Stevenson & Thorpe (2002)	Sand/air/water	Critical Velocity	Empirical	Intermittent Flow	150 – 180 microns	(40 &70) mm
Ramadan et al (2005)	Solid/gas/liquid	Mean Velocity	Mechanistic	Stratified Flow	-	70mm
Bello *et al*., (2011)	Solid/gas/liquid	MTV	Semi-mechanistic	Dispersed bubble, Annular, Slug, single phase	-	4-inch
Kesana *et al.,* (2012)	Solid/gas/liquid	Effect on Erosion	-	Slug, Annular Flow	(20,150, 300)microns	3-inch
Ravelet *et al.,* (2013)	Solid/liquid	Terminal Velocity	Semi-empirical	Intermittent, Stratified, Dispersed Flow	(5,5.5,6,8.5,10, 10.515,16)mm	100mm
Franklin (2013)	Solid/gas/liquid	Bed-load Transport	Mechanistic	Stratified Flow	-	-
Ibarra *et al.,* (2014)	Solid/gas/liquid	Critical Velocity	Semi-Mechanistic	Stratified Flow	211-297microns	4-inch
Kamyar *et al.,* (2015)	Solid/gas/liquid	Critical Velocity			Silica (20, 150, 300) microns	0.1m & 0.05m
Jiang *et al.,* (2017)	Solid/Gas	PTV	Particle Collision	Gas Flow	Alumina-1.8mm	-

3 EXPERIMENTAL INVESTIGATION

3.1 Experimental Approach

Experiments were conducted using a 2-inch (0.0504m) pipeline as:

- Water/Air Flow Test.
  This was the preliminary test aimed at progressing the fundamental understanding of the flow regimes in pipes. The detailed properties used and their ranges are in Table 3.1.

Table 3.1: Water/Air Flow Properties used in the Experiments

Properties	Range	Units
Temperature	*18.2-19.8*	*^0C*
Pipe internal diameter	*0.0504*	*m*
Air flow line internal diameter	*0.0126*	*m*
Superficial liquid velocity	*0.0663-0.3315*	*m/s*
Superficial gas velocity	*0.2292-2.8522*	*m/s*

- Water/Air Annular Flow Tests.

  These were the annular flow matrix, properties and their units which were the bedrock of the annular flow results and analysis in chapter five in this study. The properties are in Table 3.2 below.

Table 3.2: Water/Air Annular Flow Properties used in the Experiments

Properties	Range	Units
Temperature	*16.5-19.3*	*^0C*
Pipe internal diameter	*0.0504*	*m*
Air flow line internal diameter	*0.0504*	*m*
Superficial liquid velocity	*0.0501-0.2001*	*m/s*
Superficial gas velocity	*8.0774-23.7260*	*m/s*

- Water/Sand Flow [200microns, 500microns]

  These were the first sand experiments which were conducted. The experiments were used to progress the understanding of sand behaviours in single-phase flow without gas velocity. The properties and their ranges are here in Table 3.3 below.

Table 3.3: Water/Sand Flow Properties used in the Experiments

Properties	Range	Units
Temperature	*17.9-19.1*	*^0C*
Pipe internal diameter	*0.0504*	*m*
Air flow line internal diameter	*0.0126*	*m*
Superficial liquid velocity	*0.0501-0.2001*	*m/s*
Sand Diameter [200, 500] microns	*0.000200, 0.000500*	*m*

- Water/Air/Sand in Annular Flow [212microns, 500microns, 800microns]
  The experiments from water/air/sand annular flow were the hub of the research in this study, where sand transport in annular flow were investigated. The properties used and their ranges are presented here in Table 3.4.

Table 3.4: Water/Air/Sand Annular Flow Properties Used for second Experiments

Properties	Range	Units
Temperature	*18.9-21.7*	*^0C*
Pipe internal diameter	*0.0504*	*m*
Air flow line internal diameter	*0.0504*	*m*
Superficial liquid velocity	*0.0922-0.1343*	*m/s*
Superficial gas velocity	*8.4749-15.2251*	*m/s*
Sand diameter [212,500,800] microns	*0.000212, 0.000500, 0.000800*	*m*

- Physical modes of sand distribution in annular flow (***Sampling Method***)
  The physical modes of sand distributions in annular flow were carried out using a sand sampling approach. The sand sampling throat was flush-mounted internally at the base or (bottom) of the 2-inch (0.0504m) flow loop, (see Figure 3.2), while the properties used and their ranges are presented in Table 3.5 below.

Table 3.5: **Sand Sampling Properties used in the Experiments**

Properties	Range	Units
Temperature	*17.9-20.5*	*^0C*
Pipe internal diameter	*0.0504*	*m*
Air flow line internal diameter	*0.0504*	*m*
Sampling throat (pipe diameter)	*0.00292*	*m*
Superficial liquid velocity	*0.0713-0.1025*	*m/s*
Superficial gas velocity	*11.2481-18.0185*	*m/s*
Sand diameter [212,500] microns	*0.000212, 0.000500*	*m*

3.1.1 Experimental Set-Up

The experiments were conducted using a pipe with an internal diameter of 2-inch (0.0504m) at the Process Systems Engineering (PSE) Laboratory, Cranfield University. The 2-inch (0.0504m) pipeline test facility of 28.68m was a closed-loop system, where water inlet pipe was connected to the water tank and the outlet was also connected back to the same storage water tank.

On the flow loop were, 2 pairs of pressure transducers (Druck) with the upstream (T1) as (PMP 4070, S/N 2642126) and downstream (T2) as (PMP 4070, S/N 2630077) which were installed at 2.08m apart from one another. The essence of the difference was to observe the pressure behave immediately after the gas and sand entry points and the multiphase flow behaviour after symmetrically distribution of the fluids in the experiments. Other instruments installed were: light emission diode infrared sensor (LED), conductivity ring sensors of double pairs installed at 0.07m apart and two set of conductance probes also installed at 0.20m apart on the flow loop as shown in Figure 3.1. The air-line which was a 2-inch (0.0504m) has a delivery capacity of superficial gas velocity of 30m/s with air flowmeter, pressure transducers and temperature sensors also connected to it. The sand injection point to the sand sampling location (point) was 5.27m, while the sand injection point to the upstream conductance probe (S1) was 2.39m and to second probe downstream (S2) was 2.59m.

During the experiments, the water line is often open to flow to stabilize before the gas line through the second valve before the vortex air flowmeter. The air supplies were meter and the pressure similarly recorded with Pg while the temperature, also recorded as T1.These instruments were, connected to a Labview where the data were recorded. From Figure 3.1, is the sketch of the 2-inch (0.0504m) pipe flow loop, with the instruments/lines representing the colours follows:

The Red Line: Is for gas supply,

The Blue Line: Is for water supply,

The Pink Line: Represents the multiphase flow, while

The Green Line: Is for sand/water mixture (slurry flow) from the sand hopper.

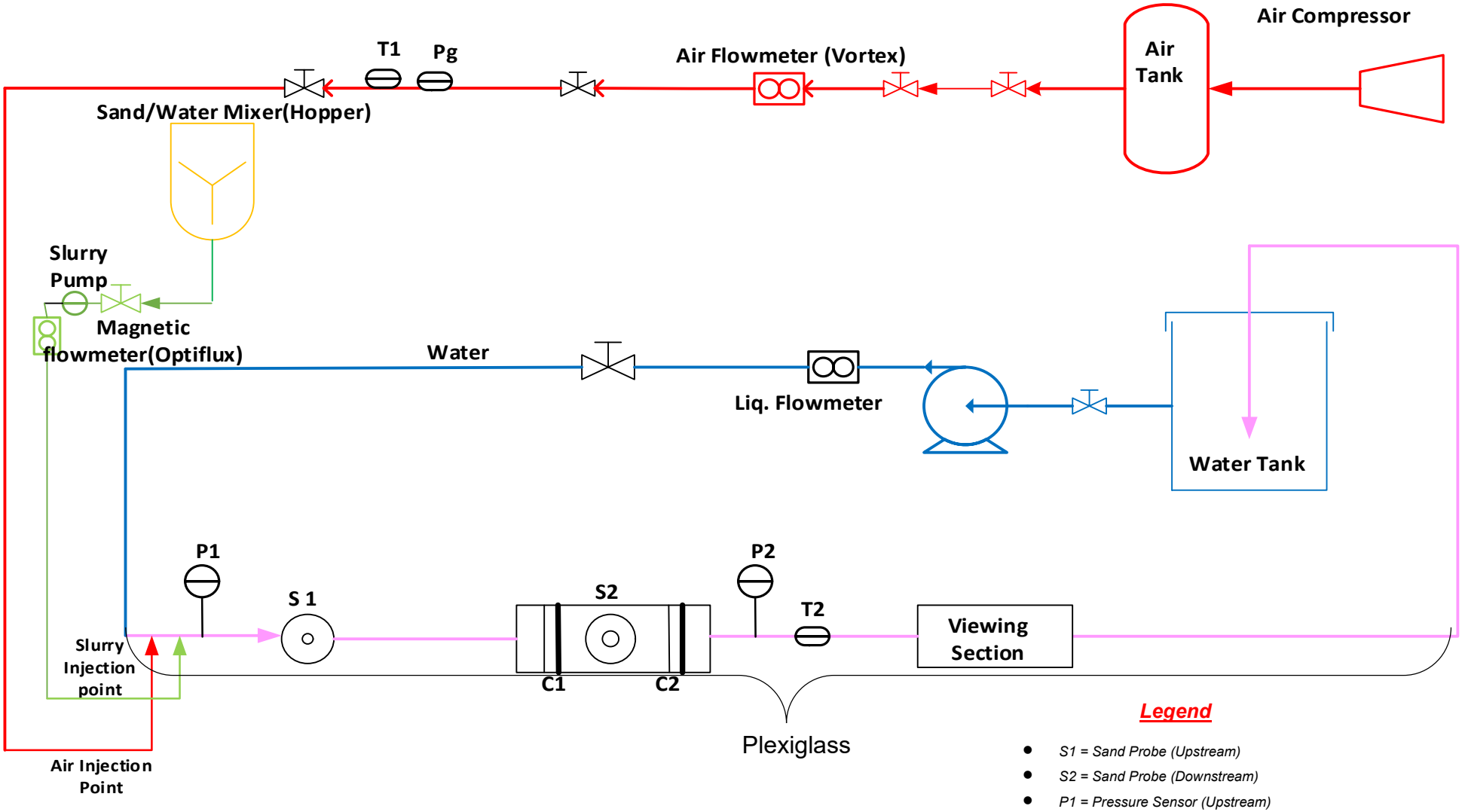

Figure 3.1: Sketch of the 2-inch Flow Loop Design used in Experiments

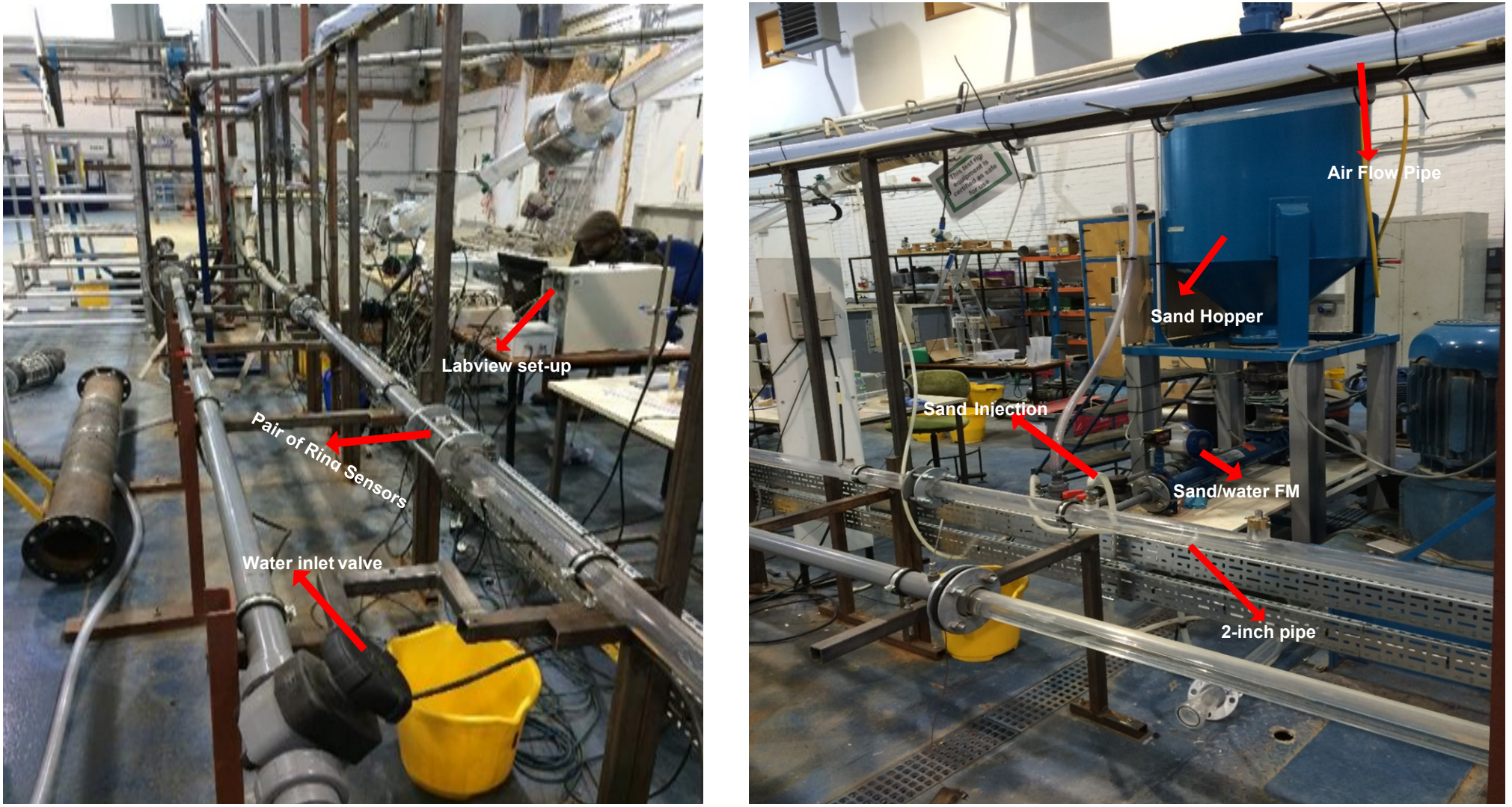

Figure 3.2: A 2-inch Pipeline Test Facility used in the Experiments

3.1.2 Why Horizontal and Sand Injection Location Important.

The experiments were conducted in horizontal flow pipe to represent the true scenarios in petroleum production flowline systems and other industries, where the fluid flows are majorly conveyed in horizontal pipes to the delivery point.

The sand injection point was located 0.08m away from the gas injection point as shown in Figure 3.1. This is to enable the gas (air) to aid the sand particles to be transported and attain steady state conditions before the measuring sand probe located at 0.5m away from the sand injection point.

3.1.3 Facility Instrumentation and Equipment

To replicate how the test facility received, supplies like: gas, water and sand in the PSE laboratory, the equipment and the instruments used will be presented as follows:

3.1.3.1 Sand Supply

The sand supply equipment usually referred to as sand hopper is blue in colour. It has an internal diameter of 0.8m with a height of 1.35m. The sand hopper has a control panel for sand pump, sand mixer and a powerflex-4 sand mixer (see Figure 3.3) which were installed to regulate the out flow of the mixed sand/water slurry flow to the 2-inch (0.0504m) experimental pipeline. Connected to the sand hopper are: NORD motor (Type SK 80L/4) which is used to rotate the sand/water mixer called chemineer. Chemineer, is installed internally in the sand hopper with the primary purpose of mixing sand/water slurry before they are pumped into the pipeline. The (IS LEROY SOMER) pump with serial number LS71/1- No D00862-2007 is used to pump the mixed sand/water slurry from the sand hopper to 2-inch (0.0504m) experimental pipeline. The mixed sand/water slurry, from the sand hopper goes through a flexible pipe with an internal diameter of 0.00635m into the 2-inch (0.0504m) pipeline immediately after the air injection point on the flow loop.

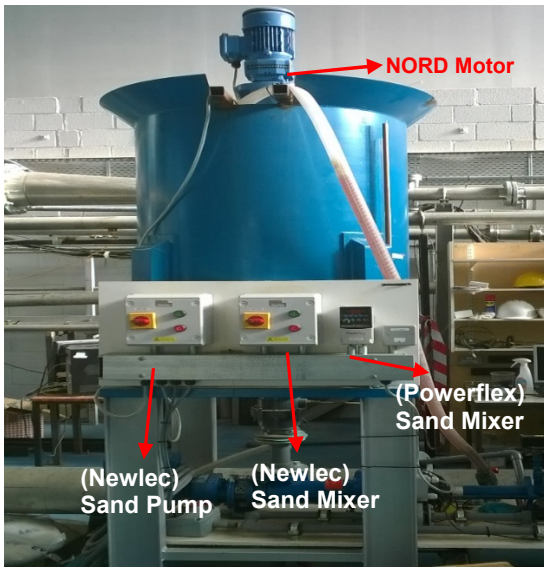

Figure 3.3: **Sand Hopper for the 2-inch Pipeline Test Facility**

3.1.3.2 Water/Sand Mixer

The water/sand mixer with Model No. (20-DTD-075), serial No. (113170-01-01) and uncertainty of ±1% was mounted on the open sand hopper with NORD motor extending outside of the sand hopper as presented in Figure 3.3. It has three blades in double sections at the tail end used for proper mixing of sand and water in the hopper. The upper blades were wider than the last blades and were separated at 0.3m apart. Attached at the upper part is the NORD motor (Type SK 80L/4) that drives the three blades for proper mixing. The total height of the water/sand mixer called Chemineer with the NORD motor is 1.53m while the height of the stainless cord from the motor to the last blades is 1m.

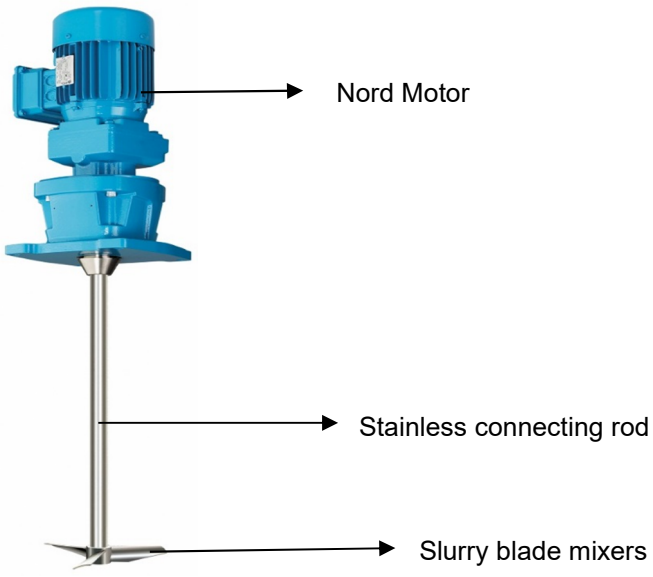

Figure 3.4: Water/Sand Mixer used for slurry mixing

3.1.3.3 Water Supply

The 2-inch (0.0504m) horizontal pipeline in the PSE laboratory, receives water from a source to function. The plastic fibre water storage tank in a cubic shape is used as a source of water supply to the 2-inch (0.0504m) horizontal test pipeline facility. It has a capacity of 4.4m^3. The plastic fibre water storage tank was connected to the 2-inch (0.0504m) pipeline through a 2-inch supply pipe that links it through a progressive cavity pump (PCP) of 90m^3/h in capacity with maximum discharge pressure of 5bar. The entire supply systems to the 2-inch (0.0504m) pipeline was in a closed loop. The plastic fibre water storage tank is internally designed into two:

- The returning chamber: where water that was initially pumped into the test facility flows back to.
- Suction chamber: this is by the side of the returning chamber that retains the returned water. The suction chamber acts as the source of the water. It supplies the water to the 2-inch (0.0504m) pipeline test facility.

More so, the water that flows into the 2-inch (0.0504m) test pipeline were always metered using an electromagnetic flowmeter, to account for its volume.

Figure 3.5: **The Plastic Fibre Water Storage Tank used in Experiments**

3.1.3.4 Gas (Air) Supply

The gas (air) was supplied via a 2-inch air or gas pipeline from the big compressor in the PSE laboratory. The compressor has a capacity of 400m^3/h with a maximum discharge pressure of 10barg. The gas was metred using a Vortex gas flow meter with a full range of [0-70m^3/h] and uncertainty of ±1%. The compressor was able to supply gas (air) through a 2-inch (0.0504m) air (gas) pipeline to the flow loop at a maximum superficial gas velocity of 30m/s. Shortly after the first run, the compressor packed up due to over loading. Therefore, the superficial gas velocity was constrained at a maximum of 23m/s from the compressor to avoid over loading or stressing it beyond its limit.

3.1.4 Instrumentation and Calibration Procedure

Instrumentation, is basically the act of measuring a process and recording the physical quantities as an output for further analysis. To account or determine the needed fluid properties or parameters in this experiments, electrical instruments were used to create, read, record and transmit the data to a usable state through data acquisition systems (Labview). In this study, some of the instruments used are: flowmeter, pressure transducers, temperature sensor, LED etc.

3.1.4.1 Liquid Flow Meter

To account for the volume of water used in the experiments. An electromagnetic flowmeter with a model number ABBK 280/0 AS and a range of 0-20m^3/h was used to account for the water that flows into the 2-inch pipeline test facility

3.1.4.2 Sand/water Flow Meter

A KROHNE magnetic flow meter (OPTIFLUX, 2300) with a serial No. A12001699 (50-60Hz, 22VA) and DN 25mm/1inch was used in metering slurry from the sand hopper. The slurry was metered, before flowing into the 2-inch (0.0504m) experimental flow pipe. Figure 3.6 is the magnetic flow meter used.

Figure 3.6: Sand/water Flow Meter connected to Pipeline from Sand Hopper

3.1.4.3 Gas (Air) Flow Meter

The gas flowmeter (Vortex) has a full range of [0-70m^3/h] and manufacturer uncertainty of ±1%. The flowmeter was used to meter the gas (air) supply from the compressor to the experimental flow loop. The flowmeter was installed over head on a horizontal pipe as shown in Figure 3.1.

Figure 3.7: Gas (Air) Flowmeter (Vortex)

3.1.4.4 Thermocouple

The temperature of the fluids was accounted using the thermocouple. Thermocouples are devices that produces electrical signal with varying temperature. With the aid of an amplifier, a measurable signal is produced and recorded in the Labview. The thermocouple devices (temperature sensors) where installed as T1 and T2 on the flow loop. T2 was installed to obtain the temperature of the fluid when they have commingled as multiphase flow in the pipe. Therefore, T2 gives detail temperature information of the fluid in the experiment as shown in Figure 3.8.

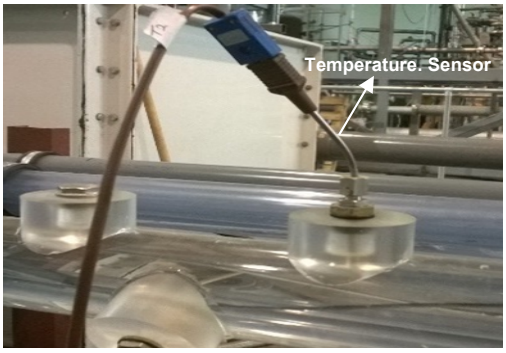

Figure 3.8: **A Thermocouple Installed on 2-inch Pipeline Test Facility**

3.1.4.5 Pressure Transducer

Pressure transducers were used to account for pressures of the fluids, as it flows via the pipeline. The pressure transducers comprise of two pairs of Druck PMP 4070; (PMP 4070, S/N 2642126, 0-100psi, 0-6bara) and (PMP 4070, S/N 2630077, 0-100psi, 0-6bara) installed at 2.08m apart. The two pairs were labelled P1 and P2. The P1 was installed at the upstream, while P2 at the downstream of the flow loop as shown in Figure 3.1. The two pairs of pressure transducers had an uncertainty of ±0.04% and ±0.06% respectively with an output range of 0-5volts direct current.

The two pairs of pressure transducers, were calibrated in the laboratory using a boast pressure sensor where the electrical output was measured with voltmeter and used in the analysis. In Figure 3.9, is the boast pressure sensor used for the pressure calibrations.

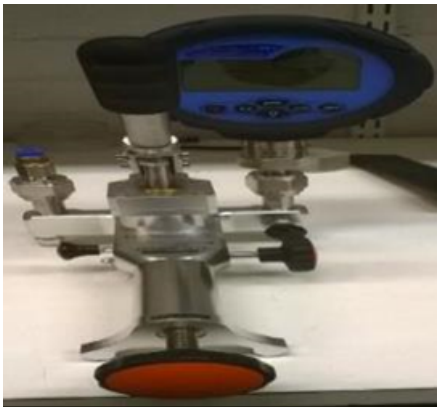

Figure 3.9: **Pressure Calibration in the Lab**

3.1.4.5.1 *Pressure Transducer Calibration*

The pressure calibration procedures are as follows:

- First, is to take the voltage device to 0.00 or close enough, like 0.1 or 0.20 as the offset voltage.
- Secondly, connect the pressure transducer to a source of voltage device and at the other end to the small pressure machine for pumping in air.
- Obtain the reading or value as follows in Table 3.6.
- Then plot readings of pressure on the vertical axis against voltage on the horizontal in a Cartesian coordinate graph.
- From the plot of pressure versus voltage above, take a slope to 0.5.

Table 3.6: Calibration data for Pressure Transducer (P1) Upstream

Input of Pressure (barg)	*Voltage (v)*
0	*0.0256*
1	*0.7475*
2	*1.4702*
3	*2.1958*
4	*2.9201*
5	*3.6425*
6	*4.3722*

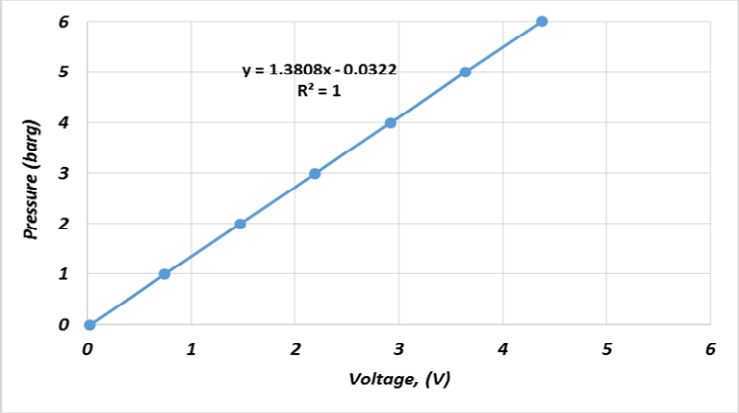

Figure 3.10: Calibration Plot of Pressure against Voltage (V) (P1) Upstream.

Table 3.7: Calibration data for Pressure Transducer (P2) Downstream

Input of Pressure (barg)	*Voltage (v)*
0	*0.0045*
1	*0.7331*
2	*1.4582*
3	*2.1845*
4	*2.9051*
5	*3.6384*
6	*4.3557*

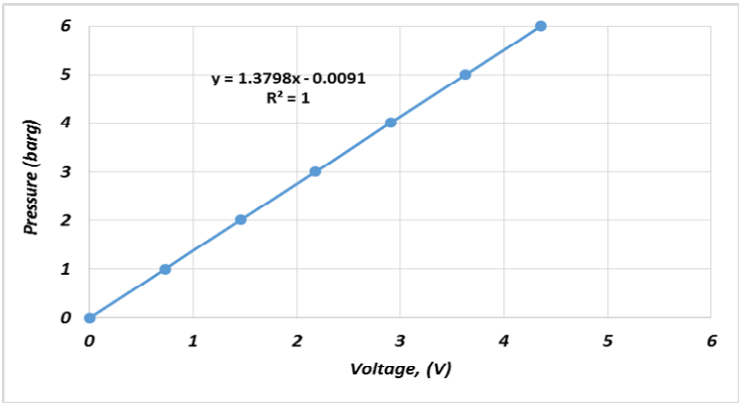

Figure 3.11: Calibration Plot of Pressure against Voltage (V) (P2) Downstream

3.1.4.6 Conductivity Ring Sensors

This is used to obtain flow values by injecting electric current into the pipes through the outer pair of electrodes and measuring the corresponding electric potential drop in between each successive electrode (Chao *et al.,* 2011). The conductivity sensors are used to measure liquid hold up. It measures a resistance based on amount of liquid fraction in the system or pipes and gives an output voltage as its readings.

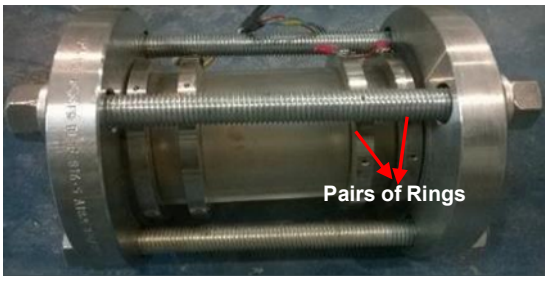

Figure 3.12: Conductivity Ring Sensors used in Experiment

3.1.4.6.1 *Conductivity Rings Calibration for Liquid Hold-up/Film Thickness*

A bench calibration for liquid hold-up/film thickness using conductivity ring sensors in annular flow, was conducted using a 50mm (I.D) with a length of 170mm (see Figure 3.12). The calibration of liquid film thickness in annular flow was achieved, using five different acryl rods inserts of 49mm, 48mm, 46mm, 42.34mm and 33.40mm with a length of 170mm respectively. Also, this calibration was repeated using different blocks as presented in (Appendix, A-1). The following were the procedures used in the calibration experiment:

- The 50mm horizontal pipe was filled with water without acryl rods and the voltage was recorded using the data digital acqusition system (Labview).
- Each of the acryl rods were inserted differently and the annulus between the 50mm (I.D) and the outer diameter of the acryl rod inserts, where filled with water and voltage were recorded in Labview at sacn duration of 60s.
- Also the the liquid fraction of each acryl rod inserts were noted using the weighing balance.
- The bench calibration was repeated three times.
- The voltage results recorded were normalized

- A graph of refernce hold-up against normalized voltage was plotted as seen in Figure 3.13 and equation (3.1) for reference liquid hold-up was obtained from it.

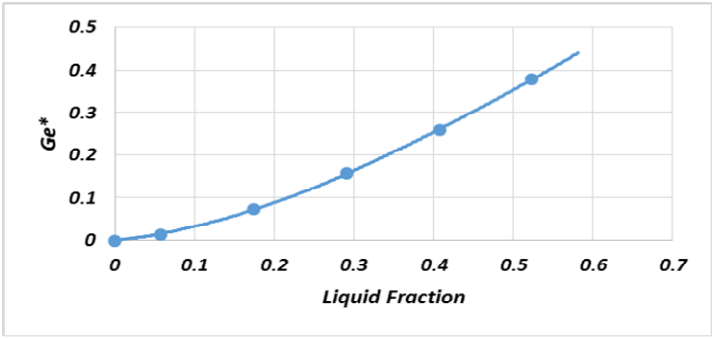

Figure 3.13: Normalized Volt against Reference liquid Fraction Calibration

Liquid hold-up reference :

$$C\ 1 = -0.2648x^3+0.9814x^2+0.2845x-0.0028\ (R^2=0.9788) \quad \textbf{(3-1)}$$

Reference film thickness equation (3.2) from probe calibration was used.

$$Y=-0.0044x^2+0.1256x+0.112 \quad \textbf{(3-2)}$$

The entire voltage recorded from the different acryl rod inserts were normalized using the equation below;

$$G^* = \frac{G}{G_l}, \frac{V}{V_w}, or\ \frac{V_{signal} - V_{air}}{V_{water} - V_{air}} \quad \textbf{(3-3)}$$

Where V is the voltage of the reading at different liquid fractions, while V water, is the voltage of the full calibration pipe with water.

3.1.4.7 Sand Probe Sensors

Sand probe sensors in the experiments, were used to serve dual purpose. They served as sand probes as configured to detect sand transport in the 2-inch (0.0504m) pipeline as aligned to the Labview. The flush mounted sand probe sensors consist of two pairs S_1 and S_2 and were installed at 0.21m apart on the flow loop as shown in Figure 3.1. They have a circular conductive plate at the centre with a diameter of 10.25mm as well as an outer circular conductive plate of 1.80mm which were duly separated by a 2.40mm circular insulator (see Figure

3.14). The sand probe sensors, detect sand by recording a decrease in voltage output.

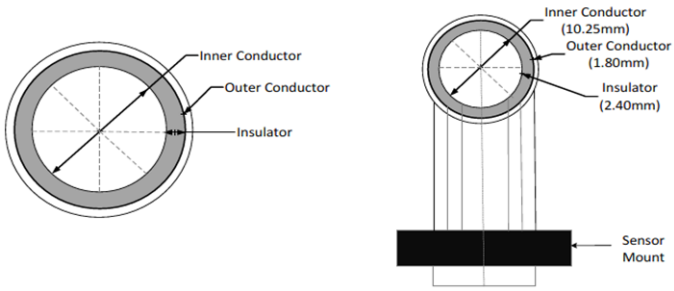

Figure 3.14: A Sketch of the Sand Probe Sensors used

3.1.4.7.1 *Calibration of Sand Probes*

- Fill the test tube that is already flushed-mounted with sand probe (film thickness probe) with known quantity of water (e.g. 50ml). Perform the experiment twice.
- Record the voltage of the sand sensor without water
- Record the voltage of the sand sensor when fill with known amount of water.
- Weigh some quantity of sand particles on the weighing balance.
- Add the known weight of the sand particles to the known volume of water in contact with sand sensor (film thickness probe). Then shake properly and record the voltage of the sand in the water in contact with the probe.
- Repeat the experiment for different sand particle sizes.

3.1.4.7.2 *Porosity*

- Weigh an empty measuring beaker and record the weight.
- Put about 50ml of water into the measuring beaker and determine the weight of the beaker and water.
- Add known quantity of sand particles to the weighed water and measuring beaker and determine the total weight (Sand/water/beaker)
- Record the increase in the volume of water when sand is added to the water in the beaker.

- Repeat the experiment for different sand particle sizes.
- Determine the actual volume.
- Determine the apparent volume.
- Divide actual volume by apparent volume to obtain your porosity.

Table 3.8: Porosity obtained

Particle Diameter(microns)	*Porosity (%)*	*Density (kg/m^3)*
212	*31.38*	*2650*
500	*30.69*	*2650*
800	*30.56*	*2650*

3.1.4.8 Film Thickness Probes

The film probe sensors are the same as the sand probe sensors. In absence of sand in the flow, the probes records for film. Although, the data are separated in the Labview, hence the readings could be simultaneously obtained if when both sand and water are in the systems running concurrently.

3.1.4.8.1 *Film Thickness Probe Calibration with solids objects*

Bench calibration of film thickness was done using three solid cylindrical pipes of 49mm, 42.34mm, and 33.40mm with a length of 170mm respectively.

A conductance (film thickness) probe used was flush mounted to a 50mm (ID) pipe. The both ends of the 50mm (ID) pipe were sealed.

Procedure

- The 50mm pipe was clamped to the base of the table in order to ensure that the water and the solids objects were stable as shown in figure 3.15.
- The empty pipe of 170mm was recorded. Full pipe of 170mm with water was also recorded.
- The solid objects were then inserted in the order, 49mm, 42.34mm, 33.40mm and all were recorded.

- The gap or space between the pipe of 50mm and the solid objects used (49mm, 42.34mm, 33.40mm), represents the ***reference film thickness*** in the bench calibration.
- Each of the experiment with the solids were repeated 3times
- The output voltage was normalized and plotted against the reference film thickness as seen in Figure 3.14

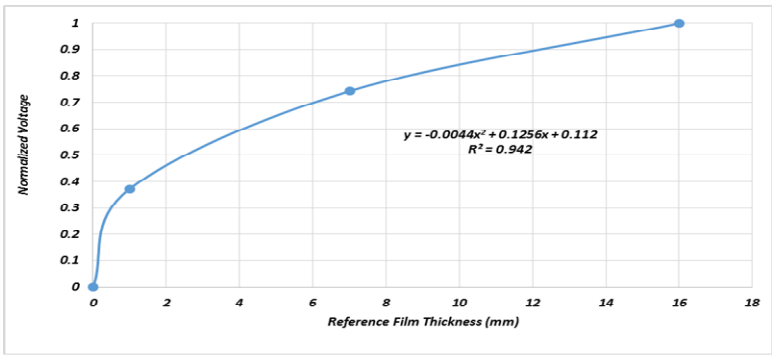

Figure 3.15: Normalized Voltage against Reference Film Thickness (mm)

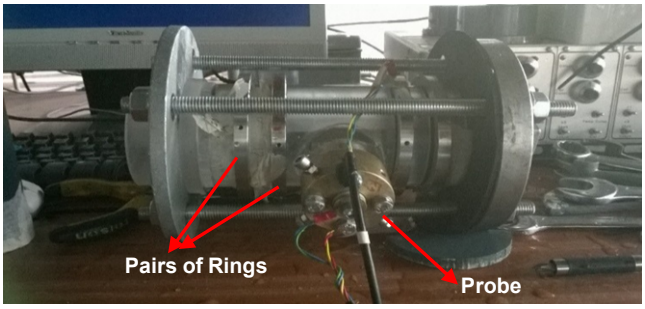

Figure 3.16: A Horizontal Calibration Pipe used for Annular Film Thickness

3.1.4.9 Re-Calibration Conducted on Annular Flow

A bench calibration for liquid hold-up using conductivity ring sensors and liquid film thickness from probes in annular flow was re-conducted after two years of the previous calibration. The new calibration was conducted using a 50mm (I.D) with a length of 154mm and five different acryl plastic blocks of: 49mm, 48mm, 47mm, 46mm and 45mm with a length of 154mm respectively. Detailed results are shown in the Appendix (Tables P-1.1 to P-1.5) for liquid hold-up and (Q-1.1 to Q-1.5) for liquid film thickness. The summary of the statistical error analysis of liquid hold-up from the new calibration compared to the previous liquid hold-up results from the first annular calbration is presented in Tables 3.9 and 3.10.

3.1.4.10 Comparing the Previous Calibration and New Calibration Results

The differences from the results of the new (liquid hold-up and film thickness) when compared with the previous (liquid holdup and liquid film thickness) results, could be attributed to instrumentation error. The previous calibrations were conducted alongside the experiments with the same conductivity box and conditions for the experiments. Again, the error margin could also be as a result of the conductivity box tuning, as the previous calibration showed a more realistic results with both liquid hold up and film thickness, even with respect to liquid entrainments. The new calibration results gave higher liquid holdup results in the entire flow conditions and likewise the film thickness results. In reality, the former calibration results is better and most realistic results in all conditions.

Table 3.9: Summary of Error of new Liquid Holdup from previous Liquid Hold-up Calibrated.

Vsl [m/s]	*Average Actual Error*	*Average Relative Error [%]*	*Standard Deviation*
0.0505	0.0187	57.2982	7.5696
0.0714	0.0336	67.4514	8.2129
0.0903	0.0395	65.4298	8.0889
0.1355	0.0489	63.0458	7.9401
0.1851	0.0573	61.5088	7.8428

Table 3.10: Summary of Statistical Error for new Film Thickness from previous ones

Vsl [m/s]	*Average Actual Error*	*Average Relative Error [%]*	*Standard Deviation*
0.0505	0.0486	30.5548	5.5276
0.0714	0.0239	12.8667	3.5870
0.0903	0.0142	7.1323	2.6706
0.1355	0.0068	3.2552	1.8042
0.1851	0.0022	0.9972	0.9986

3.1.5 Data Processing

There is no doubt that there are noise associated with signals between the transmitters and the receivers which often distorts the signal output. This is why it is necessary to filter the raw signal output to improve on the analysed results of the experimental data. In this study, the raw output signals were filtered in Matlab on the power spectral density and wavelet using the smooth function.

3.1.6 Cross-Correlation

This is a standard means of measuring the level or degree at which two signals could correlate with one another over time displacement from the experiment conducted. In all standard, cross-correlation should be similar and as well identical while crossing one another as they move towards unity from the output signals. In case they are dissimilar, cross-correlation should be zero or close enough to zero. Supposing there are two series of X(t_n) and Y(t_n), where n=0, 1, 2……..N-1, then cross-correlation well be:

$$R_{x,y} = \frac{C_{x,y}(\tau)}{\sqrt{C_y(0)C_y(0)}} \quad \textbf{(3-4)}$$

where,

$$C_{x,y} = (\tau) = \frac{1}{N-1}\sum_{n-1}^{N-\tau} X(t_n).Y(\tau + t_n) \quad \textbf{(3-5)}$$

The filtered output signal of cross-correlation for Vsl=0.0502m/s and Vsg=14.0307m/s is plotted in Figure 3.17.

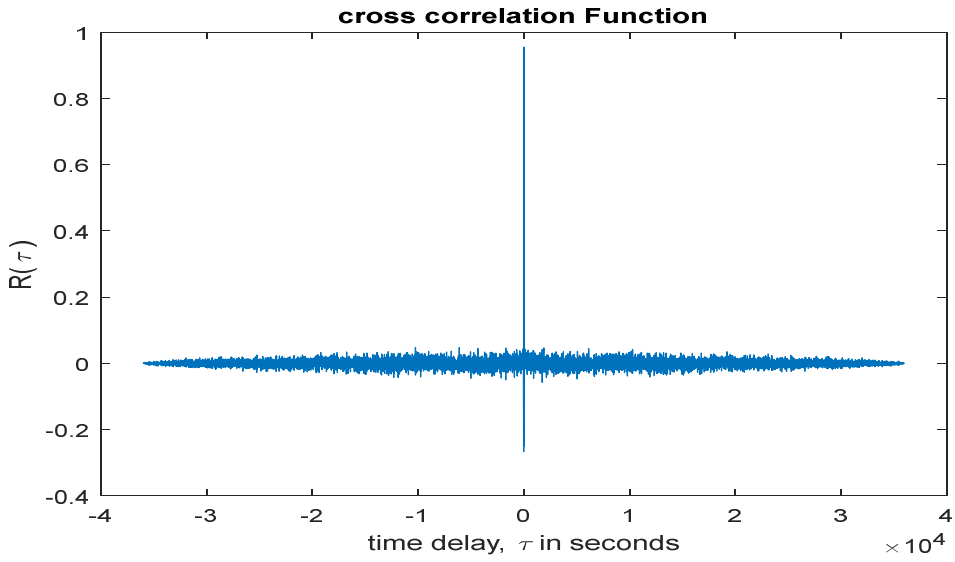

Figure 3.17: Cross-Correlation of Probe (S1 and S2) for Vsl=0.0502m/s, Vsg=14.0307m/s

3.1.7 Sand Sampling Procedure

Sand Sampling method, was adopted in evaluating physical modes of sand distributions in annular flow. The sand sampling method involves collecting samples of liquid that flows across the throttle of the sampling pipe (small) at different levels internally in the pipe.(see Figure 3.18)

3.1.7.1 Experimental Set-Up

The experiment was conducted using a 2-inch (0.0504m) flow loop of 28.68m long. A 2-inch air injection pipe was connected to the flow loop immediately after the bend at 15.81m while the sand sampling point was at a distance of 9.24m away from the air injection point. More so, the distance of the sand injection point to the sand sampling point was 5.27m. The sand sampling pipe has an internal diameter of 2.92mm (0.00292m) that is adjustable for sampling purposes at different levels internally in the pipe.

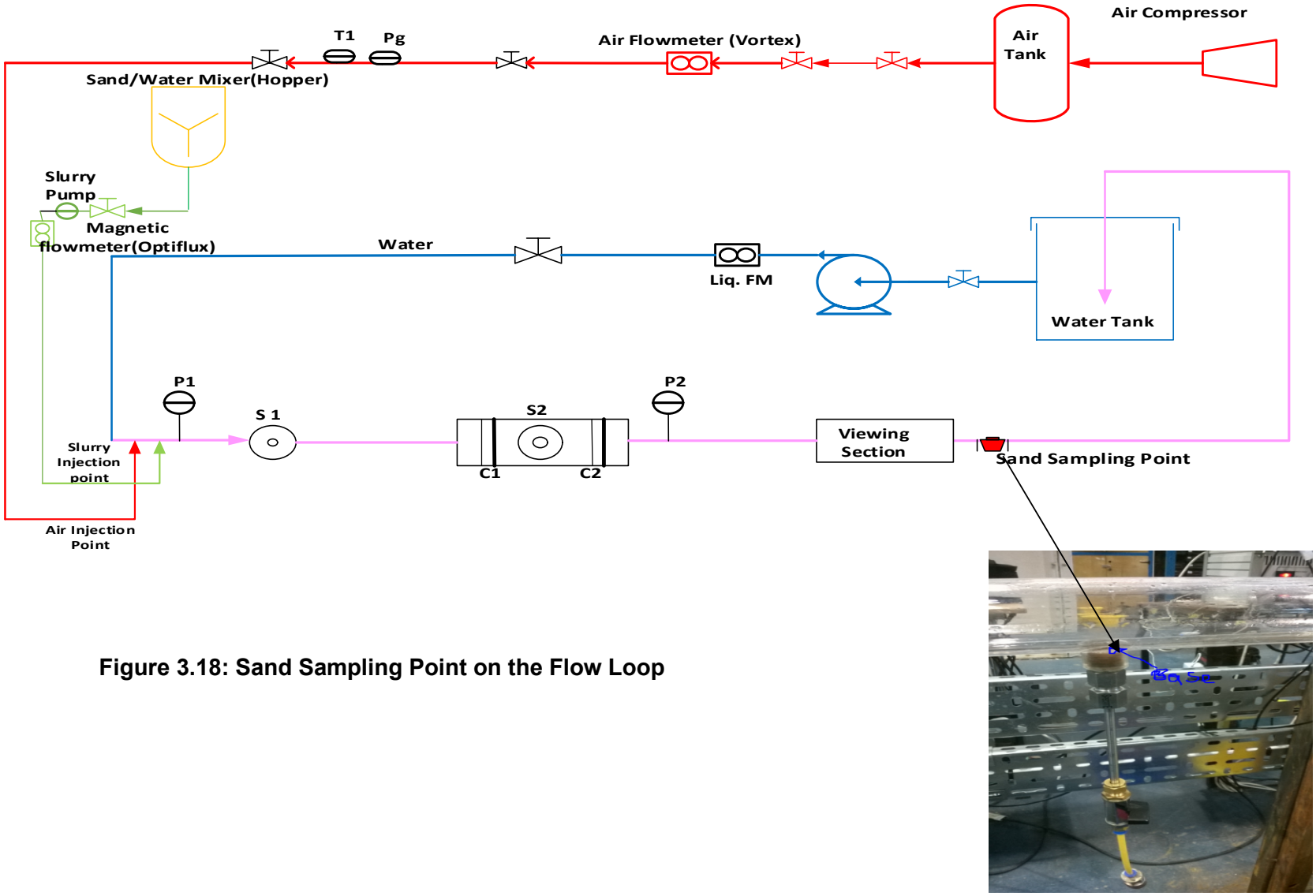

Figure 3.18: Sand Sampling Point on the Flow Loop

3.1.7.2 Experimental Procedures

Sand Sampling

- The sand sampling pipe with an internal diameter of 2.92mm (0.00292m) was properly flushed with water to ensure that the flow path is completely free from blockages.
- The sand sampling pipe was flush mounted at the bottom of the pipe where the samples were collected.
- After each sand sampling was completed, the sampling pipe was properly flushed/drained.
- Sampling experiments were done by using an adjustable flow pipe throat of 0.00292mm at different locations internally in the 2-inch pipe, from 0cm to 1.5cm, 2.5cm and finally the top wall (5cm) of the pipe internally.
- The sand samples collected with water were weighed with a known container (see Figure 3.18), properly labelled and stored for 24hours to enable the sand particles to settle.
- After 24hours, it was filtered into a known beaker (see Figure 3.21) for final drying.

Figure 3.19: Container/Storage used for Sand Sample Experiments

Drying of Sand Samples

- The drying was done using a Hot Air Tool, Leister - 230V (50/60Hz) with Serial No, 1305286146, (see Figure 3.20).
- An Empty beaker for drying samples was properly clean to make sure that there were no traces of particles.

- The cleaned empty beaker, was always weighed using a balance and the weight recorded after each sampling experiments.
- Each sand samples that were stored for 24hours were then filtered and the residue being sand and some water were heat using a Hot Air dryer in figure 3.20.
- The “Hot Air Dryer” was always adjusted to a temperature of 300^{o}C.
- After each sand samples were dried, pictures were taken and the dried sand in the beaker with the beaker were placed on the weighing balance and results were recorded.
- Again, after each drying, the beaker is always cleaned blue rolling paper before subsequent usage.

Figure 3.20: Hot Air Dry Tool

Figure 3.21: Beaker (Fishbrand) 600ml

3.2 Limitations of this Study

The experiments were conducted with 2-inch horizontal pipe flow loop. The sand hoper was only installed to the 2-inch flow loop in the PSE laboratory. The reason was to avoid sand particles damaging devices in other flow loops with wire mesh installed for other experiments in the PSE Laboratory.

Again, the water/air annular flow experiments were for superficial liquid velocity ranges of 0.0501 -0.1950m/s and superficial gas velocities in the range of

8.0774m/s – 23.7260m/s. The gas compressor with the capacity of 400m3/h could not supply beyond maximum superficial gas velocity during the experimental time. Lastly, the sand probes were only installed at 0^{o} (bottom) of the horizontal pipe.

3.3 Experimental Error and Uncertainty Analysis

Sand behaviour in annular flow, entails detail experimental measurements using instruments like flowmeters, conductivity ring-sensors for liquid hold-up, pressure transducer for differential pressures, conductivity probes for film thickness and sand detections, light emission diode infrared sensors and thermocouple for temperature measurements. The Table 3.11 below, shows the instruments used and the range of readings from the manufacturers.

Table 3.11: Instrumentation for Experimental Measurements

Instruments	*Functions*	*Accuracy-[Full Range]*
Gas Flowmeter Vortex	Air/gas Flow Metering	± 1% [0~70m^3/h]
Magnetic Flowmeter [Optiflux 2300]	Sand Flow Metering	±0.2% [0~21m^3/h]
Liquid flowmeter	Liquid Flow Metering	± 0.8% [0~20m^3/h]
Pump	Water/sand pump	[0-300L/h]
Pressure Transducer [P1]	Pressure Measurement	± 0.04% [0-6bara, 0-100psi]
Pressure Transducer [P2]	Pressure Measurement	± 0.06% [0-6bara, 0-100psi]
Conductivity Probe Sensor [S1]	Film thickness, Sand detector	±3.6% [0-3.8mm]
Conductivity Probe Sensor [S2]	Film thickness, Sand detector	±3.6% [0-3.8mm]
Conductivity Ring Sensor [C1]	Liquid hold-up	±2.3% [0-1]
Conductivity Ring Sensor [C2]	Liquid Hold-up	±2.3% [0-1]
Thermocouple [Temperature Sensors T_1-T_2]	Temperature Measurement	± 0.5% [0^{o}-100^{o} c]

It is pertinent to note, that these instruments were all installed at different location points on the experimental flow loop as shown in Figure 3.1, and because of the errors in measurement due to calibration setup, experimental setup and also experimental procedures adopted in measurements, it is imperative for all the experimental measurements presented in this study, to be subjected to uncertainty and error propagation analysis.

3.4 Error and Uncertainty

Error is a variance between the true value and the measured value. Error is judged or measured by its precision and accuracy. Accuracy represents, how close a measured value is to a true value (Carlson, 2002). Precision means, repeatable or reproducible measurements that gives same results or close results.

Error is expressed mathematically as:

$$Error = \frac{E}{100} \times F \quad \textbf{(3-6)}$$

where E represents the percentage value from the manufacturer and F is the full range of reading from manufacturer.

While uncertainty, is unsureness about calculated results, (Falcone *et al.,* 2009).

Uncertainty of the instruments (e.g. flow meters, pressure transducers, probe sensors) used in the experiments could be denoted with a symbol U in this study, and expressed as:

$$U\ (\%) = \frac{Error}{M} \times 100\ \% \quad \textbf{(3-7)}$$

Where U represents uncertainty of instruments used, M stands for mean of readings obtained from such instruments used.

In experimental measurements, there are precautions to be taken to curb the possibility of error and inaccuracies. These precautions were taken as follows:

- Calibration of instruments to aid in accuracy evaluations.

- Ensuring that instruments were in the stable conditions before taking readings
- In the horizontal pipe section, instruments were checked properly to ascertain that they were installed in horizontal position before readings were taken.
- Recording were taken with no disturbance or external vibrations on the instruments.
- Distance apart on conductivity ring sensors and probes were dully put into considerations.
- Positioning of flow meters also were considered.

From the instruments used: flow meters, conductivity ring-sensors, conductivity probes, sand/water mixer and pressure transducers, the error and uncertainty analysis will be further analysed and presented as follows:

- Water/air in annular flow.
- Water/sand flow
- Water/air/sand in annular flow (Multiphase flow).

More so, the detailed tabular results of the error and uncertainty analysis calculations could be seen in the Appendix, (Tables L-1.1 to O-1.1)

3.5 Error Propagation (Propagation of Uncertainty)

Error propagation, is the combination of several variables uncertainties for such measured quantity, to produce more accurate measurements. For example, if error propagation of superficial gas velocity were to be analysed, uncertainty of several measured values like temperature, pressure, gas flow rate will be involved to obtain it. Therefore, the combined uncertainties of these measured values are used to obtain propagation of uncertainty.

3.5.1 Superficial Liquid Velocity

The liquid flow rate measured in the experiments were recorded in litre per second. The liquid flow rates divided by pipe area represents superficial liquid velocity. The equation is given as:

$$Vsl = \frac{Q_L}{A} = \frac{Q}{\pi d^2/4} \text{ [m/s]} \quad \textbf{(3-8)}$$

From partial derivatives, the equation [3.8] becomes:

$$\delta Vsl = \frac{\delta Q_l}{\pi d^2/4} \quad \textbf{(3-9)}$$

$$\frac{\delta Vsl}{Vsl} = \frac{\frac{\delta Q_l}{\pi d^2/4}}{\frac{Q_l}{\pi d^2/4}} = \frac{\delta Q_l}{Q_l} \quad \textbf{(3-10)}$$

$$\delta Vsl = \frac{\delta Q_l}{\bar{Q}_l} \quad \textbf{(3-11)}$$

3.5.2 Superficial Gas Velocity

From my experimental set up, my superficial gas velocity could be expressed mathematically as:

$$Vsg = \frac{P_g Q_g T_2}{P_2 T_g 3600 \rho_g A} \text{ [m/s]} \quad \textbf{(3-12)}$$

where A is the pipe area (0.001984m), P_g is the gas pressure, Q_g is the gas flow rate, T_2 is Mixture (gas and liquid) temperature, T_g is the gas temperature, P_2 is pressure of gas and liquid mixture and ρ_g is gas density. These flow parameters were all measured in the experiments. From partial derivatives, Vsg becomes:

$\delta P_g = \left(\frac{\delta P_g}{P_g}\right)^2$, this is likewise the other variables in equation (3.12) to yield the derivatives in equation (3.13):

$$\delta Vsg = \sqrt{\left(\frac{\delta P_g}{P_g}\right)^2 + \left(\frac{\delta Q_g}{Q_g}\right)^2 + \left(\frac{\delta T_2}{T_2}\right)^2 - \left(\frac{\delta P_2}{P_2}\right)^2 - \left(\frac{\delta T_g}{T_g}\right)^2 - \left(\frac{\delta \rho_g}{\rho_g}\right)^2} \quad \textbf{(3-13)}$$

where,

$$\rho_g = \frac{P_2}{RT_2} \quad \textbf{(3-14)}$$

where R is gas constant.

$$\frac{\delta\rho_g}{\rho_g} = \sqrt{\left(\frac{\delta P_2}{P_2}\right)^2 - \left(\frac{\delta T_2}{T_2}\right)^2} \quad \textbf{(3-15)}$$

Substituting equation 3-15 into equation 3-13, yields:

$$\delta Vsg = \sqrt{\left(\frac{\delta P_g}{P_g}\right)^2 + \left(\frac{\delta Q_g}{Q_g}\right)^2 + \left(\frac{\delta T_2}{T_2}\right)^2 - \left(\frac{\delta P_2}{P_2}\right)^2 - \left(\frac{\delta T_g}{T_g}\right)^2 - \left(\frac{\delta P_2}{P_2}\right)^2 - \left(\frac{\delta T_2}{T_2}\right)^2} \quad \textbf{(3-16)}$$

In determining error propagation, the calculated uncertainties of the variable parameters of equation (3.12) measured are substituted into equation 3.16 to obtain the error propagation.

3.5.3 Water/Air in Annular Flow

The error propagation for Vsl, Vsg, liquid hold-up and film thickness are:

3.5.3.1 Superficial Liquid Velocity

From the above partial derivative of equation (3.8), the superficial liquid velocity (Vsl) of error propagation from the experimental matrix used are:

Table 3.12: Error Propagation for Superficial Liquid Velocity

Average Vsl [m/s]	*Error Propagation [± m/s]*
0.0505	0.0510±0.0219
0.0714	0.0714±0.0219
0.0903	0.0903±0.0219
0.1355	0.1400±0.0219
0.1851	0.2001±0.0219

The graph of Figure 3.22 was the error propagation analysis of [±0.0219] showing the error bar of the superficial liquid velocity against the number of the experimental test runs (points). This is to present the level of accuracy of the measured values of superficial liquid velocity from the experiments obtained. The detailed analysis is seen in the Appendix (Tables L-5.1 to L-5.3).

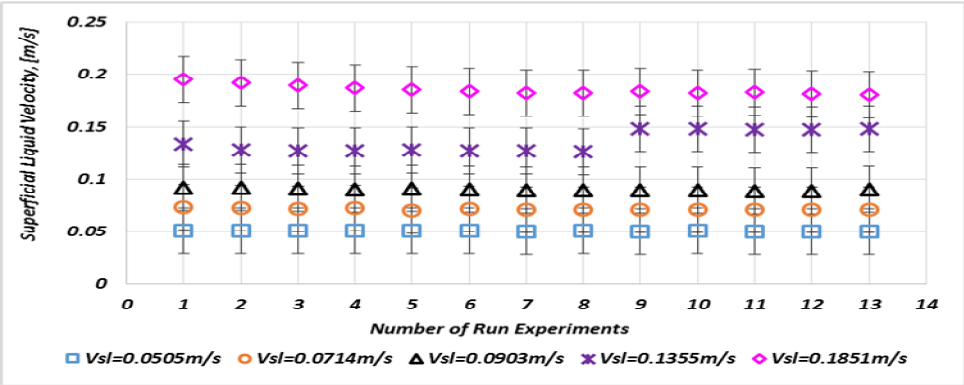

Figure 3.22: Error Propagation on Superficial Liquid Velocity

3.5.3.2 Superficial Gas Velocity

The error propagation for the superficial gas velocities used in water/air annular flow experiments is presented in Table 3.13 as follows:

Table 3.13: Error Propagation for Superficial Gas Velocity

Average Vsg [m/s]	*Error Propagation [± m/s]*
8.2699	8.2699±0.0008
9.2654	9.2654±0.0007
10.2160	10.2160±0.0006
11.2251	11.2251±0.0005
12.0675	12.0675±0.0005
13.1692	13.1692±0.0004
14.2883	14.28830.0003
15.3236	153236±0.0003
16.2262	16.2262±0.0003
17.3086	17.3086±0.0002
18.2481	18.2481±0.0002
20.3842	20.3842±0.0002
23.4575	23.4575±0.0002

The average error propagation of ±0.0004m/s for superficial gas velocity as shown in Table 3.13 was plotted on a graph of Figure 3.23. It shows a negligible error as the error bars were inconsequential, (see Figure 3.23). This means the measured values were accurate. The detail calculated table is in Appendix (Table L-6.1).

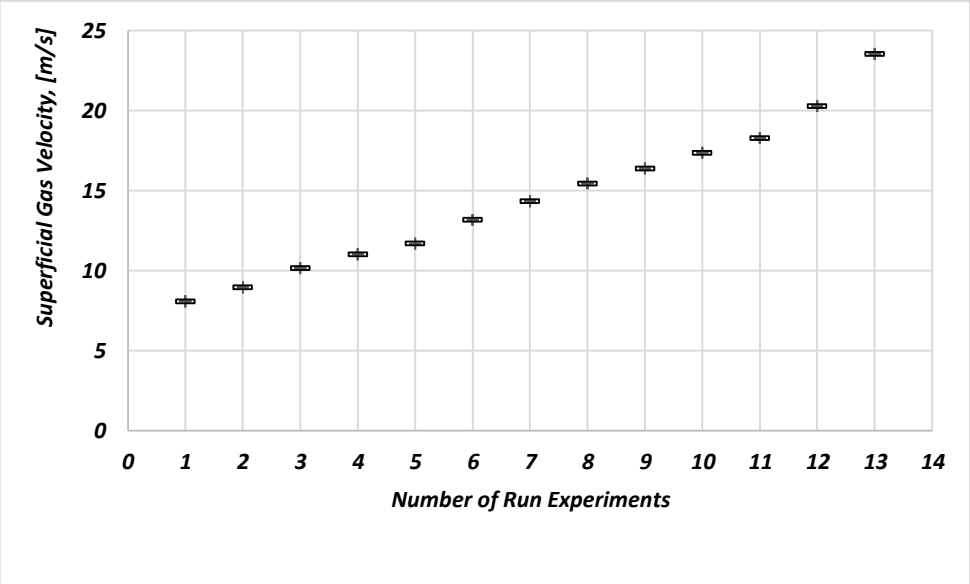

Figure 3.23: Error Propagation on Superficial Gas Velocity

3.5.3.3 Liquid Hold-Up

The error propagation for the liquid hold up is based on conductivity ring sensors' uncertainty results. The detailed error propagation results are shown in the Appendix (Table L-4.1 to L-4.3).

3.5.4 Water/Air/Sand in Annular Flow

The error propagation analysis below are for water/air/sand annular flow experiments.

The error propagation for superficial liquid velocity and superficial gas velocity in water/air/sand experiments were presented as follows;

3.5.4.1 Superficial Liquid Velocity

Table 3.14: Error Propagation (Vsl) for Water/Air/Sand in Annular Flow.

Sand(1000bbl)	*Vsl and Error Propagation*
200lb/212microns	(0.037-0.056) ±0.022m/s
200lb/500microns	(0.034-0.060) ±0.022m/s
500lb/212microns	(0.037-0.061) ±0.022m/s
500lb/500microns	(0.035-0.056) ±0.022m/s
200lb/800microns	(0.035-0.060) ±0.022m/s
500lb/800microns	(0.037-0.056) ±0.022m/s

The detailed calculations are presented in the Appendix (Tables N-1.1 to N-1.2).

4 Water/Air Flow Test Results

The preliminary results in Table 4.1 were the initial experiments conducted with water/air flow. The experiments presented a better insight on boundary conditions with respect to superficial gas velocity on flow regimes. In the experiments, half inch (1/2-inch) air-flow line was used to supply air to the 2-inch (I.D-0.0504m) flow loop from a gas compressor with a capacity of 252m^3/h and maximum discharge pressure of 7.5barg, that could only supply gas velocity below 8m/s.

The different flow regimes obtained were: plug, slug, stratified-smooth and stratified-wavy flows. The results, indeed enhanced the understanding and the concept of flow regimes with respect to different superficial gas velocities. Table 4.1 presents the flow regimes and the flow conditions.

Table 4.1: Experimental Result of Flow Patterns in 2-inch Pipe.

Flow Patterns	***Vsl [m/s]***	***Vsg [m/s]***
Stratified-Smooth Flow	0.0712	0.4871
Plug Flow	0.1484	0.2292
Slug Flow	0.3315	1.7131
Stratified -Wavy	0.0663	2.8522

From Figure 4.1, stratified-smooth flow was obtained from superficial liquid and gas velocities of 0.0712m/s and 0.4871m/s respectively. It was a smooth water/air flow in the pipe with no wavy present. This has progressed the understanding, that stratified flow, is attained at low superficial liquid and gas velocities in the pipes.

Vsl =0.0712m/s, Vsg =0.4871m/s

Figure 4.1: Stratified-Smooth Flow from 2-inch flow Pipe (Side View)

Plug flow, was presented from the experiments on superficial liquid and gas velocities of 0.1484m/s and 0.2292m/s, (see Figure 4.2). The picture in Figure 4.2, has shown that plug, flows in a bullet-shaped manner in horizontal pipes.

Vsl = 0.1484m/s Vsg = 0.2292m/s
Figure 4.2: Plug Flow from the 2-inch Flow test rig

Slug flow was presented from superficial liquid and gas velocities of 0.3315m/s and 1.7131m/s respectively from the experimental results as shown in Figure 4.3. In this case, high superficial liquid velocity and superficial gas velocity were involved, hence the flow was able to progress into waves with high magnitude in the flow loop. The waves were large, fast in motion and were observed covering the entire cross-section of the flow loop. It progresses with speed as it touches the entire pipe walls.

Vsl = 0.3315m/s, Vsg =1.7131m/s
Figure 4.3: Slug Flow from the Experiment using 2-inch Pipe

The flow observed in Figure 4.4 was a stratified-wavy flow. The flow progresses with ripples on the surface of liquid phase (water) in the pipe.

Vsl = 0.0663m/s Vsg = 2.8522m/s
Figure 4.4: Stratified-Wavy Flow from the Experiment using 2-inch Pipe.

The results of water/air flow in Table 4.1, were plotted on Taitel & Dukler (1976) flow regime map for better recognitions and understanding of the different flow positions. However, slug, plug and stratified-smooth and wavy flows matched perfectly as presented in Figure 4.5.

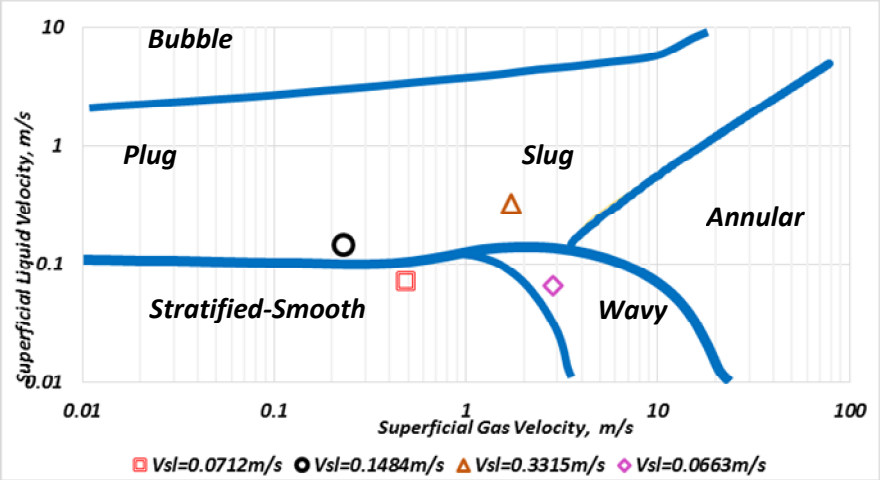

Figure 4.5: Experimental Result of Flow Regime with Taitel & Dukler (1976)

4.1 Water/Air Annular Flow Test Results

In water/air annular flow, high superficial gas velocities from 8m/s to 100m/s are required to achieve annular or annular-mist flow in horizontal pipes. Hence, a 2-inch (0.0504m, I.D) pipeline was installed to supply air from the higher compressor with a capacity of 400m^3/h (discharge pressure of 10barg) in the PSE Laboratory to the 2-inch (0.0504m, I.D) flow loop in the experiment. The ½-inch (0.0126m) air pipeline that was initially in place, was only able to supply air flow with a maximum superficial gas velocity of 8m/s, while in annular flow experiment, higher gas velocities above 8m/s were required. It was based this reason, that a second air pipe of 0.0504m was installed with its source of air (gas) from a higher gas compressor

In Table 4.2, are the properties and their ranges which were applied in water/air annular flow experiments in horizontal pipe.

Table 4.2: Experiment data for Annular Flow

Properties	Range	Units
Temperature	*16.5-19.3*	*^0C*
Pipe internal diameter	*0.0504*	*m*
Air flow line internal diameter	*0.0504*	*m*
Superficial liquid velocity	*0.0501-0.2001*	*m/s*
Superficial gas velocity	*8.0774-23.7260*	*m/s*

4.1.1 Annular Flow Regime

Annular flow is a flow regime in multiphase, where both the liquid phase and the gas phase, flows together in the pipe with the gas being the dominant phase and flows at high velocity at the centre of the pipe.

Annular flow in horizontal pipe could be presented in a flow map of superficial liquid velocity against superficial gas velocity. From the experiments that were conducted in the PSE Laboratory, the superficial liquid velocities were plotted against the superficial gas velocities in a log-log graph to present annular flow regime (see Figure 4.6). Again, to ascertain that the experiments conducted were actually annular flow, analysed data obtained were plotted on Taitel & Dukkler (1976) flow regime map for horizontal flow in pipes, as presented in Figure 4.6.

From the annular flow regime map in Figure 4.6, annular flow conditions were presented with an average superficial liquid velocities of 0.1851m/s, 0.1355m/s, 0.0903m/s, 0.0714m/s and 0.0505m/s. The transitions from high stratified-wavy flow were presented from superficial liquid velocity of 0.0505m/s and superficial gas velocities of 8m/s-12m/s as presented in Figure 4.6. While that of superficial liquid velocity of 0.0714m/s, presents the transitions from high stratified-wavy to annular-wavy flow, were on superficial velocities of 8m/s to 10m/s.

With the progress of having achieved good understanding and the plot of annular flow regime as presented in Figure 4.6, it becomes necessary to proceed further in the entire annular flow analysis like: flow behaviours, the liquid holdup, film thickness and the wave characteristics in the experiments.

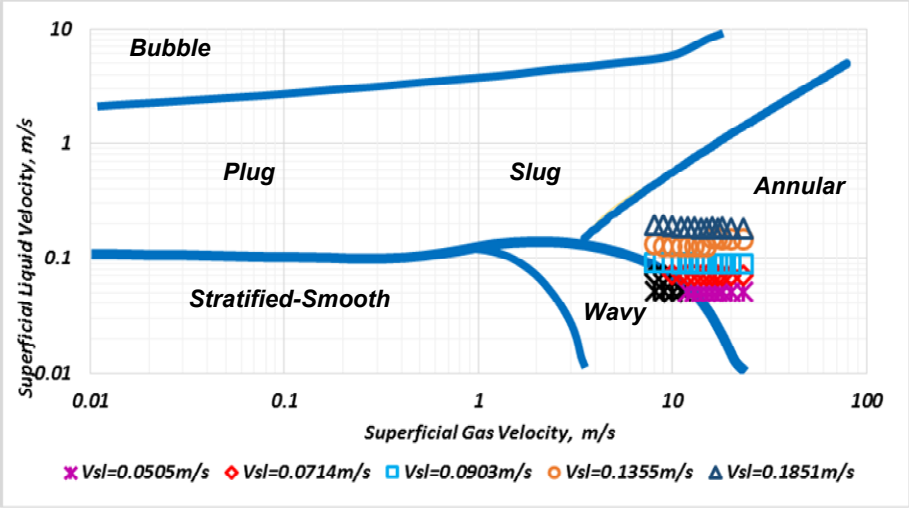

Figure 4.6: Annular Flow Regime of 2-inch Horizontal Pipe (Taitel & Dukkler, 1976)

4.1.2 Annular flow behaviour in 2-inch horizontal pipe.

From the water/air annular flow experiments, visual annular flow behaviours were carefully observed and recorded using an Olympia high digital camera. The results in Table 4.3, were compared with the flow regime map in Figure 4.6. Importantly, the flow behaviours from visual observations matched preferably with the annular regime map in Figure 4.6 as Vsl=0.0505m/s-0.0903m/s and Vsg 8.2699m/s -11.2251m/s, observed as annular-wavy flow from Table 4.3, were the same in Figure 4.6 plot.

Table 4.3: Annular flow showing flow behaviour in 2-inch horizontal pipe

¯Vsl/Vsg	8.2699	9.2654	10.2160	11.2251	12.0675	13.1692	14.2883	15.3236	16.2262	17.3086	18.2481	20.3842	23.4575
0.0505	A+S L-T	A+S L-T w-d	A+S L-T w-f	A+S L-Ts w-f	A+S L-Ts w-f	A L-Ts w-f	A L-Ts w-f wl-c	A L-Ts w-f wl-c	A L-Ts w-f wl-c	A L-Ts w-f wl-c	A L-Ts w-f wl-c	A L-Ts w-f w-cr	A L-Ts w-f w-cr
0.0714	A+S L-T w-d	A+S L-T w-d	A+S L-T w-f	A+Sr L-T w-f	A+Sr L-Ts w-f wl-c	A+Sr L-Ts w-f wl-c	A L-Ts w-f wl-c	A L-Ts w-f wl-c	A L-Ts w-f wl-c	A L-Ts w-f wl-c	A L-Ts w-f w-cr	A L-Ts w-f w-cr	A L-Ts w-f w-cr
0.0903	A+S L-T w-d	A+Sr L-T w-d	A+Sr L-T w-d	A+Sr L-T w-d	A+Sr L-T w-f	A L-Ts w-f wl-c	A L-Ts w-f wl-c	A L-Ts w-f wl-c	A L-Ts w-f wl-c	A L-Ts w-f wl-c	A L-Ts w-f w-cr	A L-Ts w-f w-cr	A L-Ts w-f w-cr
0.1355	A L-T w-d	A L-T w-ds	A L-T w-ds	A L-T w-f	A L-T w-f	A L-Ts w-f wl-c	A L-Ts w-f wl-c	A L-Ts w-f wl-c	A L-Ts w-f wl-c	A L-Ts w-f w-cr	A L-Ts w-f w-cr	A L-Ts w-f w-cr	A L-Ts w-f w-cr
0.1851	A L-T w-d	A L-T w-d	A L-T w-d	A L-T w-f	A L-T w-f	A L-T w-f	A L-Ts w-f wl-c	A L-Ts w-f wl-c	A L-Ts w-f wl-c	A L-Ts w-f w-cr	A L-Ts w-f w-cr	A L-Ts w-f w-cr	A L-Ts w-f w-cr

From Table 4.3: A = Annular flow fully, A+S = Annular-wavy with slug flow, A+Sr = Annular-slug but slug reduces, L-T = More liquid film thickness at the bottom of the pipe, L-Ts = More liquid film thickness at the bottom but moves with more speed, w-d = Wavy flow at upper walls of the pipe and drain down through the pipe walls to the bottom of the pipe, w-ds = Wavy flow at the upper pipe walls and drain down the pipe walls to the bottom of the pipe at higher speed, w-f = Wavy flow at the upper walls of the pipe with speed, wl-c = the entire pipe walls are fully covered with liquid film at high speed, w-cr = the entire pipe walls are fully covered with liquid film at very high speed at the entire walls of the pipe.

4.1.3 Annular wavy-flow at upper walls of horizontal pipes

From the experiments, annular flow was proven, to flow with more liquid film at the bottom of the pipe at all superficial liquid and gas velocities. This is because of gravity and shear stress, Sergey et al., (2014). More interestingly, annular flow behaves as wavy thin flow at the upper walls of the pipe. This was more prominent with higher superficial liquid and gas velocities, (see from Figures 4.7 and 4.8).

Figure 4.7, illustrates that wavy flow exists at the upper walls of the pipe in annular flow as seen with superficial liquid and gas velocities of 0.0501m/s and 23.2796m/s respectively. Though, the wavy progression at the upper walls of the pipe, were less compared with that of superficial liquid velocity of 0.0901m/s. This is because, the lower the superficial liquid velocity, the lower the liquid film at the bottom and upper walls of the pipe, and the less spread of the liquid film across the pipes.

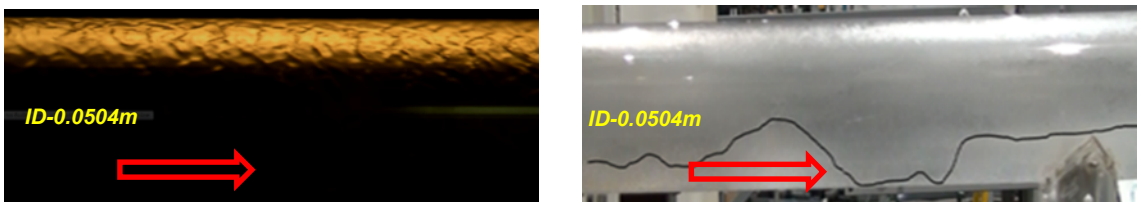

Figure 4.7:(a)Vsl =0.0501m/s, Vsg=23.2796m/s,(b) Vsl=0.0501m/s, Vsg =23.2796m/s

For Figure 4.8, the wavy tendencies were more pronounced, because more of the liquid films were distributed circumferentially across the walls of the pipe. More so, the higher the superficial liquid velocity, the thicker the film, and the more

spread the liquid film across the walls of the pipe. This is the true illustration of Figure 4.8.

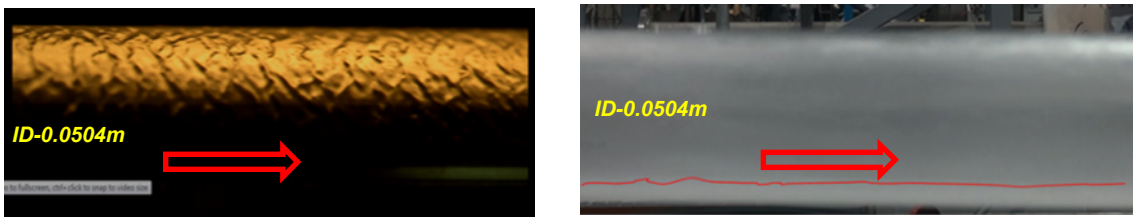

Figure 4.8:(a)Vsl=0.0901m/s, Vsg=23.5707m/s, (b) Vsl=0.0901m/s, Vsg =23.5707m/s

4.2 Liquid Hold-Up Results.

Liquid holdup results from the experiments were presented from the normalized conductivity ring signals in conjunctions with the annular flow bench calibration equation (3.1). The bench calibration involved, using different cylindrical blocks (plastic) which were inserted into the calibration tool of 50mm (I.D) with a length of 170mm.

The annular bench calibration was done horizontally, to replicate the experimental flow scenario in horizontal pipe. The results obtained were analysed and plotted to obtain a 3-order polynomial equation (3.1) which was used, on the experimental data of the conductivity ring sensor signals. From this, the annular flow liquid hold-up results were presented in Figure 4.9.

The graph of Figure 4.9 which is the liquid hold up against superficial gas velocity, has shown that liquid hold up increases with increase in superficial liquid velocity, but decreases with increase in superficial gas velocity in horizontal pipes. The was an upward projection on Vsl=0.1355m/s plot because of an increase in the Vsl values from 0.1264m/s to 0.1482m/s hence removed. This was not observed during the experiments, but the measuring instruments detected it perfectly.

In terms of level of confidence on results presented, error propagation of 0.0067m/s from the uncertainty calculations on liquid holdup, were further plotted (Figure 4.9) on Vsl=0.1851m/s, to present the level of accuracy of the measured liquid holdup values. The detailed error propagation calculations of liquid holdup are presented in the Appendix L (Tables L-4.1- L-4.3)

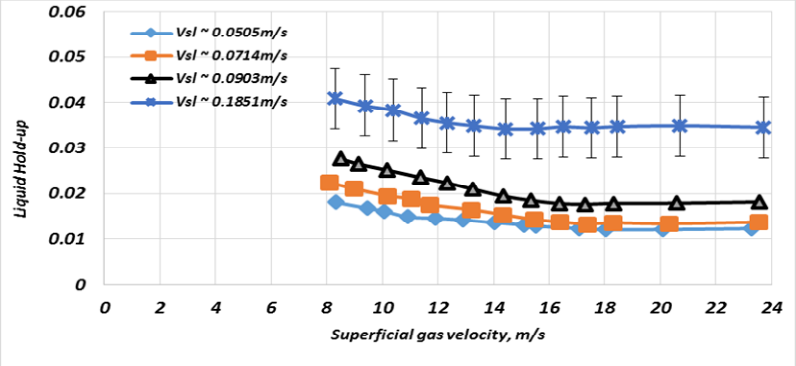

Figure 4.9: Liquid hold-up against superficial gas velocity.

4.3 Determining the Film Thickness

In determining the liquid film thickness in annular flow in this study, precautions were followed. First, to produce annular flow trend in the experiments, where the superficial gas velocity will be dominant at the core centre of the pipe. Therefore, the bench calibration was done to reflect the scenarios where there is a gas core at the centre of the pipe. The annular flow calibrations were carried out using conductance probe and conductivity ring sensors in the PSE laboratory as elaborated below in the subsections respectively.

4.3.1 Film Thickness using Conductance Probe

Experimental bench calibration with conductance probe was set up, using a 50mm (0.0504m, I.D) pipe with a length of 170mm. The annular flow calibration was achieved, using three solid cylindrical blocks (plastics) of 49mm, 42.4mm and 33.40mm which were inserted at different times with their voltage recorded. The procedures were expatiated in chapter 3 on section 3.1.38. From the bench calibrations, equation (4.1) was obtained for determining the liquid film thickness as:

$$Y = -0.0044\ X^2 + 01256\ X + 0.112 \qquad \textbf{(4-1)}$$

Where Y is the reference film thickness obtained graph in Figure 3.15, X is the experimental data (Normalized probe sensor's results).

Figure 4.10, presents the liquid film thickness results. More so, the graph of Figure 4.10, shows that the liquid film thickness, decreases with increase in

superficial gas velocity, and increases with increase in superficial liquid velocity, as average superficial liquid velocity of 0.0505m/s plot indeed, has the lowest film thickness while the superficial liquid velocity of 0.1851m/s represented the highest film thickness. Again, Figure 4.10 had also shown that, as the superficial liquid velocity becomes higher, the rate of decrease in film thickness becomes insignificant at the bottom of the pipes. This is because of gravity impact overtime on the break-up droplets. As more of the break-up droplets are lifted up, they indeed becomes heavier and with the impact of gravity, drains to the bottom of the pipes. These mechanisms were also noted by Setyawan *et al*., (2016) and (Shedd, 2001). And for these reasons, the graph of superficial liquid velocity of 0.1851m/s in Figure 4.10 seems to be a straight line with equal heights across all the superficial gas velocity conditions. However, the heights were not precisely equal as the detailed analysed results provided in the Appendix H (Table H-1.5), proved it.

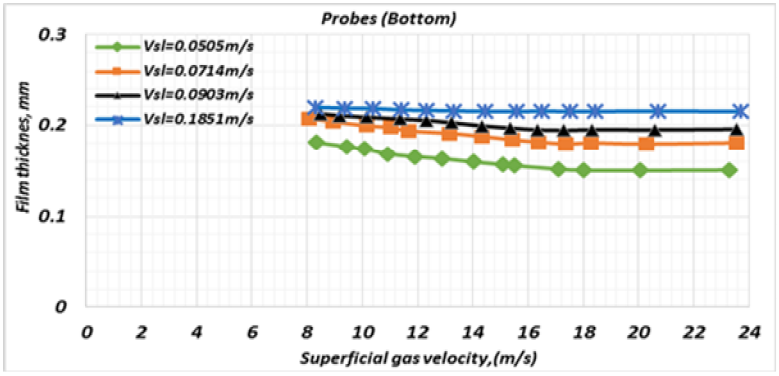

Figure 4.10: Film thickness (probe at bottom) against superficial gas velocity

4.3.2 Wave Velocity of the Film Thickness (Probe)

The graph of Figure 4.11 shows that an increase in superficial liquid velocity, increases the wave velocity in annular flow. This is because, as the liquid rate increases, momentum transfer between gas core and liquid film increases to create more waves. This is also in line with the reports of Setyawan *et al*., (2016), Fukano *et al*., (1983), Jayanti *et al*., (1990), Alamu and Azzoppardi (2011), Paras and Karabelas (1991), Mantilla (2008). Thus, the graph further illustrates that the lower the superficial liquid velocity, the lower the wave velocity. The reason is simply because of low surface tension. Low surface tension gives low wave

velocity with respect to low superficial liquid velocity (Setyawan *et al*., 2016). The higher the superficial liquid velocity, the higher the wave velocity though with a decreasing trend for surface tension. It was also observed that both superficial liquid and gas velocities affect the wave velocity. However, increase in superficial gas velocity, increases the wave velocity as presented in Figure 4.11 and also noted by Furukawa *et al*., (2010).

In all the superficial liquid velocities in Figure 4.11, the wave velocity increased till a Vsg = 18m/s and became stable across all the superficial liquid velocities. This is simply because, the wave amplitude had attained its peak both at the crest and trough with more interfacial roughness at superficial gas velocities of 18m/s across the entire flow conditions, that no further changes would impact on it.

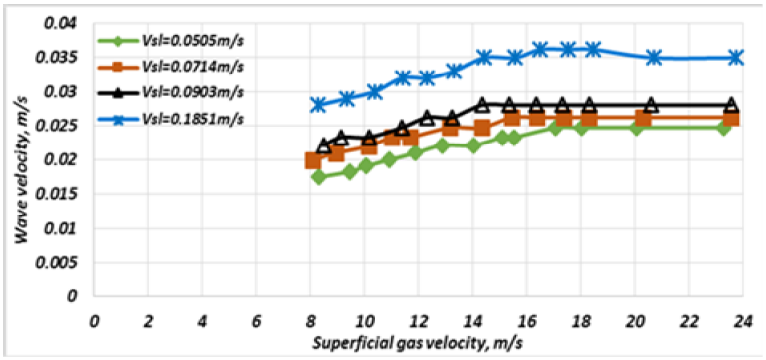

Figure 4.11: Wave velocity against superficial gas velocity

The graph of figure 4.12 is the liquid film thickness against wave velocity. It presents, how the wave velocity increases, with decrease in liquid film thickness annular flow.

For the liquid film thickness from the above statements, it means as the wave increases in the pipe, more liquid droplets were being taken up as entrainments, hence decreasing the liquid film thickness at the bottom of the pipe as superficial gas velocity increases in annular flow.

Reasons for the increase in the wave velocity against decrease in liquid film thickness could be best explained below: hence more energy is dissipated from the gas core to keep the wave in motion under high wave amplitude as superficial liquid and gas velocities increases, therefore, the faster the liquid film will be

displaced in the systems. This is with respect to the superficial liquid velocities, hence in Figure 4.12, Vsl=0.0505m/s presented lower wave velocities compared to Vsl=0.1851m/s.

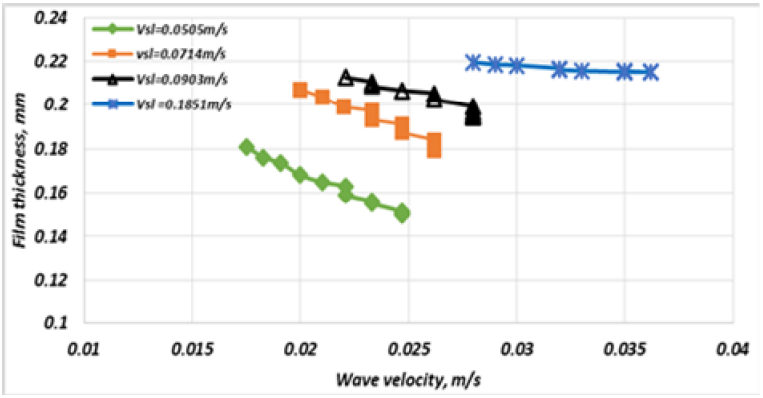

Figure 4.12: Film thickness (probe at bottom) against wave velocity

Figure 4.13 is the graph of liquid film thickness against pressure gradient. As expatiated in Figure 4.12 earlier, hence more energy is required from the gas core to keep the wave in motion annular flow, therefore, there will be more friction and wall shear stress both at the interface between the liquid phase and the gas core, and between the liquid film and walls of the pipes in horizontal flow. Based on these facts, pressure losses will be high likewise pressure gradient as presented in Figure 4.13. The pressure gradient with respect to the film thickness at the bottom of the pipe, were increasing with decrease in the film thickness. Also, the higher the superficial liquid velocity, the higher the film thickness and the higher the pressure gradient.

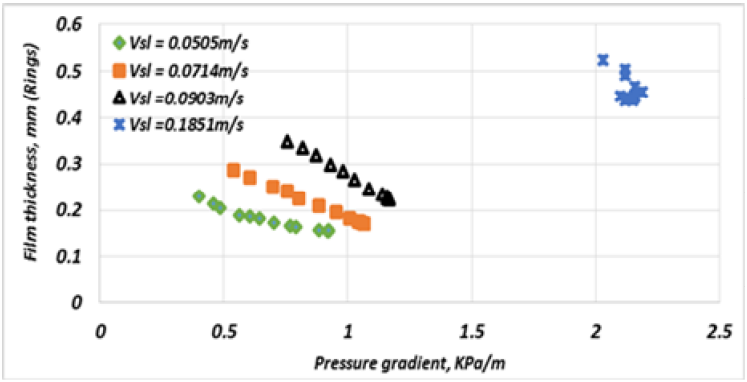

Figure 4.13: Film thickness (probe at bottom) against pressure gradient

4.3.3 Film Thickness using Conductivity Ring Sensors

Figure 4.14 is a graph of film thickness against superficial gas velocity from conductivity ring sensors. It shows that film thickness decreases with increase in superficial gas velocity as observed in Figure 4.10. The Vsl=0.1355m/s had an upward projection which was as a result of increase in Vsl in the flow loop, hence was removed. The error bar plot on average Vsl=0.1851m/s was the error propagation of ± 0.0844mm of the film thickness which shows the level of accuracy of the measured values.

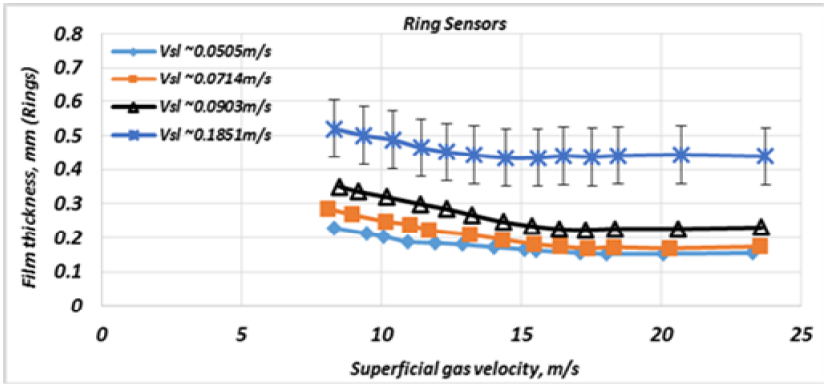

Figure 4.14: Film thickness from ring sensor against superficial gas velocity

4.3.4 Wave Frequency Analysis on Ring Sensors

Wave frequency analysis was presented using conductivity ring sensors' data from the experiments. The wave frequency results, from the experimental data were achieved using Matlab 2015 version on PSD against Frequency.

Wave frequency plot against superficial gas velocity in Figure 4.15, shows that wave frequency increases, with increase in superficial gas velocity as reported also by Setyawan *et al.,* (2016), Ousaka *et al*., (1992), Para and Karabelas (1991) and Schubring and Shedd (2008). However, the experimental results of Figure 4.15, had refuted Setyawan *et al.,* (2014), whose report presented superficial liquid velocities to have insignificant effect on wave frequency.

Figure 4.15 illustrates the impact of superficial liquid velocity on wave frequency in line with Para and Karabelas (1991) that says wave frequency decreases with increase in superficial liquid velocity. From Figure 4.15, the wave frequency of

Vsl = 0.0505m/s was presented to be higher than of wave frequency of Vsl = 0.1851m/s. Meaning, wave frequency decreases with increase in superficial liquid velocity in annular flow in horizontal pipe. The detail calculations are shown on in the Appendix (Tables I-1.1 to I-1.5).

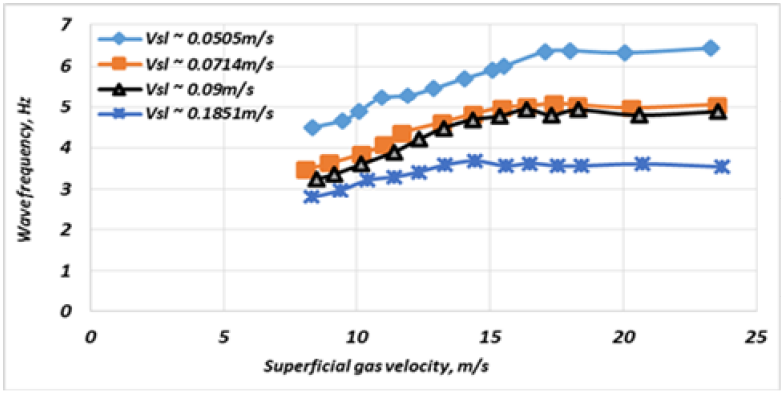

Figure 4.15: Wave frequency against superficial gas velocity

4.3.4.1 Comparing Wave Frequency from Experiments with Correlations

The results from the entire superficial liquid velocities were compared also with different existing wave frequency correlations as follows:

Figure 4.16, is the wave frequency graph of Vsl=0.0505m/s against existing correlations. The wave frequency graph of Figure 4.16, shows a trend of increase with increase in superficial gas velocity. The correlations of Ousaka *et al*., (1992), Schubring & Shedd (2008), Setyawan *et al.,* (2014) and Setyawan *et al.,* (2016) underestimated the wave frequency. While the correlation of Al-Sarkhi *et al.,* (2012) over-estimated the wave frequency when compared to the experimental wave frequency results. The reasons for the differences compared to the experimental wave frequency results, were based on assumptions made in deriving those correlations and pipe diameters considered. Mantilla (2008) was close to the experimental wave frequency results in the case of superficial velocity of 0.0505m/s.

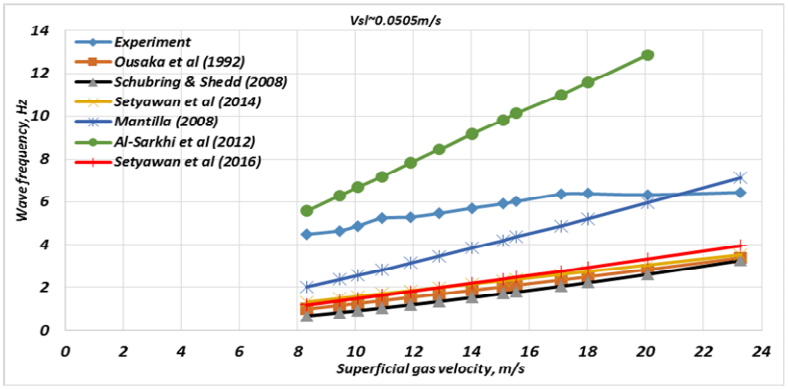

Figure 4.16: Wave frequency Vs Superficial gas Velocity (Vsl~0.0505m/s)

Again, Figure 4.17 has presented an under-estimation of wave frequency from correlation of Ousaka *et al.,* (1992), Setyawan *et al.,* (2014), Schubring & Shedd (2008) and Setyawan *et al.,* (2016), while over-estimation of wave frequency from correlation of Al-Sarkhi *et al.,* (2012). The wave frequency from the experiment was between 3.4712Hz to 5.058Hz.

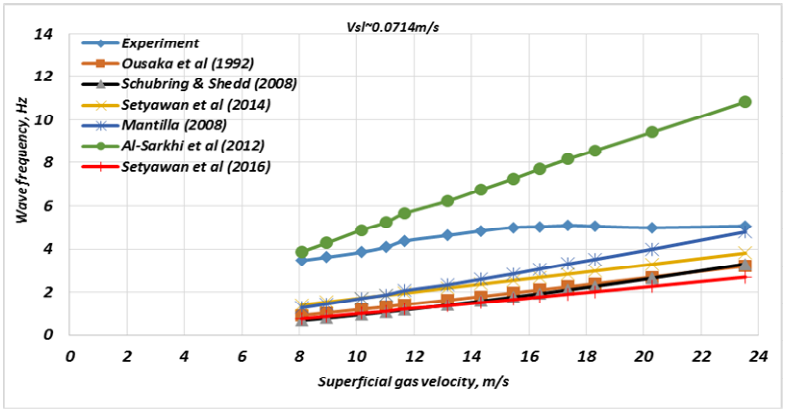

Figure 4.17: Wave frequency Vs Superficial gas velocity (Vsl~0.0714m/s)

Figure 4.18 has also shown similar trend with Figure 4.17, though with the wave frequency from the experiments being in close range with Al-Sarkhi *et al.,* (2012), on superficial gas velocities of 8m/s to 14m/s. The wave frequency from the experiments were between 3.2413Hz to 4.8847Hz while Al-Sarkhi *et al.,* (2012) correlation wave frequency were between 3.271Hz to 8.638Hz.

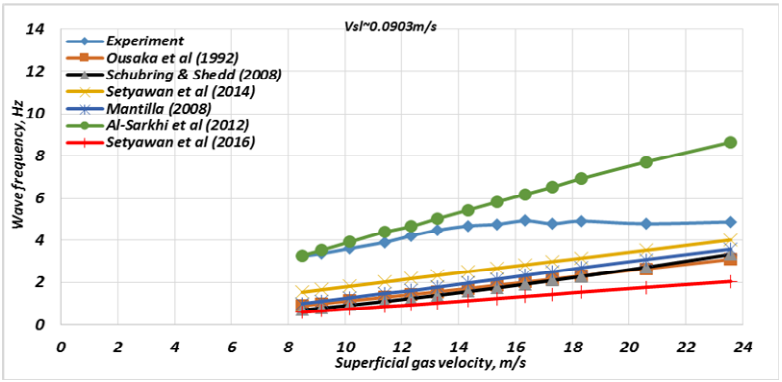

Figure 4.18: Wave frequency Vs Superficial gas velocity (Vsl~0.0903m/s)

Interestingly, Figure 4.19 has shown a close range among the correlations with the wave frequency from the experiments, and with Al-Sarkhi *et al.,* (2012) matching preferably than others. Wave frequency from Figure 4.19, were between 2.9654Hz to 4.1405Hz while that of Al-Sarkhi *et al.,* (2012) were between 2.334 Hz to 5.361Hz. It is also interesting to note, that as the superficial liquid velocity increases, the wave frequency decrease. This is because, the wave tendency decreases as the liquid film, circumferentially fills the entire walls of the horizontal pipe.

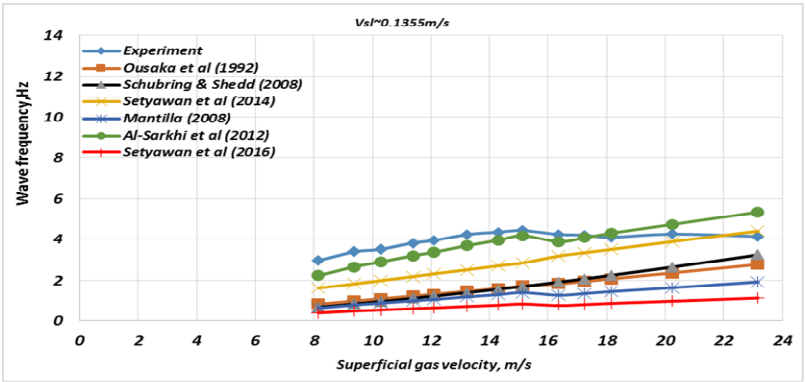

Figure 4.19: Wave frequency Vs Superficial gas velocity (Vsl~0.1355m/s)

From Figure 4.20, shows that the entire plots were already matching the measured wave frequency better. In horizontal pipe, it shows that the higher the superficial liquid velocity, the lower the wave frequency. The wave frequency from the experiments, were between 2.7945Hz to 3.5396Hz while Al-Sarkhi *et al.,* (2012) correlation wave frequency results were between 1.597Hz to 4.555Hz).

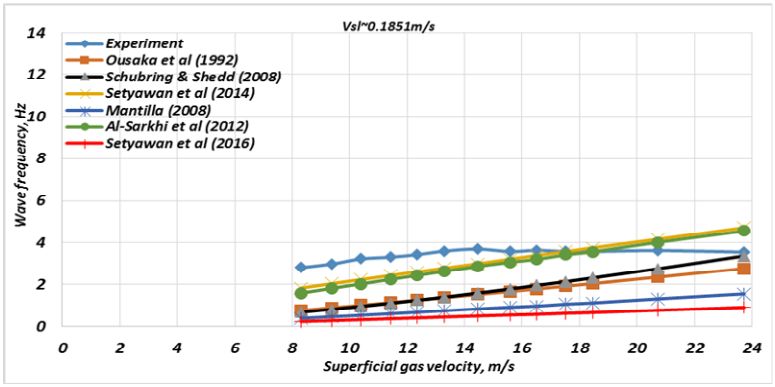

Figure 4.20: Wave frequency Vs Superficial gas velocity (Vsl~0.1851m/s)

In conclusions, the correlations and the experimental results of wave frequency had proven that superficial liquid velocity has impact on wave frequency. From the superficial liquid velocity of 0.0505m/s, the wave frequency from the experiment were between 4.499Hz to 6.4358Hz with Vsg of 8.3179m/s and 23.2796m/s respectively. While at an average superficial liquid velocity of 0.1851m/s, the wave frequency from the experiments were between 2.7945Hz to 3.5396Hz with Vsg of 8.3042m/s and 23.7259m/s respectively. This has shown, that the higher the superficial liquid velocity, the lower the wave frequency and the higher the amplitude, the more disturbing waves are created which forms ring structures across the pipe.

Lastly, the correlation results of Ousaka *et al*., (1992), Schubring & Shedd (2008), Setyawan *et al.,* (2014), Setyawan *et al.,* (2016) differed because the correlations were derived using small pipe diameters of 8.8mm to 26mm.

From the performance plot of Figure 4.21, the Al-Sarkhi *et al.,* (2012) was the only correlation that matched closely with the measured wave frequency on average Vsl=0.0903m/s, 0.1355m/s and 0.1851m/s. At low Vsl of 0.0505m/s, it was Mantilla (2008) that was close. The detailed analysis on wave frequency is presented in Appendix I (Tables I-1.1 to I-1.5)

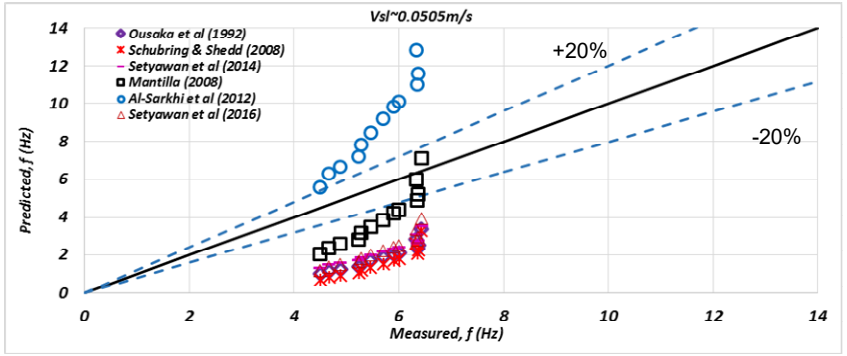

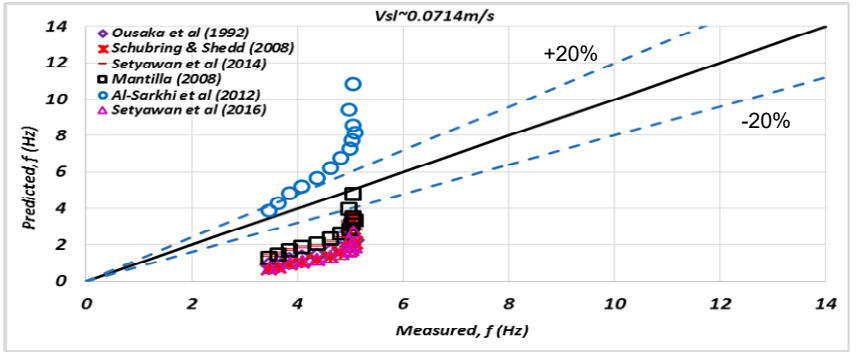

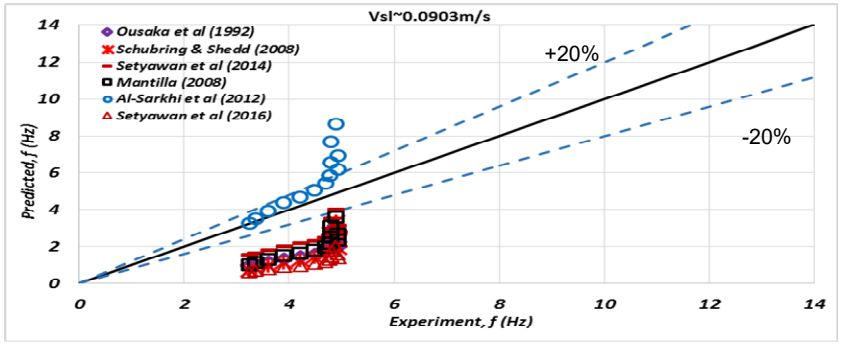

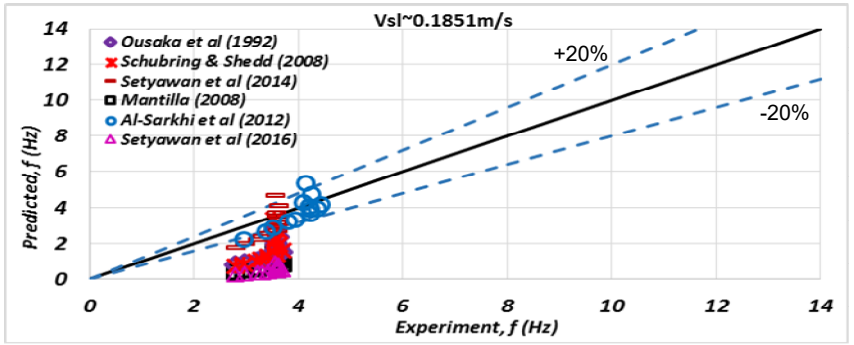

Figure 4.21: Plots of Performance to identify Correlation that matched the Experimental (Measured) Wave Frequency

4.3.5 Film Thickness using Triangular Relationship

Triangular relationship is simply the three principle system variables which are dependent on one another: pressure gradients, liquid film thickness and liquid film flow rate. It is a unique method for determining liquid film thickness in multiphase flow in pipes. Triangular relationship, represents liquid film flow rate as a function of liquid film thickness and pressure gradient in the pipes. From the pressure gradients and liquid flow rates from the experiments, the liquid film thickness using triangular relationship method, was presented; (see Figure 4.22) and the results are presented below.

Figure 4.22, is the plot of triangular relationship (liquid film thickness) against superficial gas velocity. Triangular relationship from the graph, has shown that film thickness decreases with increase in superficial gas velocity. Again, from the same Figure 4.22, it was presented that the higher the superficial liquid velocity, the higher the film thickness, hence the average Vsl of 0.1851m/s, represented the highest film thickness in the analyses.

One observation from the graph was a uniform decline among all the superficial liquid velocity. The decline in the liquid film thickness was observed with less changes as the average superficial gas velocity increases from 16.2262m/s to 23.4575m/s. The reason is because the entrained liquid droplets overtime, will become larger due to high gas velocity that results to more break-up and lifting of these liquid droplets as superficial gas velocity increases in horizontal pipe. These liquid droplets will descend back to the bottom of the pipes through the walls of the pipes, as gravity impacts on the droplets. This phenomenon, presented the liquid film thickness plots to appear nearly as a straight line in Figure 4.22.

The convergence on average Vsg=8.2699m/s to 12.0675m/s in Figure 4.22 is because, triangular relationship presented liquid film thickness, to be decreasing with increase in superficial liquid velocity, and increasing with decrease in superficial liquid velocity. This is because triangular relationship is for annular flow in vertical pipes and not horizontal flow in pipes.

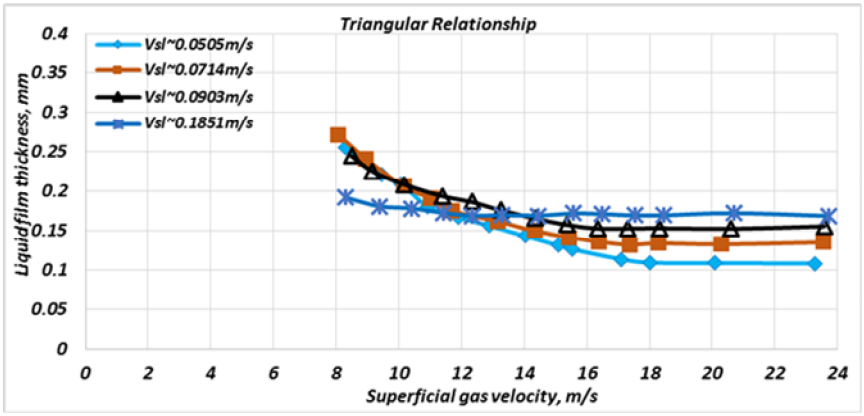

Figure 4.22: Film thickness Vs Vsg using Triangular Relationship

4.3.6 Comparing Liquid Film Thickness from different Methods

The annular flow liquid film thickness results from the experiments, were determined using the following methods:

- Conductivity Ring Sensors,
- Probes and,
- Triangular Relationship.

The results of the three methods, were plotted in Figures 4.23 and 4.24 with Vsl=0.0505m/s and 0.0714m/s respectively, while the performance plots were presented in Figure 4.25(a) and (b), and the detailed results analysis in the Appendix (Tables H-1.1 to H-1.5).

The graph of Figure of 4.23 presented a similar trend among the three methods, except the little variance from the graphs of the probes. However, conductivity ring sensors and triangular relationship plots for liquid film thickness, represents the true scenario where the liquid film thickness flows, circumferentially across entire walls of the pipes. Meanwhile, the probes only accounted for the liquid film thickness at the bottom of the pipe, hence the difference seen in Figure 4.23.

Again, the little difference between the conductivity ring sensors and the triangular relationship could also be attributed to uncertainties from bench calibration, which was used in determining film thickness for the conductivity ring sensors' method.

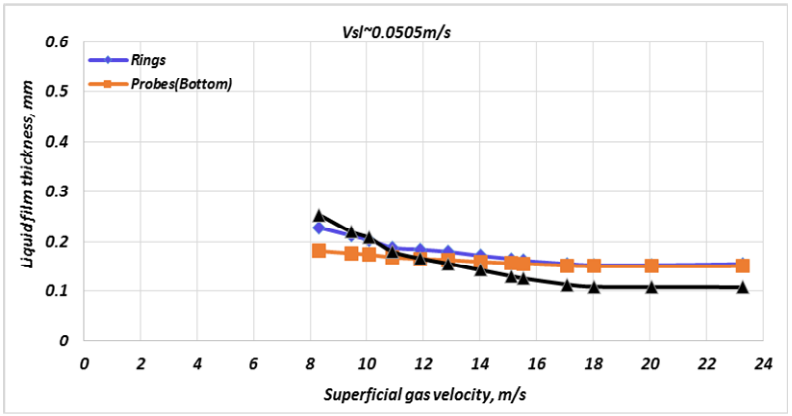

Figure 4.23: Comparing film thickness from three methods (Vsl ~ 0.0505m/s)

From figure 4.24, the film thickness from conductivity rings sensors and the triangular relationship showed similar trend while the plot from probes was a bit different from that of average superficial gas velocities of 8.2699m/s to 14.2883m/s. Again, the probe represents, only the film thickness at the bottom of the pipe which is the difference in the plots.

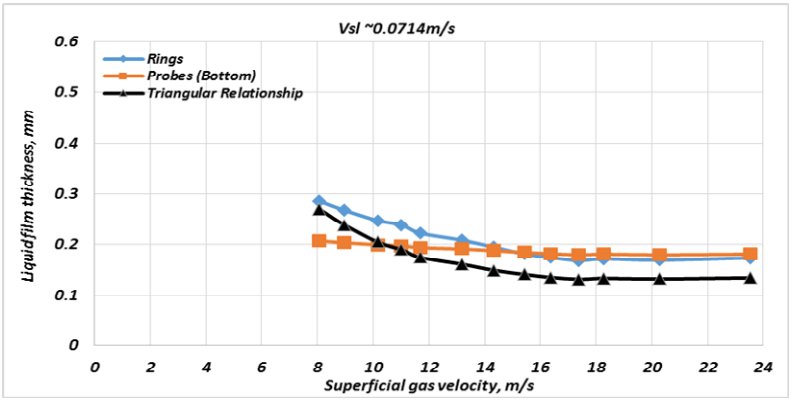

Figure 4.24: Comparing film thickness from three methods (Vsl ~ 0.0714m/s)

The graphs of Figure 4.25, is the predicted liquid film thickness from triangular relationship against the measured film thickness from conductivity ring sensors and probes. From Figure 4.25 [a], the liquid film thickness from triangular relationship under-predicted liquid film thickness, when compared with liquid film thickness from conductivity ring sensors. The plot of average Vsl=0.1851m/s was completely off, showing a wide difference while plots of Vsl=0.0505m/s and Vsl=0.0714m/s, preferably matched.

For probes, the predicted triangular relationship liquid film thickness matched better with the measured liquid film thickness from probes in all the superficial liquid velocities. This is to illustrate that probes detects liquid film thickness better than conductivity ring sensors in annular flow as seen Figure 4.25 (b). The reason could be as a result of the impact of high superficial gas velocity on conductivity ring sensors which will be a green area for future research in annular flow in pipes.

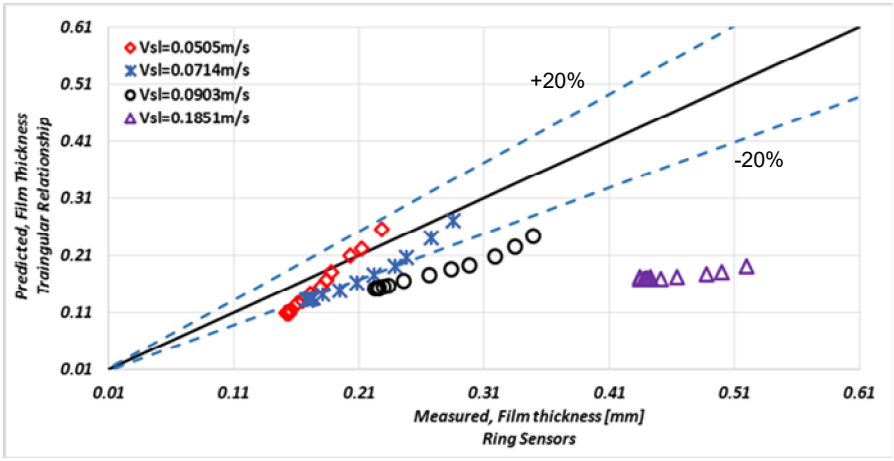

[a]

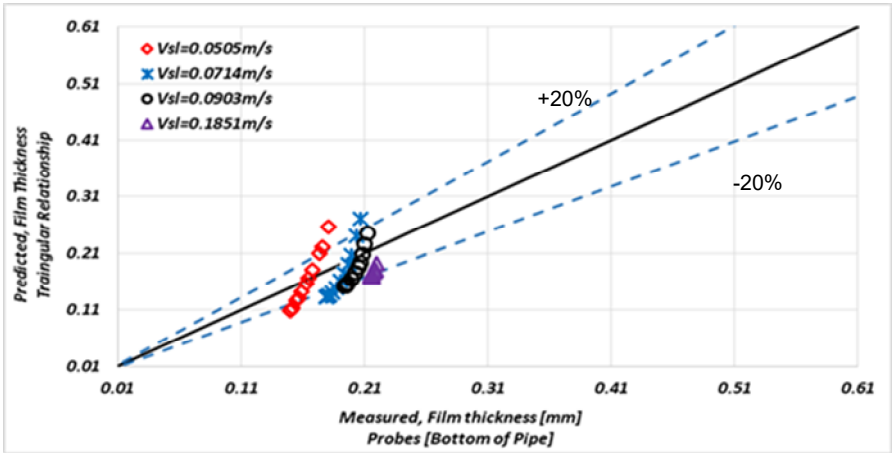

[b]

Figure 4.25 [a], [b]: Plot of Predicted against Measured Liquid Film Thickness

4.3.7 Interfacial friction factor/interfacial shear stress analysis

The interfacial friction factor and interfacial shear stress were analysed in this study. The interface between the liquid phase and the gas phase represents the untapped action regions with more information that will progress the knowledge of flow behaviours with respect to wave characteristics in annular flow

The interfacial friction factor, predicts the friction energy loss on the interface based on the velocity of the fluid and the resistance to friction. The interfacial friction factors in this study, were presented from the experiments using the following equations from Aliyu *et al.,* (2015):

$$f_i = \frac{2\tau_i}{\rho_g V_{Sg}^2} \quad \textbf{(4-2)}$$

where τ_i (interfacial shear stress)

$$\tau_i = \left(-\frac{dP}{dz} - \rho_C g \right) \frac{D - 2t}{4} \quad \textbf{(4-3)}$$

where,

$$\rho_{gC} = (1 - \varepsilon_C)\rho_L + \varepsilon_C \rho_g \quad \textbf{(4-4)}$$

and

$$H_C = \frac{\varepsilon}{\varepsilon + \gamma(1 - \varepsilon)} \quad \textbf{(4-5)}$$

and,

$$\wp = e \frac{\varepsilon}{(1 - \varepsilon)} \frac{1 - x}{x} \frac{\rho_g}{\rho_L} \quad \textbf{(4-6)}$$

Where e is entrainment, x is the gas quality, $\wp$ is the droplet, ρ_{gC} is the density of gas core, H_C is gas core void fraction, ρ_S is the slip mixture density, ρ_L is the liquid density and ε is the cross-sectional average void fraction (Aliyu *et al.,* 2015).

In determining the interfacial shear stress, equation (4.3) was used. The pressure gradient and the liquid film thickness (t), the entrainments (droplets) average void fraction were obtained from the experiments. In the calculation, the gas quality (x) was calculated from the expression as:

$$x = \frac{M_g}{(M_g + M_L)} \qquad \textbf{(4-7)}$$

Where M_g is the mass flow rate of the gas, M_L is the mass flow rate of the liquid (Kg/s, or litre/seconds). The mass liquid and gas flow rates were obtained from the experiments.

Figure 4.26 clearly shows that the interfacial friction factor decreases, with increase in superficial gas velocity in annular flow in horizontal pipes. More so, at lower superficial gas velocity, the interfacial friction factors were higher, but at higher superficial gas velocity, interfacial friction factors were lower as seen in Figure 4.26.

The reason is because, more frictions were observed at low amplitude, with low superficial gas velocity that often creates high interfacial roughness of the gas and liquid phases on the surface of liquid film thickness in horizontal pipes. At very high amplitude with respect to high superficial gas velocity, there were interfacial transfer of mass, momentum and energy which result to more liquid entrainment in annular flow (Setyawan *et al.,* 2016).

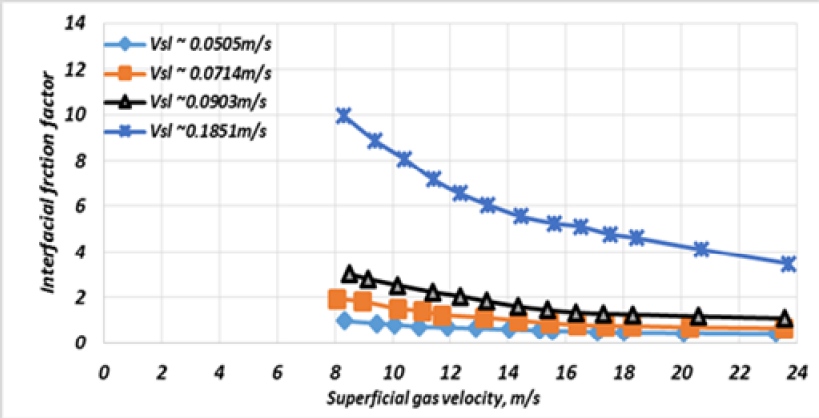

Figure 4.26: Interfacial friction factor against superficial gas velocity

Figure 4.27 illustrates that the higher the superficial liquid velocity with respect to gas velocity, the higher the interfacial friction factor and pressure gradient in annular flow in horizontal pipes. In annular flow in horizontal pipe as seen in Figure 4.27, the lower the superficial gas velocity, the higher the interfacial friction factor and the lower the pressure gradient. Meaning, interfacial friction factor decreases, with increases in superficial gas velocity, while the pressure gradient increases with increase in superficial liquid velocity.

This is because as superficial liquid velocity increases, wave amplitude also increases hence more energy will be required from the gas phase for the waves (Mantilla, 2008). However, as superficial gas velocity increases the waves become fewer and surface tension reduces, hence the decrease in interfacial friction factor.

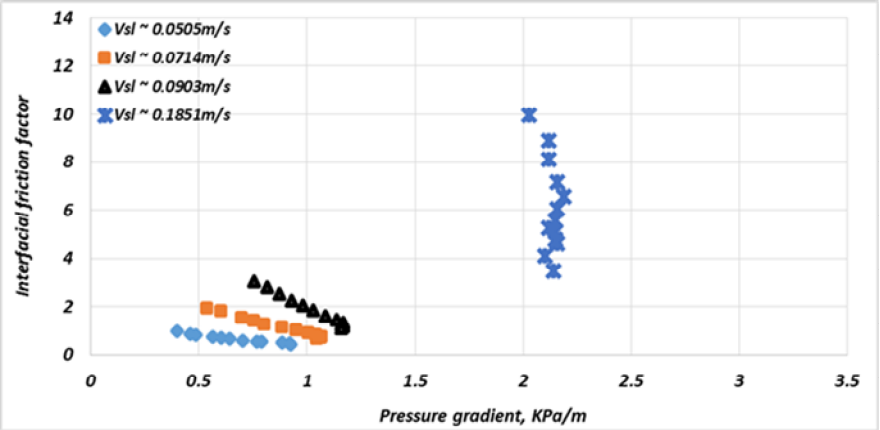

Figure 4.27: Interfacial friction factor against pressure gradient

From the graph of Figure 4.28, it shows that the higher the superficial liquid velocity, the higher the interfacial shear stress. Again, the interfacial shear stress decreases with increase in superficial gas velocity in horizontal pipes with respect to annular flow. The reason is because, interfacial roughness are more pronounced at low amplitude with surface waves and promotes pressure drops also in the pipes. At low superficial gas velocity of 8-12m/s, annular flow is transported as asymmetrical but at higher superficial gas velocity at all superficial liquid velocity conditions, annular flow behaves symmetrical. This is the more reason the interfacial shear stress is higher at all conditions at low superficial gas velocity in all the Vsl flow conditions.

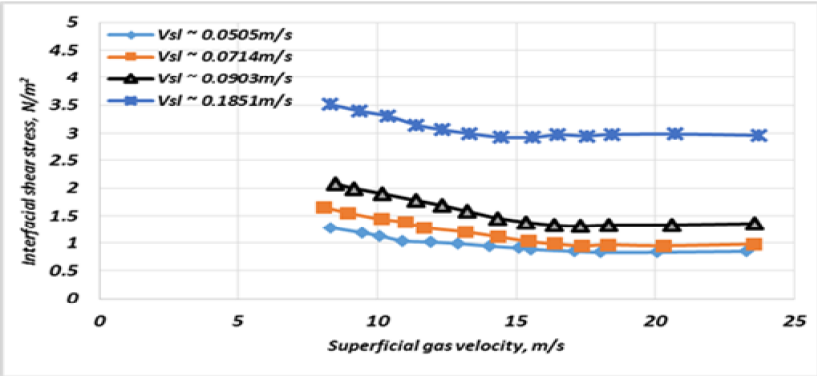

Figure 4.28: Interfacial shear stress against superficial gas velocity

In the graph of Figure 4.29, a plot of liquid film thickness against interfacial shear stress was presented to illustrate that, the higher the superficial liquid velocity, the higher the film thickness and the higher the interfacial shear stress.

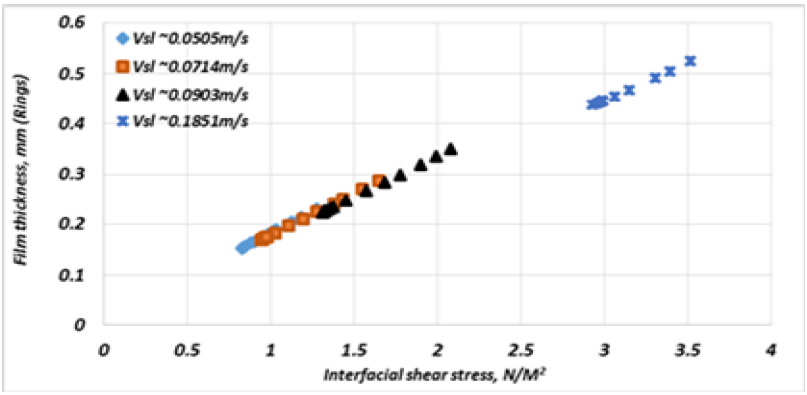

Figure 4.29: Film thickness against interfacial shear stress

The graph of interfacial shear stress against wave frequency in Figure 4.30, shows that the higher the interfacial shear stress, the lower the wave frequency as superficial liquid velocity of 0.0505m/s presents, the highest wave frequency while the superficial liquid velocity of 0.1851m/s has the lowest wave frequency. This means that, wave frequency decreases with increase in superficial gas velocity but increases with decrease in superficial liquid velocity. Also, the interfacial shear stress decrease with increase in wave frequency, and decrease in superficial liquid velocity. The reason is because wave amplitude increases with increase in superficial liquid velocity hence requires more energy from gas phase for wave movement (Mantilla, 2008), therefore the interfacial shear stress will be higher as seen in Figure 4.27.

Lastly, the higher the superficial liquid velocity, the higher the wave velocity and the lower the surface tension, hence the lower the wave frequency as fewer waves are presented in Figures 4.34, 4.38 and 4.40.

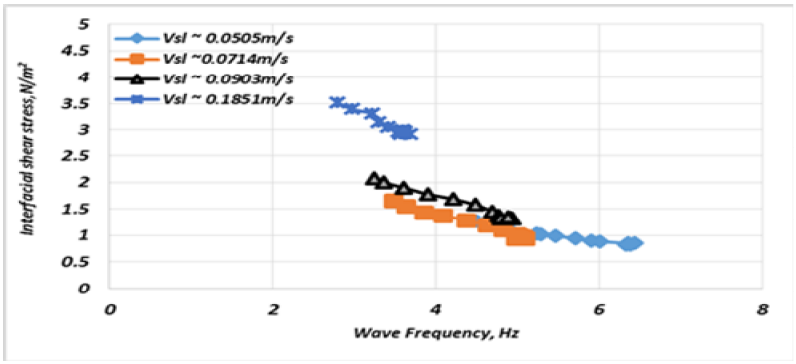

Figure 4.30: Interfacial shear stress against wave frequency

The graph of interfacial shear stress against interfacial friction factor illustrates a typical trend of increase in interfacial shear stress and interfacial friction factor with respect to superficial liquid velocity. This means that, the higher the superficial liquid velocity, the higher the interfacial shear stress and the higher the interfacial friction factor as Vsl =0.1851m/s presents the highest, while Vsl =0.0505m/s, the lowest from Figure 4.31. This is simply because, the higher the superficial liquid velocity, the higher the amplitude hence more interfacial transfer of mass, momentum and energy to liquid entrainment, therefore the higher the interfacial shear stress and interfacial friction factor.

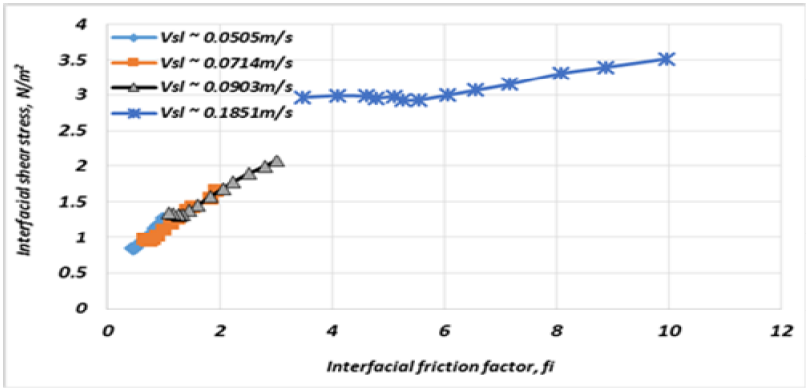

Figure 4.31: Interfacial shear stress against interfacial friction factor

Figure 4.32 of interfacial friction factor against wave frequency shows similar trend with figure 4.30. Superficial liquid velocity of 0.0505m/s has the highest

wave frequency and the lowest interfacial friction factor while 0.1851m/s has the highest interfacial friction factor but the lowest wave frequency.

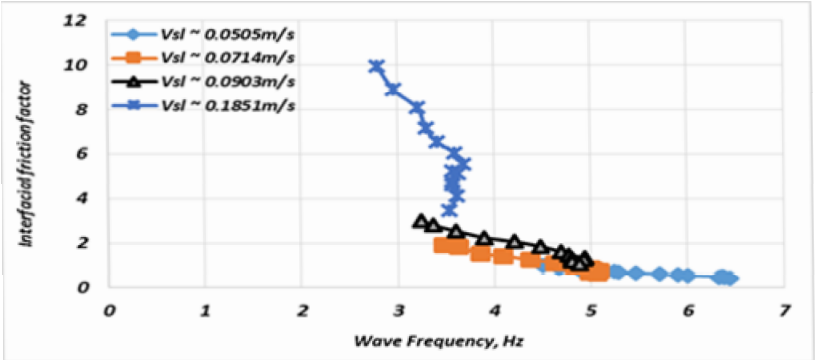

Figure 4.32: Interfacial friction factor against wave frequency

4.4 Probability Density Function/Void Fraction in Annular Flow

The void fractions against time in Figures 4.33 and 4.34 illustrates that, the lower the superficial liquid velocity the shorter the wave circle in the pipe as seen on Vsl=0.0508m/s, Vsg=10.0773m/s and likewise 0.0501m/s and Vsg=23.2796m/s respectively. While the higher the superficial liquid velocity, the longer the wave circle in horizontal pipes as shown on Vsl=0.1892m/s and Vsg=10.3927m/s as well as Vsl=0.1805m/s and Vsg=23.7259m/s respectively.

Probability time series describes the statistical distribution of the instantaneous film thickness. For Vsl=0.0508m/s with Vsg=10.0773 and 0.0501m/s with respect to Vsg=23.2796, Figures 4.33 and 4.34 have illustrated, that the lower the superficial liquid velocities, the higher the void fraction and thin the liquid film thickness in the pipe. As superficial liquid velocity increases, the void fraction likewise decreases while the film thickness increases. More details of the PDF and the void fraction analysis are presented in the Appendix (Table G-1.3). The PDF plot against void fraction in Figures 4.33 and 4.34, were used to further illustrate that the flow regimes were annular. The closer the PDF plot with Void fraction, the more uniform the flow as seen in Figure 4.33, while the more wider or spread with respect to void fraction, the more the disturbance flow in the pipe.

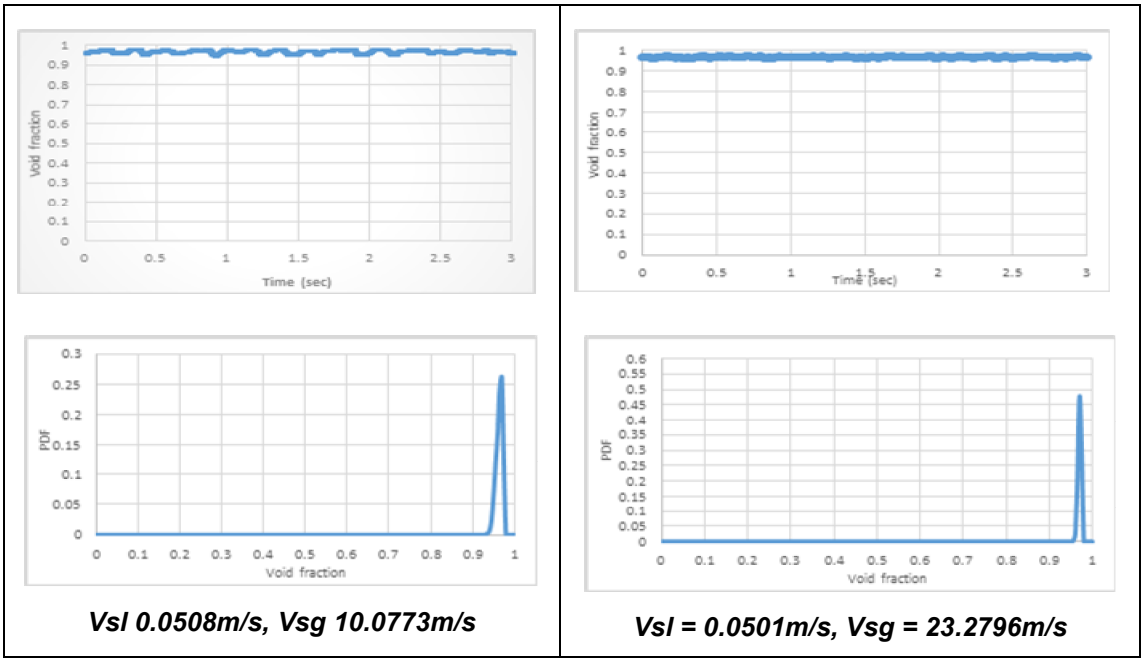

Vsl 0.0508m/s, Vsg 10.0773m/s

Vsl = 0.0501m/s, Vsg = 23.2796m/s

Figure 4.33: Vsl 0.0508m/s, Vsg 10.0773m/s Vsl = 0.0501m/s, Vsg = 23.2796m/s

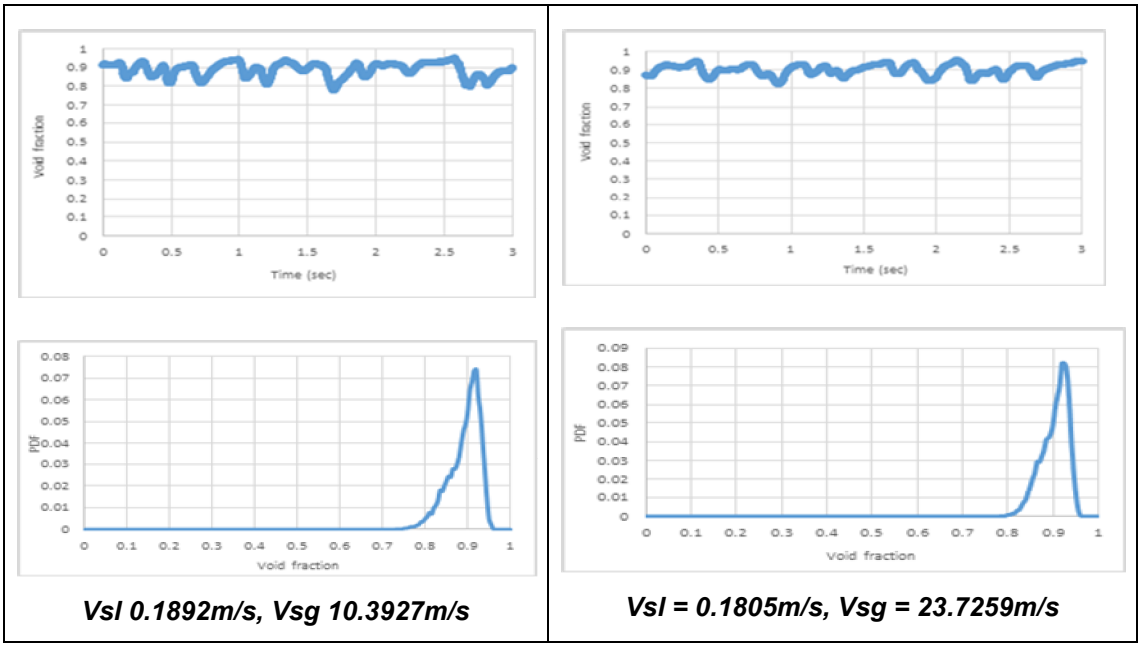

Vsl 0.1892m/s, Vsg 10.3927m/s

Vsl = 0.1805m/s, Vsg = 23.7259m/s

Figure 4.34: Vsl 0.1892m/s, Vsg 10.3927m/s Vsl = 0.1805m/s, Vsg = 23.7259m/s

4.5 Power Spectral Density Analysis on Film Thickness

In Figures 4.35 and 4.36 (a) and (b), presents the power spectral density (PSD) of the liquid film thickness with dominant frequency, where strong effect of gas flow rate with respect to wave energy, were felt.

Thus, dominant frequency goes with more disturbance waves that covers much portion of the pipe circumference, (Paras and Karabelas, 1991). As the superficial gas velocity increases, the wave also becomes more uniformly distributed around the pipe circumference.

Figures 4.35 and 4.36 (a) and (b), have illustrated that, increase in superficial liquid velocity, decreases wave amplitude and wave frequency (see Figure 4.15), as wave amplitude requires more energy from the phase to keep the wave in motion. In Figure 4.35, (a), the highest frequency was 6.5Hz, while in Figure 4.36 (a), the highest frequency was 6.2Hz. For more detailed analysis from the experiments, see Appendix G (Table G-1.4)

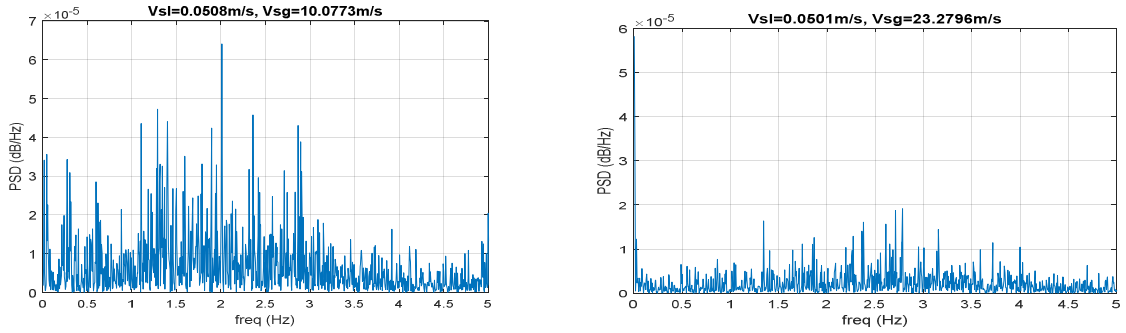

Figure 4.35: (a). Vsl = 0.0508m/s Vsg = 10.0773m/s (b). Vsl = 0.0501m/s, Vsg = 23.2796m/s

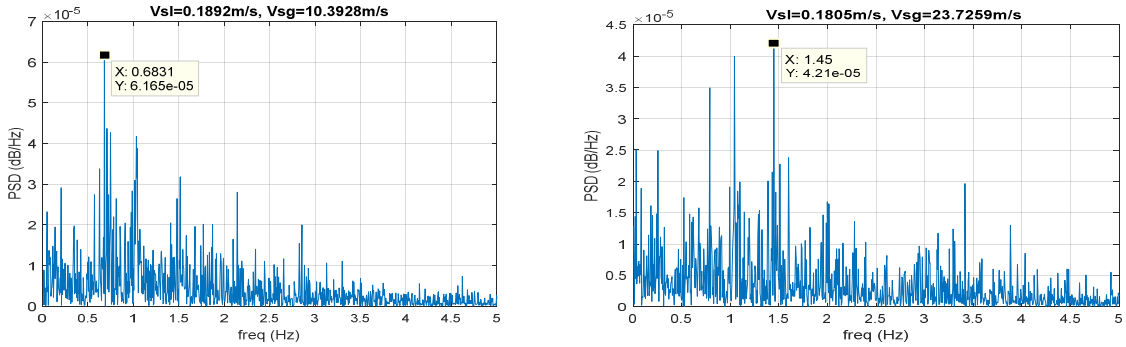

Figure4.36: (a). Vsl = 0.1892m/s Vsg = 10.3927m/s (b). Vsl = 0.1805m/s, Vsg = 23.7259m/s

4.6 Wavelet Analysis on Film Thickness

The essence of the wavelet is to present more insight on liquid film thickness signals in line with the power spectral density (PSD) graphs in Figures 4.35 and 4.36 (a) and (b), earlier presented. Again, wavelet is less complex compared to PSD, in analysing any experimental data on signals, as also noted by Jones and

Zuber (1975), Vince and Lahey (1982). Wavelet provides better understanding of time-resolved frequency information even with the aid of a scalogram, McClusky *et al.,* (2002).Wavelet analysis, comprises of various applications called wavelet family. They are Haar, Daubechies, Symlets, Coiflets, Biorthogonal, Reverse Biorthogonal, Meyer, Gaussian, Mexican, Morlet, Complex-Morlet (Gabor), Shannon, Fejer-Korovkin, etc. The choice from the family is based on accurate extraction of signals from your experimental data. In this study, the symlet application was used, and the results presented in Figures 4.37 and 4.38.

More so, the analysis in Figures 4.37 and 4.38 were based on continuous wavelet transforms (cwt) McClusky *et al.,* (2002), on the liquid film thickness signals in annular flow. The wavelet (cwt) was used on the liquid film thickness data to analyse:

- Frequency-time variation and,
- Scalogram.

The cwt wavelet on the film thickness analysis of each signal from the experimental data in Figures 4.37 and 4.38, covers (36011 data points) from a scan duration of 180s. The scalogram, presents a space (frame) on the abscissa using (**50 frame interval**) as **1s** with the frequency on the ordinate from 1-31, while the coloration represents the wavelet energy density.

The graph of Figure 4.37 (a) and (b) for superficial liquid and gas velocities of 0.0508m/s and 10.0773m/s and that of 0.0501m/s and 23.2796m/s presents, the magnitude of wavelet signals at a given time and frequency. The wavelet for Figures 4.37 (a) and (b) had illustrated further the liquid film thickness with respect time, with similar trend with the liquid film thickness in Figure 4.39. This has shown that at low superficial liquid and gas velocities of 0.0508m/s and 10.0773m/s and that of 0.0501m/s and 23.2796m/s, ripple waves were dominant.

According to McClusky *et al.,* (2002), the dominant frequency in the scalogram is attributed to passage of more gas bubble in the flow. The wave signals were more on the lower superficial liquid velocities. As seen in Figures 4.35 and 4.36 (a) and (b), the higher the superficial liquid velocity the more the wave signal decreases.

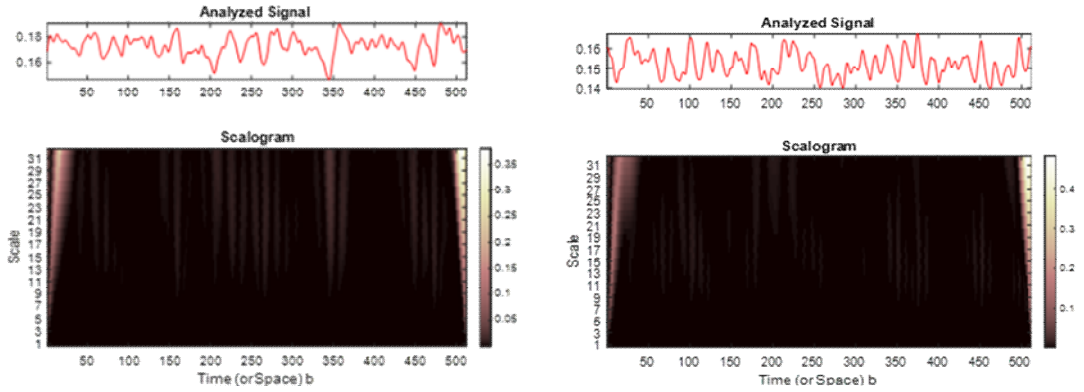

Figure 4.37: (a). Vsl=0.0508m/s, Vsg=10.0773m/s, (b). Vsl=0.0501m/s, Vsg = 23.2796m/s

The graph of Figure 4.38 has shown that the wave signal decreases with increase in superficial liquid velocity. This is also similar to the results of Figure 4.40 which is for liquid film thickness with respect to time. At this point, the liquid film has been distributed circumferentially across the walls of the pipes. The wavelet illustrated that at higher superficial liquid velocity, the higher the film thickness in the pipe. Again, the scalogram had shown the higher the superficial liquid velocity, the lower the wave frequency in line with Figure 4.15. More so, Figure 4.38 presented similar trend with Figure 4.40, showing a more spread (long lived) wave, high liquid film thickness, higher amplitude and low frequency from the scalogram. With these attribute, Figure 4.38 represents a disturbance wave in annular flow.

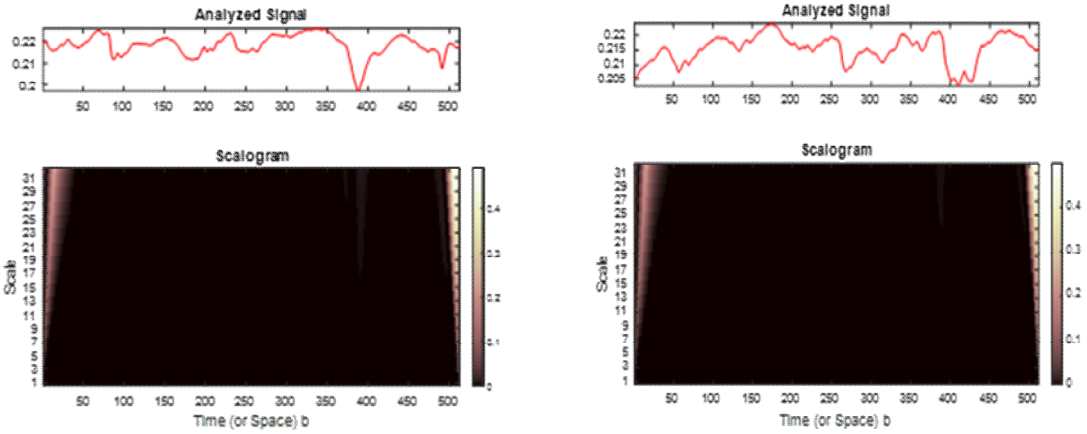

Figure 4.38: (a). Vsl=0.1892m/s, Vsg=10.3927m/s (b).Vsl=0.1805m/s, Vsg=23.7259m/s

4.7 Film thickness with time series analysis

The graphs of liquid film thickness with time in Figures 4.39 and 4.40, were used to further illustrate that annular-wavy flow conditions in horizontal pipes, decreases with increase in the superficial liquid velocity as similarly reported by Paras and Karabelas (1991). Thus, the liquid film thickness from superficial liquid velocity of 0.0508m/s presents high wavy flow at the bottom of the pipe compared to the liquid film thickness from superficial liquid velocity of 0.1892m/s. The reason is because of low impact of inertial forces, low velocity and surface tension influence at low superficial liquid velocity.

Further illustrations from the graph of Figure 4.39 has shown that, at low superficial liquid velocity, the ripple wave effect is prominent. From Figures 4.39, 4.40 (a) & (b), the waves were thickly dominant at the peak of an average liquid film thickness of 0.1892mm, while the waves were sparsely presented at an average liquid film thickness of 0.23mm, in all the flow conditions respectively. This has further ascertained that, there are more annular-wavy flow at lower superficial liquid and gas velocities as presented in Table 4.3 (chapter 4) from the visual observation results.

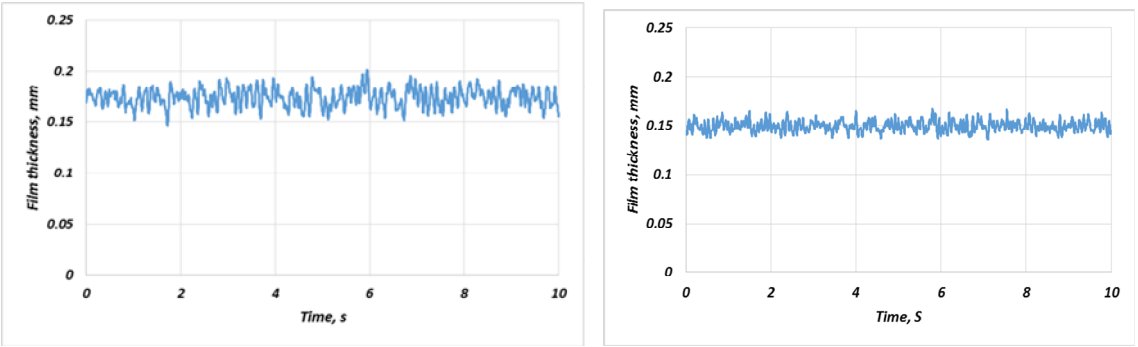

Figure 4.39: (a). Vsl = 0.0508m/s vsg =10.0773m/s (b). Vsl = 0.0501m/s Vsg = 23.2796m/s

Figure 4.40 (a) and (b), were graphs of liquid film thickness against high superficial liquid velocities with average Vsl of 0.1892m/s and 0.1805m/s and Vsg of 10.3927m/s and 23.7259m/s respectively. The results, presented a sparsely and great decrease in waves spikes compared to Figure 4.39 (a) and (b).

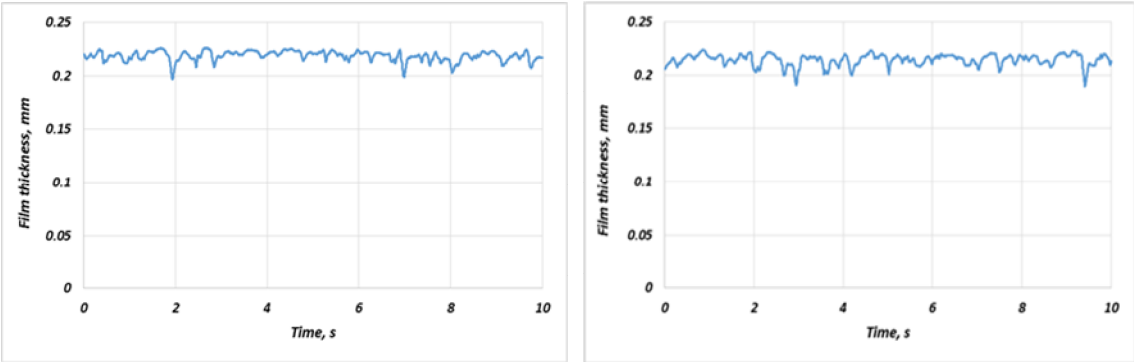

Figure 4.40: (a). Vsl=0.1892m/s, Vsg=10.3927m/s (b). Vsl=0.1805m/s, Vsg=23.7259m/s

4.7.1 Pressure Gradient and Superficial Gas Velocity

The graph of pressure gradient against superficial liquid velocity for 0.0505m/s as obtained from the experimental results, is presented in Figure 4.41: The results were preferably in match with Dukler *et al.,* (1964) and Beggs & Brill (1973) correlations for annular flow in horizontal pipes.

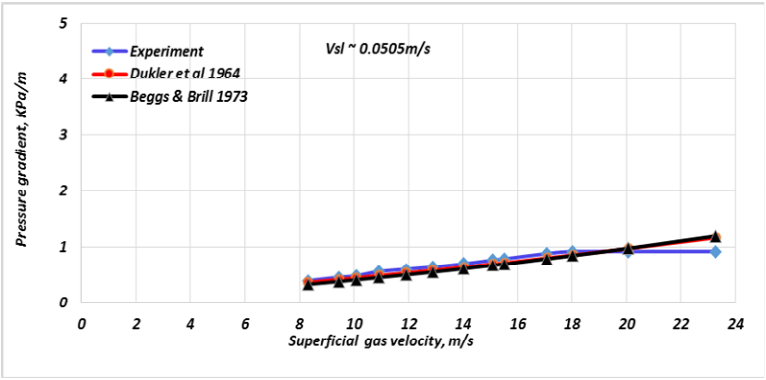

Figure 4.41: Pressure gradient Vs Superficial gas velocity (Vsl ~0.0505m/s)

The experimental result of pressure gradient in Figure 4.42 also matched with the correlations of Dukler *et al.,* (1964) and Beggs & Brill (1973). It shows that pressure gradient increases with increase in superficial gas velocity and also with increase in superficial liquid velocity.

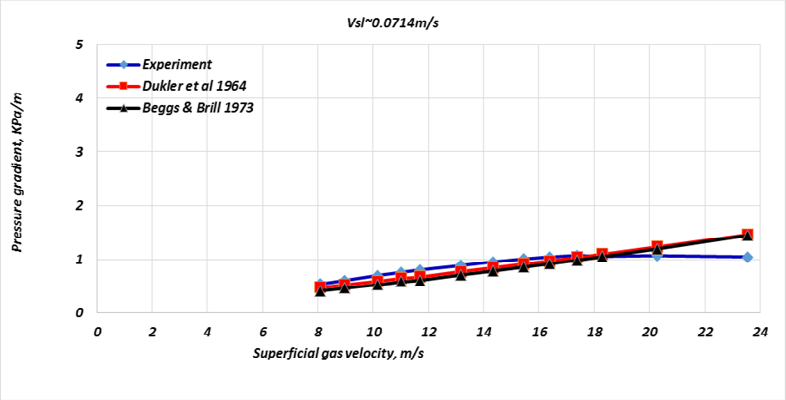

Figure 4.42: Pressure gradient Vs Superficial gas velocity (Vsl ~ 0.0714m/s)

Also the pressure gradient from Figure of 4.43, matched preferably with that of Dukler *et al.,* (1964) and Beggs & Brill (1973). However, the slight decline from the pressure gradient from the experiments could be attributed to the fact that the wave reduces at that point hence less pressure losses were also recorded. It is an indication of less friction loss. This is also shown in Figure 4.15, where the wave frequency were no longer increasing with increase in the superficial gas velocity, but rather becoming a uniform straight plan.

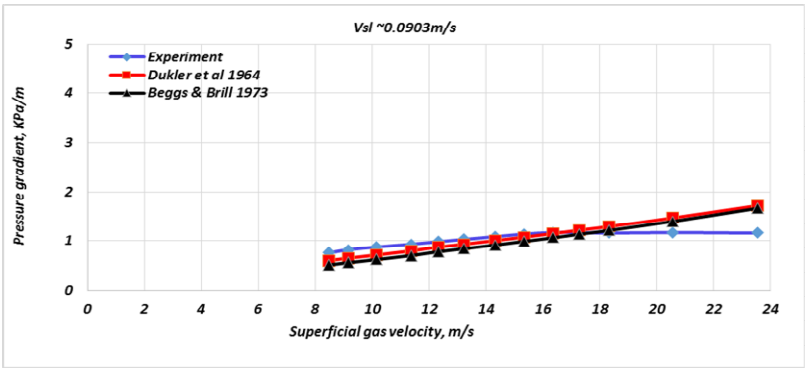

Figure 4.43: Pressure gradient Vs Superficial gas velocity (Vsl ~ 0.0903m/s)

Figure 4.44 also shows a good match apart from the decline in the experimental result plot. The little upward projection was as an increase in the superficial liquid velocity from 0.1264m/s to 0.1482m/s, which were evidenced in the plots of the experiments (measured) and the predictive pressure gradient correlations.

The further decline of the experimental pressure gradient plot, compared to the predicted Dukler *et al.,* (1964) and Beggs & Brill (1973) was simply to show, that

at high superficial gas velocity the pressure losses decreased as wave frequency, no longer impact on the changes. The Dukler *et al.,* (1964) and Beggs & Brill (1973) over predicted it the measured pressure gradient.

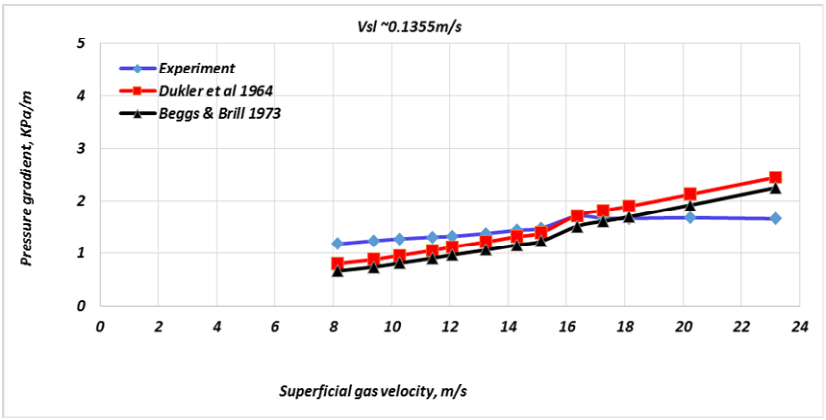

Figure 4.44: Pressure gradient Vs Superficial gas velocity (0.1355m/s)

From Figure 4.45, the experimental pressure gradient presented the same trend with Figures 4.38 and 4.40 which simply illustrated that the wave decreased as the superficial liquid velocity increases. This means, the pressure gradient also decreased as pressure losses were minimised. Therefore, Dukler *et al.,* (1964) and Beggs & Brill (1973) over-predicted.

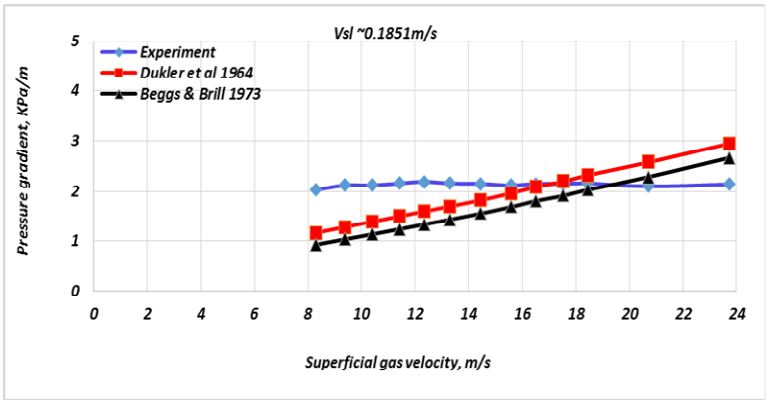

Figure 4.45: Pressure gradient Vs Superficial gas velocity (Vsl~0.1851m/s)

The performance graph of Figure 4.46 clearly presented how preferably the predicted Dukler *et al.,* (1964) and Beggs & Brill (1974) matched the experimental pressure gradient. Except for the results of average superficial liquid velocities of 0.1355m/s and 0.1851m/s which under estimated and slightly over estimated the measured pressure gradient results. The predictive correlations were able to

match better in the case of Vsl=0.0505m/s, 0.0714m/s and 0.0903m/s. The reason is simply because the pressure gradients were not much because of the impact of the gas velocity hence much wave were also observed as seen in Figures 4.37 and 4.39.

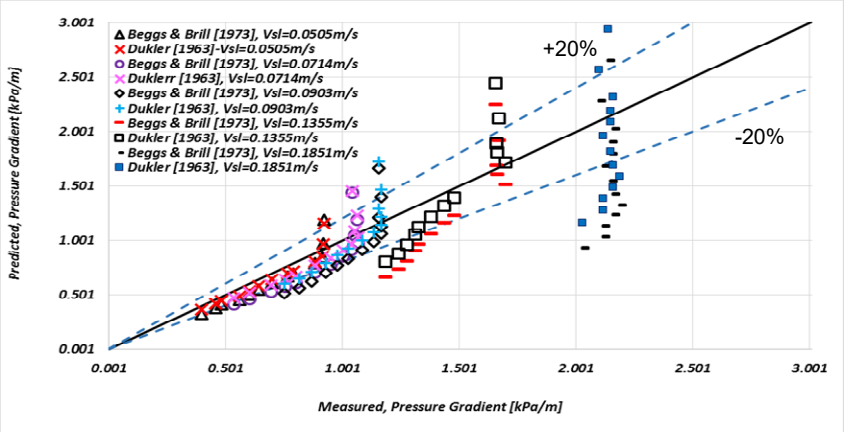

Figure 4.46: A Plot of Predicted against the Experimental Pressure Gradient

Higher slippage in fluid flow signifies resistance of the liquid phase in the pipeline. Therefore Figure 4.47, illustrates that in annular flow, more slippage occurs at low superficial liquid velocity. The film thickness is very thin therefore will create more wall shear stress, more wave but less interfacial shear stress in the flow hence the wave oscillation circle is short. Therefore, the pressure gradient will be low while the slip will be high as presented in Figure 4.47.

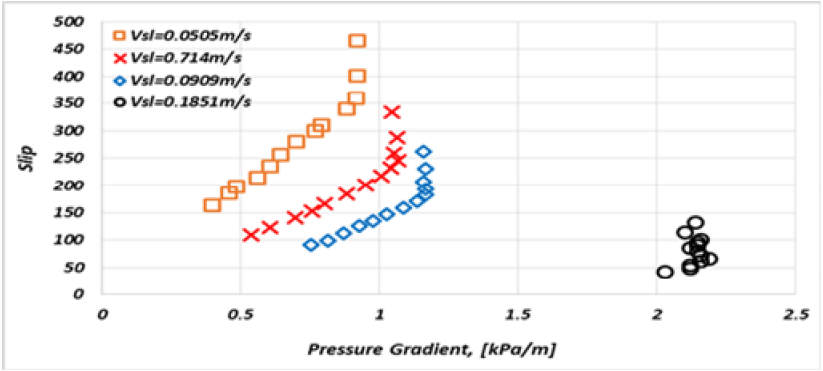

Figure 4.47: A Plot of Slip against Pressure Gradient, [kPa/m]

The graph of Figure 4.48, also illustrated that annular in pipe is a non-homogenous flow. Slip ratio increases with increase in superficial gas velocity. Although, plot of average Vsl of 0.0714m/s, 0.0903m/s, 0.1355m/s and

0.1851m/s converged and crosses each other as the Vsg increases from Vsl=16.3867m/s. This means at higher superficial liquid velocity, there are negligible changes in slip ratio in annular flow as annular flow is fully established and the flow behaviour tends to be the same in the pipes as the disturbance wave, takes the centre stage with the film circumferentially flowing across the walls of the pipes from Vsg of 14m/s.

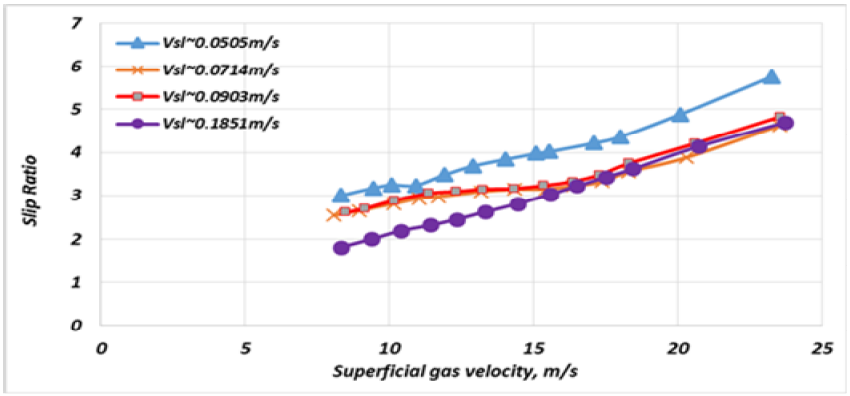

Figure 4.48: A Plot of Slip Ratio against Superficial Gas Velocity.

4.8 Chapter Summary

Water/air annular flow experiments, were conducted with analysed results presented to show that annular flow could be attained from a superficial gas velocity of 8m/s in the pipe with high superficial liquid velocity of 0.0903m/s. The detailed annular flow behaviours revealed that at low superficial gas and liquid velocities, annular flow behaves as annular-wavy flow in the pipe while at high superficial gas and liquid velocities such tendencies, do not exist. In the flow conditions analysed, more liquid film thickness were presented at the bottom of the pipe with wavy flow structures at the upper walls of the pipe as in Figures 4.7 and 4.8.

To understand the dynamics of annular flow in pipes: annular flow characteristics like liquid film thickness, wave velocity, wave frequency, interfacial friction factor, pressure gradient were analysed. Liquid film thickness in all the flow matrix in this study were observed decreasing with increase in gas velocity while increasing with increase in liquid velocity. The decreasing tendency with gas velocity was because of liquid entrainment. The liquid entrainments, were accounted for using

Pan and Hanratty (2002b) correlation. The correlation gave the more realistic results among other correlations compared from the experimental data. This was further proven by Magrini *et al.,* (2012) analysis on liquid entrainment correlations for horizontal pipes where Pan and Hanratty (2002b) was presented as a correlation that preferably, predicts liquid entrainment.

Wave velocity and wave frequency also increases with increase in superficial gas velocity in annular flow. For wave frequency, it was observed that both superficial liquid and gas velocities have great impact on wave frequency against the observation noted by Setyawan et al., (2014) that superficial liquid has negligible effect. In annular flow in horizontal pipe, it was also observed that the lower the superficial liquid velocity, the lower the amplitude and the higher the wave frequency. This is because more ripple waves occur at low liquid velocity hence more energy is used that results to high frequency. However, several correlations were compared with the obtained wave frequency in this study, but Al-Sarkhi *et al.,* (2012) preferably matched better as the superficial liquid velocity increases from 0.0903m/s to 0.1851m/s.

Also, the pressure gradient, interfacial friction factor and interfacial shear stress were presented, using experimental measured data. For interfacial friction factor and interfacial shear stress, it was observed that they decrease, with increase in superficial gas velocity. This is because of interfacial mass transfer, momentum change and more energy dissipated which aid in more liquid entrainments as the superficial gas velocity increases. Again, the higher the superficial liquid velocity, the higher the interfacial friction factor and the interfacial shear stress in annular flow in horizontal pipe as presented in this study.

On the probability density function (PDF) and wavelet (Symlet) analysis, it was presented that the lower the superficial liquid velocity, the higher the ripple waves while the higher the superficial liquid velocity, the more the disturbance waves as shown in Figures 4.37, 4.38, 4.39 and 4.40. More importantly, the power spectral density (PSD) had shown that in annular flow in horizontal pipes, more energy is dissipated with the dominant frequency showing the strong effects of superficial gas velocity in the flow.

5 Sand Transport Flow Results

5.1 Water/Sand Flow Test (Visual Observation)

Single-phase flow experiments with sand was carried out using a 2-inch flow loop, to investigate sand behaviours in the pipes. In the experiments, sand particles of 500microns and 200microns and sand concentration of 200lb/1000bbl and 500lb/1000bbl were used. The flow regimes (sand) presented were: saltation, scoring and sand dune in both 200microns and 500microns.

One other observation, was that of 500microns where the sand dune recorded, was different from the sand moving dune in that of 200microns with respect to superficial liquid velocity. In 500microns, the sand dune, was presented at superficial liquid velocity as low as 0.0980m/s while that of 200microns, sand dune was recorded at 0.1210m/s. This is because of gravity effect that acted on the larger particles' size of 500microns.

Table 5.1: Water/Sand Test with Flow Regimes.

Sand Concentration	***200 microns***	***VSL [m/s]***
200lb/1000bbl	Saltation	*0.1403-0.2100*
	Scoring	*0.2925-0.3241*
	Dune	*0.1910-0.2739*
	Sand Bed	*0.1105-0.1908*
	500 microns	***VSL [m/s]***
500lb/1000bbl	Saltation	*0.1120-0.2127*
	Scoring	*0.2110-0.2652*
	Dune	*0.0980-0.2102*
	Sand Bed	*0.0581*

As seen in Table 5.1, the flow regime obtained were saltation, scoring, dune, and sand bed. Again, the above sand flow regime shown in the Table are further expatiated below:

The picture in Figure 5.1, is sand bed from the experiments. Because of low superficial liquid velocity, the sand were presented as bed at the bottom of the pipe. This is quite similar to the experimental results of Angelson *et al*., (1989) where sand bed was observed also at low superficial liquid velocity of 0.1507m/s. Though, there is a stable height of the sand bed from Figure 5.1, but at the top of the sand bed (height), sand particles were rolling in the direction of liquid flow in the horizontal pipe. This is because of the water movement in the pipe.

Figure 5.1: Sand bed for 200microns at bottom of pipe (Vsl =0.1208m/s).

As the superficial liquid velocity increases, the sand bed becomes a moving dune. At average superficial liquid velocity of 0.1910m/s, the 200microns sand particles became a slow moving dunes as presented in Figure 5.2 which is also close to Angelson *et al.,* (1989) results on moving dune.

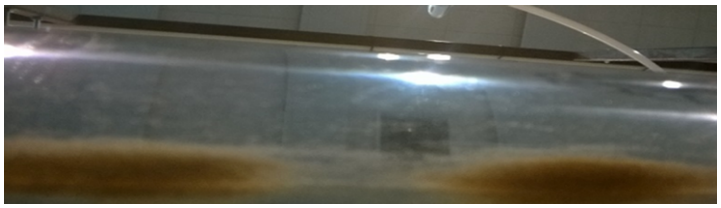

Figure 5.2: Moving dune at bottom of pipe (Vsl = 0.1910m/s)

With more increase in superficial liquid velocity to an average of 0.3241m/s, sand particles moved in close proximity, on the walls of the pipe in a scouring manner as presented in Figure 5.3 in this work.

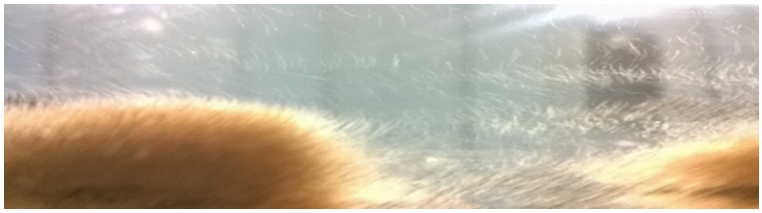

Figure 5.3: Sand scoring for 200microns at bottom of pipe (Vsl = 0.3241m/s)

The entire results from Figures 5.1, 5.2 and 5.3 were compared with that of Angelson *et al*., (1989). However, the results from this study were in proximity with the presented results of Angelson *et al*., (1989) as shown In Table 5.2 and Figure 5.4 even though their results, were presented from an experiment carried out using 1-inch pipe.

Table 5.2: Study Results compared with Angelson et al., (1989) Results

Experimental Results	***Angelson et al (1989) using 1-inch with 200microns***	***This Study (2-Inch) 200microns (200lb/1000bbl)***	***Average of This Study***
Sand Bed	*0.15m/s*	*0.1105-0.1908*m/s	*0.1507m/s*
Moving Dune	*0.15-0.3m/s*	*0.1910-0.2739*m/s	*0.2325m/s*
Scouring	*0.35m/s*	*0.2925-0.3241*m/s	*0.3083m/s*

Table 5.2 is the comparison results of the study with the reported results of Angelson *et al.,* (1989). The little difference from the average results on moving dune and sand scouring could be attributed to the difference in pipe diameter used.

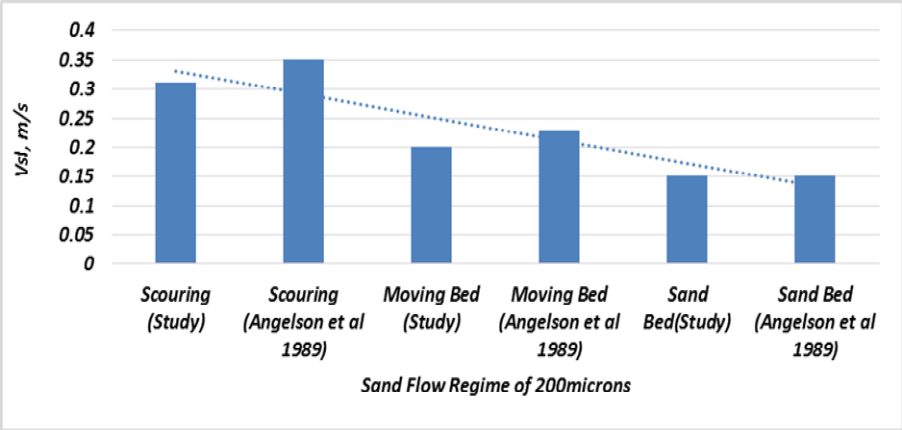

Figure 5.4: Comparing sand flow regime (200microns) with Angelson et al., (1989)

The bar chart of Figure 5.4 is to show the entire results of this study and Angelson *et al.,* (1989). Both experiment were carried out using sand particles' size of 200microns but different pipe diameters as indicated in Table 5.2 respectively. In

comparison, the results were fairly close irrespective of the difference in the pipe diameters of 2-inch in my study to 1-inch used by Angelson *et al.,* (1989).

The minimum transport velocity condition (MTC) from Table 5.3 increases, as sand particles and sand concentration increases. From sand particles size of 150microns to 200microns on the same sand concentration of 500lb/1000bbl, MTC increased from 0.2330m/s to 0.3142m/s. This means that, the higher the sand concentration the higher the particle-particle interactions in the system and the higher the minimum transport velocity. Also, MTC or critical velocity increases as sand particle sizes increases as presented in Table 5.3 because large particles create more frictions and increase in drag forces in the pipe as noted by Kamyar *et al.,* (2015).

Table 5.3: Water/Sand Flow Experimental results (MTC)

Sand Concentration	*Sand Particle Sizes (Microns)*	*MTC (m/s)*
200lb/1000bbl	*500*	*0.2602*
500lb/1000bbl	*200*	*0.3142*
500lb/1000bbl	*150*	*0.2330*

5.2 Water/Sand Flow Test (Instrumentation)

Sand transport in single-phase flow was carried out using a 2-inch flow loop shown in Figure 3.1 with the aid of 2 pairs of conductivity probes: S1 (upstream), and S2 (downstream) installed at 0.20m apart at the bottom of the horizontal pipe (see Figure 3.1). During the experiment, empty pipe and full pipe with water were recorded for the purpose of normalizing the experimental results. This was indeed repeated on every experiment carried out on daily basis and mathematically expressed as:

$$N = \frac{V_{two-phase} - V_{empty}}{V_{fullpipe} - V_{empty}} \quad \textbf{(5-1)}$$

Where N is for normalized Voltage of (S1, S2 or C1, C2), $V_{two\text{-}phase}$ is the voltage of the two-phase experimental, V_{empty} is for voltage of empty pipe and $V_{full\text{-}pipe}$ is for full water voltage of the calibration pipe.

In the experiments, the data were recorded based on: sampling rate (200Hz) and scan duration (120s) for single-phase with sand, while 180s-water/air/sand in annular flow. The scan duration was 120s because it was a single-phase flow and could attain steady-state flow easily hence there was no gas involved. The normalized voltage against time series are shown below with the left-hand side as snapshot from Sony camera used during the experiment.

The graph of Figure 5.5 shows a sand dune from conductance probe used. The graph shows that at the beginning time, the sands were rolling until a dune was formed between 60s and 115s in the pipe. This was also presented by Angelson *et al.,* (1989) as a rolling bed that breaks into a slow moving dunes. The dip signifies that more sand particles were compacted in that region which increases the resistivity of the probe at that region.

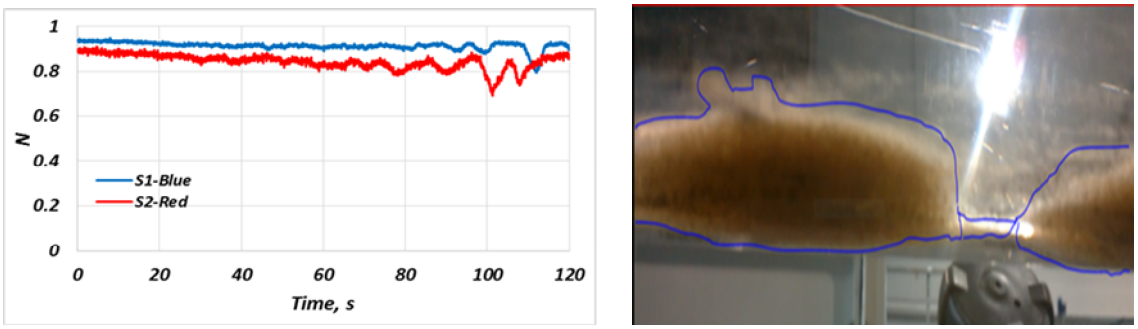

Figure 5.5: Sand dune, Vsl = 0.1504m/s (212microns, 200lb/1000bbl) - both are same

The graph of Figure 5.6 illustrates a typical saltation flow of sand in a pipe. The sand particles are not close but rather scattered as they keep bouncing or jumping in motion along the bottom of the pipe as presented also by Wicks (1971). Again, from Figure 5.6, the upstream probe (S1, blue) and the downstream probe (S2, red) were seen with little spike in a straight line manner with little dip along spikes which justifies saltation in the sand flow regime in the pipe.

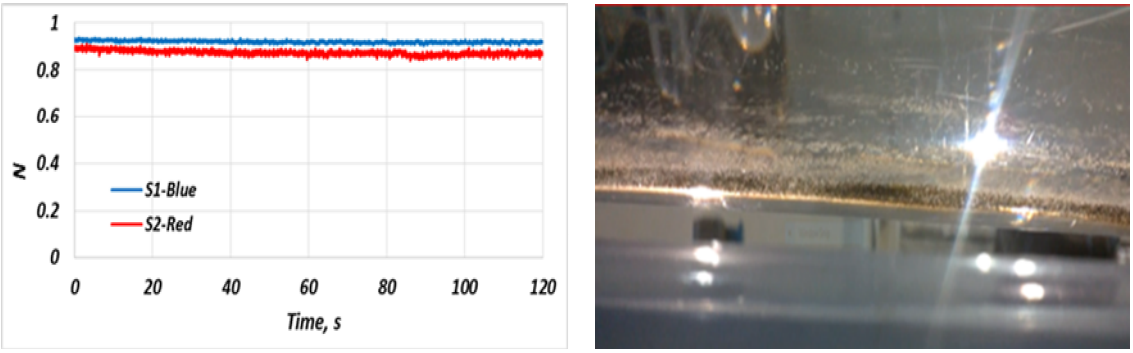

Figure 5.6: Saltation, Vsl = 0.1775m/s (212microns, 200lb/1000bbl) - both are same

As superficial liquid velocity increases from 0.18m/s to 0.20m/s, the flow regime changes from saltation to streaks. It means, that majority of the sand particles came in close proximity unlike saltation with the walls of the pipe as they scours along the bottom of the pipe. Again, from the graph of Figure 5.7, you could easily point out the difference from that of saltation. In this graph of figure 5.7, the spikes of both probes (S1, blue) and (S2, red) are with little or no dip on it unlike that of figure 5.6 where there are little dip on it.

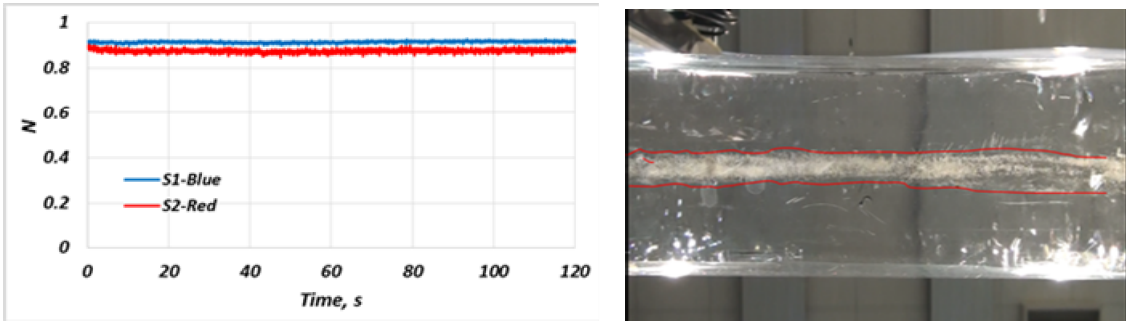

Figure 5.7: Streaks, Vsl =0.1967m/s (212microns, 200lb/1000bbl)

In the case of figure 5.8 with a superficial liquid velocity of 0.2427m/s, the spikes from both probes (S1, blue) and (S2, red) became more fused together compared to the previous graphs of figure 5.5, 5.6 and 5.7. From graph of Figure 5.8, the sand particles became fully suspended in the liquid flow in horizontal pipe.

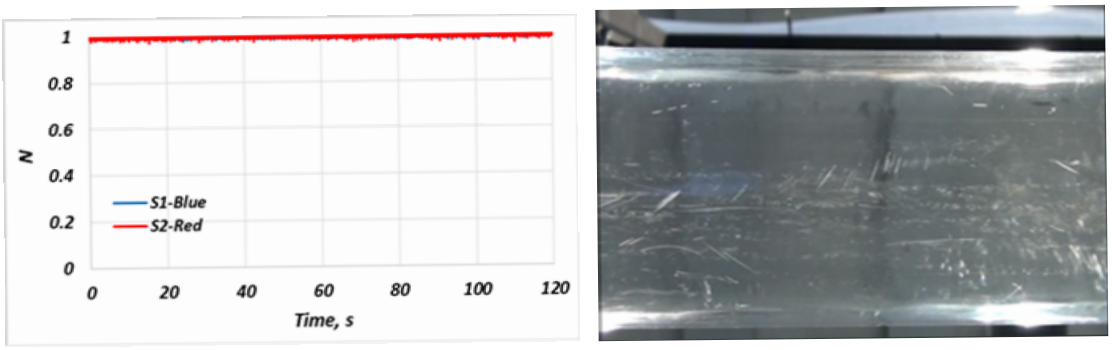

Figure 5.8: Suspension, Vsl 0.2427m/s (212microns, 200lb/1000bbl)

In Figure 5.9, the resistivity effects of the sand probe were felt more as it presents more signals of a sand dune in the pipe. It is because the sand particles' sizes are higher compared to 212microns. However, gravity effect aided in the sand particles as a result of its sizes as more were found in the picture on the left-hand side of Figure 5.9. The dip on the normalized voltage against time series were a typical sand dune as a of result resistivity effect of the probe.

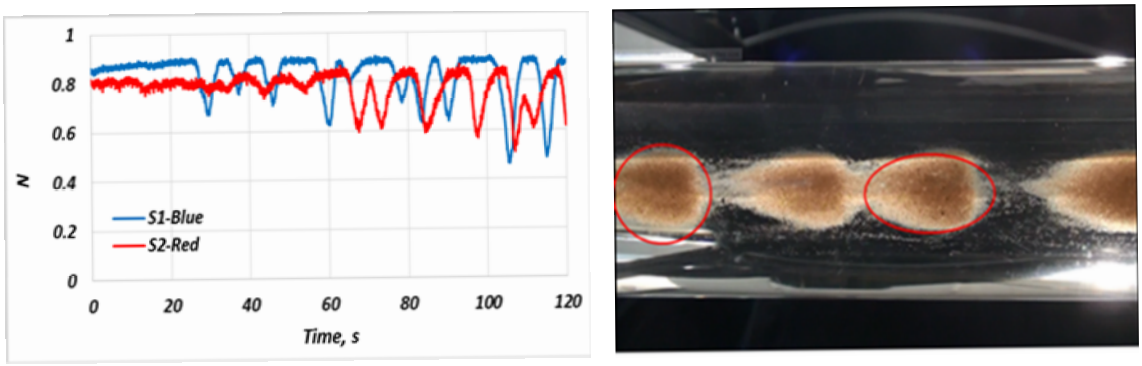

Figure 5.9: Sand dune, Vsl = 0.1527m/s (500microns, 200lb/000bbl) - both are same

Saltation was more pronounced in Figure 5.10 compared to Figure 5.6, because of the particles' size used. 500microns exhibited more gravity effect compared to the particle size of 212microns, hence more of the sand particles were felt by the probe compared to Figure 5.6 where the dips on the graph were less. Thus, more sand particles were found bouncing at the bottom of the pipe in Figure 5.10, hence the dip recorded by both probes.

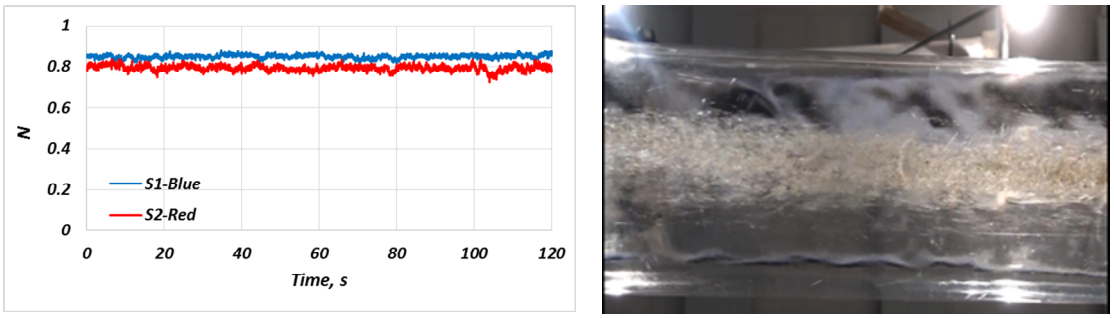

Figure 5.10: Saltation, Vsl = 0.1783m/s (500micron, 200lb/1000bbl)

Sand streaks were recorded as superficial liquid velocity increases. Majority of the sand particles were in proximity with the walls as they scour along the bottom of the pipe.

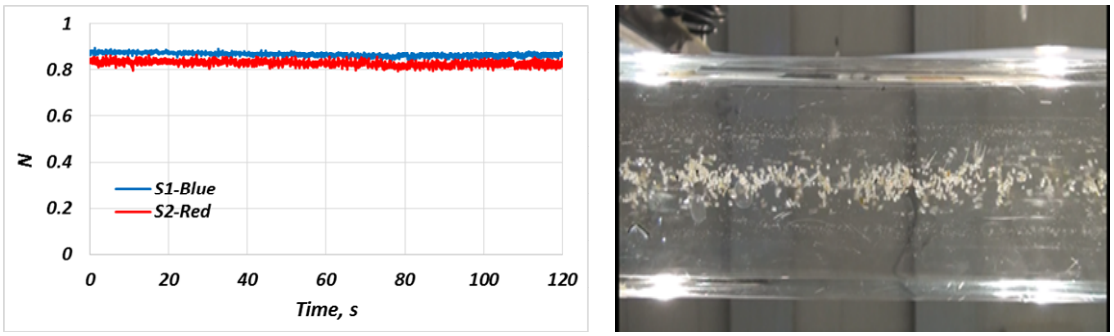

Figure 5.11: Sand Streak, Vsl = 0.1949m/s (500microns, 200lb/1000bbl)

Suspension was fully recorded at superficial liquid velocity of 0.25m/s. At this point, the spikes from both probes of S1 (blue) and S2 (red) fuses together with no dip observed. The sand particles were fully suspended in the liquid flow in the horizontal pipe

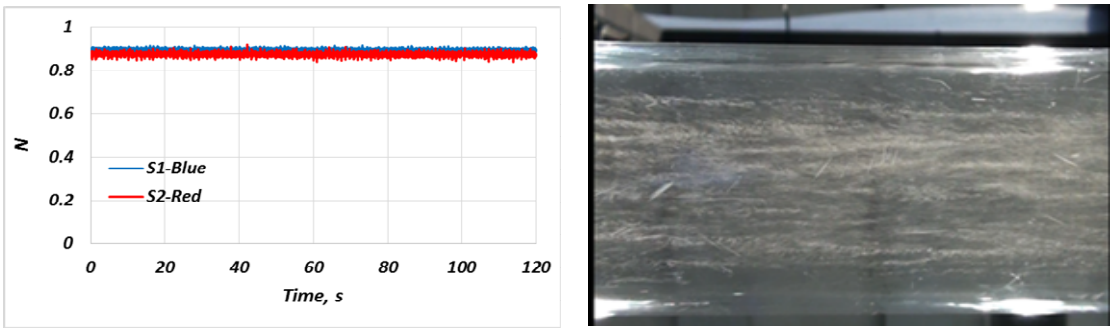

Figure 5.12: Suspension, Vsl = 0.2486m/s (500microns, 200lb/1000bbl).

Figure 5.13 was a case of high sand concentrations and sand particles' size. The graph shows the spikes from both probes with many dips representing sand dune at the bottom of the pipe. The effect were felt much with little gap between the two probe of S1 (blue) and S2 (red) which illustrates that sand particles were accumulated between saltation were seen at the tail end. Meaning, the sand particles started bouncing much later with aid of the liquid velocity in the pipe.

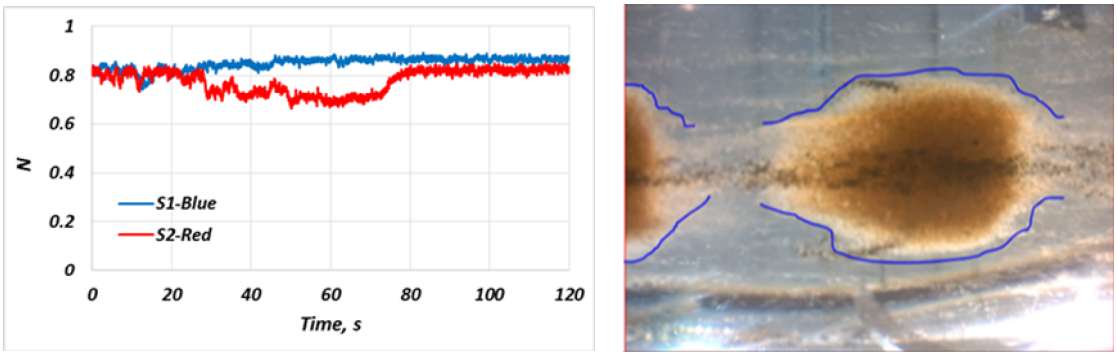

Figure 5.13: Sand dune/saltation, Vsl = 0.1481m/s (500microns, 500lb/1000bbl)

Saltation as presented from the graph of Figure 5.14 with sand particles' size of 500microns and sand concentration of 500lb/1000bbl in the pipe. According to Wicks (1971), gravity effect and buoyancy forces with increase in the liquid velocity aids sand particles to be bouncing or sliding even with the sizes are bigger.

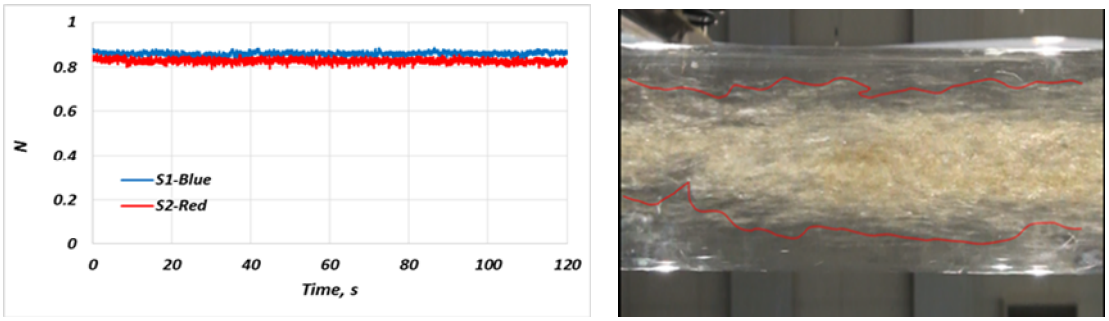

Figure 5.14: Sand Saltation, Vsl = 0.1772m/s (500microns, 500lb/1000bbl)

Sand streaks were recorded from the graph of Figure 5.15. Though, with the two probes fusing together as a result of the sand particles bouncing. The little dip on the spikes means, there were resistivity effects from the sand particles, hence the probes recorded more number of sand at that point.

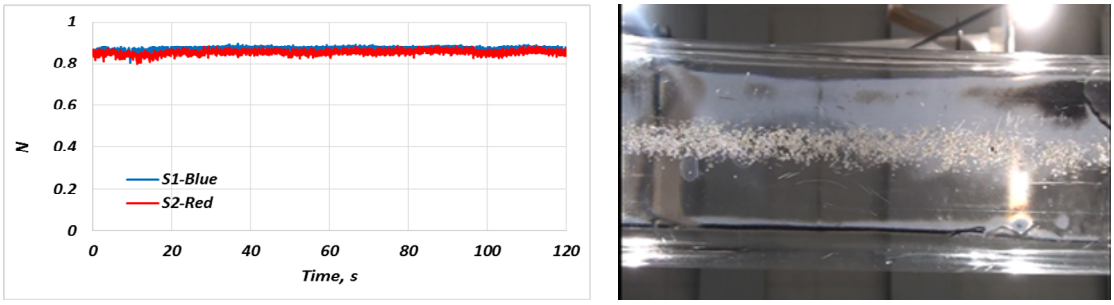

Figure 5.15: Sand Streaks, Vsl = 0.1931m/s (500microns, 500lb/1000bbl)

The graph of Figure 5.16 shows that the flow regime was a full suspension of sand flow in the pipe. The spikes even with the high sand concentration and particles' sizes, still shows similar trend as that of Figure 5.12 with sand concentration of 200lb/1000bbl and Figure 5.8 which was 200lb/1000bbl of sand concentration.

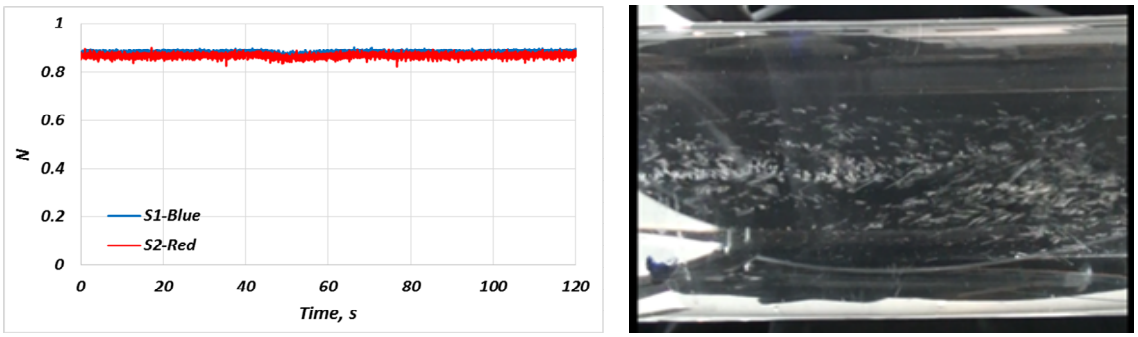

Figure 5.16: Sand Suspension, Vsl = 0.2466m/s (500microns, 500lb/1000bbl)

.

5.3 Water/Air/Sand Annular Flow (instrumentation)

Water/air/sand annular flow experiments were conducted using superficial gas velocities between 8.0959m/s to 15.9312m/s and superficial liquid velocities (0.0922m/s-0.1343m/s) respectively. The sand particle's sizes and concentration used were: 212microns-200lb/1000bbl, 212microns-500lb/1000bbl and 500microns-500lb/1000bbl.

On the experimental set up, the same 2-inch sand flow loop in Figure 3.1 was used with two film thickness probes (conductivity probes) of S1 (upstream) and S2 (downstream) installed at the bottom of the pipe to detect sand transport/behaviour in the horizontal pipe. Also, the experimental set-up was installed in a Labview with the following conditions being applied: scan rate (1000Hz), sampling rate (200Hz) and scan duration (180s). Scan duration of 180s was used to enable the flow attain steady-state flow conditions in the pipe.

5.3.1 Sand Flow Regime/Behaviour in Annular Flow

From the experiments, the two probes of S1 (blue) and S2 (red) spikes look widely spread compared to the single-phase of water/sand, earlier presented. This is because of much effect of the superficial gas velocity which is the dominant phase in annular flow compared to the single-phase where there is no gas involved. The liquid and the sand in the pipe with the aid of the dominant gas phase tend to behave like bubble of gas across the walls of the pipe thereby resulting to the broad spread of spikes presented in the following graphs of Figures 7.1 to 7.6. The reason is because gas is dominant and as well dissolves more in the liquid phase as bubble, thereby weaken the viscosity tendency of the water. Through, break-up and droplet lifting mechanism, the liquid spreads across the pipe as droplets or bubbles with thin film at the bottom depending on the superficial liquid velocity.

The graph of Figure 7.1 (a) is that of Vsl=0.1126m/s and Vsg=9.3775m/s. The sand particles were 212microns with sand concentration of 200lb/1000bbl, while Figure 7.1 (b) is that of water/air without sand. From the superficial velocities of both graphs of figure (a) and (b) which seems similar, the normalized volts of the

probes S1 (blue) and S2 (red) against time should have also shown similar spikes hence both were from the same probes at the bottom of the pipe. This is to show that the probes detected sand transported that is the reason while Figure 5.17 (a) has a different signals/spikes from Figure 5.17 (b) even when the superficial velocities were almost the same. Comparing the graph of Figure 5.17 (a) with the previous graphs of Figure 5.6, 5.10 and 5.14, then the flow regime (sand) could be presented as sand saltation. Irrespective of the high superficial gas velocity, the sand has been seen moving as sand saltation. Again, Figure 5.17 (a) has more spikes compared to Figure 5.17 (b) because the sand concentration in Figure 5.17 (a) has changed the flow density, hence more energy was dissipated to keep the flow in motions.

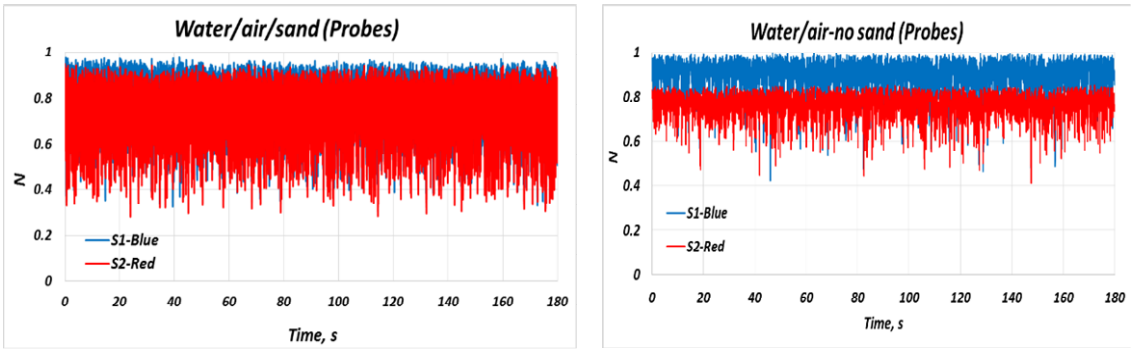

(a). Vsl = 0.1126m/s Vsg = 9.3775m/s ***(b) Vsl=0.1275m/s, Vsg = 9.3771m/s***

Figure 5.17: (a) Sand Saltation (212microns, 200lb/1000bbl) (b) Water/air-no sand

The graph of Figure 5.18 (a) still shows that the probes were detecting sand saltation in the liquid film at the bottom of the pipe. Though, Figure 5.17 (a) had a mild spikes which also depicts sand saltation but it is more pronounced in Figure 5.18 (a) even with dip on the upper surface of the plot which indicates that sand saltation was detected by the probes. Thus, Figure 5.18 (b) should have shown the same spikes (signals) with Figure 5.18 (a), if the probes were not detecting sand particles in the flow. In this case, both plots were seen different even when the superficial liquid and gas velocities were similar to have shown similarity in the signals/spikes hence they were from the same probes of S1 (blue) and S2 (red). This has proven that the probes actually detected sand particles irrespective of the high superficial gas velocity in annular flow.

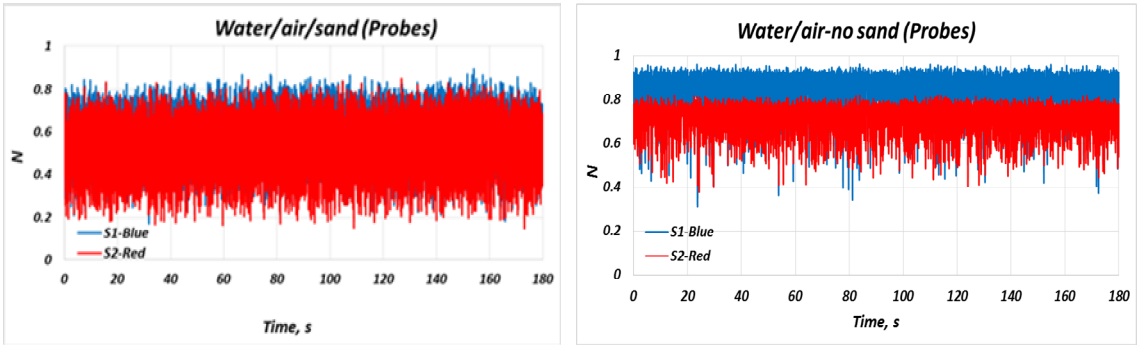

(a). Vsl = 0.1145m/s Vsg = 14.9179m/s (b) Vsl = 0.1269m/s, Vsg = 14.2926m/s

Figure 5.18: (a) Sand saltation (212microns, 200lb/1000bbl) (b) Water/air-no sand

The graph of Figure 5.19 (a) has sand particle size of 212microns with sand concentration of 500lb/1000bbl. The trend is not different from the previous ones seen in figures 5.17 and 5.18 respectively. The sand flow regime is that of saltation in liquid film at the bottom of the pipe. Figure 5.19 (b) shows that the blue and the red spikes were being detected in similar manner like sand, but the normalized volts from the plot were different from plot (a) indicating that (a) was detected and particles.

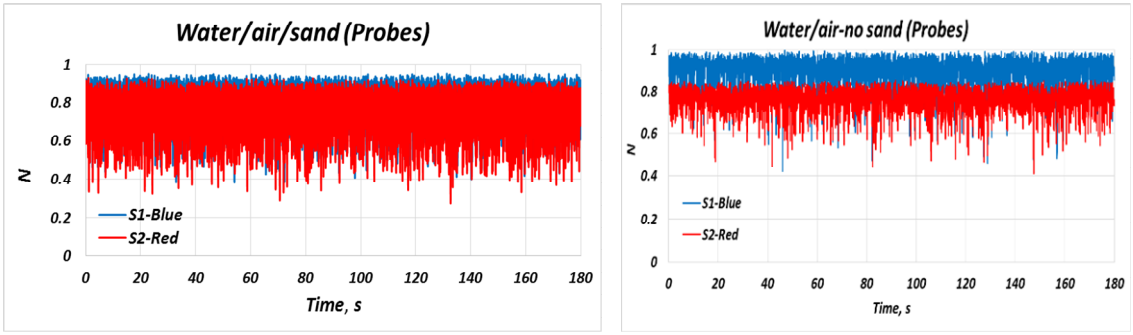

(a). Vsl = 0.1252m/s Vsg = 8.9535m/s (b) Vsl=0.1275m/s, Vsg = 9.3771m/s

Figure 5.19: (a) Sand Saltation (212microns, 500lb/1000bbl) (b) Water/air-no sand

The above Figure 5.20 with sand particles of 212microns and sand concentration of 500lb/1000bbl shows more pronounced signals/spikes on the upper surface compared to Figure 5.19. Though, the difference could be attributed to more superficial gas velocity in Figure 5.20 which must have led to more bouncing or jumping of sand particles at the bottom of the pipe.

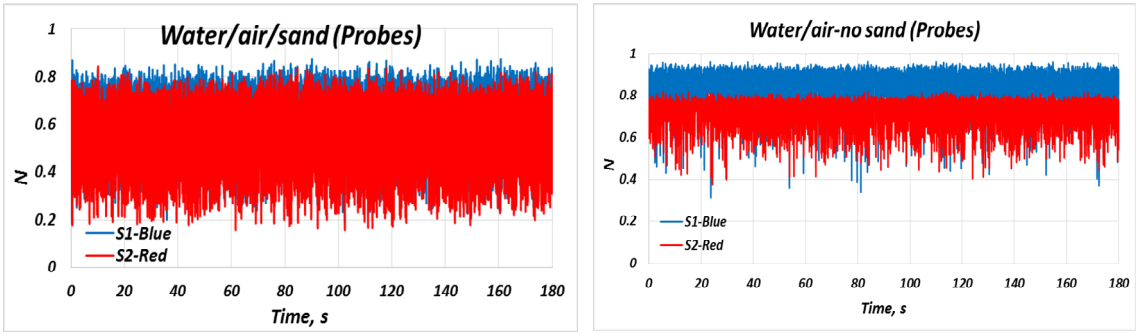

(a). Vsl = 0.1248m/s Vsg = 14.5936m/s *(b) Vsl = 0.1269m/s, Vsg = 14.2926m/s*

Figure 5.20: (a) Sand saltation (212microns, 500lb/1000bbl) (b) Water/air-no sand

From Figure 5.21 if the plot of water/air/sand could be said to have the two regime observed. At the upper part of the plot which is S1-probe (upstream) shows a typical suspension spikes when compared to Figures 5.8, 5.12 and 5.16 while the blue spikes (S2-downtream) shows a typical saltation in the flow. Again, comparing Figure 5.21 and Figure 5.21 or Figure 5.22 shows that there two flow regime (sand) of saltation and suspension were being detected in the flow.

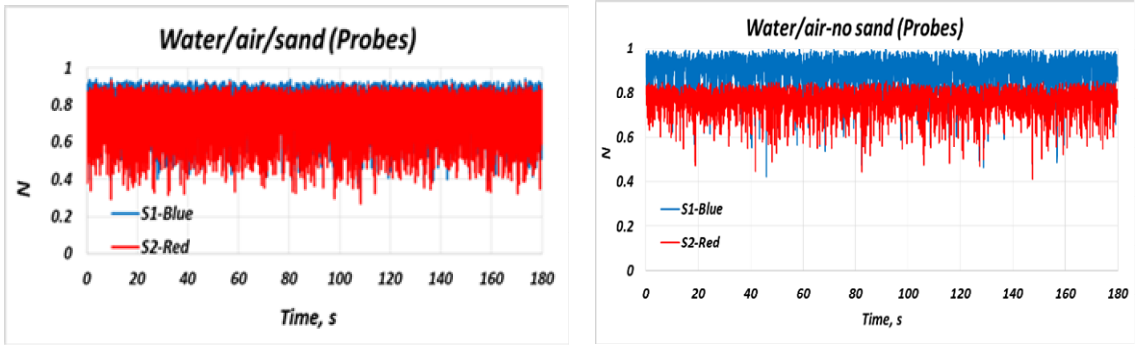

(a). Vsl = 0.1256m/s Vsg = 8.7601m/s *(b) Vsl=0.1275m/s, Vsg = 9.3771m/s*

Figure 5.21: (a) Sand Saltation (500microns, 500lb/1000bbl) (b) Water/air-no sand

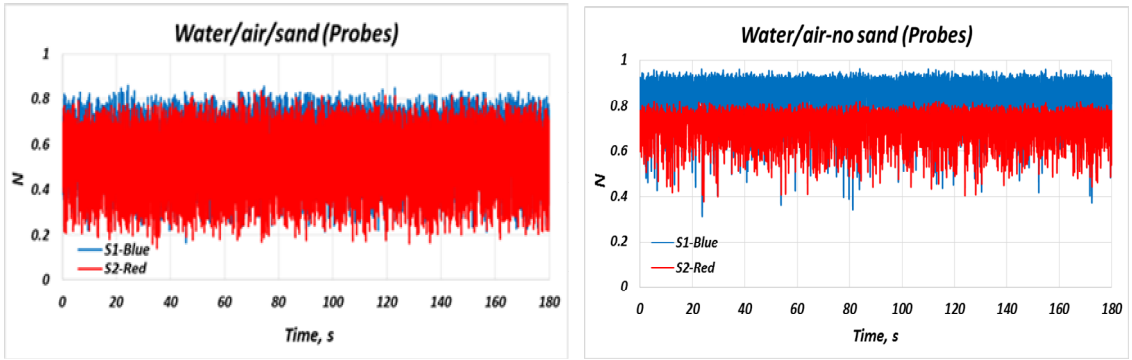

(a). Vsl = 0.1236m/s Vsg = 14.4325m/s *(b) Vsl = 0.1269m/s, Vsg = 14.2926m/s*

Figure 5.22: (a) Sand saltation (500microns, 500lb/1000bbl) (b) Water/air-no sand

Sand particles when they are larger, are more dispersed to one another compared to when the sand particles are smaller in sizes.

In conclusion, the flow regimes (sand) in annular flow as detected from the film thickness probes were majorly: saltation and suspension. This is found only with the lower superficial gas velocity as seen in Figures 5.17(a), 5.19(a) and 5.21(a). It is interesting to note that spikes from the various graphs illustrates the impact of the sand particles. Again, full saltation were prominent in Figures 5.18(a), 5.20(a) and 5.22(a). It was not a mistake that the spikes presented on the graphs in Figures 5.18(a), 5.20(a) and 5.22(a) were rougher on high superficial gas velocities of 14.9179m/s, 14.5936 and 14.4325m/s. This implies that the sand particles were bouncing in good numbers across the probes. More so, it was detected from the signals' analysed in Figures 5.17(a), 5.19(a) and 5.21(a) that the lower the superficial gas velocity, the less the spikes at the top while the rougher the spikes at the bottom of the graphs. This indicates streaks cum saltation when compared to Figures 5.11, 5.14 and 5.15.

Finally, the striking difference between Figures 5.17(a) and 5.17(b) to 5.22(a) and 5.22(b) even when their flow conditions were similar, shows that the probes were detecting sand particles in annular flow. In the case of the water/air only from the (b) sides, illustrated similar spikes but with the blue (S1) and the red (S2) were clearly differentiated while the water/air/sand were more spread across each other which indicates that more energy were dissipated from the gas phase in terms of water/air/sand flow experiments to keep the liquid phase with the sand particles in motions. However, the rough spikes on water/air only, were the liquid droplets or bubbles in the liquid film which the probe sensors also detected. So basically, two major flow regimes (sand) exist in annular flow in horizontal pipe. And these are: sand saltation and suspension from the experimental analysis.

5.3.2 Power Spectral Density (PSD) of Sand in Annular Flow.

The power spectral density (PSD) of sand transport in annular flow was analysed to see the effect of sand on annular flow behaviour in horizontal pipe. It was observed, after the analysis of both sand in annular flow and annular flow without sand, that sand in liquid film aids in increase of wave amplitude as more energy

were dissipated from the gas phase to keep the wave in motion as presented in Table 5.4.

The power spectral density of Vsl=0.1126m/s, Vsg=9.3775 with 212microns-200lb/1000bbl has presented a distinct difference from that of Vsl=0.1275m/s, Vsg =9.3771m/s without sand. This has shown, that more energy were dissipated in Vsl=0.1126m/s, Vsg=9.3775 with 212microns-200lb/1000bbl. Therefore, sand particles are proven to be transported in the liquid film in annular flow as also presented in Figures 5.28 and 5.29 which were obtained from the sand sampling method. Again, this has further proven the probes' results of Figures 5.17 to 5.22 that sand particles are transported in the film in as much as in suspension.

Having achieved this, effect of sand particles and sand concentration will be further analysed to see sand impact on wave velocity.

Table 5.4: PSD of Sand in Annular Flow compared with Annular Flow without Sand.

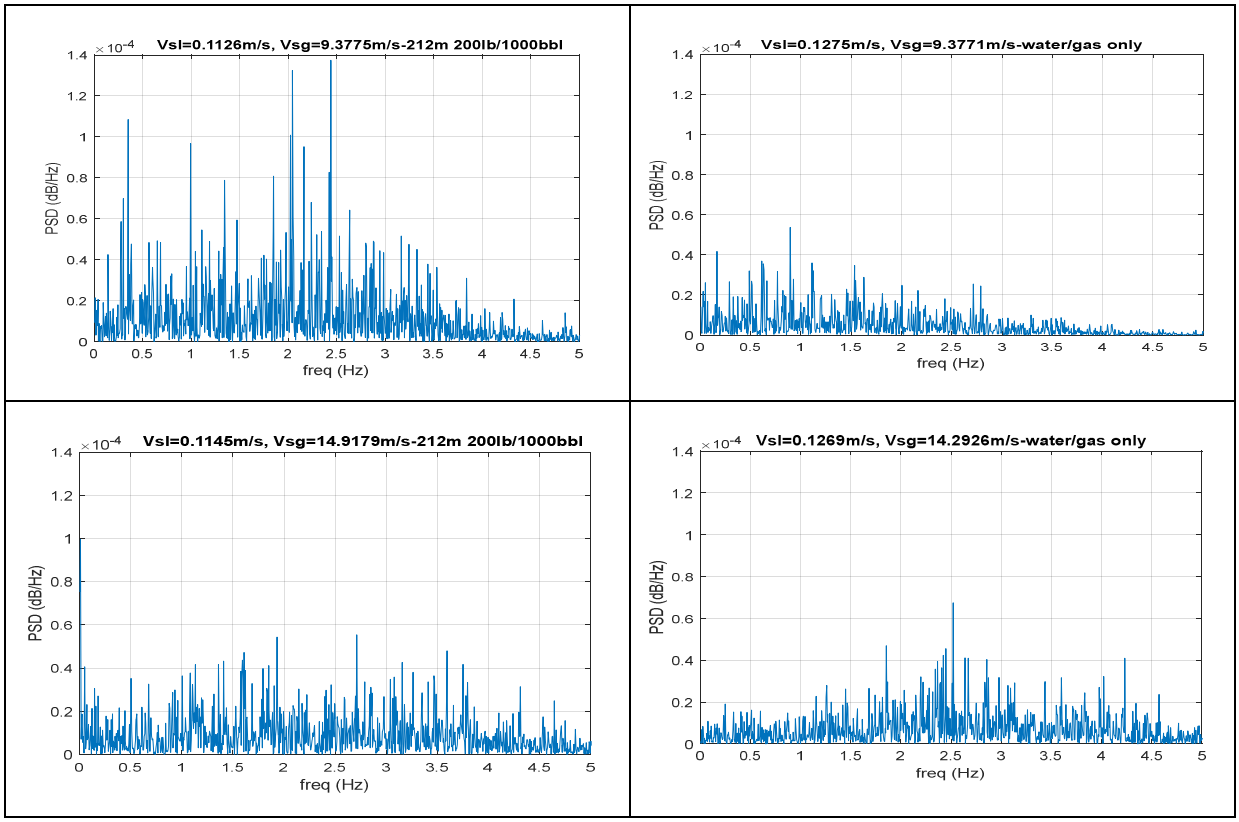

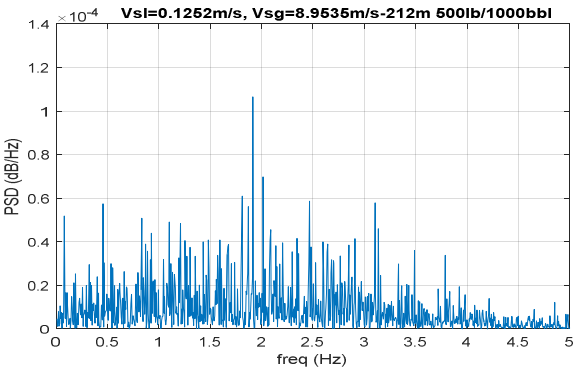
Vsl=0.1252m/s, Vsg=8.9535m/s-212m 500lb/1000bbl
PSD (dB/Hz)
freq (Hz)

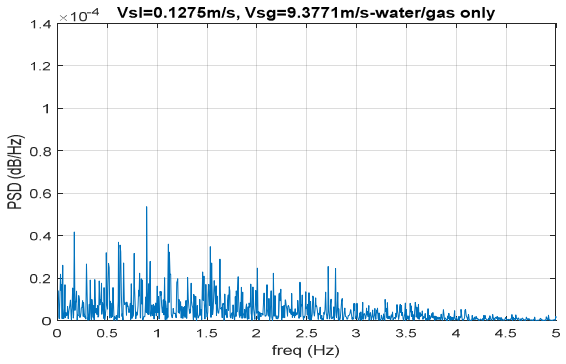
Vsl=0.1275m/s, Vsg=9.3771m/s-water/gas only
PSD (dB/Hz)
freq (Hz)

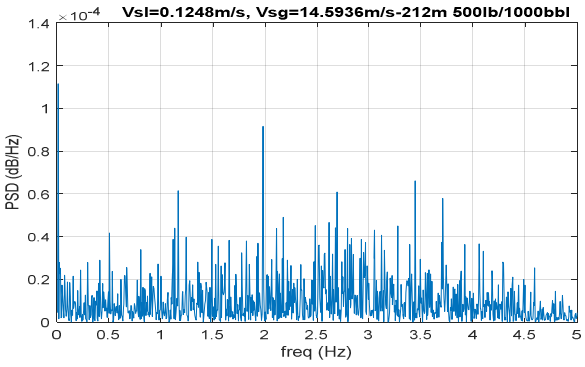
Vsl=0.1248m/s, Vsg=14.5936m/s-212m 500lb/1000bbl
PSD (dB/Hz)
freq (Hz)

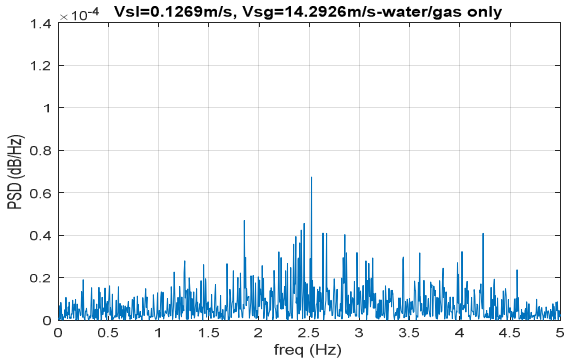
Vsl=0.1269m/s, Vsg=14.2926m/s-water/gas only
PSD (dB/Hz)
freq (Hz)

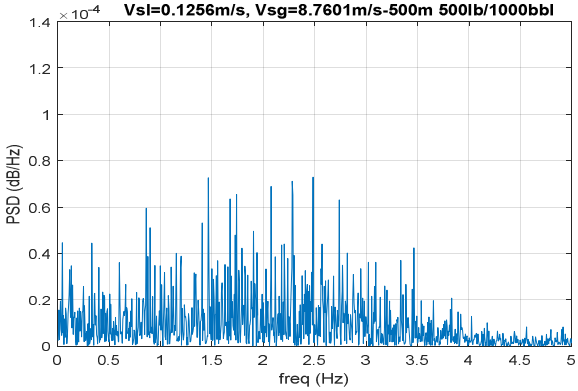
Vsl=0.1256m/s, Vsg=8.7601m/s-500m 500lb/1000bbl
PSD (dB/Hz)
freq (Hz)

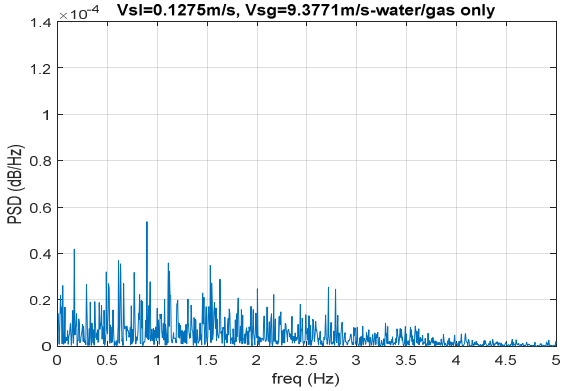
Vsl=0.1275m/s, Vsg=9.3771m/s-water/gas only
PSD (dB/Hz)
freq (Hz)

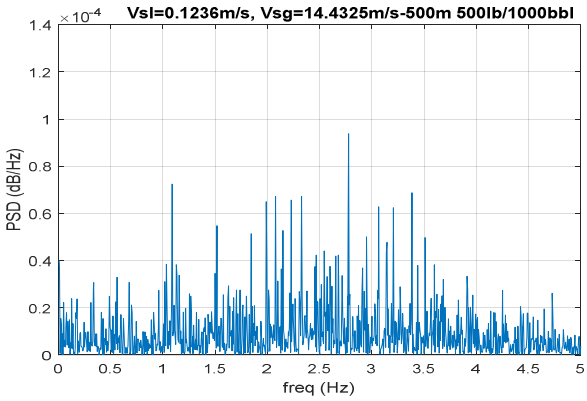
Vsl=0.1236m/s, Vsg=14.4325m/s-500m 500lb/1000bbl
PSD (dB/Hz)
freq (Hz)

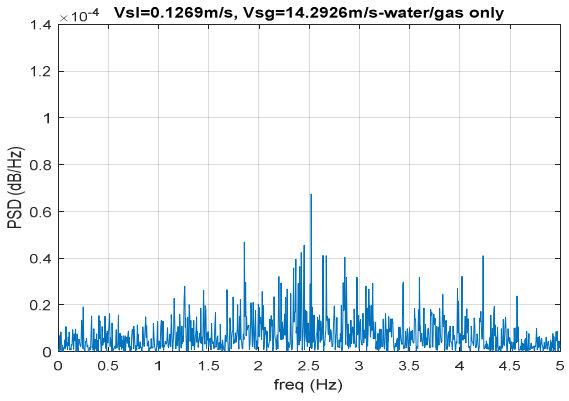
Vsl=0.1269m/s, Vsg=14.2926m/s-water/gas only
PSD (dB/Hz)
freq (Hz)

5.3.3 Effect of Sand Particle's Sizes/Concentration on Wave Velocity

Effect of sand particle's sizes and sand concentration were analysed from water/air/sand annular flow to present how sand affects wave velocity. From Table 5.4 and Figure 5.23, we discovered that sand particle's sizes and sand concentration have negligible impact on wave velocity in annular flow in horizontal pipe. For better understanding, the distinct difference between wave amplitude and wave velocity is: wave amplitude is the distance from the wave centre to either the top (crest) or bottom (tough) and measured in metres while wave velocity is the speed and direction. However, superficial liquid and gas velocities impacted much from Table 5.5 on wave velocity, while sand particle's sizes and sand concentration were negligible as 212microns (500lb/1000bbl) with Vsl=0.0983m/s and Vsg= 8.9650m/s presented the same wave velocity as that of 200microns (800lb/1000bbl).with Vsl=0.0922m/s and Vsg=8.8898m/s.

Also, 212microns (500lb/1000bbl) with Vsl and Vsg=0.1248m/s and 14.5936m/s had the same wave velocity with 500microns (500lb/1000bbl), 800microns (200lb/1000bbl) and 800mirons (500lb/1000bbl), because the superficial liquid and gas velocities were similar.

However, this is a clear evidence that sand particles' sizes and sand concentration do not have effect on wave velocity, rather superficial liquid and gas velocities affects wave velocity greatly, though more importantly, the superficial liquid velocity.

Table 5.5: Effect of Sand Particles on Wave Velocity in Annular Flow

lb/1000bbl	Grain Size(micron	Vsl [m/s]	Vsg [m/s]	Wave Velovcity [m/s]	Vsl [m/s]	Vsg [m/s]	Wave Velovcity [m/s]
500	212	0.0983	8.9651	0.0175	0.1024	14.4564	0.0221
500	212	0.1252	8.9535	0.0200	0.1248	14.5936	0.0247
500	212	0.1343	8.9811	0.0210	0.1304	14.8428	0.0262
200	212	0.0961	10.4769	0.0191	0.0951	14.9132	0.0221
200	212	0.1126	9.3775	0.0200	0.1145	14.9179	0.0233
200	212	0.1264	8.9792	0.0210	0.1209	14.9517	0.0262
200	500	0.1017	9.0558	0.0175	0.1003	15.2251	0.0221
200	500	0.1152	9.1572	0.0200	0.1184	14.5038	0.0233
200	500	0.1243	9.2351	0.0210	0.1289	14.4386	0.0262
500	500	0.1087	8.4749	0.0168	0.1003	15.2251	0.0233
500	500	0.1256	8.7601	0.0200	0.1236	14.4325	0.0247
500	500	0.1288	9.2246	0.0200	0.1265	14.6875	0.0248
200	800	0.0922	8.8898	0.0175	0.1010	14.9812	0.0221
200	800	0.1178	9.0353	0.0191	0.1155	15.1954	0.0247
200	800	0.1263	8.7283	0.0210	0.1239	15.1237	0.0262
500	800	0.1014	9.2332	0.0183	0.1039	14.5006	0.0221
500	800	0.1209	9.0533	0.0191	0.1179	15.1651	0.0247
500	800	0.1289	8.9116	0.0200	0.1257	15.0489	0.0262

The superficial liquid velocity on Table 5.5 was obtained by adding the liquid flow rates and the slurry flow rates from the sand hopper divided by the area of the pipe.

The graph of Figure 5.23 for superficial liquid velocity of averagely 0.1125m/s in all the sand particles' sizes and sand concentration showed that the sand transport has negligible effect on wave velocity as earlier mentioned. Irrespective of the differences in sand particle's sizes and sand concentration, the wave velocity were lumped together on the graph of Figure 5.23. The little gap observed on the graph of Figure 5.23 is the difference seen on the superficial liquid and gas velocities.

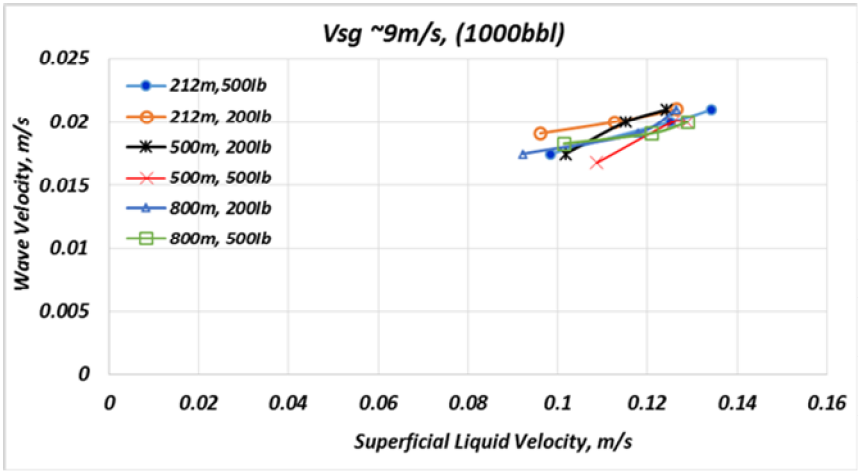

Figure 5.23: Wave Velocity vs Vsl on Sand Particle Sizes/Sand Concentrations

Figure 5.24 has also shown that sand particles' sizes and sand concentration have no impact on wave velocity in annular flow in horizontal pipes. Behold the plots of Figure 5.24 were more close to one another as the superficial gas velocity increased compared to graph of Figure 5.23. This has shown that sand particles or sand concentration in annular flow have no impact on wave velocity.

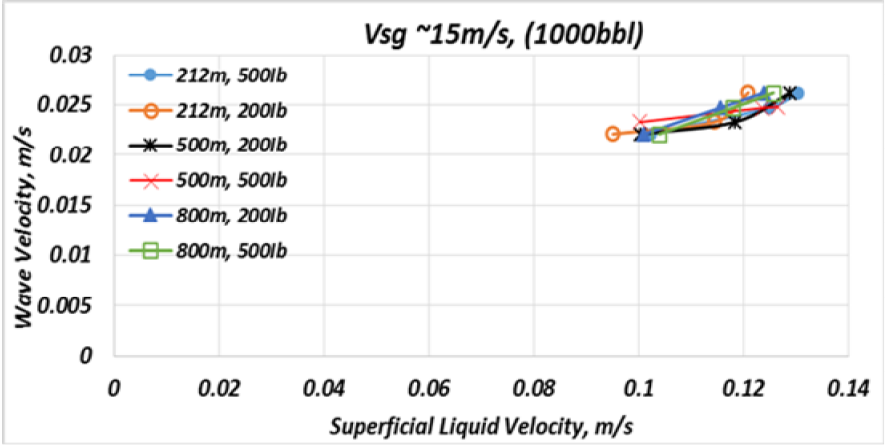

Figure 5.24: Wave Velocity vs Vsl on Sand Particle sizes/Sand Concentration

5.3.4 Effect of Sand Particles' Sizes/Sand Concentration on Wall Shear Stress.

Effect of sand particles' sizes and sand concentration were investigated in annular flow in horizontal pipe in this study, with the experimental pressure gradients. The sand particles' sizes were 212microns, 500microns with sand concentration of 200lb and 500lb. Wall shear stress was obtained from the measured pressure gradient and pipe diameter.

The graph of Figure 5.25 of wall shear stress against film thickness shows the dominant effect of superficial gas velocity on wall shear stress in annular flow. The graph was a plot of sand particles' size and sand concentration of 212microns-200lb/1000bbl with the slight difference in superficial liquid velocity but different superficial gas velocity. Indeed, superficial gas velocity presented much impact on wall shear stress. Again, Figure 5.25 had illustrated that the higher the superficial liquid velocity, the higher the film thickness with respect to superficial gas velocity and the higher the wall shear stress. The detailed calculated results are in Appendix (Table R-1.1).

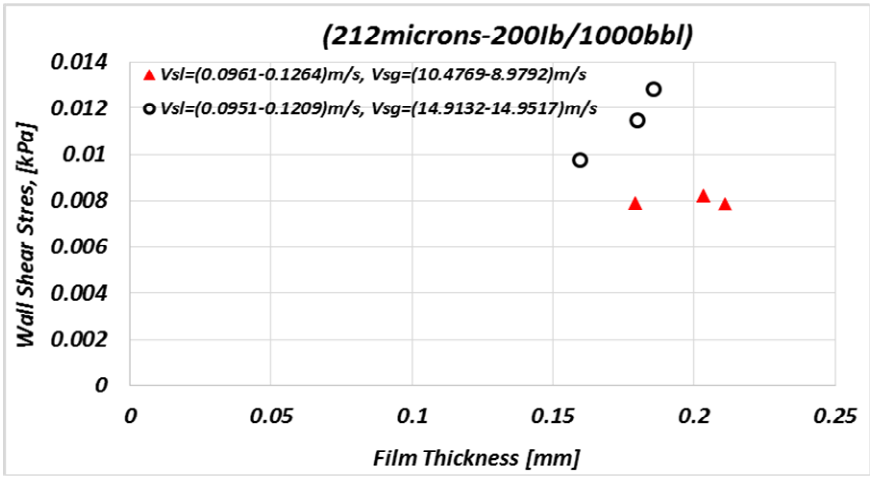

Figure 5.25: Wall Shear Stress against Film Thickness- Effect of Gas velocity felt.

The graph of figure 5.26 was a wall shear stress against film thickness with the same sand concentration of 500lb, but different sand particles' sizes. The superficial gas and liquid velocities where slightly different. The plots preferably matched one another, which illustrates that sand particles' sizes have no impact on the wall shear stress in annular flow from the experiments.

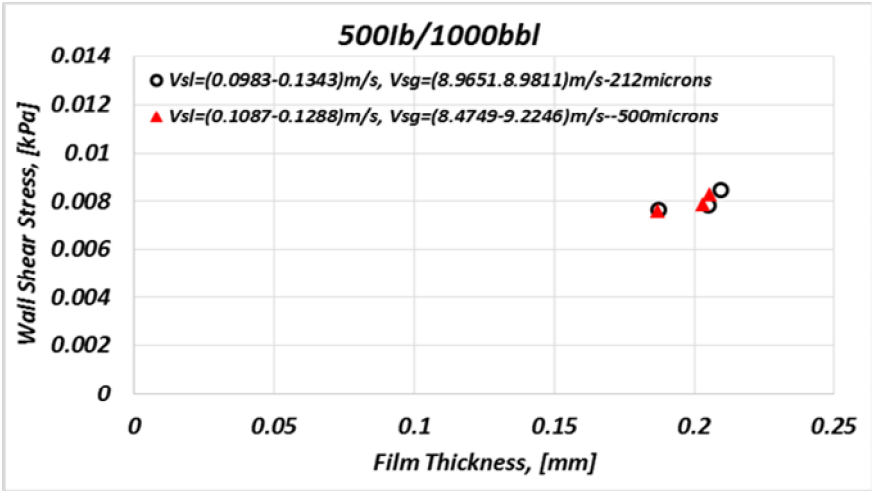

Figure 5.26: Wall Shear Stress against Film Thickness- Effect of Particle Sizes.

The graph of 5.27 was wall shear stress against film thickness with same sand particles' size of 212microns but different sand concentration of 200lb and 500lb. Again, the superficial gas and liquid velocities were slightly different and similar to the flow conditions in Figure 5.26.

It was amazing to observe the slight difference on the plots against what was observed in Figure 5.26. The plot of Figure 5.27 clearly illustrated that sand concentration indeed, have impact on wall shear stress because if the superficial gas and liquid velocity were close enough, the same results as presented on plot in Figure 5.26 should have been expected in Figure 5.27. Again, this has proven that sand particles are indeed being transported in the liquid film at the bottom of the horizontal pipe in annular flow.

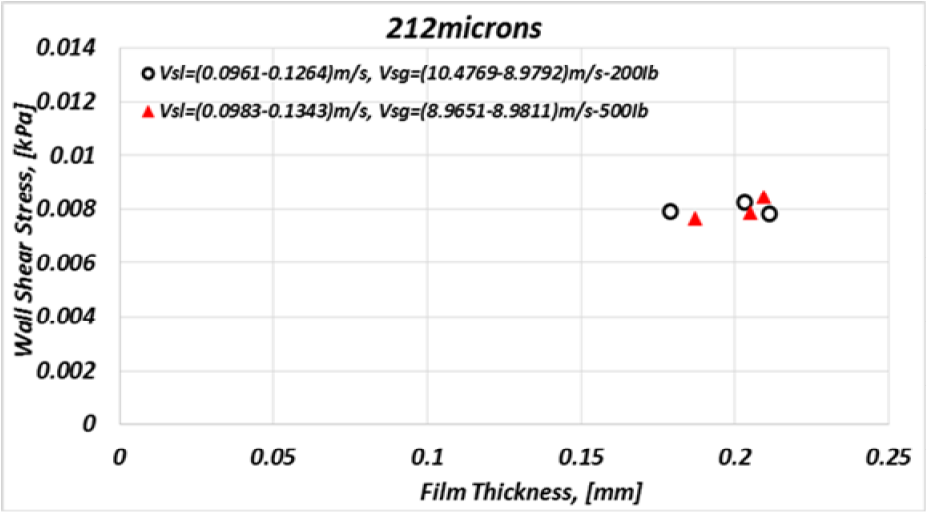

Figure 5.27: Wall Shear Stress against Film Thickness- Effect of Concentration felt.

5.4 Physical Modes of Sand Distribution in Annular flow (Sampling Method)

The physical modes of sand distribution were investigated using sand sampling method. The experiments on sand sampling shows that the higher the velocity, the higher the sand particles transported in the pipe. This simply means, increase in superficial gas velocity also increases sand movement and sand lifting/entrainment in the gas core in annular flow.

Figure 5.28 results was quite different from Figure 5.29 results obtained. Figure 5.28 was conducted using Vsl=0.0732m/s with 212microns-200lb/1000bbl. The results illustrates that small particles are transported more in the gas core than in the liquid film thickness as discovered in Figure 5.29. This means the smaller the particles, the lighter they are easily lifted and transported with respect to high gas velocities. At a height of 2.5cm (0.025m) in the internal diameter of the horizontal

pipe of 2-icnh (0.0504mm) flow loop, where the gas core was dominant, presented more sand particles being transported. Again, at a height of 1.5cm (0.015m) in the internal diameter, more sand particles were also detected from the sampling experiments. While at the bottom of the pipe where the sampling throat was flush mounted, less sand particles were detected. At the upper walls of the internal pipe diameter, negligible sand particles were transported.

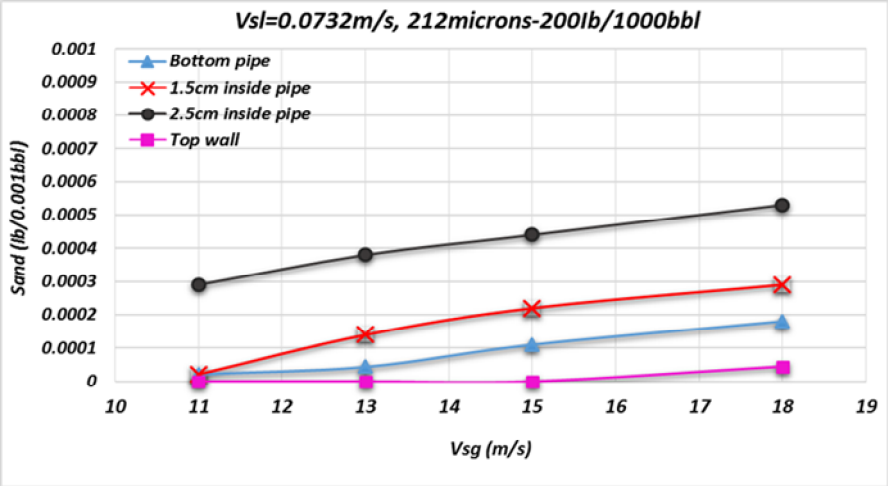

Figure 5.28: Sand Distribution in the Pipe for Vsl=0.0732m/s, 212microns.

In Figure 5.29, presents a distinct sand flow behaviours in the pipe with sand particles' size of 500microns and Vsl=0.1042m/s. At 2.5cm (0.025m) the results showed an increase in sand particles being transported in the gas core from Vsg=15.0122m/s to 18.0010m/s. while at the bottom, At the bottom of the pipe, more sand transportations were presented in the graph of figure 5.29. Reasons for having more sand particles being transported at the liquid film is because of gravity impact. The sand particles are bigger in sizes (500microns) compared to 212microns in Figure 5.28, therefore gravity could have impacted in having more of the sand particles at liquid film in the bottom of the pipe.

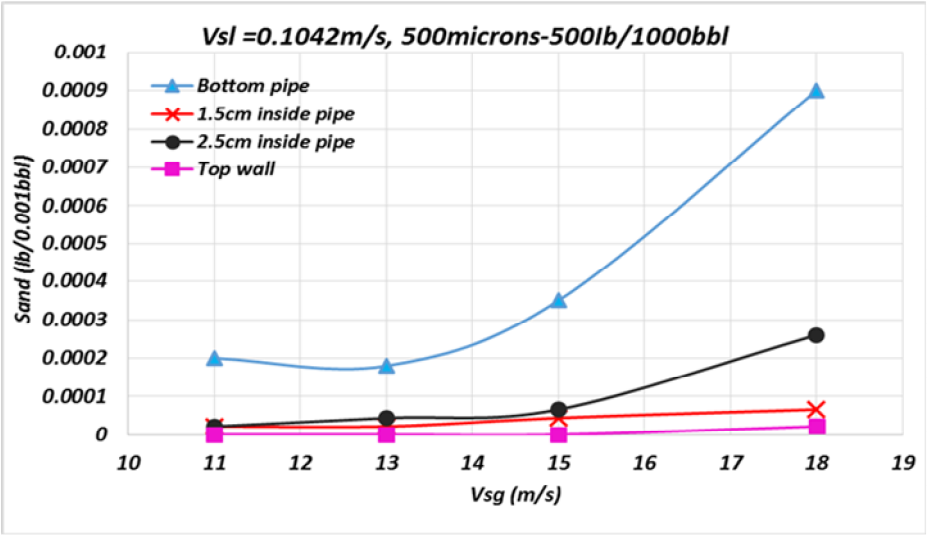

Figure 5.29: Sand Distribution in the Pipe for Vsl=0.1042m/s, 500microns.

In conclusion, from both Figures 5.28 and 5.29, it has shown that the larger particles of 500microns were easily influenced by gravity, while the smaller particles are transported in the gas core in annular flow. Again, increases in superficial gas velocity, increased the sand concentration at the bottom of the pipe in Figure 5.29.

With respect to the same Figure 5.29, it was clear, that the sand particles were transported in the liquid film at the bottom of the pipe as gravity impacted more on the film droplets so also on the larger sand particle sizes, subject to superficial gas velocity in annular flow.

While in Figure 5.28 with low superficial liquid velocity, low sand concentration of 200lb and small sand particle sizes of 212microns; the sand particles were transported more in the gas core than at the bottom of the pipe. Therefore, the lighter the sand particles, the more suspended they are transported through the gas core in annular flow. Again, it shows that the higher the superficial gas velocity, the more sand concentration are lifted and transported in the gas core if the sand particles are small and the superficial liquid velocities are low.

5.5 Chapter Summary

Water/sand flow experiments were conducted using 200microns, 212microns and 500microns with sand concentrations of 200lb and 500lb. The experiments

were presented on visual observations and the use sand probes to detect sand behaviours. The analysed results of the sand probes for Figures (5.5 - 5.16) further complimented the visual pictures of sand flow regime on the lift hand side which were taken with a low resolution camera during the experiments. From both results, it was observed that at low superficial liquid velocity, sand moves as moving bed with traces of sand dune. This is because the lower the superficial liquid velocity, the lower the buoyancy forces to lift the sand particles and the higher the effect of gravity which impacts on the sand particles, especially the larger ones that are transported slowly as moving dunes at the bottom of the horizontal pipe. With increase in superficial liquid velocity to an average of 0.31m/s, the sand particles were presented to be transported as scoring. The visual observation results were compared with Angelson *et al.,* (1989) results as reported in Table 5.2 with close similarities. On minimum transport condition (MTC), it was also discovered that MTC increases with increase in sand particle sizes as presented also by Kamyar *et al*., (2015). The reason is because, the larger the sand particles' sizes, the more friction and the higher the drag forces on the pipe walls as force of gravity would aid them to be transported at the bottom of the pipe.

On flow regime (sand), both the visual observations and sand probe results presented the following flow regimes in water/sand flow: Suspension, Saltation, streaks and moving dunes as seen in Figures 5.5 - 5.16 in this study.

The novelty is being able to use film thickness probe which is majorly used for film thickness, to detect the different flow regimes (sand) in water/sand flow experiments in this study. The work had also presented that the lower the superficial liquid velocity, the more the sand particles are transported as sand dune in horizontal pipes.

In contribution to knowledge, the experiments have presented the minimum transport velocity (MTV) for different sand particles and concentration in Table 5.3. Also, the MTV results have shown that both sand concentration and particle sizes, have significant impact on minimum transport velocity in water/sand flow in horizontal pipes.

Water/air/sand annular flow experiments were conducted to investigate sand behaviours and its effect in annular flow. The experiments, were conducted using two different sets of superficial liquid velocities ranging from (0.0922m/s-0.1304m/s) and superficial liquid velocities of 0.0732m/s and 0.1042m/s (sand sampling) with respect to superficial gas velocities ranging from 8.4749m/s to 18.2251m/s with sand sampling included respectively. Sand particles of 212microna, 500microns and 800microns were used with sand concentration of 200lb and 500lb only.

Sand probes that were used in the experiments, presented tremendous sand behaviours in annular flow as seen in Figures 5.17 to 5.22 in this study. However, saltation and suspension were detected and presented as the major flow regime (sand) in annular flow. Again, from the power spectral density analysis shown on Table 5.17, water/air/sand annular flow showed that sand contributed to the increase of wave amplitude in the liquid film compared to the water/air annular flow analysis without sand. This also has further proven, that sand particles are indeed transported at the bottom of the pipe as presented in Figures 5.28 and 5.29. Effect of sand particles' sizes and sand concentration were also analysed. The results seen in Figure 5.24 had shown that both sand particle sizes and sand concentration have negligible impact on wave velocity in annular flow. While on wall shear stress, sand particles' sizes had no impact on wall shear stress but sand concentration impacted on wall shear stress as seen in Figure 5.27. In all, superficial gas velocity created much impact as seen in Figure 5.25.

From the sand sampling experiments, which were conducted to compliment the sand probe results, Figures 5.28 and 5.29 illustrated that sand particles are transported at the bottom of the pipe and at the gas core region. For 212microns in Figure 5.28, the sand particles were transported mostly at the gas core than at bottom of the pipe. This is simply, because the lighter the sand particles, the easier they could be lifted. For 500microns in Figure 5.29, sand particles were transported majorly at the bottom of the pipe because of gravity effect. Finally, transported sand particles increases in concentration with increase in superficial gas velocity.

6 OLGA Simulations

In this study, the experimental results presented were measured using different instruments like pressure transducers, probes, conductivity ring sensors, LED and flowmeters (gas, water). Therefore, it is necessary to compare these measured results with OLGA simulation results.

OLGA which is a multi-fluid dynamic model was developed on physical principles from: continuity equations, momentum, energy and correlations. Therefore comparing the measured with the simulations models using OLGA will be useful and important.

In applying OLGA in this study, the transient approach was adopted. The experimental data obtained were simulated using OLGA (2015) as follows: water/air annular flow and water/air/sand annular flow in horizontal pipes. The essence was not to validate but to compare the measured (experiments) results with OLGA simulation models. The aim of comparing OLGA with the experimental results is to identify potential areas where further advances in multiphase flow modelling could be made.

The simulations were made possible using the following OLGA input options;

- Library Material for the pipe walls and particle (particle density, diameter and capacity)
- Case definition
- FA Model
- Flow components
- Nodes
    - ✓ Inlet
    - ✓ Outlet
- Run Results

The detailed input values/screenshots to show how it was simulated, are presented in the Appendix (Table G-1.6).

6.1 OLGA Flow Geometry Setup

OLGA flow geometry of 12m long was setup for the simulations. This was the distance from the beginning of the Plexiglas to the delivery water fibre storage tank as presented in Figure 3.1. The 12m distance was necessary because the entire measuring devices used in the experiments for measurements e.g. pressure sensor T1, conductance probe upstream and downstream (S1 and S2), conductivity ring sensors (C1 & C2), pressure sensor (P2) and temperature sensor (T2) were all installed within this 12m distance. The air injection point and the sand injection point were just at the source point on the horizontal flow geometry setup.

In the design, the angle of elevation was set at zero in all the sections with the results point at section 5. The reason was simply to enable the fluids flowing under high superficial gas velocity to stabilize before the results were recorded in OLGA

6.1.1 OLGA Flow Model

OLGA is modelled for only two flow regimes: distributed and separated flow. The distributed flow is consists of slug and dispersed bubble flow, while the separated flow is consists of stratified (smooth and wavy) and annular flow. Annular flow is modelled similarly to stratified flow regime (OLGA, 2015). Hence, annular flow was not excluded from stratified flow model, this study will expatiate more on stratified flow.

OLGA stratified flow is consist of two flow models, namely: OLGA flow model and OLGA HD flow model. The two could be distinguished as follows: OLGA stratified flow model uses average bulk velocities and friction model while OLGA HD stratified flow model, uses 2D velocity distribution over cross-sectional area of pipes and friction model in handling separated flow regime problems.

Annular flow is treated similarly in OLGA as stratified flow regime, therefore the transient OLAG HD was chosen in the option segment. More so, OLGA HD stratified flow model was improved for more reliable predictions in gas pipelines by resolving the inconsistency of the 1D models, combining 3D consistency with

the speed of 1D (axial) and accounting for 2D velocity distribution over the pipe cross sections in the system, Staff et al., (2010), Biberg et al., (2015). It means the 1D conservation equations in combination with the 2D velocity distribution, produces a 3D of a slowly evolving flow that will be able to predict 1-3 fluid layers in the system, (OLGA, 2015). From the flow geometry, the following liquid hold-up results were presented.

6.1.2 OLGA Liquid Hold up Model.

There are no specific liquid hold-up correlations like Beggs & Brill (1973), Abdul-Majeed (1996) used in OLGA. The liquid hold-up is modelled with the conservation equations. They are imbedded in both mass and momentum equations, which requires mathematical derivatives to further extract the liquid-hold-up equations in the manner they were used in OLGA. A typical example of the liquid hold-up equation is given in equation (2-121).

6.1.3 OLGA Sand Transport Model.

In OLGA, two distinct model options were considered in sand transport in multiphase flow, namely: the simple particle flow and the advanced particle flow models.

The simple particle flow model predicts sand (solid) particles that are suspended only in a phase (e.g. gas phase only or liquid phase only). The conservation equations in simple particle flow model in OLGA were derived for the mass of particles with respect to the carrier phase only. While the advance particle flow model predicts sand (solid) particles that are transported either as in more phases (e.g. water/gas/oil) and with sand deposition inclusive, (OLGA, 2015). Also, the conservations equations in the advance particle flow model, were derived for suspension (total mass of suspended particles in oil, water and gas simultaneously) and the sand particles in the bed.

More so, the sand particle flow conditions in OLGA could be group into: stationary bed (no-moving dune), moving bed and no bed (suspension of sand particles).

In simulating sand particles in OLGA, the following equations are necessary:

Fluid sand particle viscosity:

$$\frac{\mu_{fp}}{\mu_{fp}^{n}} = \left(1 - \frac{\omega}{0.75}\right)^{K} \quad \textbf{(6-1)}$$

Where k= -2.0025, ω is for volume fraction for particles in the fluid that were suspended, μ_{fp} is for fluid particle viscosity (kg/m.s).

Slip velocity for turbulent flow:

$$S_v = C\left(d_p\left(\frac{\rho_p - \rho_t}{\rho_t}\right)\right)^{m} \quad \textbf{(6-2)}$$

For laminar flow, the slip velocity is expressed as:

$$S_v = C\left(\rho_p - \rho_t\right)\left(\frac{d_p^{2}}{\mu_{fp}}\right) \quad \textbf{(6-3)}$$

Where m = 0.5, C is constant (2.9452 and 0.32673) for turbulent and laminar flow respectively , d_p is diameter of sand particles (m), ρ_p is the sand particle density (kg/m^3), ρ_t is the fluid flow density (kg/m^3), and S_v is slip velocity (m/s).

The particles Reynold's number was presented in OLGA based on the slip velocity of the phase where the particles are transported. Therefore the particles Reynold's number is expressed as:

$$N_{\mathrm{Re}} = \frac{S_v \rho_t d_p}{\mu_{fp}} \quad \textbf{(6-4)}$$

Sand particle deposition is expressed as:

$$\alpha_p = \frac{L_s}{A_p}\rho_p s_v \cos(\phi) C_s \quad \textbf{(6-5)}$$

The sand entrainment in fluid is expressed as:

$$\varepsilon_p = \frac{L_s}{A_p}\rho_p s_v \cos(\phi) C_s \quad \textbf{(6-6)}$$

Where α_p is for particle depositions, ε_p is for entrained particles in the fluid, ρ_p is the sand particle density (kg/m^3), L is bed-suspended particle interface length (m), A_p is cross-section area of pipes (m^2), ϕ is particle moving angle, C_s and C_b are for concentration of suspended particles (bed) and concentration of particles in bed respectively and S_v is slip velocity (m/s).

Based on these models, OLGA was able to predict the following results on liquid hold up and sand transport in annular flow which were compared with the measured results in this study.

6.2 Liquid Hold –Up (OLGA).

The graph of Figure 6.2 was a result of OLGA simulation with the measured liquid hold-up for Vsl=0.0505m/s. OLGA liquid hold up presented a preferable trend with the measured liquid hold-up in annular flow in horizontal pipe. This has justified the physical models or correlations as it predicted closely with the measured values from the experiments.

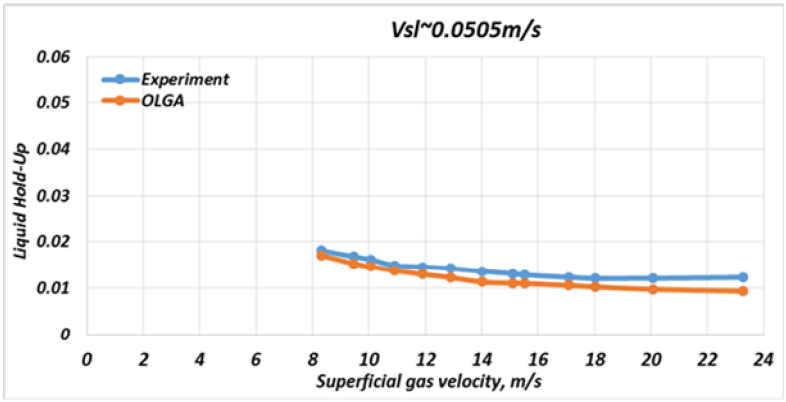

Figure 6.1: OLGA/Experiment (Measured) Liquid Hold-Up for Vsl=0.0505m/s

Figure 6.3 presents another similar trend between the measured (experiment) liquid hold-up and the OLGA simulation results. The gap between the measured and the OLGA liquid hold-up is simply based on the liquid entrainment which the measured seems to take into consideration more than OLGA did. Liquid entrainment if not properly accounted could be responsible because the entrained droplets when over or underestimated will impact on the liquid holdup

results. Also, the variance could be attributed to assumptions and conditions (e.g. pipe diameters) considered in the development of models used.

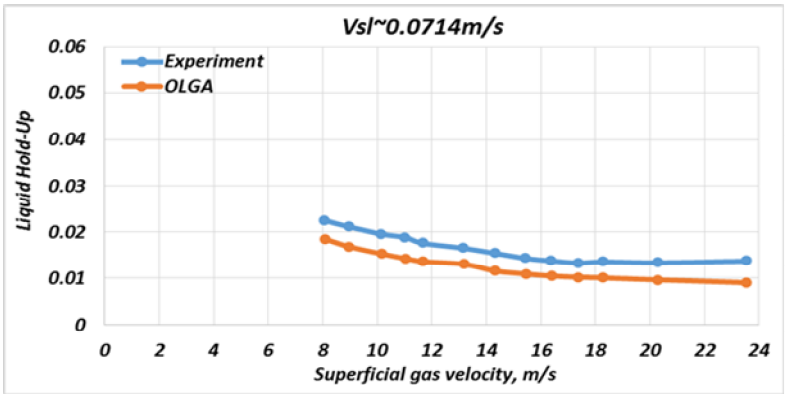

Figure 6.2: OLGA/Experiment (Measured) Liquid Hold Up for Vsl=0.0714m/s.

Figure 6.4 illustrated that the higher the superficial liquid velocity, the more the liquid entrainment from the OLGA simulation results, compared to the measured. The differences were basically from the liquid entrainments which were accounted for in the experiments using Pan and Hanratty (2002b) correlation. The correlation presented the most realistic results among other correlations compared using the experimental data. This was further proven, by Magrini *et al.,* (2012) ranking analysis on liquid entrainment correlations for horizontal pipes where Pan and Hanratty (2002b), was presented as the best correlation that preferably, predicts liquid entrainment. In summary, the OLGA and the measured results for Vsl=0.0903m/s seems similar with the same trend even though they were unable to match perfectly.

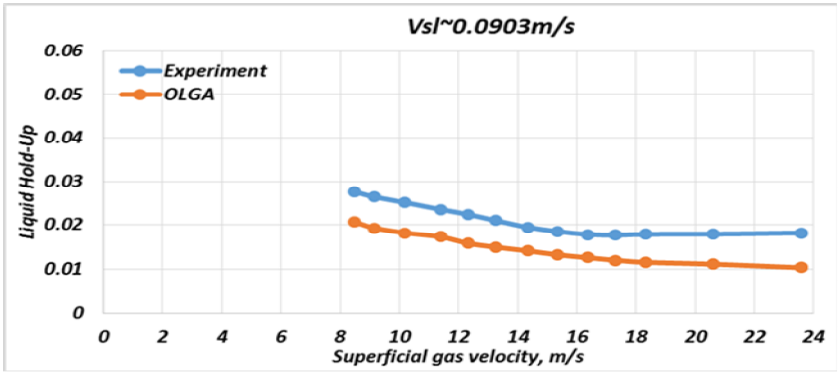

Figure 6.3: OLGA/Experiment (Measured) Liquid Hold-Up for Vsl=0.0903m/s.

From Figure 6.5, the measured liquid hold up and OLGA liquid hold up also had a similar trend as the superficial gas velocity increases. Although, OLGA under-predicted the measured liquid up. Again, this is because of liquid entrainment which were taken into cognizance in the experiments.

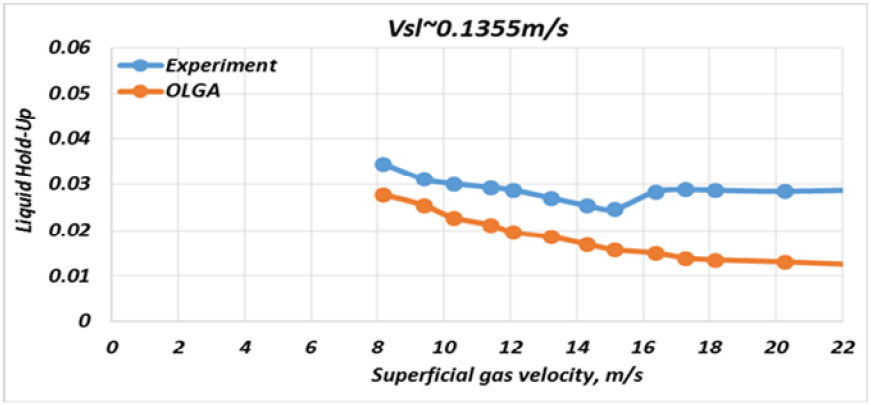

Figure 6.4: OLGA/Experiment (Measured) Liquid Hold-Up for Vsl=0.1355m/s.

The graph of Figure 6.6 showed that OLGA matched the measured liquid hold-up in the cases of Vsl=0.0505m/s, 0.0714m/s while 0.0903m/s and 0.1355m/s were under predicted. The under predicted cases, could be because of liquid entrainments which were accounted in this study, also could be the principles behind the development of the models used in the simulator (e.g. pipe diameters and assumptions adopted). Therefore, the measured is better than the predicted OLGA result obtained.

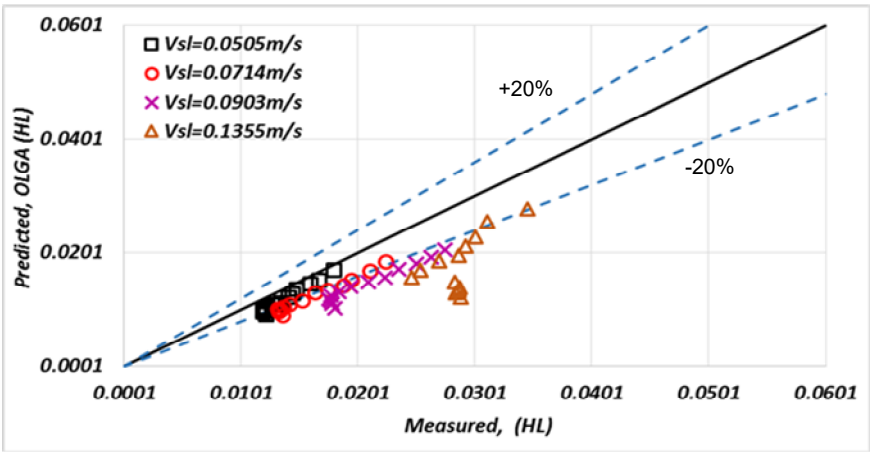

Figure 6.5: OLGA against Experiment (Measured) Liquid Hold-Up

In conclusion is the statistical error analysis showing OLGA liquid hold-up deviation of from the measured liquid hold-up, presented in Table 6.1, while the detailed statistical error analysis are presented in the Appendix (Tables S-1.1 to S-1.2).

Table 6.1: Summary of Statistical Error for OLGA Hold-up variance from Measured Hold-up.

Vsl [m/s]	*Average Actual Error*	*Average Relative Error [%]*	*Standard Deviation*
0.0505	0.0018	13.2610	3.6416
0.0714	0.0038	25.5132	4.8490
0.0903	0.0063	30.3882	5.5125
0.1355	0.0106	37.1871	6.0981

6.3 Sand Simulation (OLGA)

Water/air/sand annular flow experimental data in horizontal pipes were simulated with OLGA and compared with measured results, (see Figures 6.11 and 6.12). Again, OLGA presented good results in agreement with most of the measured results like the sand sampling in Figures 5.28 and 5.29.

Figure 6.7 is the flow regime (sand) simulation in annular flow presented by OLGA. The flow regime (sand) also illustrated that, sand particles are suspended in annular flow in pipes which OLGA referred to as “No Bed”. While the experimental results presented it as sand saltation.

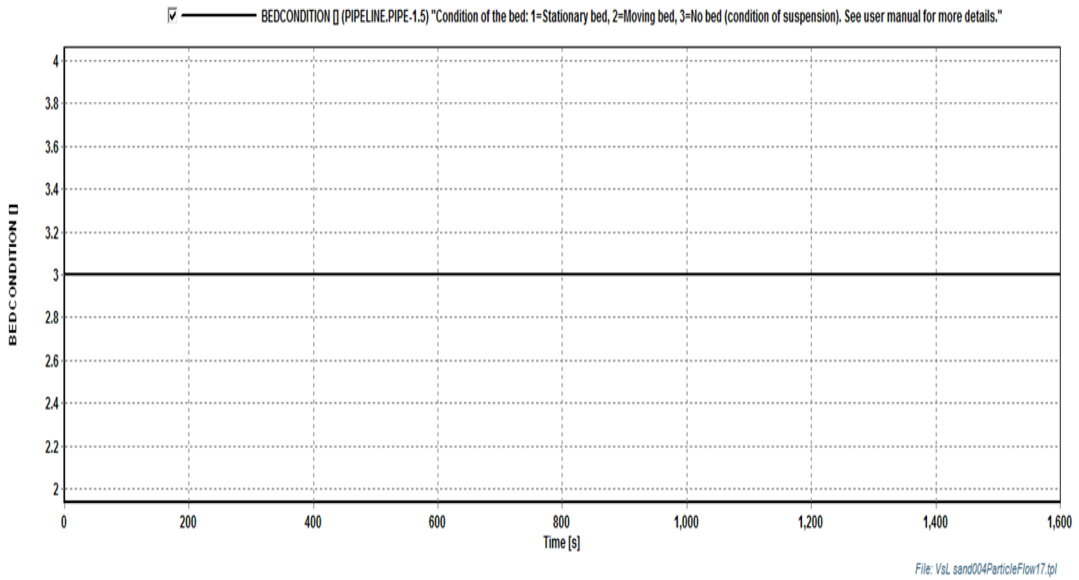

Figure 6.6*:* Sand Flow Regime in Sand Transport in Annular Flow (Vsl=0.1145m/s and Vsg = 14.9179m/s, 212microns, 200lb)

Figure 6.8 is the OLGA simulation in annular flow showing the accumulated mass particles' flow in water. This means, sand particles are being transported in the liquid film which is in agreement with Figure 5.18 (saltation) from sand probe results and the Figures 5.28 and 5.29 from the sand sampling results.

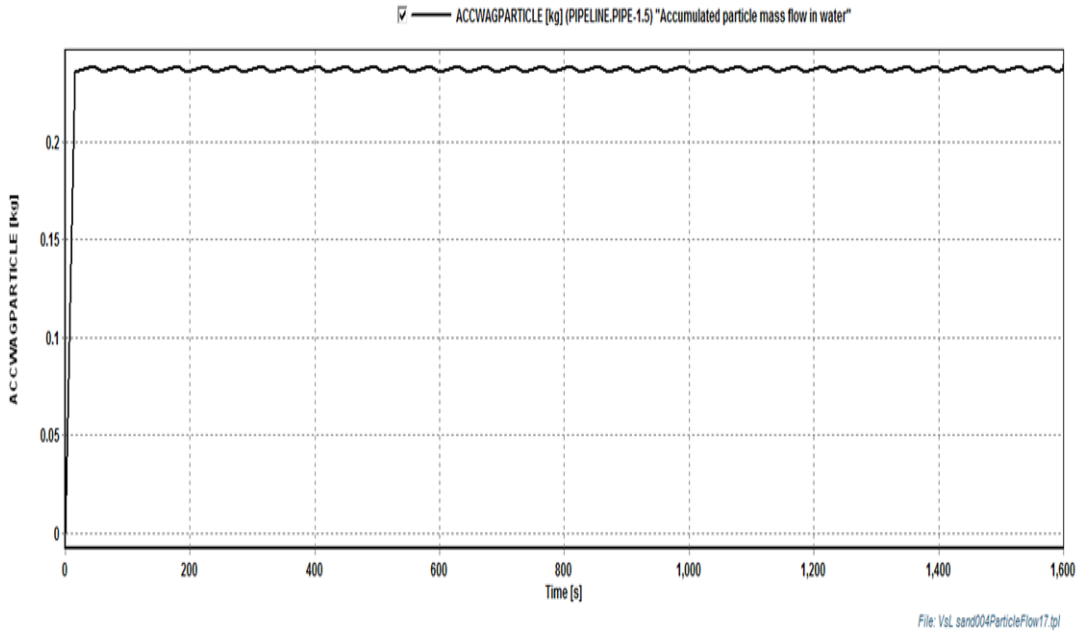

Figure 6.7: Particle Mass flow in water in Annular Flow (Vsl=0.1145m/s and Vsg = 14.9179m/s, 212microns, 200lb)

Figure 6.9 is OLGA simulation results, showing the accumulated mass particles' flow in suspension. It shows, how sand particles are also transported in the gas core which is in agreement sand sampling results in Figures 5.28 and 5.29.

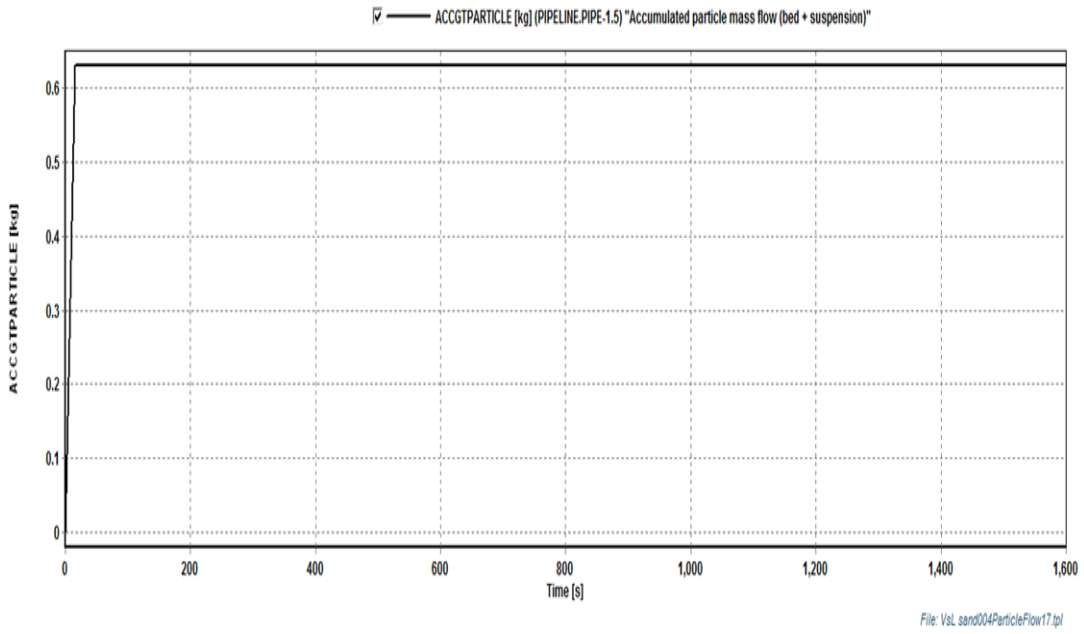

Figure 6.8: Particle Mass flow in Suspension in Annular Flow (Vsl=0.1145m/s and Vsg = 14.9179m/s, 212microns, 200lb)

Figure 6.10 presents OLGA simulation results, showing the accumulated volume of sand particles in both the gas core and in the liquid film in annular flow. This was also in agreement with the actual volume of the sand particles in the experiment as shown in Table 6.2. Again, it shows that sand particles increases in the pipe as flow progress, meaning there were more sand particles being lifted along in the pipeline.

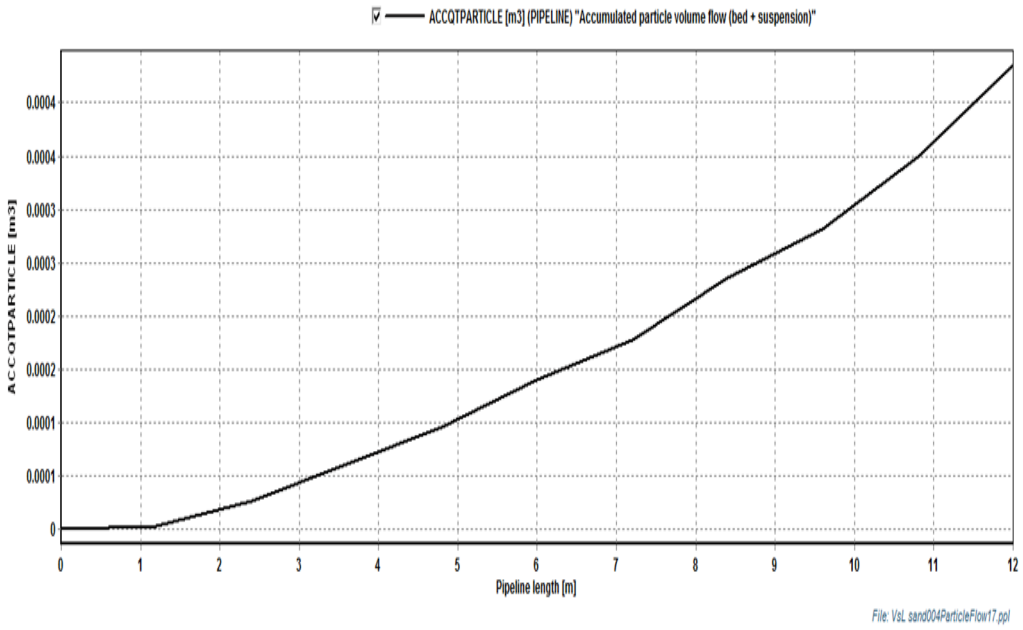

Figure 6.9: Particle Volume Flow both in Water + Suspension (Vsl=0.1145m/s and Vsg = 14.9179m/s, 212microns, 200lb)

Figure 6.11 is a plot of total sand particle mass transport in the experiments, compared with the OLGA simulated results. OLGA results matched with the Vsl = 0.1145m/s, Vsg =14.9179m/s (212microns-200lb/1000bbl), but underestimated that of Vsl = 0.1236m/s, Vsg = 14.4325m/s (500microns-500lb/1000bbl) and Vsl=0.1257m/s, Vsg=15.0489m/s (800microns-500lb/1000bbl) respectively, (see Figure 6.11). In conclusion OLGA simulations predicts, smaller sand particles better than the bigger 500 micron and 800microns.

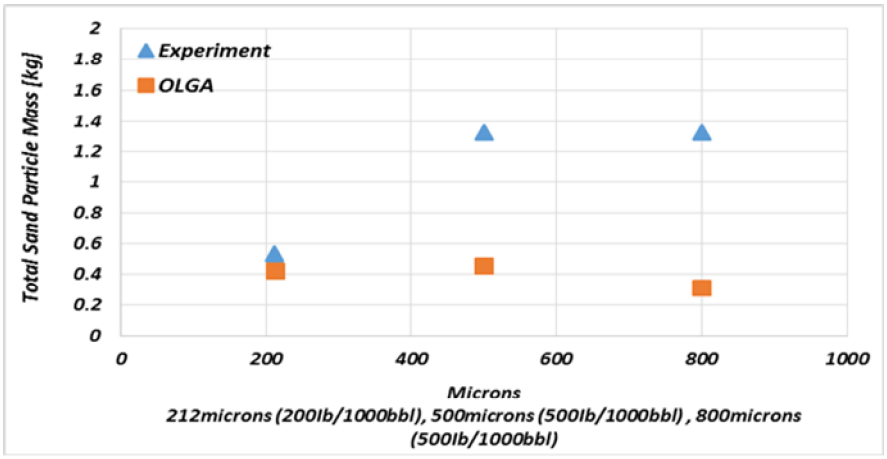

Figure 6.10: Comparison of Total Sand Particle Mass Used in Experiment and OLGA Simulated Results

Figure 6.12 is the comparison plot of OLGA sand concentration by volume with the measured. Again, Figure 6.12 presented a similar trend with figure 6.11. In this plot, the sand concentration of Vsl = 0.0500m/s, Vsg =14.9179m/s (212microns-200lb/1000bbl) matched perfectly with that of the experiment while Vsl=0.0514m/s, Vsg=14.4325m/s (500microns-500lb/1000bbl) and Vsl=0.1257m/s, Vsg=15.0489m/s (800microns-500lb/1000bbl) were far apart. Again, 212microns were smaller in size and as such will be much in number which attributed cumulatively to the volume observed by OLGA simulations.

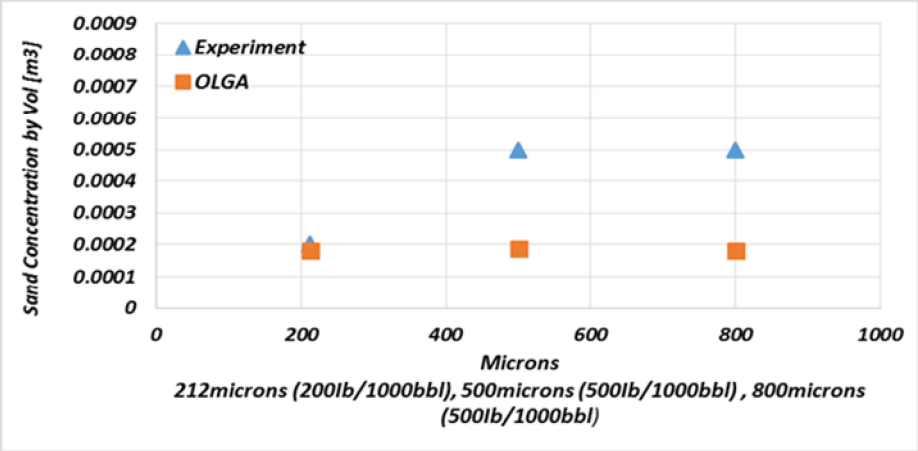

Figure 6.11: Comparison of Sand Concentration by Volume in Experiment and OLGA Simulated Results

In conclusion, OLGA presented good results in the case of sand particles' sizes of 212microns as seen in Figures 6.11 and 6.12. This is because, 212microns are smaller in size and as such will be much in volume (numbers) which attributed cumulatively to the volume observed by OLGA simulations

OLGA simulation results on water/air/sand flow, aligned with the results of the sand probes and the sand sampling. For flow regime (sand), sand probes were able to justify that sand particles were transported as saltation in the liquid film while OLGA presented it as suspension (No Bed). From OLGA further results on water/air/sand flow, accumulated particle mass were accounted for, in the both liquid film and in the gas core.

Further comparison had shown total sand concentrations by volume from OLGA matching closely with the experimental results while those of the larger sand

particle sizes were underestimated by OLGA. This is because the smaller the sand particles, the much space and volume it occupies. OLGA underestimated the larger ones to illustrate that the larger the sand particles, the less lifting and suspension. The summary of the statistical error analysis showing OLGA simulation margin from the experiments (measured) with respect to water/air/sand annular flow experiments in horizontal pipe is shown in Table 6.2.

Table 6.2: Summary of Statistical Error Margin of OLGA from Experiment.

			M[kg]		Cv [m3]	
Vsl[m/s]	Vsg[m/s]	Sand Particles[microns]	Actual Error	Relative Error[%]	Actual Error	Relative Error[%]
0.1145	14.9179	212(200lb/1000bbl)	0.1073	20.2403	0.00002	9.8068
0.1236	14.4325	500(500lb/1000bbl)	0.8684	65.5368	0.0003	62.6159
0.1257	15.0489	800(500lb/1000bbl)	1.0135	76.4903	0.0003	63.8437

More water/air/sand flow simulation results are presented in the Appendix F (1.2)

The comparisons between the OLGA sand simulation results and the experimental results showed that OLGA requires improvement with respect to water/air/sand annular flow in horizontal pipes, particularly for large sand particle sizes. For small particle size of 212microns, OLGA matched preferably with the experimental results (see Figures 6.11 and 6.12), but under-predicted sand concentration and total particle mass in the system when larger particle size of 500microns and 800micrns were involved.

For liquid hold-up in water/air annular flow, OLGA matched better on low superficial liquid velocity. As the superficial liquid velocity increases, the margin between OLGA and the measured values became more pronounced (see Figures 6.2 and 6.3). Again, OLGA was unable to replicate the hump in Figure 6.5, which is the fluctuation or flow rate change during the experiments. In summary, OLGA liquid hold-up model should be reviewed and if possible different liquid hold-up correlations be made available based on pipe diameters and flow conditions. Using the concept of stratified flow regime flow model to predict

annular flow as rightly presented in OLGA 2015 manual, will not present favourable results. This is because annular flow goes with higher gas velocity and more symmetrical flow across the pipe compared to stratified flow. The entire mechanism of entrainment is also different compared to stratified flow.

7 Conclusions

Experimental investigations on sand transport in annular flow in horizontal pipe were presented in this study, using a 2-inch (0.0504m, ID) closed flow loop, connected to a digital data acquisition systems. The investigations were on: annular flow behaviours, sand transport, effect of sand on annular flow behaviour, and physical modes of sand distribution in annular flow. Results presented from the experiments, were further compared with a widely used commercial software OLGA. The essence was to present further advances in multiphase flow modelling, if such need arises in course of comparing with the measured results.

The experiments conducted, could be grouped into: water/air flow, water/air annular flow, water/sand flow and water/air/sand annular flow experiments.

- Water/air flow experiments investigated as water/air flow and water/air annular flow experiments. Water/air flow experiments which were analysed and plotted on Taitel & Dukler (1976) flow regime map were presented, with the aim of progressing the understanding of the different flow regimes (plug, slug, stratified-smooth, stratified-wavy flows) and their behaviours .

  Water/air annular flow experiments were the bedrock of the investigations, as detailed annular flow behaviours were presented to progress the understanding before adventuring into sand transport in annular flow. Among the key features investigated were: liquid holdup, film thickness, wave velocity, wave frequency, interfacial shear stress and pressure gradient.

  Liquid film thickness was extensively investigated using three methods: the probe, conductivity ring sensors and triangular relationship. In all the methods and at all flow conditions, liquid film thickness decreased with increase in superficial gas velocity, but increases with increase in superficial liquid velocity. Wave velocity and wave frequency, also exhibited similar characters as both were increasing with increase in superficial gas velocity. More so, several correlations for wave frequency e.g. Ousaka *et al*.,(1992), Shubring & Shedd (2008), Setyawan *et al.,*

(2014), Mantilla (2008), Al-Sarkhi *et al.,* (2012) and Setyawan *et al.,* (2016), were compared with the obtained wave frequency in this study. Although, Al-Sarkhi *et al.,* (2012) preferably matched with the measured from Vsl (0.0903m/s to 0.1851m/s). Lastly, the liquid film thickness results were further analysed using Probability density function, power spectral density and wavelet for better understanding.

- Water/sand flow experiments were conducted using 200microns and 500microns. From visual observations, saltation, sand scoring, sand moving dunes and sand beds were presented as the flow regime (sand). For 500microns in particular, the sand moving dunes were presented at lower superficial liquid velocity compared to the sand moving dunes with 200mcirons. This is to illustrate the influence of gravity on sand particle transports. From the analysis in Table 6.1, it was clear that the higher the superficial liquid velocity, the more the flow regimes (sand) changes. The flow regimes (sand) presented in this study were compared with Angelson *et al.,* (1989) results. The results were similar as sand beds at Vsl=0.1507m/s and moving dunes of Vsl=0.2325m/s were the same with the results presented. Meanwhile, Angelson *et al.,* (1989) used 1-inch while 2-inch was used in this study, which accounted for the little difference in results.
- Water/air/sand annular flow experiments, were conducted using sand particles' sizes of 200microns, 500microns and 800microns with sand concentration of 200lb and 500lb. From the analysis, saltation and suspension were the main flow regimes (sand) presented in this study. To further verify the results, sand sampling experiments were conducted, which proved that the larger sand particles' size of 500microns are largely transported at the bottom of the pipe, meaning saltation while the smaller particles' size of 212microns were largely transported at the gas core, which signified suspension.

  On effect of sand particles' size and concentration in annular flow, sand particles' size does not appear to have an impact on wave velocity and

wall shear stress, while sand concentration affects wall shear stress, but not wave velocity.

- OLGA dynamic multiphase flow simulator was used to compare the experimental results. OLGA simulation results on water/air/sand aligned with the results from sand probes and sand sampling. For flow regime (sand), sand probes were able to justify that sand particles were transported as saltation in the liquid film while OLGA presented it as suspension, (no bed). OLGA also presented a preferable results in the case of sand particles' size of 212microns, this is because sand particles' size of 212microns are smaller and as such would be much in number which attributed cumulatively to the volume presented by OLGA simulations.

7.1 Recommendations for Future Work.

- For future work on annular flow, large pipe diameter of (3-inch) should be experimented. This is to investigate if there are effects of pipe diameter size on sand transport in annular flow when compared with the results in this study.

- Future experiments on sand transport on annular flow with sand probes to be installed at 0^0, 45^0, 90^0 and 180^0 are recommended. This study, only concentrated on (0^0).

- Future experiment should involve sand coated with paints for better visual observations.

- Future experiments should be focused on, how the sand particles in the gas core are being transported by focusing on the conditions of the sand particles: Is it imbedded inside (coated) the droplets if not, are they moving randomly in the gas core? These requires more attention in sand transport in annular flow.

- Further attempt should be made using isokinetic approach for sand sampling. This will complement the effort made in the research.

- What could be the sand particle velocity if they are transported as dry sand in the gas core region (using PIV)? This should be investigated.

- Water/air/oil/sand annular flow could be investigated with 2-inch and 4-inch pipelines with the aid of CMC to see the effect of sand on annular flow in both horizontal and vertical pipes.

REFERENCES

Admiraal, D.M (2003) “Influence of Pipe Angle on Bedload Transport in an Inclined Pipe” Int. J. Sediment Res., 18(2): 122-129.

Afshin Goharzadeh., Peter Rodgers., Chokri Touati (2008) “Influence of Slug Flow on Hydraulic Sand Dune Migration in Horizontal Pipelines” Proceedings of IMECE2008, 2008 ASME International Mechanical Engineering Congress and Exposition October 31 –November 6, 2008, Boston, Massachusetts, USA.

Akilli, H, Levy, E, K and Sahin, B (2001) “Gas-Solid Flow Behaviour in a Horizontal Pipe after 90^0 Vertical-to-Horizontal Elbow” Power Technology, Vol.116, pp.43-52, *Elsevier*.

Alamu, M. B. and Azzopardi, B. J. (2011) “Wave and Drop Periodicity in Transient Annular Flow”, Nuc., Eng. Des. 241(12), pp. 5079-5092.

Aliyu, M. A., Lao, L. and Yeung, H. (2015) “A Comparative Analysis of Interfacial Friction Factor Correlation for Adiabatic Co-Current Gas-Liquid Annular Two-Phase Flow in Large Diameter Pipes” Proc., World Congress on Mechanical, Chemical and Material Engineering, Barcelona, Spain, July 20-21, No. 280, pp. 281-289.

Al-Lababidi, S., Yan, W., and Yeung, H (2012) “Sand Transportation and deposition Characteristics in Multiphase Flow in Pipelines” J. Energy Resources Technology 134, 034501 (2012), DOI:10.1115/1.4006433.

Al-Sarkhi, A., Sarica, C. and Magrini, K. (2012) “Inclination Effects on Wave Characteristics in Annular Gas-Liquid Flows” AIChE J. 58(4), pp. 1018-1029.

Anderson, R. J and Russell, T. W. F., (1970) “Circumferential Variation of Interchange in Horizontal Annular Two-Phase Flow”, *Ind. Engrg. Chem. Fundam.* 9, 340-344.

Angelsen, S., Kvernvold, O., Lingelem, M and Olsen, S (1989) “Long-Distance Transport of Unprocessed HC Sand settling in Multiphase Flow Lines” Multi-phase Flow-Proceedings of the 4th International Conference, 149-170.

Ankur, (2011) http://www.cheresour.com/per-api-rp-14e/

Asmund Huser and Oddmund Kvernvold, (1998) “Prediction of Sand Erosion in Process and Pipe Components” Det Norske Veritas, Veritsaveien1, N-1322 Hovik, NORWAY. Proc. 1st North American Conference on Multiphase Technology. Banff, Canada 1998. Ed.J.P. Brill, G.A. Gregory. BHR group Conf. Series. Publ. No 31 pp. 217-227

Azzopardi, B. J (1986) “Disturbance Wave Frequencies, Velocities and Spacing in Vertical Annular Two-Phase Flow” Nuclear Engineering and Design, Vol.92, pp. 121-133.

Balasubramaniam, R., Rame, E., Kizito, J. and Kassemi, M. (2006) “Two-Phase Flow Modeling: Summary of Flow Regimes and Pressure Drop Correlations in Reduced and Partial Gravity” National Center for Space Exploration Research, Cleveland, Ohio.

Beggs, H. D and Brill, J.P (1973) “A Study of Two-Phase Flow in Inclined Pipes” *Journal of Petroleum Technology*, Vol. 25, (5), pp. 607-617.

Bello, O.O., Kurt, M.R and Catalin, T (2005) “Particle Holdup Profile in Horizontal Gas-Liquid-Solid Multiphase Flow Pipeline” Chemical Engineering & Technology, 28 (12), 1546-1653.

Bendlksen, K. H., Malnes, D., Moe, R and Nuland, S (1991) “The Dynamic Two-Fluid Model OLGA: Theory and Application” SPE Production Engineering, vol.6, Issue 02.

Biberg, D., Staff, G. and Hoyer, N. (2015) “Accounting for Flow Model Uncertainties in Gas-Condensate Field Design using the OLGA High Definition Stratified Flow Model” BHR Group multiphase.

BP Statistical Review of World Energy, June, 2016.

Butterworth, D. (1972) “Air-Water Annular Flow in a Horizontal Tube”, *Prog. Heat Mass Transfer,* 6, 235-251.

Cairns, R. C., Lawther, K. R and Turner, K. S., (1960) “Flow Characteristics of Dilute Small Particle Suspension”, *Brit. Chem. Eng.,* Vol. 5, pp. 849-856.

Carlson, G. A. Experimental Errors and Uncertainty Lecture note, 2000-2002.

Chao, T, Dong, F and Shi, Y (2011) “Data Fusion for Measurement of Water Holdup in Horizontal Pipes by Conductivity Rings” IEEE, 978-1.

Chien, S and Ibele, W., (1964) “Pressure Drop and Liquid Film Thickness of Two-Phase Annular and Annular-Mist Flows”, ASME J. Heat Transfer, 86, pp. 80-86.

Chisholm, D (1967) “A Theoretical Basis for the Lockhart-Martinelli Correction for Two-Phase Flow” International Journal of Heat Mass Transfer, 10, pp. 1767-1778.

Coiado, E.M and Diniz, M.G (2001) “Two-Phase (Solid-Liquid) Flow in Inclined Pipes” J. Braz. Soc. Mech. Sci, Vol.23, no 3, Rio de Janeiro.

Condolios, E and Chapus, E. E., (1963) “Transporting Solid Materials in Pipelines”, *Chem. Eng*., Vol. 24, pp. 93-98.

Cousins, E. B. and Hewitt, G. F., (1968) “Liquid Phase Mass Transfer in Annular Two-Phase Flow; Droplet Deposition and Liquid Entrainment” UKAEA Report AERE-R5657.

Cuson, A.K and Hutchings, I.M (1983) “Influence on Erodent Particle Shape on the Erosion on Mild Steel” Proc. of the 6th Int. Conf. on Erosion by Liq. and Sol. Impact, Cavenish, 1983.

Dallman, J. C, Jones, B. G and Hanratty, T.J (1979) “Interpretation of Entrainment Measurements in Annular Gas-Liquid Flows” Int. J. Heat and Mass Transfer, Vol. 2, pp. 681-693, Hemisphere, Washington, D.C.

Danielson, T.J (2007) “Sand Transport Modeling in Multiphase Pipeline” Offshore Technology Conference.

Doron, P. and Barnea, D (1996) “Flow Pattern Maps For Solid-Liquid Flow in Pipes” International Journal Multiphase Flow. Vol.22, No.2, pp. 273-283.

Dukler, A.E, Wicks Moye and Cleveland (1964) “Frictional Pressure Drop in Two-Phase: A. A Comparison of Existing Correlations for Pressure Loss and Hold Up” *AIChE Journal,* Vol. 10 (1), pp. 38-43.

Durand, R (1953) “Basic Relationships of the Transportation of Solids in Pipes-Experimental Research” The Minnesota International Hydraulics Convention, University of Minnesota, Minneapolis, MN, pp. 89-103.

Durand, R. (1952) “The Hydraulic Transportation of Coal and Solid Materials in Pipe” Pt 1, London Colloquium of the National Coal Board, Neyrpic, Grenoble-Beauver,

Ellul, I.R., Saether, G., Mack, L.P and Shippen, E (2004) “The Modeling of Multiphase Systems under Steady-State and Transient Conditions – A Tutorial” Pipeline Simulation Interest Group, Annual Meeting in Palm Springs, California, 20-22 October.

Eltoukhy, M. A. R (2013) “Effect of Pipe Inclination on the Pipe Flow Head Losses for different Sand Concentration” International Journal of Civil Engineering and Technology (IJCIET) ISSN 0976-6308, Vol.4, no 3, May/June.

Eo Hwak Lee, Hee Cheon NO., Seung Hun Yoo., Kyung Won Lee and Chul-Hwa Song (2010) “Freezing Technique for Measuring and Predicting the Size of Droplets in a Horizontal Annular Flow” Department of Nuclear and Quantum Engineering, Korea Advanced Institute of Science and Technology, 373-1 Guseong-dong, Yuseong-gu, Daejeon 305-701, Republic of Korea, Nuclear Engineering and Design 240 (2010) 1795-1802, ELSEVIER.

Falcone, G, Hewitt, G.F and Richardson, S.M (2003) “ANUMET: A Novel Wet Gas Flowmeter” SPE Annual Technical Conference and Exhibition, Denver, Colorado, U.S.A. 5-8October.

Franklin, E. M (2013) “Prediction of Bed-load Transport by Gas-Liquid Stratified Flow in Horizontal Ducts” Applied Mathematical Modelling 37, pp. 5627-5636, Elsevier.

Fukano, F (1998) “Measurement of Time Varying Thickness of Liquid Film Flowing with High Speed Gas Flow by a Constant Electric Current Method” *Nucl.Eng. Des.* 184, pp. 363-377.

Fukano, T., Ousaka, A., Morimoto, T. and Sekoguchi, K. (1983) “Air-Water Annular Two-Phase Flow in a Horizontal Tube” (2nd Report, Circumferential Variations of Film Thickness Parameters), Bulletin of the JSME, 26(218).

Furukawa, T., Matsuyama, F. and Sadatomi, M. (2010) “Effects of Reduced Surface Tension on Liquid Film Structure in Vertical Upward Gas-Liquid Annular Flow” J. Power Energy System. 4(1), pp. 1-11.

Gawas, K., Karami, H., Pereyra, E., Al-Sarkhi, A. and Sarica, C. (2014) “Wave Characteristics in Gas-Oil Two-Phase Flow in Large Pipe Diameter” Int. J. Multiphase Flow, 63, pp. 93-104.

Gillies, R.G., McKibben, M.J and Shook, C.A (1997) “Pipeline Flow of Gas, Liquid and Sand Mixture at Low Velocities” The Journal of Canadian Petroleum Technology, 36, No.9, 36-42.

Guruprasad Kulkarni, Ravindra Devi, Biju Dasan, Paul Mathew, Yough Zhang, Emad Gharaibah and John Daniel Friedemann (2012) “Sand Erosion Experiments and Model Development for UNS NO6625 Clading and UNS S32750” Offshore Technology Conference, Houston, Texas.

Han, H, Zhu, Z and Gabriel, K (2006) “A Study on the Effect of Gas Flow Rate on the Wave Characteristics in Two-Phase Gas-Liquid Annular Flow” *Nuclear Engineering and Design, Vol., 236,* pp. 2580-2588.

Haugen, K., Kvernvold, O., Ronold, A and Sandberg, R (1995) “Sand Erosion of Wear Resistant Materials: Erosion in Choke Valves” Wear 186-187(1995) no.:179-188

Helgeland Sannæs, B and Johnson, G.W. (2010) “A comparison of OLGA with Two and Three-Phase High Pressure Pipe Flow Experiments: Flow Regime Prediction” BHR Group multiphase.

Hewitt, G.F and Hall-Taylor, N.S (1970) “Annular Two-Phase Flow” Pergamon Press.

Hill, A.L (2011) “Determining the Critical Flow Rates for Low-Concentration Sand Transport in Two-Phase Pipes Flow by Experimentation and Modeling” Ms Thesis, the University of Tulsa, Ok, USA.

Hughmark, G. A (1961) “Aqueous Transport of Settling Slurry” *Industrial and Engrg. Chem,* Vol. 55, pp. 389-390.

Ibarra, R., Mohan, R.S and Shoham, O (2014) “Critical Sand Deposition Velocity in Horizontal Stratified Flow” SPE International Symposium and Exhibition on Formation Damage Control, Lafayette, Louisiana, USA, 26-28th February.

Ishii, M and Mishima, K (1989) “Droplets Entrainment Correlation in Annular Two-Phase Flow” International Journal of Heat and Mass Transfer, Vol. 32, No. 10, pp. 1835-1846.

Jayanti, S, Hewitt, G. F and White, S. P (1990) “Time-dependent Behaviour of the Liquid Film in Horizontal Annular Flow” International Journal of Multiphase Flow, 16(6), pp. 1097-1116.

Jensen, P., Kvernvold, O and Sandberg, R (1991) “An Experimental Investigation of the Erosion Characteristics in Bean Chokes” VERITEC Report no.: 91-3059

Jiang, Z., Hagemier, T., Buck, A. and Tsotsas, E. (2017) “Experimental Measurement of Particles Collision Dynamics in a Pseudo-2D Gas-Solid Fluidized Bed” Chemical Engineering Science, S0009-2509(17) 30271-3.

Jones, O. C. and Zuber, N. (1975) “The Interrelation between Void Fraction Fluctuation and Flow Patterns in Two-Phase Flow” Int. J. Multiphase Flow, 2, pp. 273-306.

Kamyar Najmi., Alan L. Hill, Brenton S. Mclaury, Siamack A. Shirazi and Selen Cremaschi (2015) “Experimental Study of Low Concentration Sand Transport in Multiphase Air-Water Horizontal Pipelines” Journal of Energy Resources Technology, vol. 137. (032908-1)-(032908-10).

Kan Wai Choong, Lim Pei Wen, Lim Lay Tiong, Francis Anosike, Mohd Amin Shoushtari and Ismail bin Mohd Saaid (2014) “A comparative Study on Sand Trnsport Modeling for Horizontal Multiphase Pipeline” Faculty of Geosciences

and Petroleum Engineering, Universiti Teknologi PETRONAS (UTP) Tronoh, Malaysia, Scandpower Petroleum Technology Sd Bhd, Kuala Lumpur, Malaysia, Research Journal of Applied Science, Engineering and Technology 7(6): 1017-1024, February 15, 2014.

Keeys, R. K. F, Ralph, J. C and Roberts, D. N (1970) “Liquid Entrainment in Adiabatic Stream Water Flow at 500 and 1000psi” AERE-R-6293.

Kesana, N.R., Throneberry, J.M., Mclaury, B.S., Shirazi, S.A and Rybicki, E.F,(2012) “Effect of Particle Size and Viscosity on Erosion in Annular and Slug Flow” Proceedings of the ASME 2012 International Mechanical Engineering Congress & Exposition IMECE2012, November 9-15, 2012, Houston, Texas, USA.

King, M.J.S., Farhurst, C.P and Hill, T.J., (2000) “Solids Transport in Multiphase Flows Application to High Viscosity Systems” *Energy Sources Tech Conf, New Orleans,* pp. 14-17.

Kumar, R., Gottmann, M. and Sridhar, K. R. (2002) “Film Thickness and Wave Velocity Measurements in Vertical Duct” Transactions of ASME 124, pp. 634-642.

Kuncoro, B., Ulumuddin, B and Palar, S (2001) “Sand Control for Unconsolidated Reservoirs” Unocal Indonesia Company, Proceeding Simposium Nasional Iatmi, Yogyakarta, 3-5, oktober.

Kvernvold, O and Sandberg, R (1993) “CRDN 617: Production Rate Limits in Two-Phase Flow Systems: Erosion in Piping System for Production of Oil and Gas” DNV Report no.:93-3252

Laurinat, J. E., (1982) “Studies on the Effects of Pipe Size on Horizontal Annular Two-Phase Flows”, PhD Dissertation, University of Illinois at Urbana-Champaign.

Lawrence, P. A and Steven, R (2003) “Research Developments in Wet Gas Metering with V-Cone Meters” NSFMW.

Lin, P. Y (1985) “Flow Regime Transitions in Horizontal Gas-Liquid Flow”, PhD. Thesis, Univ. of Illinois, Urbana.

Magrini, K. L, Sarica, C, Al-Sarkhi, A and Zhang, H, Q (2012) “Liquid Entrainment in Annular Gas/Liquid Flow in Inclined Pipes” accepted at SPE Annual Technical Conference and Exhibition, Florence, Italy, 19-22 September, 2010, Published on SPE Journal, June, 2012.

Mantilla, I. (2008) “Mechanistic Modelling of Liquid Entrainment in Gas in Horizontal Pipes” PhD thesis, University of Tulsa, Tulsa, Oklahoma.

Mantilla, I., Gomez, L., Mohan, R., Shoham, O., Kouba, G and Roberts, R. (2009) “Modelling of Liquid Entrainment in Gas in Horizontal Pipes, Proc., ASME 2009 Fluids Engineering Division Summer Meeting, Colorado, USA, Vol. 1, No FEDSM2009-78459, pp. 979-1007.

McClusky, H. L., Holloway, M. V., Beasley, D. E. and Ochterbeck, J. M. (2002) “Continuous Wavelet Transforms of Instantaneous Wall Pressure in Slug and Churn Upward Gas-Liquid Flow” Journal of Fluid Engineering, Vol. 124, pp. 625-633.

Meng, H.S and Ludema, K.C (1995) “Wear Models and Predictive Equations; their form and Content” Wear 181-183 (1995) 443-457.

Meyer-Peter, E and Müller, R., (1948) “Formulas for Bed-load Transport” *Proceedings of the 2nd Meeting of the international Association for Hydraulic Structures Research,* pp. 39-64.

Mori, K., Kondo, Y., Kaji, M. and Yagishita, T. (1999) “Effects of Liquid Viscosity on Characteristics of Waves in Gas-Liquid Two-Phase Flow (Characteristics of Huge Waves and Disturbance Waves). JSME Int. J. Ser. B – Fluids Therm. Eng. 42, pp. 658-666.

Namie, S and Ueda, T (1972) “Droplet Transfer in Two-Phase Annular Mist Flow: Part 1. Experiment of Droplet Transfer Rate and Distributions of Droplet Concentration and velocity. Bull. JSME15 (90), 1568-1580.

Newitt, D. M., Richardson, J. F., Abbott, M. and Turtle, R. B., (1955) “Hydraulic Conveying of Solids in Horizontal Pipes”, *Trans. Inst. Chem. Eng.,* Vol. 33, 2, pp. 93-113.

Nguyen, T., Nguyen, A and Nieh, S (1989) “An Improved Isokinetic Sampling Probe for Measuring Local Gas Velocity and Particle Mass Flux of Gas-Solid Suspension Flows” Department of Mechanical Engineering, The Catholic University of America, Washington, DC 20064(USA), Powder Technology, 59 (1989) pp. 183-189.

Noah, D. M. (2005) “Measuring Pump Efficiency Uncertainty Considerations” Journal of Energy Resource Technology, Petroleum Division of ASME, Vol. 127, pp. 280-284

OLGA (2015) “Dynamic Multiphase Flow Simulator (user Manuel), Version 2015.2.

Oliemans, R. V, Pots, B. F. M and Trompe, N (1986) “Modelling of Annular Dispersed Two-Phase Flow in Vertical Pipes” Int. J. Multiphase Flow, Vol. 12, No.5, pp. 711-732.

Orell, A., (2007) “The Effect of Gas Injection on the Hydraulic Transport of Slurries in Horizontal Pipes” Chemical Engineering Science, 62, 6659-6676.

Oroskar, A.R and Turian, R.M (1980) “The Critical Velocity in Pipeline Flow of Slurries” AIChE J. 26(4), 550-558.

Oudeman, P (1993) “Sand Transport and Deposition in Horizontal Multiphase Trunklines of Subsea Satellite Developments” SPE Production & Facilities, 8(4), 237-241.

Ousaka, A and Kariyasaki, A., (1992) “Distribution of Entrainment Flow Rate for Air-Water Annular Two-Phase Flow in a Horizontal Tube” *JSME Int. J. Ser*. 2 35-II (3):354-360.

Ousaka, A, Deendarlianto, Kariyasaki, A and Fukano, T (2006) “Prediction of Flooding Gas Velocity in Gas-Liquid Counter-Current Two-Phase Flow in Inclined Pipes” *Nuclear Engineering and Design, Vol., 236,* pp. 1282-1292.

Ousaka, A., Morioka, I. and Fukano, T. (1992) “Air-Water Annular Two-Phase Flow in Horizontal and near Horizontal Tubes: Disturbance Wave Characteristics and Liquid Transportation” J. Multiphase Flow, 6(9), pp. 80-87.

Paleev, I. I and Filipovich, B. S., (1966) “Phenomena of Liquid Transfer in Two-Phase Dispersed Annular Flow”, *Int. J. Heat Mass Transfer*, 9, 1089.

Pan, L. and Hanratty, T. J (2002) (a) “Correlation of Entrainment for Annular Flow in Vertical Pipes” Int. J. Multiphase Flow, Vol. 28(3), pp. 363-384.

Pan, L. and Hanratty, T. J (2002) (b) “Correlation of Entrainment for Annular Flow in Horizontal Pipes” Int. J. Multiphase Flow, Vol. 28(3), pp. 385-408.

Paras, S. V and Karabelas, A. J (1991) “Droplet Entrainment and Deposition in Horizontal Annular Flow” Int. J. Multiphase Flow, Vol. 17, pp. 455-468.

Paras, S. V. and Karabelas, A. J., (1991) “Droplet Entrainment and Deposition in Horizontal Annular Flow”, *Int. J. Multiphase Flow,* 17 (4), pp. 455-468.

Pearce, D. L. and Fisher, S. A. (1979) A Theoretical Model for describing Horizontal Annular Flows, *In Two-Phase Momentum, Heat and Mass Transfer in Chemical, Process and Energy Engineering Systems, pp. 327-333, Hemisphere/McGraw-Hill, Washington, D.C.*

Peysson, Y. (2004) “Solid/Liquid Dispersion in Drilling and Production” Oil & Gas Science and Technology, IFP, Vol. 59, No. 1, pp. 11-21.

Prandtl, (1904) Ãœber Flussigkeitsbewegung bei sehr Kleiner Reibung: Verhandl, III int, Math, Kongr, Heidelberg.

Ramadan, A., Skalle, P and Saasen, A (2005) “Application of a Three-Layer Modelling Approach for Solids Transport in Horizontal and Inclined Channels” Elsevier, Chemical Engineering Science, vol.60, pp. 2557-2570.

Rao, K.V.L (1978) “Liquid Nitrogen Cooled Sampling Probe for the Measurement of Spray Drop Size Distribution in Moving Liquid-Air Sprays” Presented at 1st Int. Conf. on Liquid Atomization and Spray Systems, Tokyo, Japan (1978).

Ravelet, F., Bakir, F., Khelladi, S. and Rey, R. (2013) “Experimental study of hydraulic transport of large particles in horizontal pipes” Experimental Thermal and Fluid Science, Elsevier, Vol. 45, pp.187.

Salama, M.M (1998) “Sand Production Management” Offshore Technology Conference, Annual Proceedings, Field Drilling and Development Systems, 4, 743-751.

Salem, Al-lababidi (2014) “Introduction to Sand Erosion” Power Point presentation at Cranfield University, Oct, lecture room, October, 2014.

Sawant, P., Ishii, M., Hazuku, T., Takamasa, T., and Mori, M. (2008) “Properties of Disturbance Waves in Vertical Annular Two-Phase Flow” *Nuclear Engineering and Design, Vol., 238, pp*. 3528-3541.

Schubring D. and Shedd, T. A., (2008) “Wave Behaviour in Horizontal Annular Air-Water Flow”, *International Journal of Multiphase Flow*, 34, pp. 636-646.

Schubring, D and Shedd, T. A. (2008) “Wave Behaviour in Horizontal Annular Air-Water Flow” International Journal of Multiphase Flow, 34, pp. 636-646.

Scott, D.S and Rao, P.K (1971) “Transport of Solid by Gas-Liquid Mixtures in Horizontal Pipes” The Canadian Journal of Chemical Engineering: Canadian Society for Chemical Engineering, 1957-Hoboken, NJ: Wiley, Vol 49, No.3, pp.302-309.

Sergey, V. Alekseenko, Andrey, V. Cherdantsev, Mikhail, V. Cherdantsev, Sergey, V. Isaenkov, Sergey, M. Kharlamov and Dmitriy, M. Markovich (2014) “Formation of Disturbance Waves in Annular Gas-Liquid Flow” Kutateladze Institute of Thermophysics, Novosibirsk, Russia, Novosibirsk State University, Novosibirsk, Russia, 17th International Symposium on Applications of Laser Techniques to Fluid Mechanics, Lisbon, Portugal, 07-10 July, 2014.

Setyawan, A., Indarto and Deendarlianto (2016) “The Effect of the Fluid Properties on the Wave Velocity and Wave Frequency of Gas-Liquid Annular Two-Phase Flow in a Horizontal Pipe” Experimental Thermal and Fluid Science, ELSEVIER, Vol. 71, pp 25-41.

Setyawan, A., Indarto, Deendarlianto. And Prasetyo (2015) “Effects of Surface Tension on the Liquid Holdup and Wave Characteristics in Horizontal Annular Two-Phase Flow” Appl. Mech. Mater. 771, pp. 248-251.

Shedd, T. A., (2001) “Characteristics of the Liquid Film in Horizontal Two-Phase Flow”, Thesis for Doctor of Phil. in Mechanical Engineering the University of Illinois at Urbana-Champaign.

Shoeb, A. and Clifford, G. (2005) “Wavelets; Multiscale Activity in Physiological Signals” J. Biomedical Signal and Image Processing Spring, 2005.

Soeppyan F.B, Cremaschi, S, Sarica, C, Subramani, H.J and Kouba, G. E (2013) “Model Parameter Fine-tuning and Ranking Methodology to Improve the Accuracy of Threshold Velocity Predictions for Solid Particle Transport” Journal of Petroleum Science and Engineering, Vol 110, pp. 210-224.

Sommerfeld, M and Huber, N (1999) “Experimental Analysis and Modelling of Particle-Wall Collisions” International Journal of Multiphase Flow, Vol. 25, pp. 1457-1489.

Sommerfeld, M, (2003) “Analysis of Collision Effects for Turbulent Gas-Particle Flow in a Horizontal Channel: Part I, Particle Transport” International Journal of Multiphase Flow, Vol. 29, pp. 675-699.

Staff, G., Biberg, D., Vanvik, T., Hoyer, N., Nossen, J., Holm, H. and Johansson, P.S (2015) “Validation of OLGA HD against Transient and Pseudo-Transient Experiments from the SINTEF Large Diameter High Pressure Flow Loop” BHR Group multiphase.

Stevenson, P and Thorpe, R. B., (1999) “Towards understanding Sand Transport in Subsea Flowlines” BHR Group Multiphase ’99.

Stevenson, P and Thorpe, R.B (2002) “Velocity of Isolated Particles along a Pipe in Stratified Gas-Liquid Flow” American Institute of Chemical Engineers Journal, Vol. 48, No.5, pp. 963-969.

Stevenson, P and Thorpe, R.B (2003) “Energy Dissipation at the Slug Nose and the Modelling of Solids Transport in Intermittent Flow” Canadian Journal of Chemical Engineering, 81(2), 271-278.

Stevenson, P., Thorpe, R.B., Kennedy, J.E and McDermott, C (2001) ”The Transport of Particles at Low Loading in near-Horizontal Pipes by Intermittent Flow” Chemical Engineering Science, 56, 2149-2159.

Sunday, I and Andrew, F (2010) “Sand Failure Mechanism and Sanding Parameters in Niger Delta Oil Reservoirs” International Journal of Engineering Science and Technology 2, no. 5 (2010): 777-782.

Taitel, Y and Dukler, A. E., (1976) “A Model for Predicting Flow Regime Transitions in Horizontal and Near Horizontal Gas-Liquid Flow” *AICHE J.*, Vol. 22, pp. 47-55.

Takahashi, H, Masuyama, T and Noda, K (1989) “Unstable Flow of a Solid-Liquid Mixture in a Horizontal Pipe” International Journal of Multiphase Flow, 15(5), pp. 831-841.

Talaghat, M. R., Esmaeilzadeh, F. and Mowla, D. (2009) “Sand Production Control by Chemical Consolidation” Journal of Petroleum Science and Engineering, Vol. 67, pp. 34-40.

Tayebi, D., Nuland, S., and Fuchs, P., (2000) “Droplet Transport in Oil/Gas and Water/Gas Flow at High Gas Densities. *Int. J. Multiphase Flow*, 26 (5), pp. 741-761.

Tellas, A. S and Dukler, A. E., (1970) “Statistical Characteristics of Thin, Vertical, Wavy Liquid Films” Ind. Eng. Chem. Fundam., 9(3), pp. 412-421.

Thomas, D.G (1964) “Transport Characteristics of Suspension: Part IX. Representation of periodic Phenomena on a Flow Regime Diagram for Dilute Suspension Transport” Oak Ridge National Laboratory, Oak Ridge, Tennessee, American Institute of Chemical Engineers Journal, Vol.10, No 3, pp. 303-308.

Tso, C. P. and Sugawara, S. (1990) “Film Thickness Prediction in a Horizontal Annular Two-Phase Flow” Int. J. Multiphase Flow, Vol. 16, No. 5, pp. 867-884.

Tsuji, Y. and Morikawa, Y.(1982) “LDV Measurements of an Air-Solid Two-Phase in a Horizontal Pipe” Journal of Fluid mechanics, Vol. 120, pp. 385-409.

Turian, R.M and Yuan, T.F (1977) “Flow of Slurries in Pipelines” American Insitute of Chemical Engieers Journal, AIChE J, 23, pp. 232-243

Turian, R.M., Hsu, F.L., Ma, T.W, (1987) “Estimation of the Critical Velocity in Pipeline Flow of Slurries” Power Tech, 51, 35-47.

Vince, M. A. and Lahey, R. T. (1982) “On the Development of an Objective Flow Regime Indicator” Int. J. Multiphase Flow, 8, pp. 93-124.

Wagner, K (1982) “Investigation on the Influence of the Grain Size Distribution for Horizontal Hydraulic Conveying of Solids in the Heterogeneous Regime” Thesis, Karlsruhe.

Wallis, G. B (1968) “Phenomena of Liquid Transfer in Two-Phase Dispersed Annular Flow” Int. J. Heat Mass Transfer, 11(4), pp. 783-785.

Weber,M (1986) “Improved Durand-Equation for Multiphase Application” International Symposium on Slurry Flows, pp. 61-66.

Weidong, L., Fangde, Z., Rongxian, L., Lixing, Z. (1999) “Experimental Study on the Characteristics of Liquid Layer and Disturbance Waves in Horizontal Annular Flow” J. Therm. Sci. 8(4), pp. 235-242.

Wicks, M (1971) “Transport of Solids at Low Concentration in Horizontal Pipes” Shell Pipeline Corporation, R & D Laboratory, Houston, Texas, Publisher: Oxford; Pergamon, pp.101-123.

Wicks, M. and Dukler, A. E., (1960) “Entrainment and Pressure Drop in Concurrent Gas-Liquid Flow: Air-Water in Horizontal Flow” *AIChE. J*, 6, 463.

Wilkes, N. S., Azzopardi, B. J and Thompson, C. P. (1983) “Wave Coalescence and Entrainment in Vertical Annular Two-Phase Flow” International Journal of Multiphase Flow, 9 (4), pp. 383-398.

Willem, J.D and Van Dijck (1958) “Gas-Liquid Separator with Porous Wall Suction” The Hague, Netherlands, assignor to Shell Development Company, New York, N.Y, Publication Nunmber US2857979 A, 28 October, 1958.

Williams, L. R., (1990) “Effect of Pipe Diameter on Horizontal Annular Flow Two-Phase Flow”, PhD Dissertation, University of Illinois at Urbana-Champaign.

Wilson, K. C (1987) “Analysis of Bed Load Motion at High Shear Stresses” Journal of Hydrologic Engineering, ASCE 113 (1), pp. 97-103.

Wilson, K. C. (1979) “Deposition Limit Nomograms for Particles of various Densities in Pipeline Flow” Proceeding Hydro-transport 6 Conference, BHRA, Cranfield, UK, pp. 1-12.

Worster, R. C (1952) “Proceedings of Colloquium on Hydraulic Transport of Coal, National Coal Board, London.

Yan, W., Hu, X., Osho, Y and Yeung, H (2011) “Experimental Study on Sand Transport Characteristics in Water and Air-Water Flow in Dip Pipeline” In: Hunt, A.P. (Ed), 15th international Conference on Multiphase Production technology. BHR Group Limited, Cranfield, UK, pp, 51-68.

Zandi, I and Govatos, G., (1967) “Heterogeneous Flow of Solids in Pipelines” Journal of the Hydraulics Division, ASCE, Vol. 93, No. HY3, Proc. Paper 5244, May, pp. 145-159.

Zhang, G.J and Ishii, M (1995) “Isokinetic Sampling Probe and Image Processing System for Droplet Size Measurement in Two-Phase Flow” *Int. J. Heat Mass Transfer*. Vol. 38. No 11, pp. 2019-2027.

Zhao, Y., Markides, C. N., Matar., O. K. and Hewitt, G. F. (2013) “Disturbance Wave Development in Two-Phase Gas-Liquid Upwards Vertical Annular Flow” Int. J. Multiphase Flow, Vol.55. pp. 111-129.

Zhaochen Jiang, Thomas Hagemeier, Andreas Buck and Evangelos Tsotsas (2017) “Experimental Measurements of Particle Collision Dynamics in a Pseudo-

2D Gas-Solid Fluidized Bed" *Chemical Engineering Science, reference CES 13558.S0009-2509, Elsevier.*

APPENDICES

A-1: Calibration Using New sets of Blocks for Annular Flow

Conductivity Rings Calibration for Liquid Hold-Up

A bench calibration for liquid hold-up using conductivity ring sensors for annular flow was conducted using a 50mm (I.D) with a length of 154mm. The calibration was achieved using five different acryl rods of 49mm, 48mm, 47mm, 46mm and 45mm with a length of 154mm respectively.

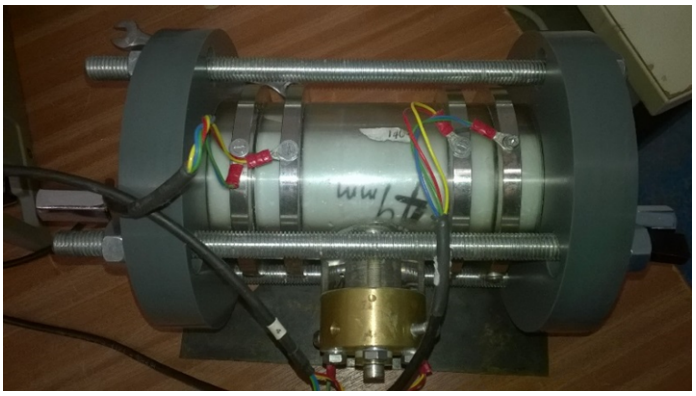

Figure A-1.1: Calibration Set-up

Figure A-1.2: *Acryl-Plastic Rods or Blocks*

The following were the procedure and process used in the calibration experiment;

- The 50mm horizontal pipe was filled with water without acryl rods and the voltage was recorded using the data digital acqusition system (Labview).

- Each of the acryl rods were inserted differently and the annulus between the 50mm (I.D) and the outer diameter of the acryl rod inserts, where filled with water and voltage were recorded in Labview at sacn duration of 60s.
- Also the the liquid fraction of each acryl rod inserts were noted using the weighing balance.
- The bench calibration was repeated three times.
- The voltage results recorded were normalized
- A graph of normalized voltage against Liquid hold up was plotted with equation for liquid hold-up obtained from it.
  C1 =y= 0.6601X – 0.0039 (R^2 = 0.9962)
  C2 = y= 0.681X – 0.006 (R^2 = 0.9947)
- The above equation of C1 and C2 were used to obtain the final liquid hold-up from the experimental data.

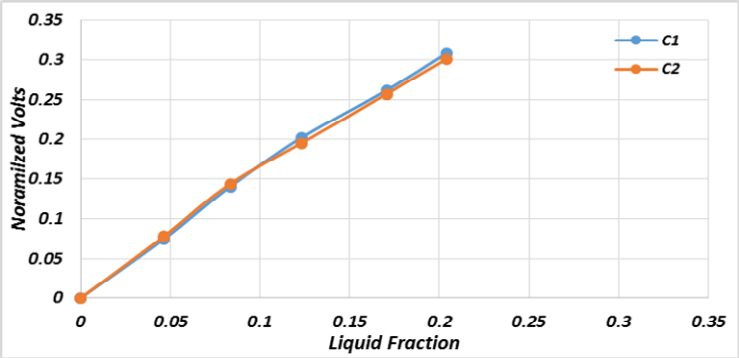

Figure A-1.3: **Liquid Hold-Up calibration from Conductive Ring Sensors**

Film Thickness Probe Calibration with solids objects

Bench calibration of film thickness was done using three solid cylindrical pipes of 49mm, 48mm, 47mm, 46mm and 45mm with a length of 154mm respectively.

A conductance (film thickness) probe used was flush mounted to a 50mm (ID) pipe. The both ends of the 50mm (ID) pipe were sealed.

Procedure

- The 50mm pipe was clamped to the base of the table in order to ensure that the water and the solids objects were stable.

- The empty pipe of 154mm was recorded. Full pipe of 154mm with water was also recorded.
- The solid objects were then inserted in these order, 49mm, 48mm, 47mm 46mm and 45mm and were recorded.
- The gap or space between the pipe of 50mm and the solid objects used (49mm, 48mm, 47mm, 46mm and 45mm), represents the ***reference film thickness*** in the bench calibration.
- Each of the experiment with the solids were repeated 3times
- The output voltage was normalized and the plotted against the reference film thickness yield the equation for film thickness as
  $Y = -0.0253X^2 + 0.2532X + 0.016$ ($R^2 = 0.9949$)

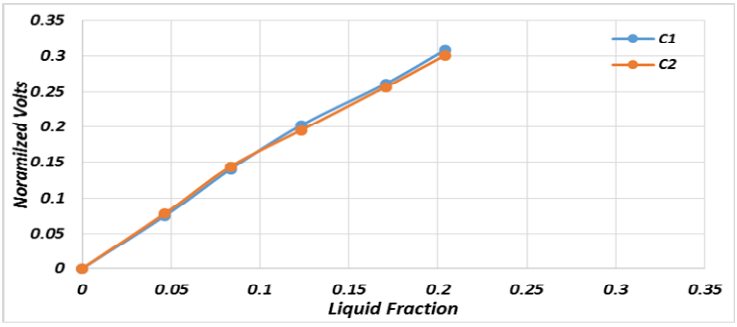

Figure A-1.4: Film Thickness Probe Calibration with solids objects

Conductivity Rings Calibration for Film Thickness

A bench calibration for liquid film thickness using conductivity ring sensors for annular flow was conducted using a 50mm (I.D) with a length of 154mm. The calibration of liquid film thickness for annular flow was achieved using five different acryl rods inserts of 49mm, 48mm, 47mm, 46mm and 45mm with a length of 154mm respectively. The following were the procedure and process used in the calibration experiment;

- The 50mm horizontal pipe was filled with water without acryl rods and the voltage was recorded using the data digital acqusition system (Labview).
- Each of the acryl rods were inserted differently and the annulus between the 50mm (I.D) and the outer diameter of the acryl rod inserts, where filled with water and voltage were recorded in Labview at sacn duration of 60s.

- Also the the liquid fraction of each acryl rod inserts were noted using the weighing balance.
- The bench calibration was repeated three times.
- The voltage results recorded were normalized
- A graph of normalized voltage against reference film thickness was plotted with equations as;

  C1 = y= 0.0618X + 0.0098 (R^2 = 0.9951)

  C2 = y= 0.0598X + 0.0129 (R^2 = 0.9925)
- The above equations of C1 and C2 could be used to obtain the final film thickness from the experimental data.

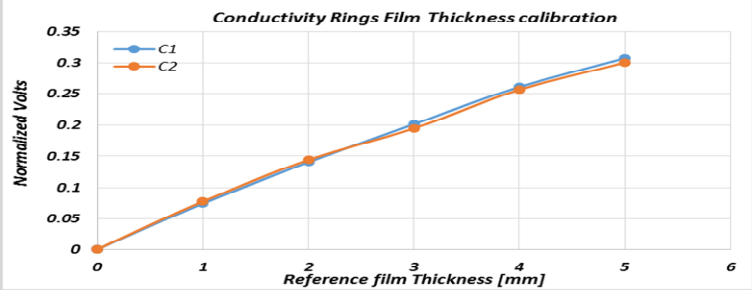

Figure A-1.5: Conductivity Rings Film Thickness Calibration

Below are the old and the new final liquid hold-up obtained from the calibration graphs and equations from the 2015 and the 2017 calibrations conducted. The average actual error and the average standard deviation were calculated as shown in the Tables.

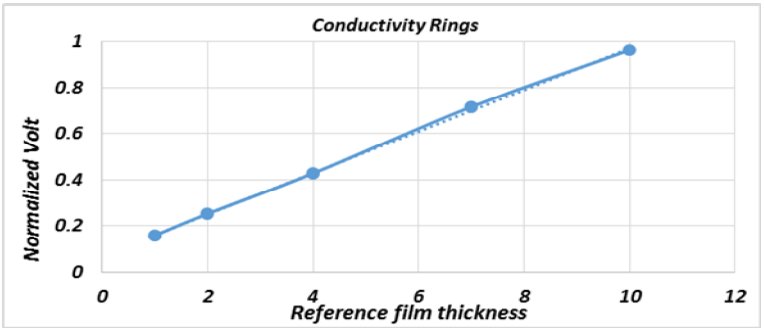

Figure A-1.6: Conductivity Rings Film Thickness Calibration (Old)

The reference film thickness calibration equation is Y=-0.0044x +0.1256x +0.112 (R^2 0.9992).This is the old calibration conducted.

The liquid film thickness could also be obtained from Tso and Sugawara (1990) equation below:

$$\delta = \frac{D}{2}\left(1 - \sqrt{(\varepsilon g)}\right) \quad \textbf{(3-4)}$$

where D is pipe diameter, εg is void fraction.

For the liquid hold-up, the newly obtined results presented a higher liquid hold-up compared to the previous results. While the liquid film thickness obtained from the new calibration was in close range with the previous results. Below are the statistical error analysis results:

Table A-1.0.1: Summary of Statistical Error for new Liquid Hold-up from previous Liquid Hold-up Calibrated.

Vsl [m/s]	*Average Actual Error*	*Average Relative Error [%]*	*Standard Deviation*
0.0505	0.0187	57.2982	7.5696
0.0714	0.0336	67.4514	8.2129
0.0903	0.0395	65.4298	8.0889
0.1355	0.0489	63.0458	7.9401
0.1851	0.0573	61.5088	7.8428

Table A-1.0.2: Summary of Statistical Error for new Film Thickness from previous ones

Vsl [m/s]	*Average Actual Error*	*Average Relative Error [%]*	*Standard Deviation*
0.0505	0.0486	30.5548	5.5276
0.0714	0.0239	12.8667	3.5870
0.0903	0.0142	7.1323	2.6706
0.1355	0.0068	3.2552	1.8042
0.1851	0.0022	0.9972	0.9986

In conclusion, the differences from the results of the new (liquid hold-up and film thickness) when compared with the previous (liquid holdup and liquid film thickness) results, could be attributed to instrumentation error. The previous calibrations was conducted alongside the experiments with the same conductivity box and condition for the experiments. Again, the error margin could also be as a result of the conductivity box tuning, as the previous calibration showed a more realistic results with both liquid hold up and film thickness, even with respect to liquid entrainments.

The new calibration results gave a high liquid holdup in the entire flow conditions with thin (low) film thickness. In reality, the former calibration results is better hence it presents most realistic results in all conditions, having compared them in this study.

B-2: Liquid Hold-Up in Annular Flow

Mathematical Development of Liquid Hold-Up in Annular Flow

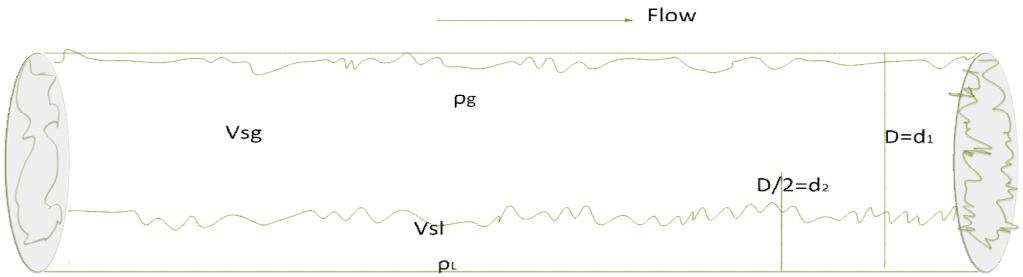

In developing an equation for liquid hold up in annular flow, the flowing assumption will be made.

- That the full pipe will be regarded as the diameter.
- That the liquid hold up occupies half or less than the entire diameter of the pipe.
- The length is less significant in developing the equation.
- Viscosity is less important.
- Will assume mass as liquid or gas mass flow rate.

To model it, the density of gas and the density of the liquid will be of paramount as follows;

Density = Mass divide by volume.

$$\rho = \frac{M}{V} \qquad \textbf{[B-1]}$$

For the purpose of two-phase flow, density will be classified as liquid or gas density as below;

$$\rho_L = \frac{M_L}{V} \text{ and } \rho_g = \frac{Mg}{V} \qquad \textbf{[B-2]}$$

Therefore, for the liquid phase;

$$\rho_L = \frac{M_L}{V} \qquad \textbf{[B-3]}$$

Above equation B.3 could also be expanded as;

$$\rho_L V = M_L \qquad \textbf{[B-4]}$$

The interest is on V, hence we make V the subject of the formula by dividing through by liquid density as;

$$\frac{\rho_L V}{\rho_L} = \frac{M_L}{\rho_L} \quad \textbf{[B-5]}$$

$$V = \frac{M_L}{\rho_L} \quad \textbf{[B-6]}$$

However, mass liquid flow rate is a function of liquid density, superficial gas velocity and cross-section area of the pipe.

Thus, the above equation B.6 becomes;

$$V = \frac{\rho_L V_{SL} A}{\rho_L} \quad \textbf{[B-7]}$$

So equation B.7 reduces to;

$$V = V_{SL} A \quad \textbf{[B-8]}$$

But volume is a function of area and height or thickness,

$$V = A \times h \quad \textbf{[B-9]}$$

Therefore the equation becomes;

$$Ah = V_{SL} A \quad \textbf{[B-10]}$$

Divide through by Area, the above equation will yield;

$$\frac{Ah}{A} = \frac{V_{SL} A}{A} \quad \textbf{[B-11]}$$

$$h_L = V_{SL} \quad \textbf{[B-12]}$$

Following the same procedure, the density of gas which will be,

$$h_g = V_{Sg} \quad \textbf{[B-13]}$$

For annular flow in pipes, the gas velocity is always higher than the liquid velocity. Also the gas occupies more space in term of height in the pipe than the liquid phase. Therefore the liquid height is divided by the gas height to obtain liquid hold as follows,

$$\frac{h_L}{h_g} = H_L = \frac{V_{SL}}{V_{Sg}} \qquad \textbf{[B-14]}$$

Again, note that,

$$V_{SL} = \frac{q_L}{A}, V_{Sg} = \frac{q_g}{A} \qquad \textbf{[B-15]}$$

Thus, equation B.14 when substituted into equation B.15 yields;

$$H_L = \frac{V_{SL}}{V_{Sg}} = \frac{\frac{q_L}{A}}{\frac{q_g}{A}} \qquad \textbf{[B-16]}$$

Therefore, liquid hold-up in annular becomes;

$$H_L = \left(\frac{q_L}{q_g}\right)\left(\frac{d_1}{d_2}\right) \qquad \textbf{[B-17]}$$

The above equation B.17 of liquid hold-up was compared with the measured liquid hold-up from the experiments and other published liquid hold-up as shown in figures B.1.1-B.1.10.

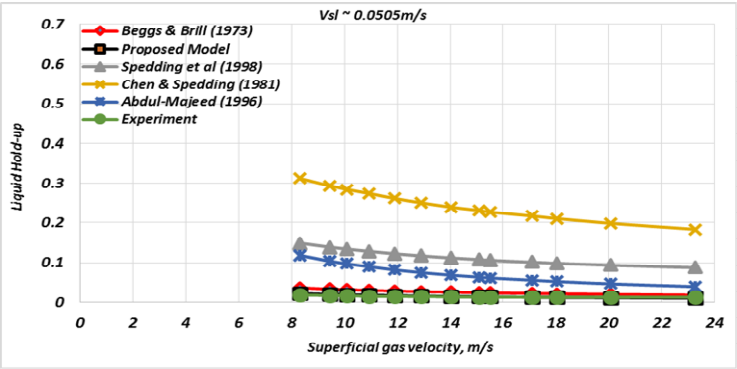

Figure B-1.1: Proposed Model, Measured and other Liquid Hold-up (Vsl=0.0505m/s)

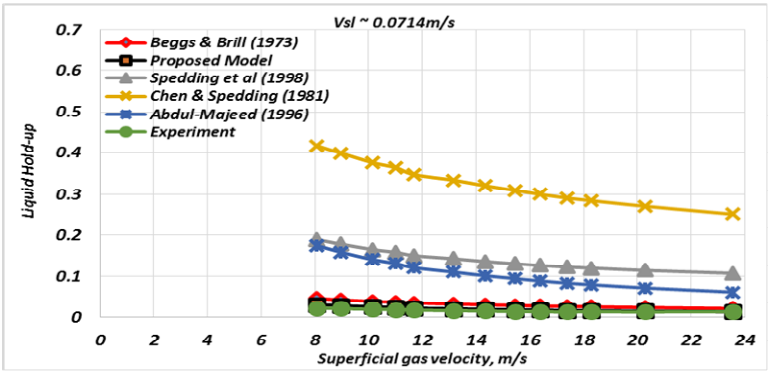

Figure B-1.2: Proposed Model, Measured and other Liquid Hold-up (Vsl=0.0714m/s)

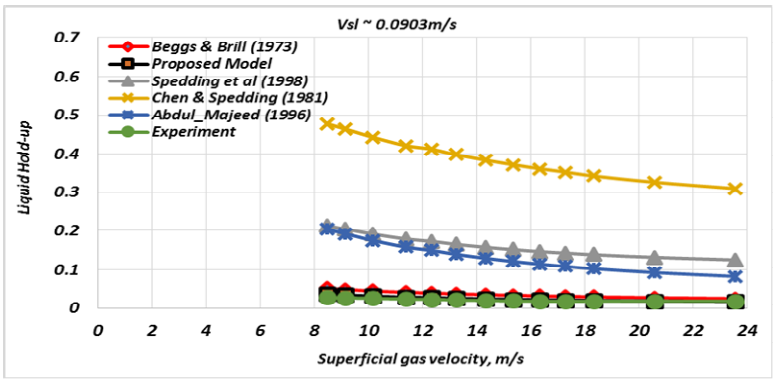

Figure B-1.3: Proposed Model, Measured and other Liquid Hold-up (Vsl=0.0903m/s)

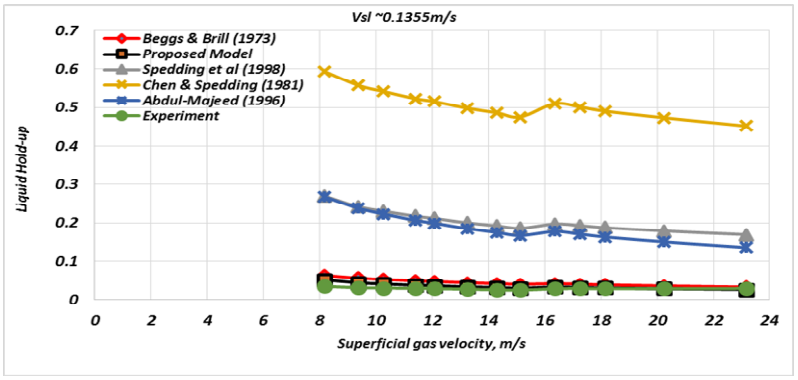

Figure B-1.4: Proposed Model, Measured and other Liquid Hold-up (Vsl=0.1355m/s)

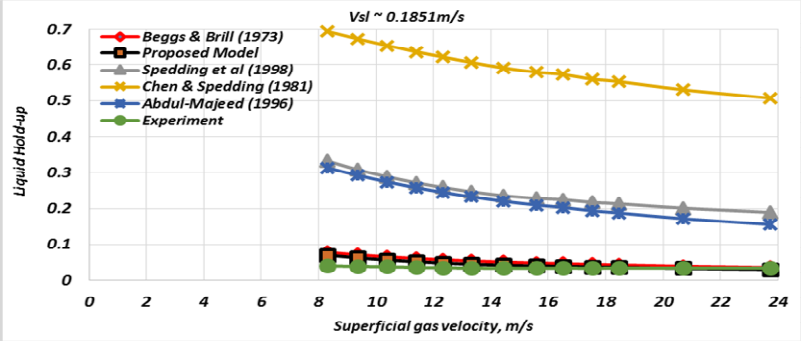

Figure B-1.5: Proposed Model, Measured and other Liquid Hold-up (Vsl=0.1851m/s)

B-2.1: Liquid Hold-Up Proposed Model/Beggs & Brill (1973) Against Measured

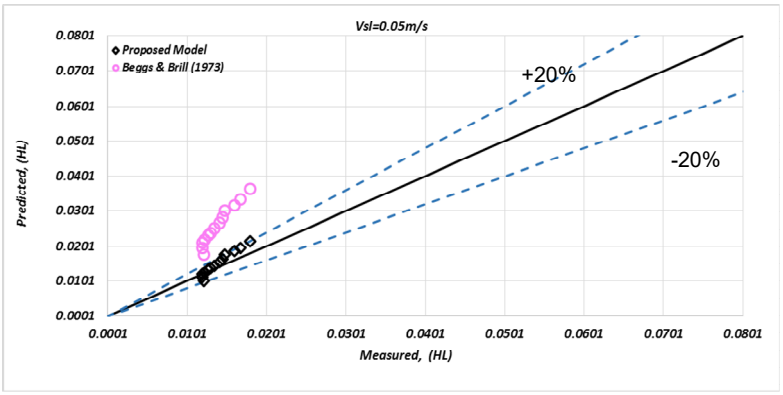

Figure B-2.1: Proposed Model/Beggs & Brill (1973) Vs Measured (Vsl=0.0505m/s)

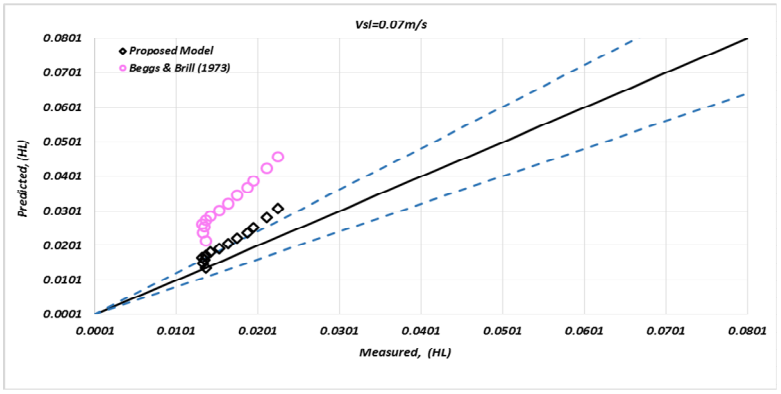

Figure B-2.2: Proposed Model/Beggs & Brill (1973) Vs Measured (Vsl=0.0714m/s)

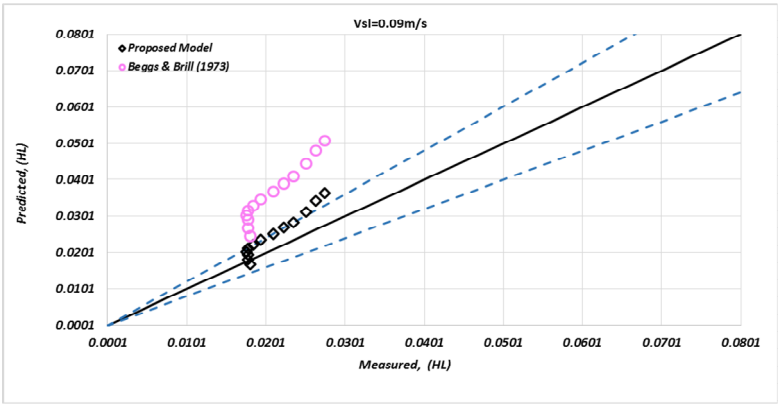

Figure B-2.3: Proposed Model/Beggs & Brill (1973) Vs Measured (Vsl=0.0903m/s)

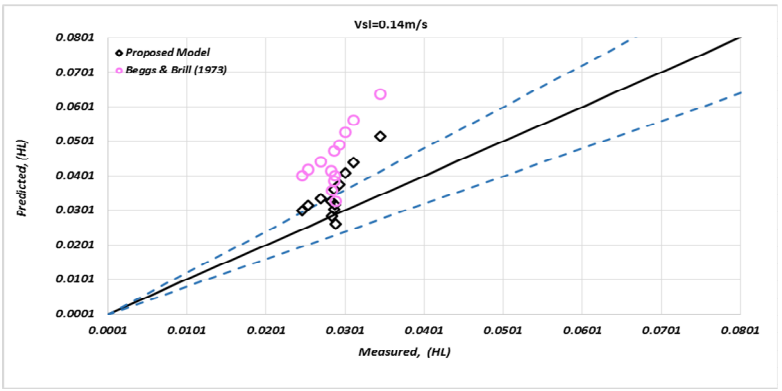

Figure B-2.4: Proposed Model/Beggs & Brill (1973) Vs Measured (Vsl=0.1355m/s)

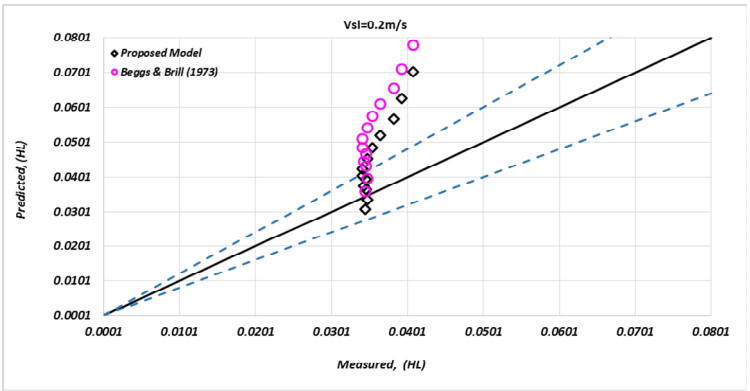

Figure B-2.5: Proposed Model/Beggs & Brill (1973) Vs Measured (Vsl=0.1851m/s)

C-1.Calculation on Solid Concentration by Volume

100% =1,000,000

M = Density x Volume.

If 100% = 1,000,000

a. CV? , 200lb of sand particles.

Therefore,

$$CV = \frac{M}{V}, \quad CV = \frac{200}{1000000} = 0.0002$$

Calculating the total mass particles used becomes,

$$M = \rho V$$

Where density of particle used is 2650[kg/m^3], V = Cv.

$$M = 0.0002\,x2650 = 0.53kg$$

b. 500lb.

$$Cv = \frac{500}{1000000} = 0.0005$$

$$M = 0.0005 \times 2650 = 1.325\,kg$$

D-1: Uncertainty of Pump Efficiency

To determine the uncertainty of the pump used in my experiment, the overall pump efficiency measurement will be expressed as;

$$\eta = \frac{P_d Q_d}{T\omega} \quad \textbf{(D-1)}$$

Where

Pd = Discharge pressure of the pump,

Qd = Volumetric flow rate measured at discharge port of the port,

T = Shaft torque,

ω = Angular velocity of the shaft.

For the purpose of the pump uncertainty analysis, the overall pump efficiency will be further expatiated as;

- Torque efficiency
- Volumetric efficiency

Where torque efficiency could be expressed as;

$$\eta_t = \frac{V_d P_d}{T} \quad \textbf{(D-2)}$$

Volumetric efficiency as;

$$\eta = \frac{Q_d}{V_d \omega} \quad \textbf{(D-3)}$$

Expanding the above equations (D.2) and (D.3) to determine the uncertainty of the overall pump efficiency could be achieved using Taylor series by define as uncertainty as noted by Noah, (2005) as;

$$\varepsilon = \frac{\eta' - \eta}{\eta} \quad \textbf{(D-4)}$$

Apply Taylor series on equation (D.4) on the experimental measured values will yield the following;

$$\varepsilon = \left(\frac{\partial \varepsilon}{\partial P_d}\right)^{'}\left(P_d - P^{'}{}_d\right) + \left(\frac{\partial \varepsilon}{\partial Q_d}\right)^{'}\left(Q_d - Q^{'}{}_d\right) + \left(\frac{\partial \varepsilon}{\partial T}\right)^{'}\left(T - T^{'}\right) + \left(\frac{\partial \varepsilon}{\partial \omega}\right)^{'}\left(\omega - \omega^{'}\right) \qquad \textbf{(D-5)}$$

Look at it from the general overall pump efficiency equation earlier expressed in equation (D.1), the equation (D.5) could be expressed as;

$$\left(\frac{\partial \varepsilon}{\partial P_d}\right)^{'} = -\frac{1}{P^{'}{}_d} \qquad \textbf{(D-6)}$$

$$\left(\frac{\partial \varepsilon}{\partial \omega}\right)^{'} = \frac{1}{\omega^{'}} \qquad \textbf{(D-7)}$$

$$\left(\frac{\partial \varepsilon}{\partial T}\right)^{'} = \frac{1}{T^{'}} \qquad \textbf{(D-8)}$$

$$\left(\frac{\partial \varepsilon}{\partial Q_d}\right)^{'} = -\frac{1}{Q^{'}{}_d} \qquad \textbf{(D-9)}$$

Putting the above equations into equation (D.5) yields the overall pump efficiency as;

$$\varepsilon = -\frac{\left(P_d - P^{'}{}_d\right)}{P^{'}{}_d} - \frac{\left(Q_d - Q^{'}{}_d\right)}{Q^{'}{}_d} + \frac{\left(T - T^{'}\right)}{T^{'}} + \frac{\left(\omega - \omega^{'}\right)}{\omega^{'}} \qquad \textbf{(D-10)}$$

Also using the Taylor series expansion equations (D.6), (D.7), (D.8), and (D.9) into equations (D.2) and (D.3) will yield;

Torque efficiency

$$\varepsilon_t = -\frac{\left(V_d - V^{'}{}_d\right)}{V^{'}{}_d} - \frac{\left(P_d - P^{'}{}_d\right)}{P^{'}{}_d} + \frac{\left(T - T^{'}\right)}{T^{'}} \qquad \textbf{(D-11)}$$

Volumetric efficiency becomes;

$$\varepsilon_v = -\frac{\left(Q_d - Q^{'}{}_d\right)}{Q^{'}{}_d} + \frac{\left(V_d - V^{'}{}_d\right)}{V^{'}{}_d} + \frac{\left(\omega - \omega^{'}\right)}{\omega^{'}} \qquad \textbf{(D-12)}$$

Summarizing the entire uncertainty equations (D.11) and (D.12), the following could be obtained in accordance with Noah, (2005).

$$\left(T - T^{'}\right) = \pm \beta_t T_{\max} \quad \textbf{(D-13)}$$

$$\left(V - V^{'}{}_d\right) = \pm \beta_v V_{\max} \quad \textbf{(D-14)}$$

$$\left(\omega - \omega^{'}\right) = \pm \beta_\omega \omega_{\max} \quad \textbf{(D-15)}$$

$$\left(P_d - P^{'}{}_d\right) = \pm \beta_p P_{\max} \quad \textbf{(D-16)}$$

$$\left(Q_d - Q^{'}{}_d\right) = \pm \beta_q Q_{\max} \quad \textbf{(D-17)}$$

Where β represents the accuracy range of full scale from the manufacturers.

In conclusion, the uncertainty of overall pump efficiency could be expressed mathematically by substituting equations D.13, D.14, D.15, D.16 and D.17 into D.10 as;

$$\varepsilon = \pm \left[\beta_p \frac{P_{\max}}{P^{'}{}_d} + \beta_q \frac{Q_{\max}}{Q^{'}{}_d} + \beta_t \frac{T_{\max}}{T^{'}} + \beta_\omega \frac{\omega_{\max}}{\omega^{'}} \right] \quad \textbf{(D-18)}$$

E-1.1: Water/Air in Annular Flow - Error and Uncertainty Analysis.

For the water/air annular flow experiments, the average flow matrix used were Vsl = (0.0501, 0.0714, 0.0903, 0.1400 & 0.2001) [m/s] while the Vsg were (8.2699, 9.2654, 10.2160, 11.2251, 12.0675, 13.1692, 14.2883, 15.3236, 16.2262, 17.3086, 18.2481, 20.3847 & 23.4575) [m/s]. Thus, the error and uncertainty analysis are elaborated as follows;

Differential Pressure Measurement (Pressure Transducer)

The pressure transducers used were P_1 (P-up) and P_2 (P-down). The differential pressure measurement for error analysis was calculated as follows; for error result;

$$\Delta P = P_1 - P_2 \quad \textbf{E-1.1}$$

$$\delta(\Delta P) = \sqrt{\delta(P_1)^2 + \delta(P_2)^2} \quad \textbf{E-1.2}$$

where,

$$Error\ , \delta(P_1) = \frac{E}{100} \times F \quad \textbf{E-1.3}$$

$$Error\ , \delta(P_2) = \frac{E}{100} \times F \quad \textbf{E-1.4}$$

For uncertainty analysis result;

$$U\,(\%) = \frac{\delta(\Delta P)}{M(P_1) - M(P_2)} \times 100\ \% \quad \textbf{E-1.5}$$

The error analysis result for the superficial liquid velocities with respect to superficial gas velocities is 0.0043[bar] and uncertainty results are shown in table E-1.1 below;

Table E-1.1: Uncertainty Result for Differential Pressure (Water/Air in Annular Flow).

Average Vsl [m/s]	*Average Vsg [m/s]*	*DP=P_1-P_2 [bar]*	*Average Uncertainty [± %]*
0.0505	8.2699-23.4575	0.0446-0.0551	8.6031
0.0714	8.2699-23.4575	0.0474-0.0575	7.9998
0.0903	8.2699-23.4575	0.0517-0.0598	7.5753
0.1355	8.2699-23.4575	0.0603-0.0697	6.5908
0.1851	8.2699-23.4575	0.0772-0.0794	5.4573

Flow Meter (Gas Flow Rate)

The error analysis result of the gas flow meter from the experimental flow matrix is 0.1556[bar] while the uncertainty results are shown in Table E-1.2.

Table E-1.2: Uncertainty Result for Gas Flow Rate (Water/Air in Annular Flow)

Average Vsl [m/s]	*Average Vsg [m/s]*	*Qg [L/s]*	*Average Uncertainty [± %]*
0.0505	8.2699-23.4575	9.5864-20.0167	1.1478
0.0714	8.2699-23.4575	8.0774-23.5416	1.1009
0.0903	8.2699-23.4575	10.2527-21.5380	1.0600
0.1355	8.2699-23.4575	10.3275-22.5677	1.0168
0.1851	8.2699-23.4575	11.2538-23.7582	0.9474

Flow Meter (Liquid Flow Rate)

The error analysis result obtained from the flow matrix is 0.0444[bar] while the uncertainty results are shown in Table E-1.3 below;

Table E-1.3: Uncertainty Result for Liquid Flow Rate (Water/Air in Annular Flow)

Average Vsl [m/s]	*Average Vsg [m/s]*	*QL [L/s]*	*Average Uncertainty [± %]*
0.0505	8.2699-23.4575	0.1035-0.1015	43.4464
0.0714	8.2699-23.4575	0.1485-0.1431	30.7024
0.0903	8.2699-23.4575	0.1871-0.1827	24.2902
0.1355	8.2699-23.4575	0.2667-0.2955	16.5145
0.1851	8.2699-23.4575	0.3953-0.3659	11.8503

E-1.2: Water/Sand Flow

The uncertainties of the instruments used are;

Differential Pressure Measurement (Pressure Transducer)

For the differential pressure measurement, P_1 (P-up) and P_2 (P-down) the error analysis result was 0.0043[bar] while the uncertainty results are in Table E-1.4 below.

Table E-1.4: Uncertainty for differential pressure for Water/sand flow

Sand [1000bbl]	*Average Vsl [m/s]*	*DP=P_1-P_2 [bar]*	*Average Uncertainty [± %]*
200lb/212microns	0.1504-0.2983	0.0398-0.0415	10.7045
200lb/500microns	0.1527-0.2945	0.0378-0.0402	11.1625
500lb/500microns	0.1481-0.2958	0.0380-0.0402	11.2323

Flow Meter (Liquid Flow Rate)

For the water/sand flow test, the error analysis result was 0.0444[bar] while the average uncertainty results are shown in Table E-1.5.

Table E-1.5: Uncertainty results for liquid flow rate in water/sand flow test

Sand [1000bbl]	*Average Vsl [m/s]*	*Qw [L/s]*	*Average Uncertainty [± %]*
200lb/212microns	0.1504-0.2983	0.3004-0.5955	11.0569
200lb/500microns	0.1527-0.2945	0.3048-0.5879	10.9985
500lb/500microns	0.1481-0.2958	0.2957-0.5906	11.1342

Flow Meter (Water/Sand Mixture Flow Rate) from Sand Hopper

The uncertainty results are shown in Table E-1.6 below;

Table E-1.6: Uncertainty results for water/sand mixture flow rate from sand hopper

Sand [1000bbl]	*Average Vsl [m/s]*	*Qw.s [L/s]*	*Average Uncertainty [± %]*
200lb/212microns	0.1504-0.2983	0.1403-0.1235	9.1514
200lb/500microns	0.1527-0.2945	0.1152-0.1176	9.7568
500lb/500microns	0.1481-0.2958	0.1431-0.1397	8.2809

E-1.3:Water/Air/Sand in Annular Flow (Multiphase Flow)

For water/air/sand in annular flow, two different concentrations were used (200lb and 500lb) while three different sand particle sizes were used (212microns, 500microns and 800microns).

The experiment on water/air/sand flow was conducted to determine sand behaviour/transport in annular flow. And based on high flow of gas in the experiment in order to achieve annular flow, the error and uncertainty analysis are needful to determine the accuracy of the experiment.

Differential Pressure Measurement (Pressure Transducer)

The different pressure measurements have an error of 0.0043[bar] for all the sand conditions. The uncertainty results analysed are shown in table E-1.7 below;

Table E-1.7: Uncertainty results for differential pressure in Water/sand flow test

Sand [1000bbl]	*Average Vsl [m/s]*	*DP=P_1-P_2 [bar]*	*Average Uncertainty [± %]*
200lb/212microns	0.0372-0.0568	0.0492-0.0570	8.3418
200lb/500microns	0.0349-0.0601	0.0456-0.0576	8.5149
500lb/212microns	0.03716-0.0613	0.0459-0.0586	8.3960
500lb/500microns	0.0350-0.0563	0.0461-0.0571	8.3549
200lb/800microns	0.0345-0.0605	0.0478-0.0601	8.2186
500lb/800microns	0.0374-0.0563	0.0468-0.0578	8.3955

Flow Meter (Liquid Flow Rate)

The uncertainty results for water/air/sand (liquid flow rate) are shown in Table E-1.8 below while the error was obtained as 0.0444***[L/s] .***

Table E-1.8: Uncertainty for liquid flow rate for Water/air/sand in annular flow

Sand [1000bbl]	*Average Vsl [m/s]*	*Qw [L/s]*	*Average Uncertainty [± %]*
200lb/212microns	0.0372-0.0568	0.0742-0.1135	46.9596
200lb/500microns	0.0349-0.0601	0.0697-0.1201	50.1206
500lb/212microns	0.03716-0.0613	0.0742-0.1225	45.8412
500lb/500microns	0.0350-0.0563	0.0699-0.1124	48.7288
200lb/800microns	0.0345-0.0605	0.0689-0.1209	49.8291
500lb/800microns	0.0374-0.0563	0.0748-0.1125	48.1186

Flow Meter (Gas Flow Rate)

The uncertainty results analysis obtained are shown in Table E-1.9. The error was the same in all flow matrix conditions as 0.0156[L/s].

Table E-1.9: Uncertainty results for gas flow rate from water/air/sand in annular flow.

Sand [1000bbl]	*Average Vsl [m/s]*	*Qg[L/s]*	*Average Uncertainty [± %]*
200lb/212microns	0.0372-0.0568	11.4698-15.5961	1.2273
200lb/500microns	0.0349-0.0601	10.3105-15.2978	1.2263
500lb/212microns	0.03716-0.0613	10.2489-15.7403	1.2565
500lb/500microns	0.0350-0.0563	9.8283-15.3699	1.2683
200lb/800microns	0.0345-0.0605	10.1437-15.9312	1.2739
500lb/800microns	0.0374-0.0563	10.4341-15.6679	1.2607

Flow Meter (Water/Sand Mixture Flow Rate) from Sand Hopper

Again, the uncertainty results analysis obtained are shown below in Table E-1.10 while the error was the same in all the flow matrix used as 0.01167 [L/s] with the details shown in appendix E.4.

Table E-1.10: Uncertainty results (water/sand mixture flow rate) from water/air/sand in annular flow.

Sand [1000bbl]	*Average Vsl [m/s]*	*Qw.s[L/s]*	*Average Uncertainty [± %]*
200lb/212microns	0.0372-0.0568	0.1174-0.1277	9.3159
200lb/500microns	0.0349-0.0601	0.1331-0.1370	8.5261
500lb/212microns	0.03716-0.0613	0.1219-0.1377	8.4953
500lb/500microns	0.0350-0.0563	0.1469-0.1401	8.0766
200lb/800microns	0.0345-0.0605	0.1349-0.1263	8.8565
500lb/800microns	0.0374-0.0563	0.1276-0.1384	8.3742

F-1.1: Statistical Error Analysis Used

The statistical error analysis was done to determine the margin between the measured and OLGA simulation results. The experiments were measured using different instruments like pressure transducers, probes, pairs of ring, LED and flow meter (gas, water), while OLGA was build or developed based on physical models from continuity equations, momentum, energy and correlations. Therefore comparing the measured and those of physical models in necessary.

The statistical parameters used are;

Relative Error,

$$Ei = \frac{(ei_{measured} - ei_{OLGA})}{ei_{measured}} \times 100\ \% \quad \textbf{(F-1)}$$

Average Actual Error,

$$\bar{N} = \frac{1}{N}\sum_{1}^{N} ei \quad \textbf{(F-2)}$$

Standard Deviation

$$Std_dev = \sqrt{\frac{\sum_{1}^{N}\left(ei - \bar{N}\right)}{N-1}} \quad \textbf{(F-3)}$$

F-1.2: OLGA plotted for Water/Air/Sand Annular Flow.

The following are the OLGA simulation of water/air/sand annular flow showing the results;

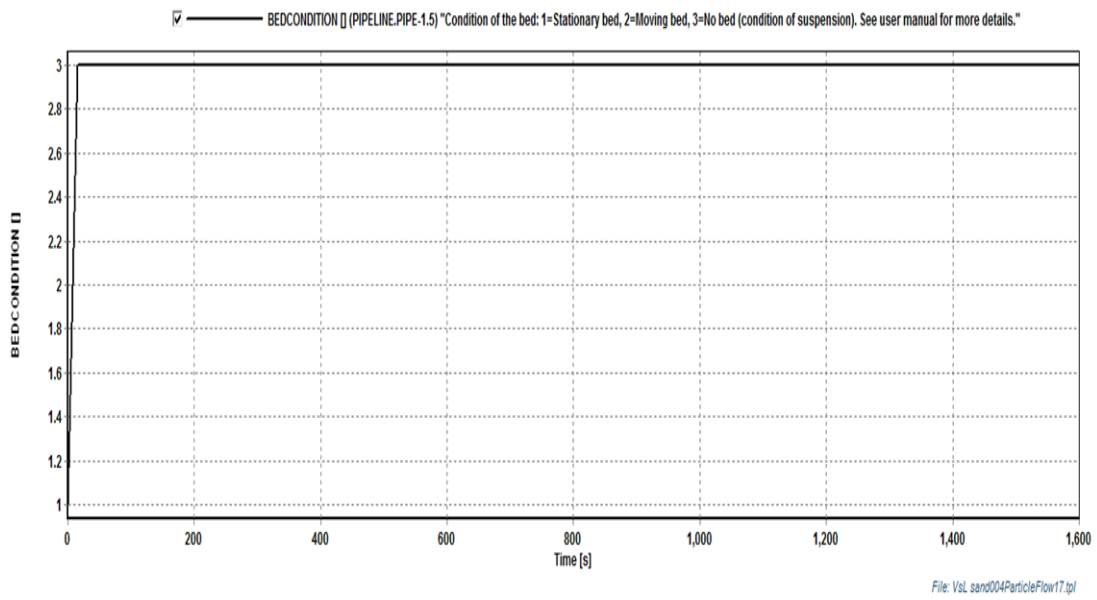

Figure F-1.1: Sand Flow Regime in Sand Transport in Annular Flow (Vsl=0.1236m/s and Vsg = 14.4325m/s, 500microns, 500lb/1000bbl)

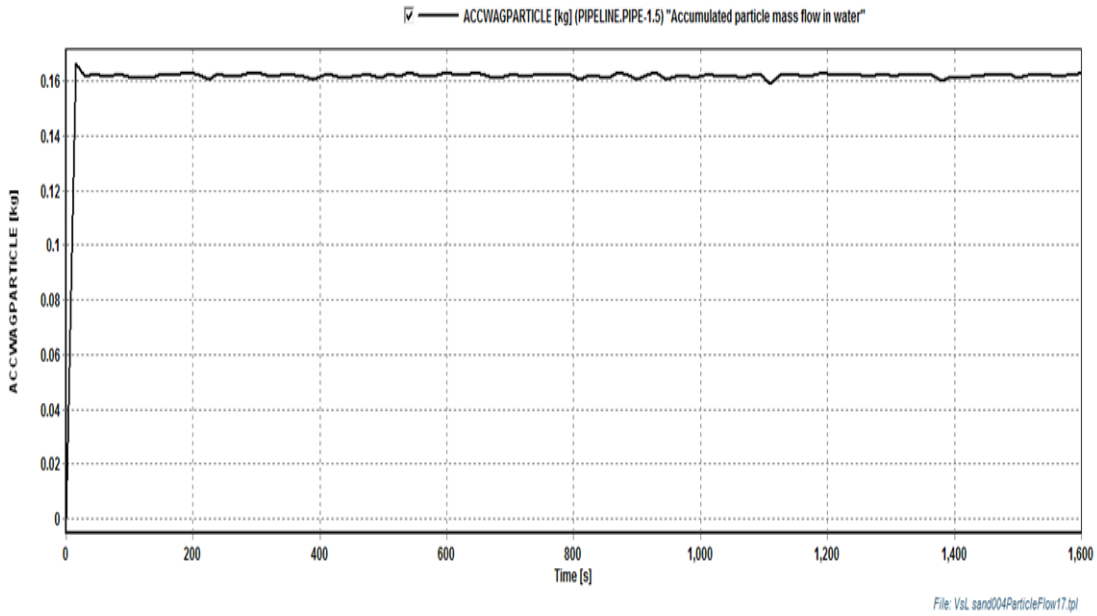

Figure F-1.2: Particle Mass flow in water in Annular Flow (Vsl=0.1236m/s and Vsg = 14.4325m/s, 500microns, 500lb/1000bbl)

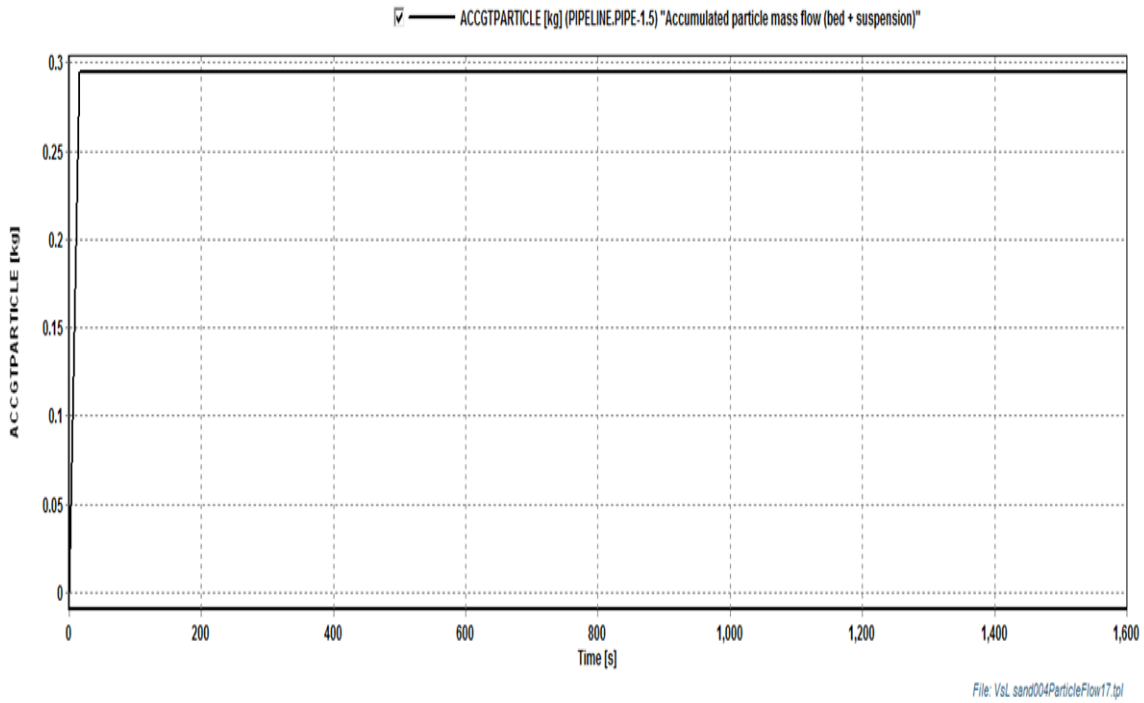

Figure F-1.3: Particle Mass flow in suspension in Annular Flow (Vsl=0.1236m/s and Vsg = 14.4325m/s, 500microns, 500lb/1000bbl)

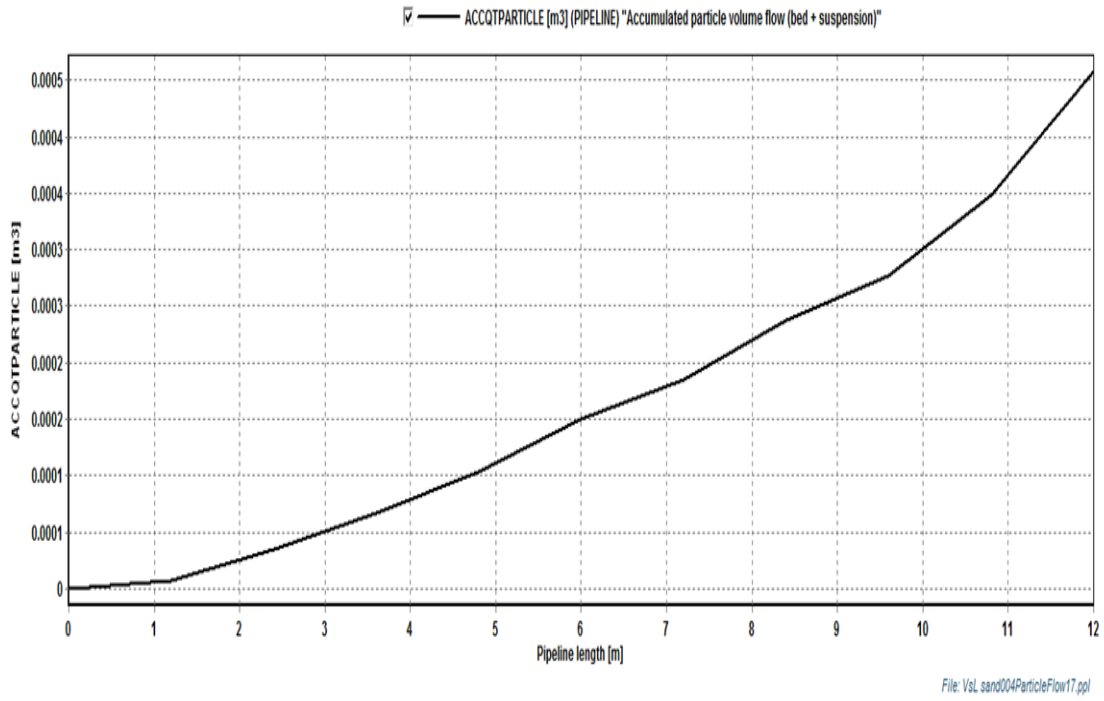

Figure F-1.4: Sand Particle Volume in water in Annular Flow with Length (Vsl=0.1236m/s and Vsg = 14.4325m/s, 500microns, 500lb/1000bbl)

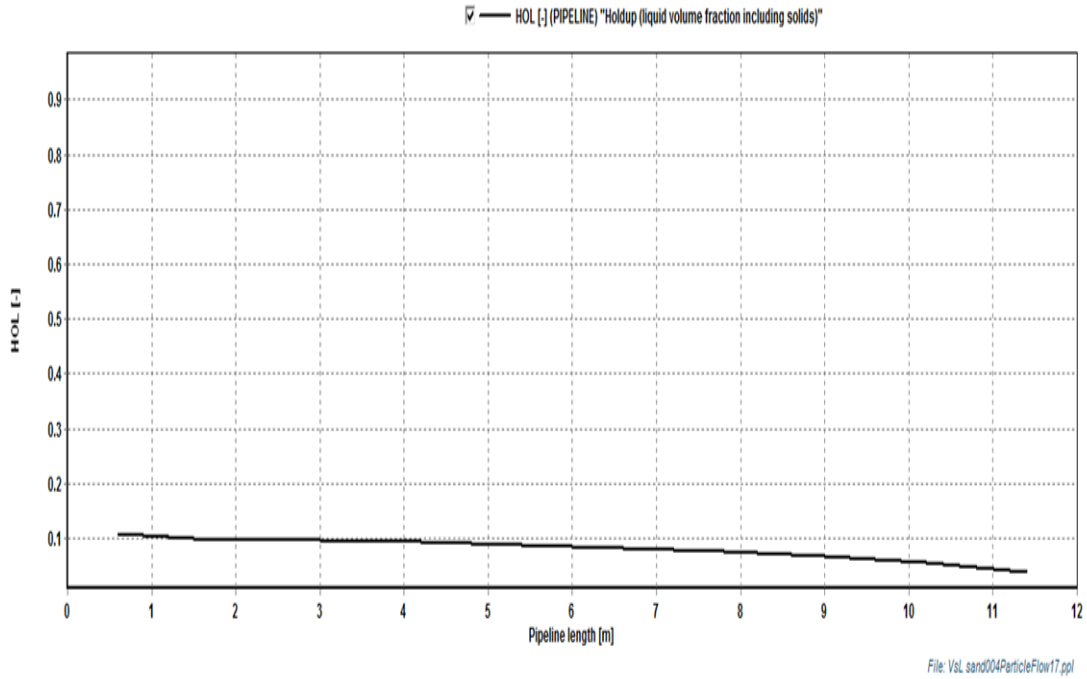

Figure F-1.5: Liquid Hold-up in Annular Flow with the Length (Vsl=0.1236m/s and Vsg = 14.4325m/s, 500microns, 500lb/1000bbl)

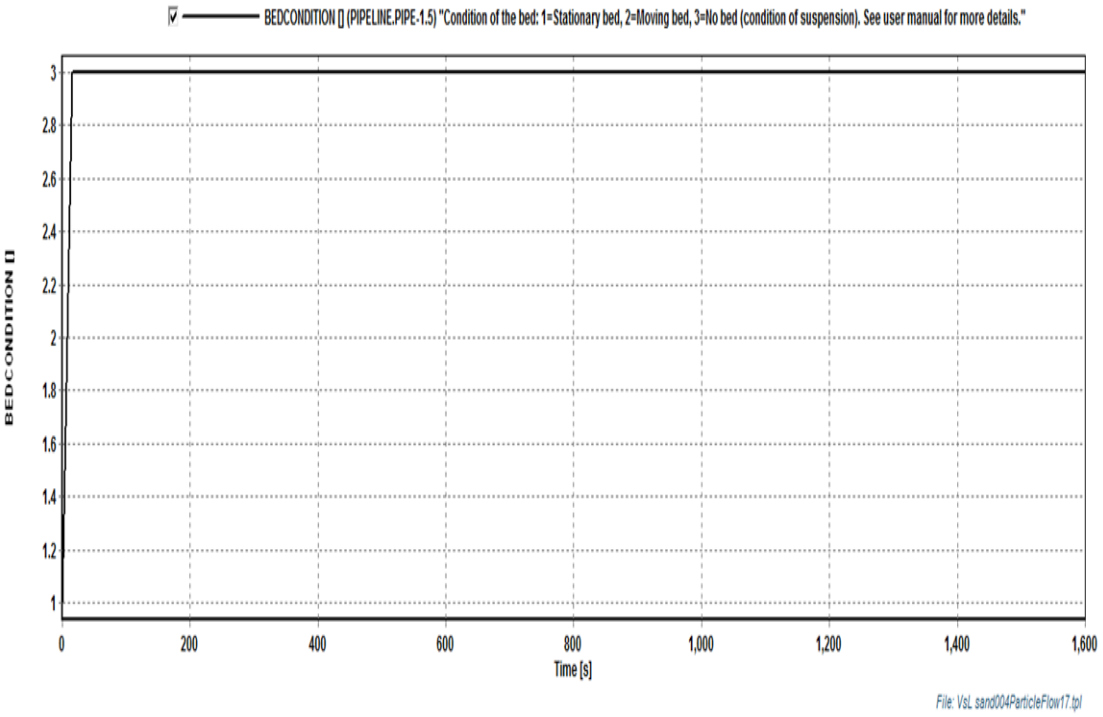

Figure F-1.6: Sand Flow Regime in Sand Transport in Annular Flow (Vsl=0.1257m/s and Vsg = 15.0489m/s, 800microns, 500lb/1000bbl)

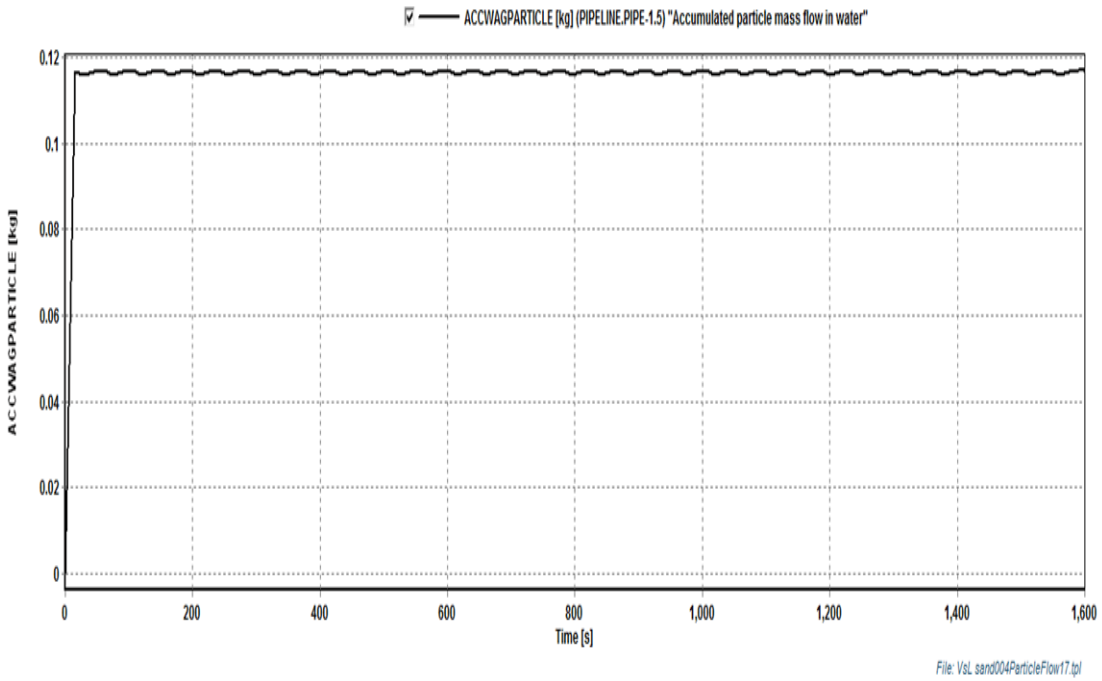

Figure F-1.7: Particle Mass flow in water in Annular Flow (Vsl=0.1257m/s and Vsg = 15.0489m/s, 800microns, 500lb/1000bbl)

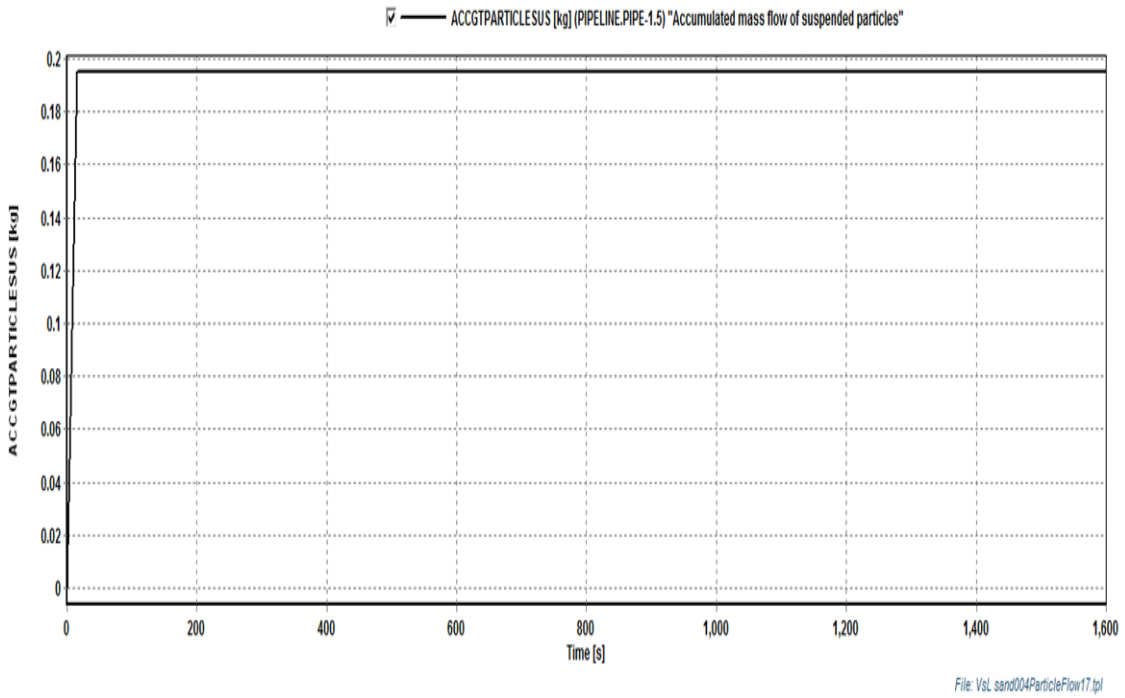

Figure F-1.8: Particle Mass flow in suspension in Annular Flow (Vsl=0.1257m/s and Vsg = 15.0489m/s, 800microns, 500lb/1000bbl)

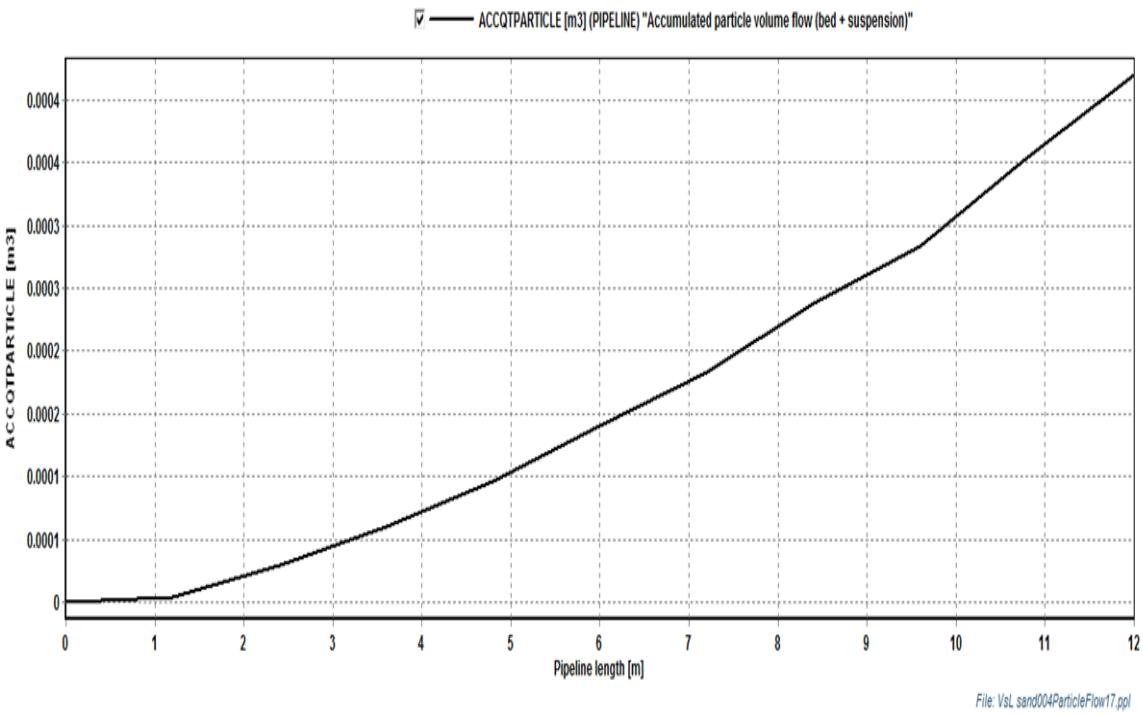

Figure F-1.9: Sand Particle Volume in water in Annular Flow with Length (Vsl=0.1257m/s and Vsg = 15.0489m/s, 800microns, 500lb/1000bbl)

Table G-1.1: Annular Flow in 2-inch pipe

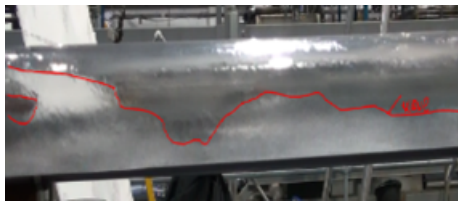 *Vsl=0.0508m/s, Vsg = 10.0773m/s*	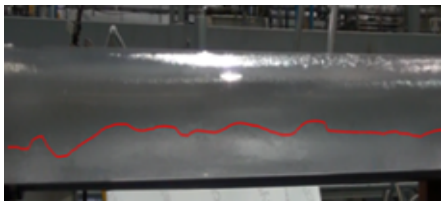 *Vsl=0.0502m/s, Vsg = 14.0307m/s*	*Vsl=0.0504m/s, Vsg = 17.0857m/s*	*Vsl=0.0501m/s, Vsg = 23.2796m/s*
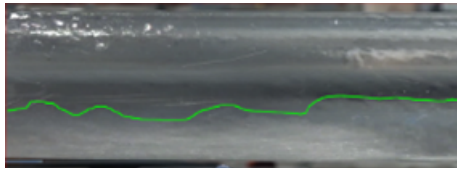 *Vsl=0.0721m/s, Vsg = 10.1592m/s*	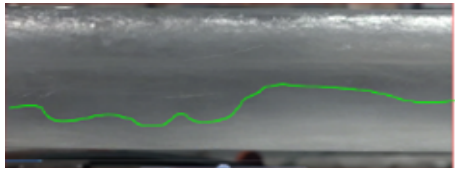 *Vsl=0.0713m/s, Vsg = 14.3349m/s*	*Vsl=0.0706m/s, Vsg = 17.3721m/s*	*Vsl=0.0706m/s, Vsg = 23.5416m/s*
Vsl=0.0910m/s, Vsg = 10.1754m/s	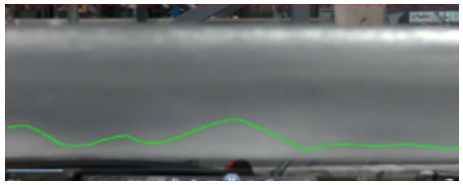 *Vsl=0.0899m/s, Vsg = 14.3424m/s*	*Vsl=0.0893m/s, Vsg = 17.3035m/s*	*Vsl=0.0901m/s, Vsg = 23.5707m/s*
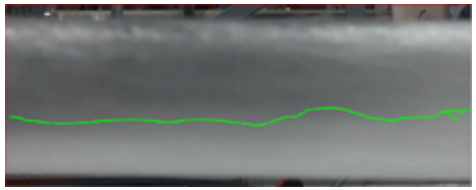 *Vsl=0.1892m/s, Vsg = 10.3928m/s*	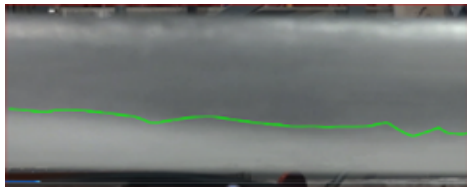 *Vsl=0.1819m/s, Vsg = 14.4407m/s*	*Vsl=0.1822m/s, Vsg = 17.5279m/s*	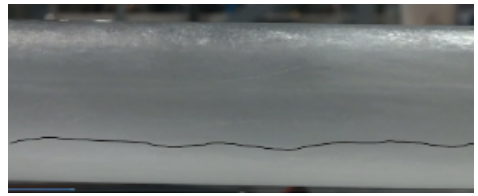 *Vsl=0.1805m/s, Vsg = 23.7259m/s*

Flow direction

Table G-1.2: Wavelet Analysis on Film Thickness in Annular Flow

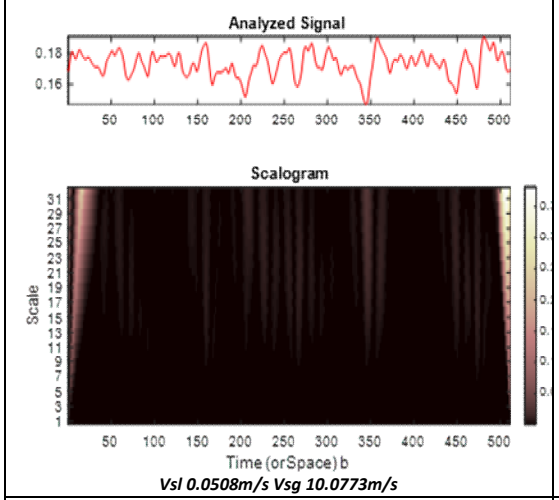

Vsl 0.0508m/s Vsg 10.0773m/s

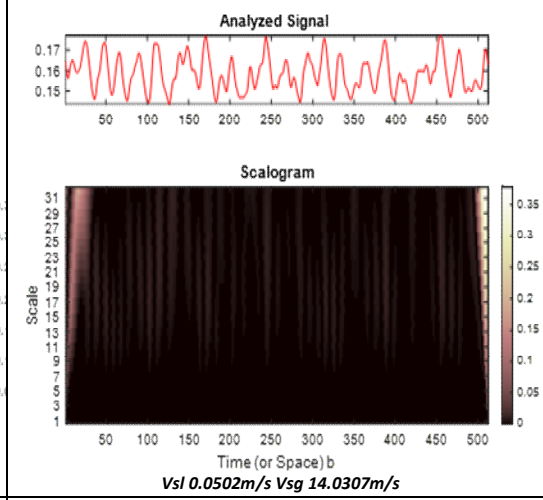

Vsl 0.0502m/s Vsg 14.0307m/s

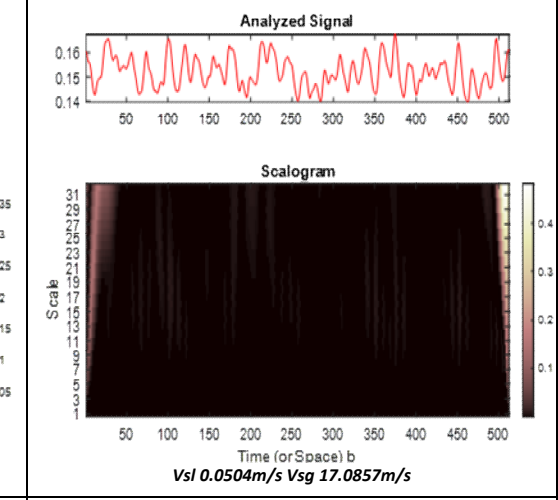

Vsl 0.0504m/s Vsg 17.0857m/s

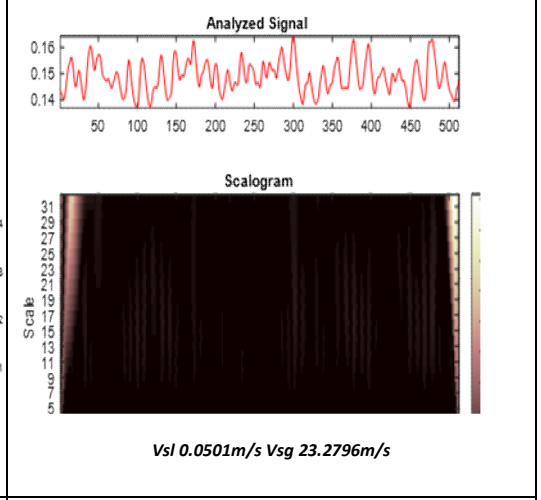

Vsl 0.0501m/s Vsg 23.2796m/s

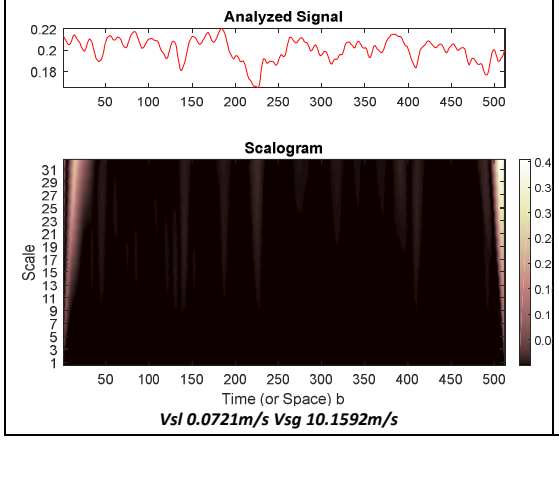

Vsl 0.0721m/s Vsg 10.1592m/s

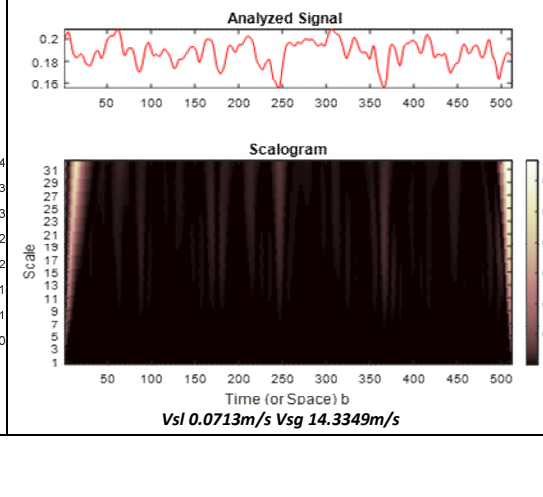

Vsl 0.0713m/s Vsg 14.3349m/s

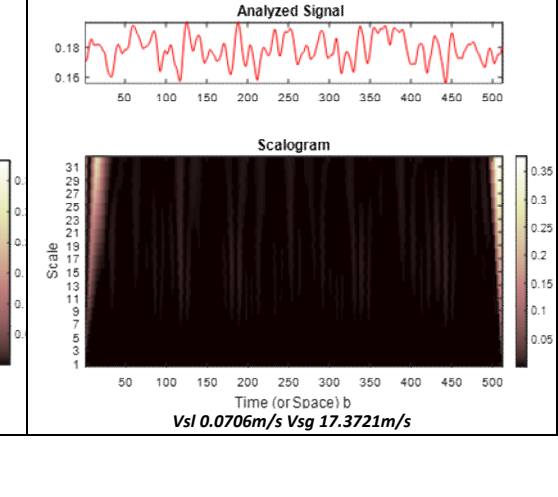

Vsl 0.0706m/s Vsg 17.3721m/s

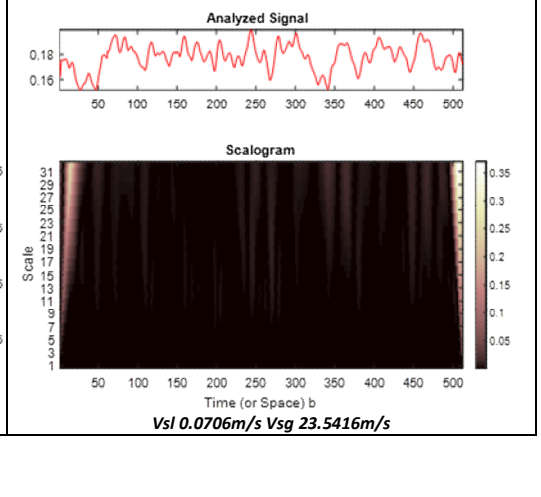

Vsl 0.0706m/s Vsg 23.5416m/s

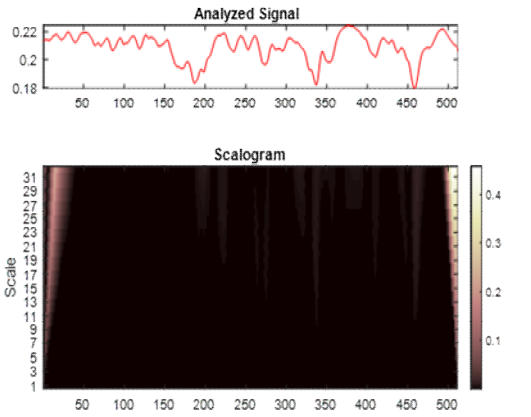

Vsl 0.0910m/s Vsg 10.1754m/s

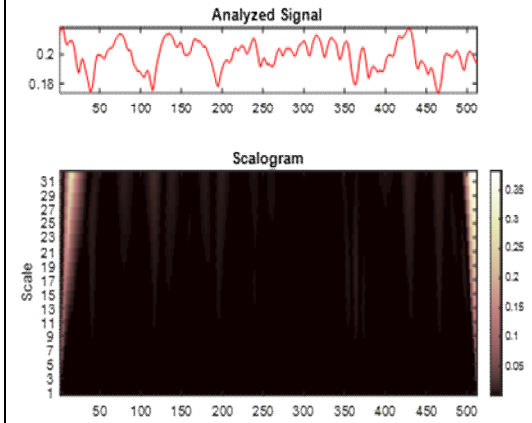

Vsl 0.0899m/s Vsg 14.3424m/s

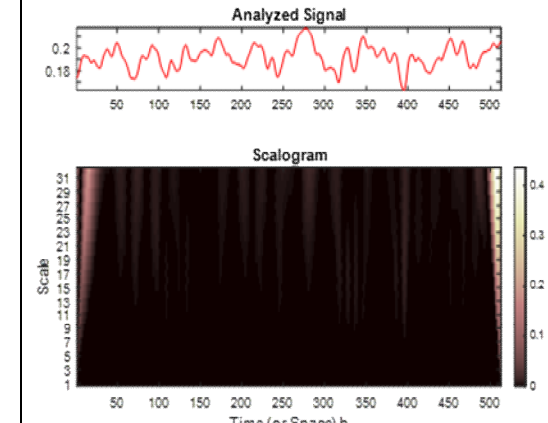

Vsl 0.0893m/s Vsg 17.3035m/s

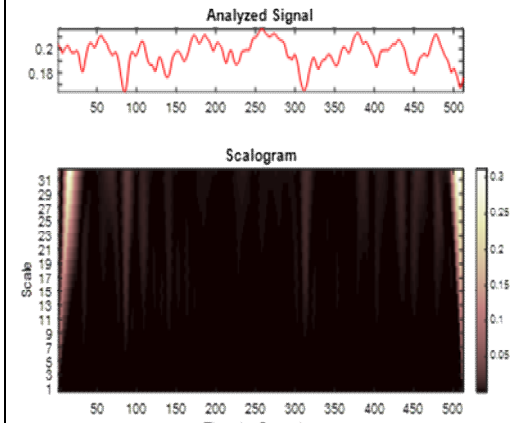

Vsl 0.0901m/s Vsg 23.5707m/s

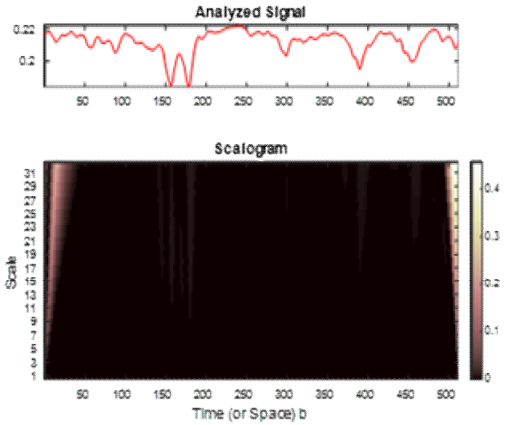

Vsl 0.1272m/s Vsg 10.2753m/s

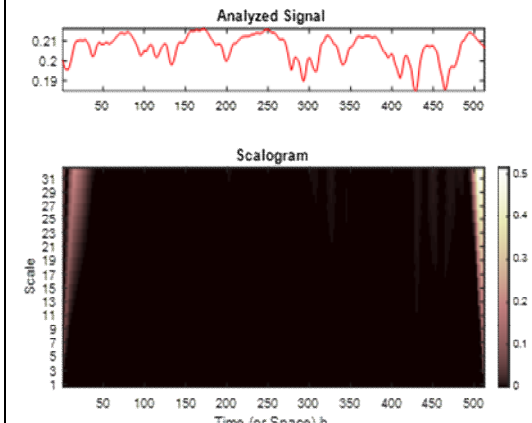

Vsl 0.1269m/s Vsg 14.2926m/s

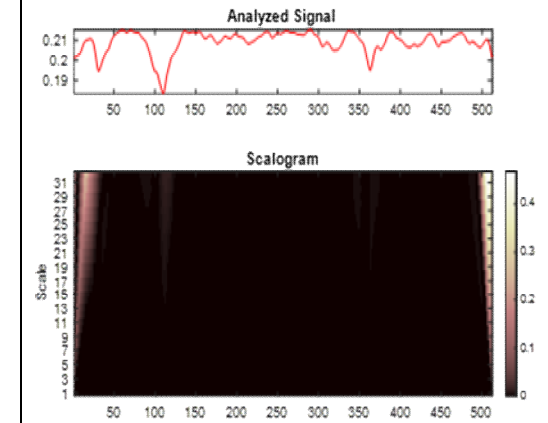

Vsl 0.1482m/s Vsg 17.2538m/s

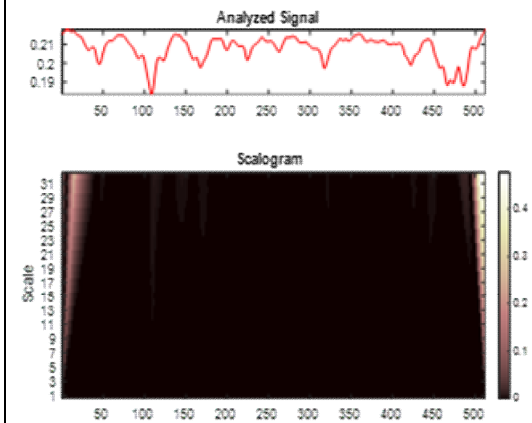

Vsl 0.1479m/s Vsg 23.1697m/s

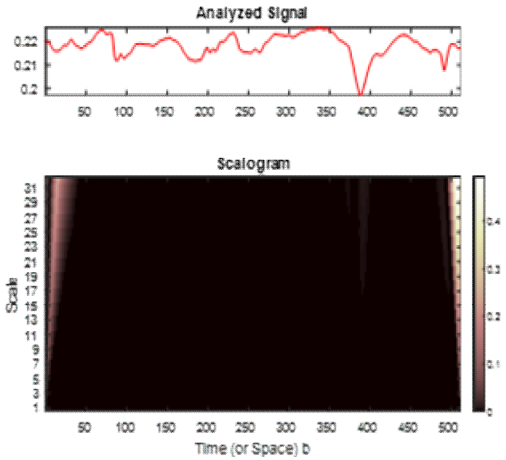

Vsl 0.1892m/s Vsg 10.3928m/s

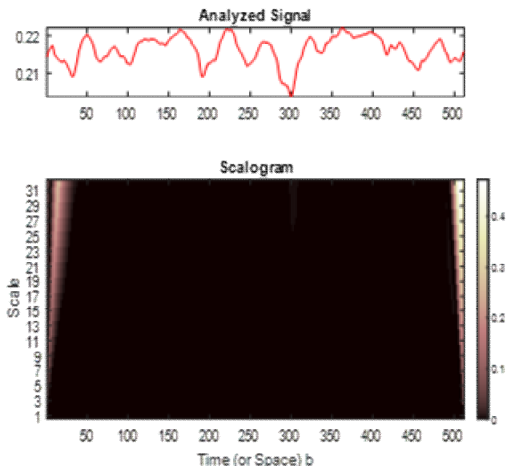

Vsl 0.1819m/s Vsg 14.4407m/s

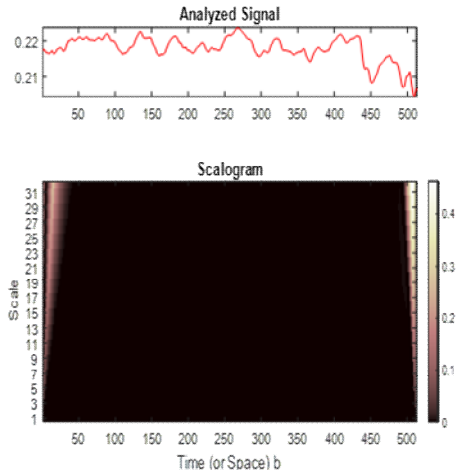

Vsl 0.1822m/s Vsg 17.5279m/s

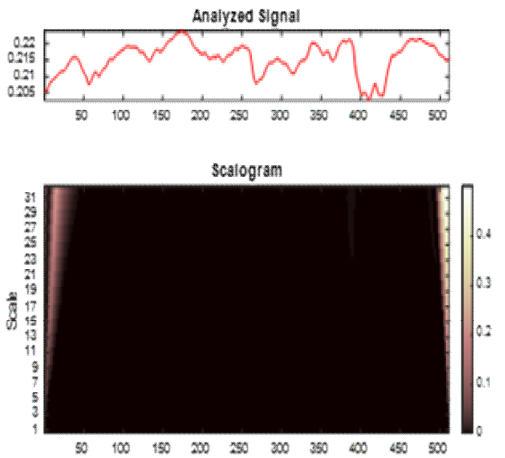

Vsl 0.1805m/s Vsg 23.7259m/s

Table G-1.3: Analysis on Void fraction vs Time and PDF vs Void fraction in Annular flow (2-inch pipe)

Vsl = 0.0508m/s, Vsg =10.0773m/s	*Vsl = 0.0502m/s, Vsg =14.0307m/s*	*Vsl = 0.0504m/s, Vsg =17.0857m/s*	*Vsl = 0.0501m/s, Vsg =23.2796m/s*
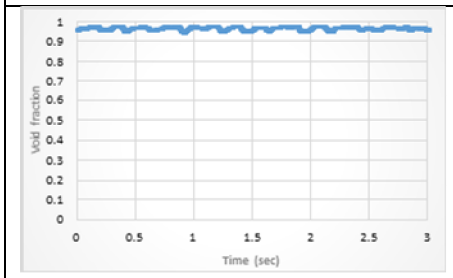	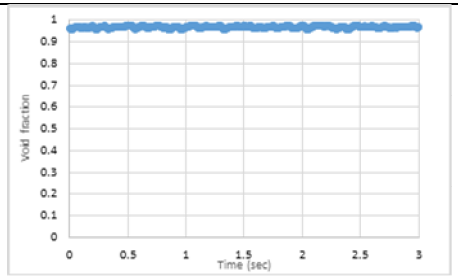	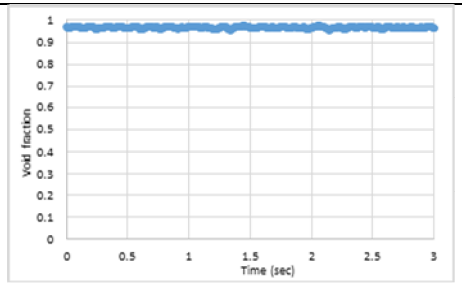	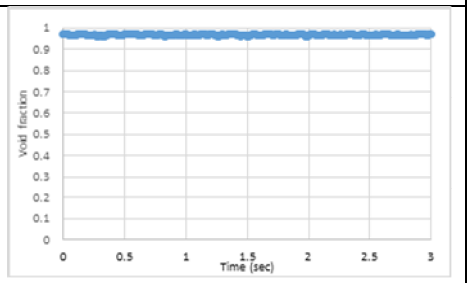
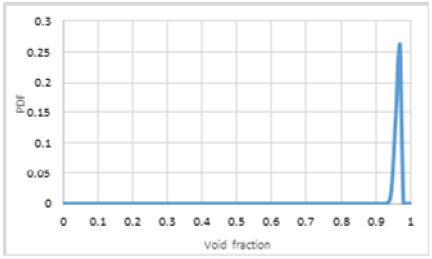	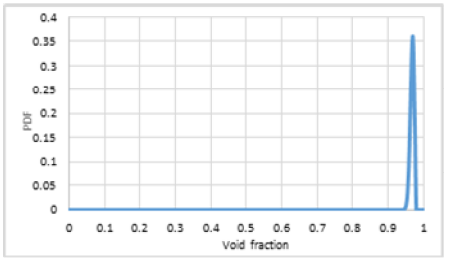	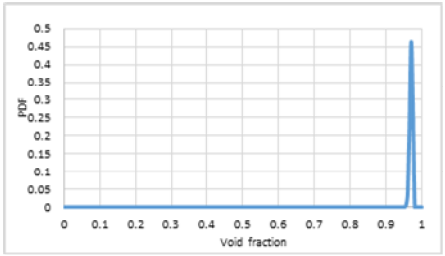	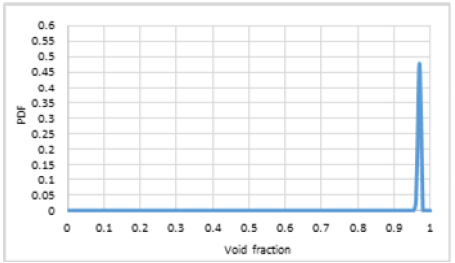
Vsl = 0.0721m/s, Vsg =10.1592m/s	*Vsl = 0.0713m/s, Vsg =14.3349m/s*	*Vsl = 0.0706m/s, Vsg =17.3721m/s*	*Vsl = 0.0706m/s, Vsg =23.5416m/s*
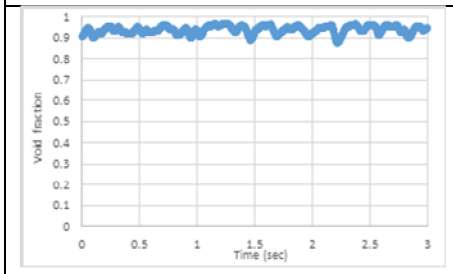	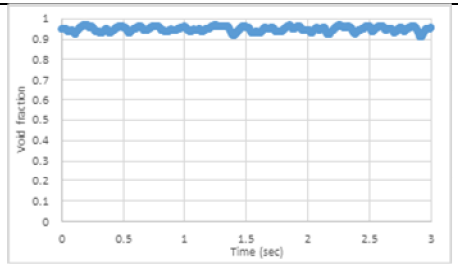	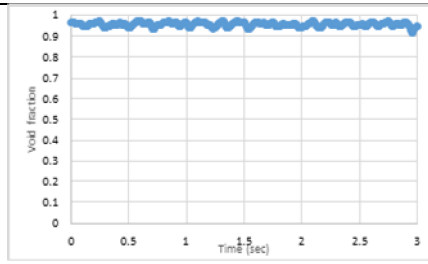	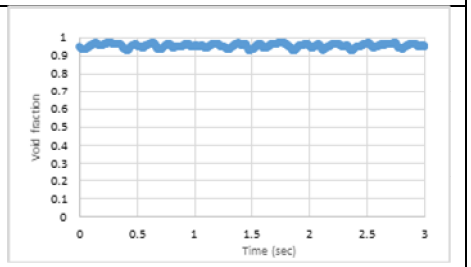

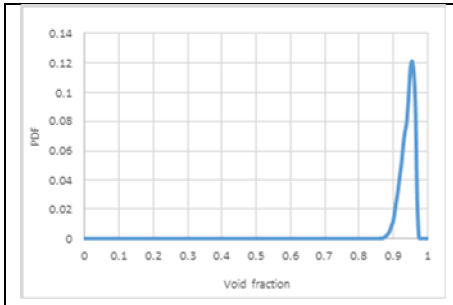	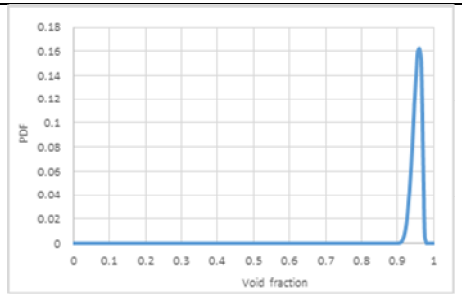	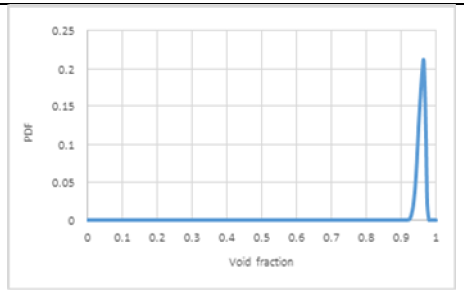	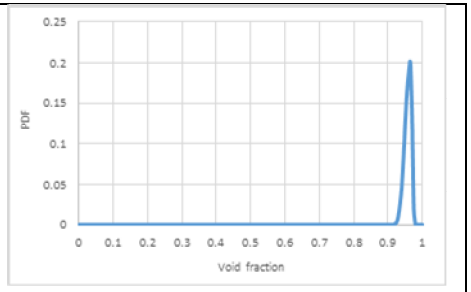
Vsl = 0.0910m/s, Vsg =10.1754m/s	***Vsl = 0.0899m/s, Vsg =14.3424m/s***	***Vsl = 0.0893m/s, Vsg =17.3035m/s***	***Vsl = 0.0901m/s, Vsg =23.5707m/s***
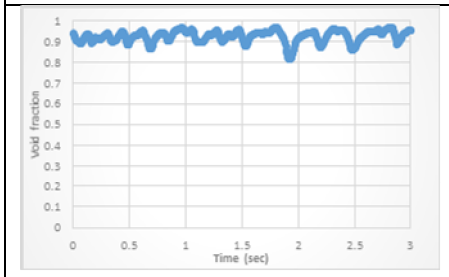 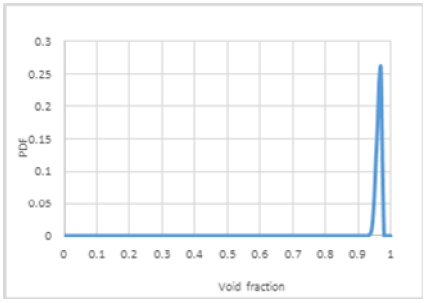	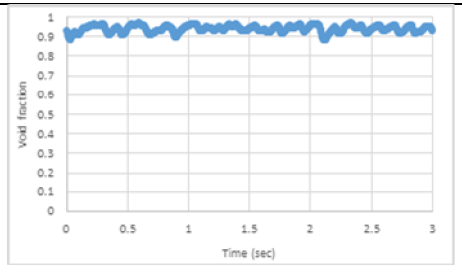 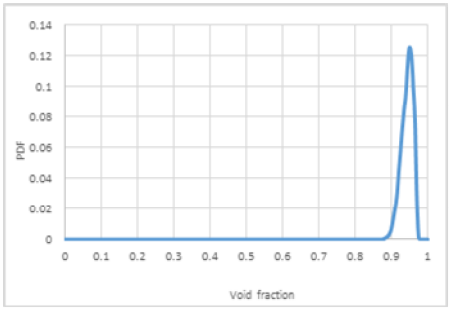	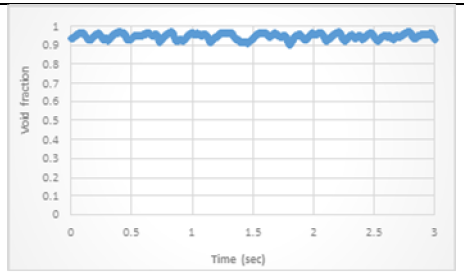 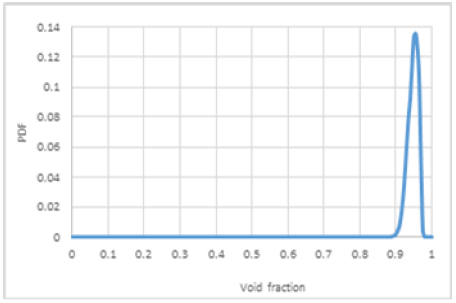	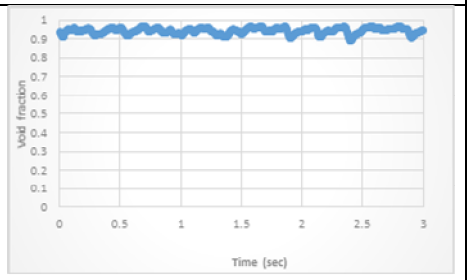 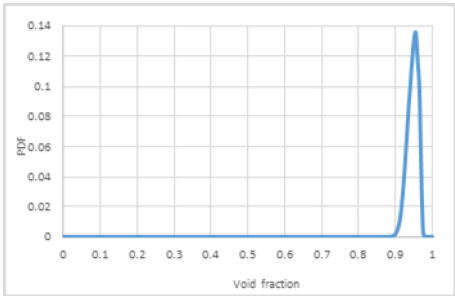
Vsl = 0.1272m/s, Vsg =10.2753m/s	***Vsl = 0.1269m/s, Vsg =14.2926m/s***	***Vsl = 0.1482m/s, Vsg =17.2538m/s***	***Vsl = 0.1479m/s, Vsg =23.1697m/s***

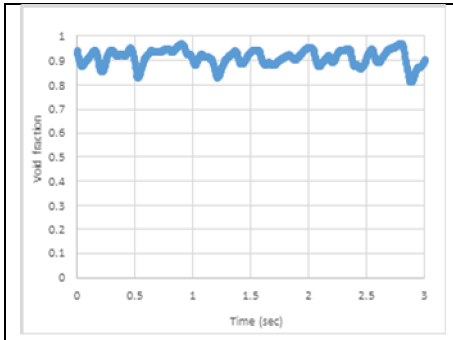

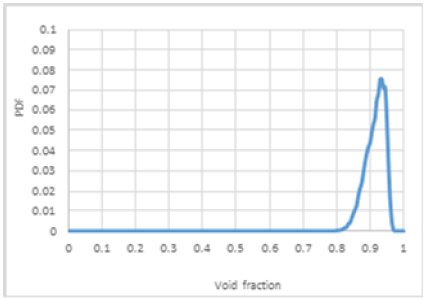

Vsl = 0.1892m/s, Vsg =10.3928m/s

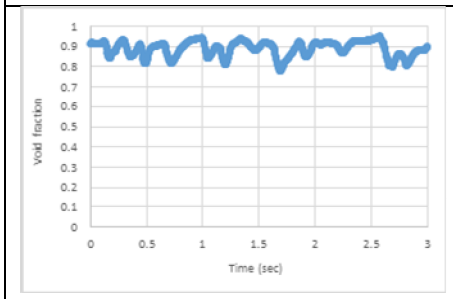

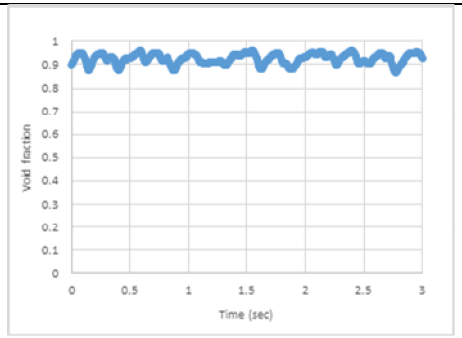

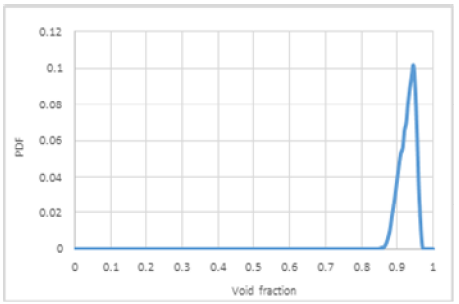

Vsl = 0.1819m/s, Vsg =14.4407m/s

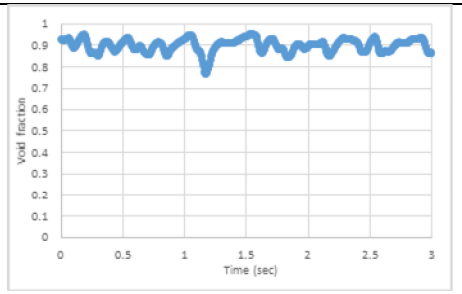

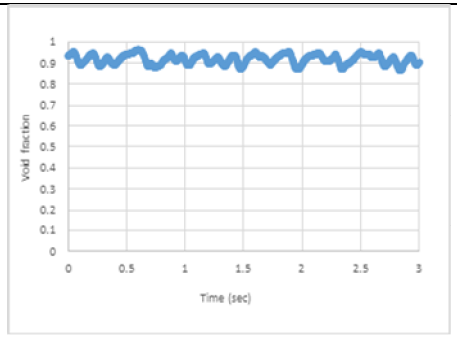

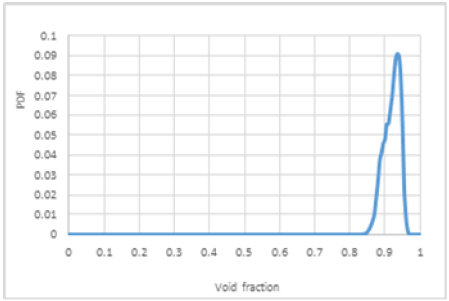

Vsl = 0.1822m/s, Vsg =17.5279m/s

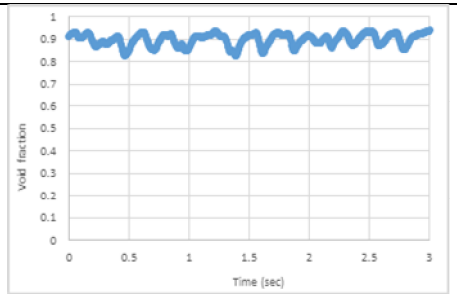

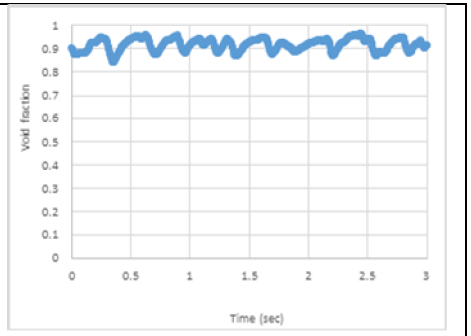

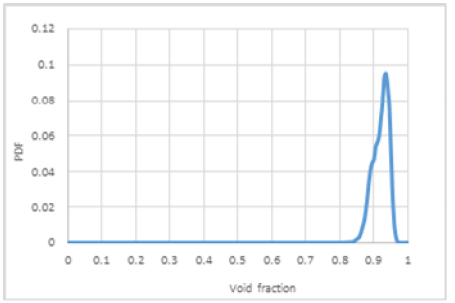

Vsl = 0.1805m/s, Vsg =23.7259m/s

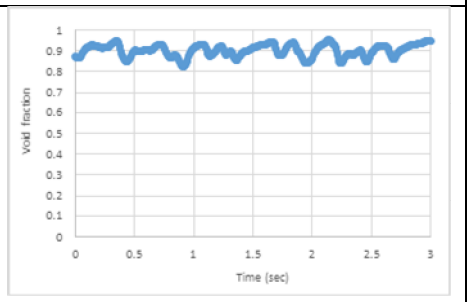

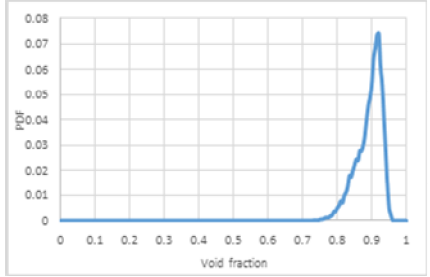
PDF
0.08
0.07
0.06
0.05
0.04
0.03
0.02
0.01
0
0 0.1 0.2 0.3 0.4 0.5 0.6 0.7 0.8 0.9 1
Void fraction

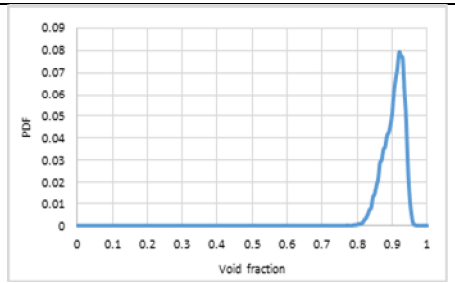
PDF
0.09
0.08
0.07
0.06
0.05
0.04
0.03
0.02
0.01
0
0 0.1 0.2 0.3 0.4 0.5 0.6 0.7 0.8 0.9 1
Void fraction

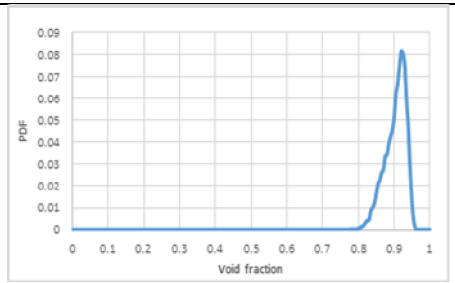
PDF
0.09
0.08
0.07
0.06
0.05
0.04
0.03
0.02
0.01
0
0 0.1 0.2 0.3 0.4 0.5 0.6 0.7 0.8 0.9 1
Void fraction

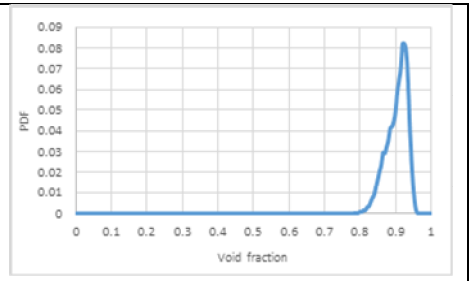
PDF
0.09
0.08
0.07
0.06
0.05
0.04
0.03
0.02
0.01
0
0 0.1 0.2 0.3 0.4 0.5 0.6 0.7 0.8 0.9 1
Void fraction

Table G-1.4: PSD Analysis for Water/Air in Annular Flow on Film Thickness

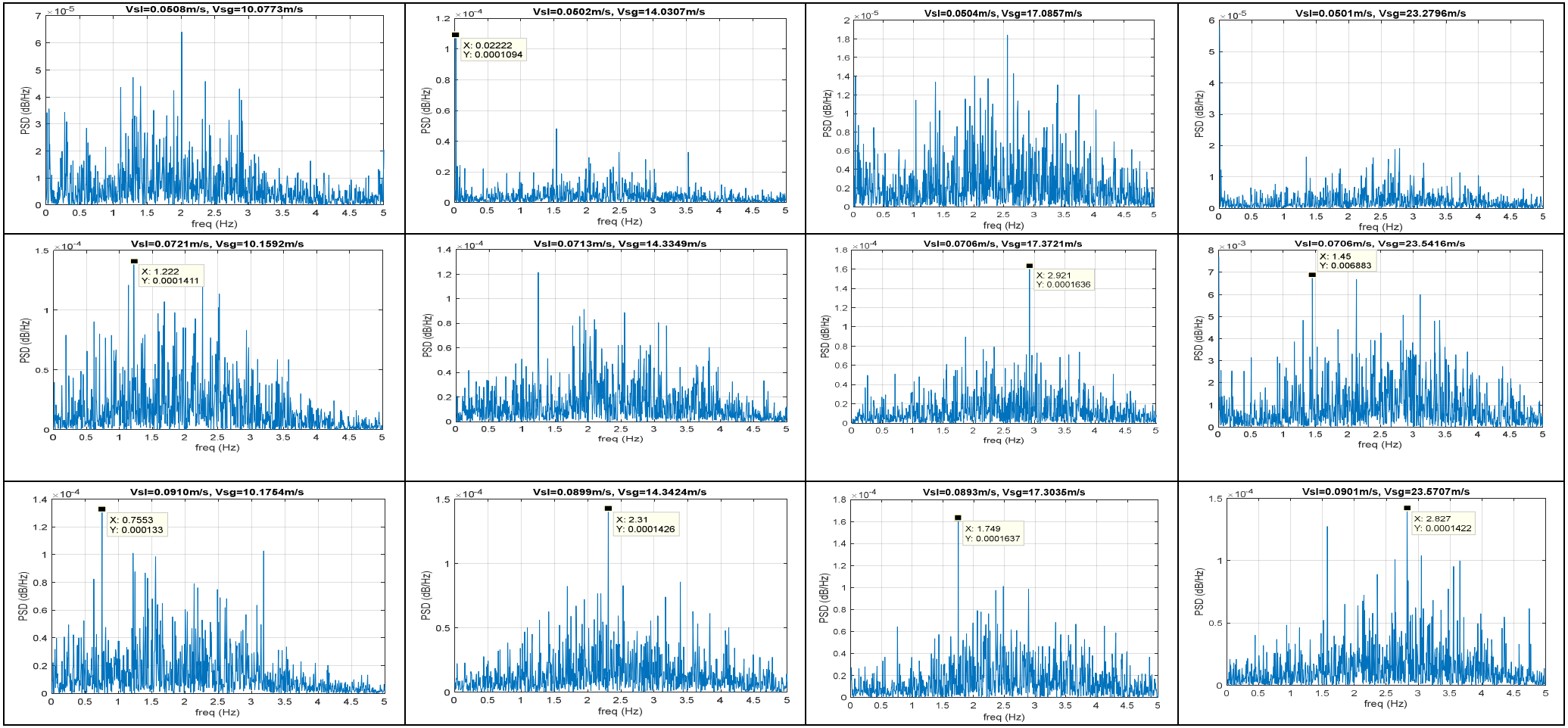

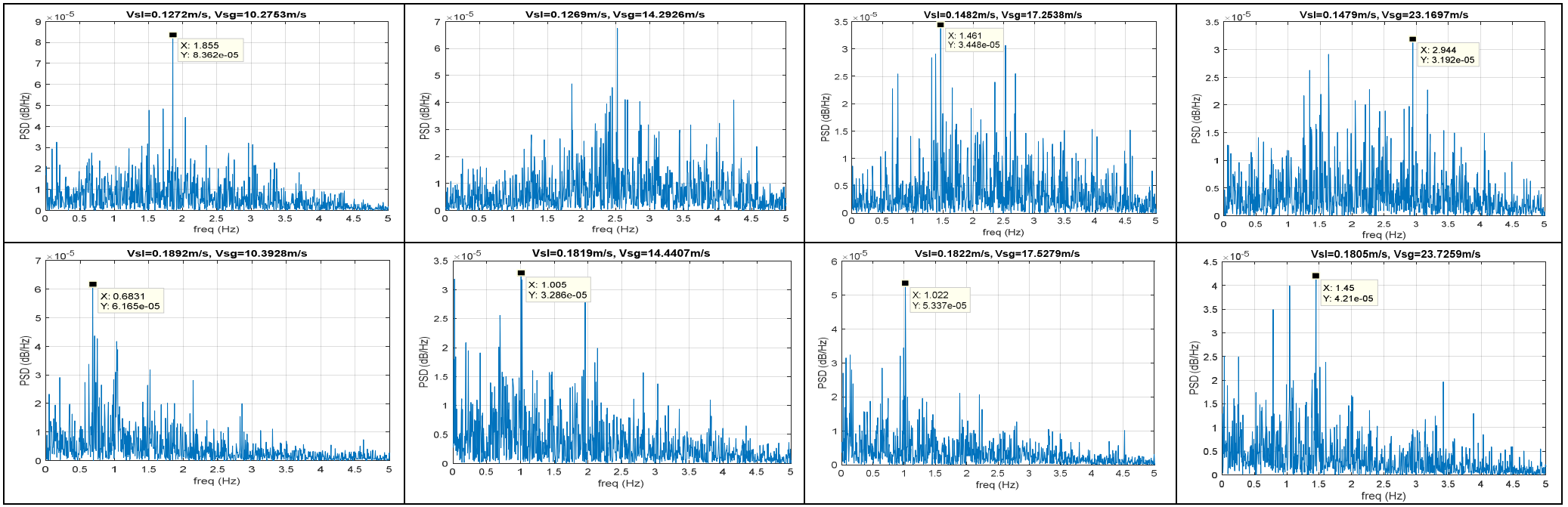
Vsl=0.1272m/s, Vsg=10.2753m/s
X: 1.855
Y: 8.362e-05
Vsl=0.1269m/s, Vsg=14.2926m/s
Vsl=0.1482m/s, Vsg=17.2538m/s
X: 1.461
Y: 3.448e-05
Vsl=0.1479m/s, Vsg=23.1697m/s
X: 2.944
Y: 3.192e-05
Vsl=0.1892m/s, Vsg=10.3928m/s
X: 0.6831
Y: 6.165e-05
Vsl=0.1819m/s, Vsg=14.4407m/s
X: 1.005
Y: 3.286e-05
Vsl=0.1822m/s, Vsg=17.5279m/s
X: 1.022
Y: 5.337e-05
Vsl=0.1805m/s, Vsg=23.7259m/s
X: 1.45
Y: 4.21e-05
PSD (dB/Hz)
freq (Hz)

Table G-1.5: Sand Sampling Results

Vsl=0.0724 Vsg=11.0521m/s (Bottom) *(212microns; 200lb/1000bbl)*	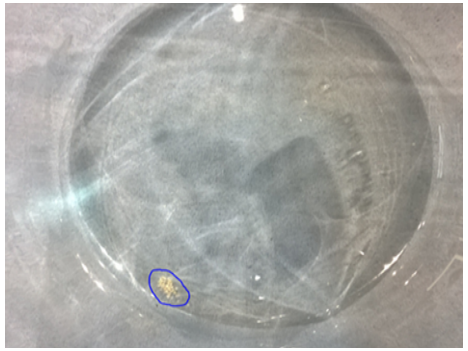 **Vsl=0.0722m/s Vsg=13.0810m/s (Bottom)** *(212microns; 200lb/1000bbl)*	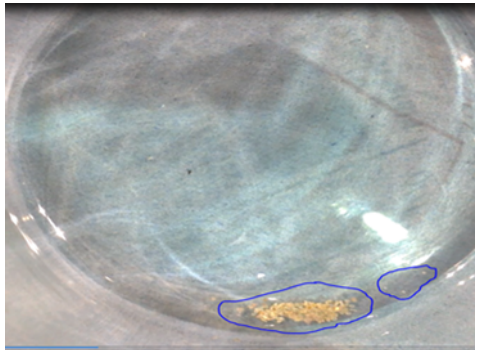 **Vsl=0.0704, Vsl=15.8127m/s (Bottom)** *(212microns; 200lb/1000bbl)*	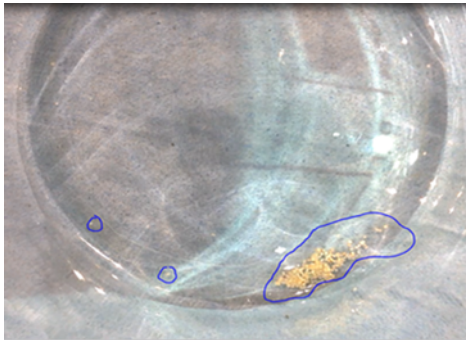 **Vsl=0.07022m/s, Vsg=18.1021m/s (Bottom)** *(212microns; 200lb/1000bbl)*
Vsl=0.0752m/s Vsg=11.4510m/s (1.5cm) *(212microns; 200lb/1000bbl)*	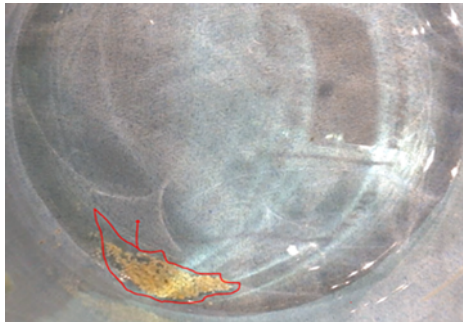 **Vsl=0.0711m/s Vsg=13.8950m/s (1.5cm)** *(212microns; 200lb/1000bbl)*	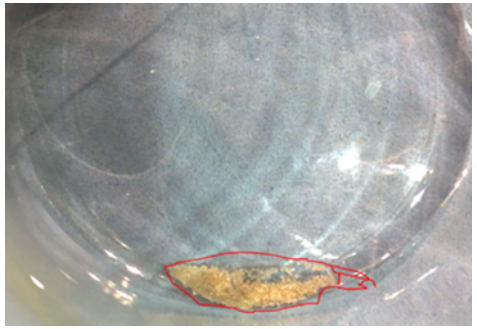 **Vsl=0.0768m/s,Vsl=15.0341m/s(1.5cm)** *(212microns; 200lb/1000bbl)*	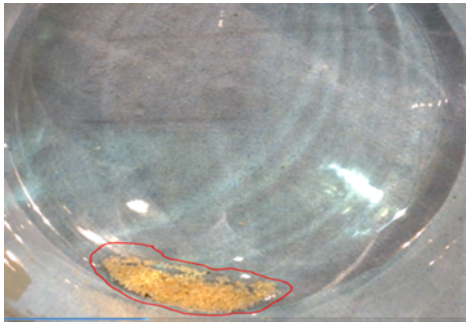 **Vsl=0.0753m/sVsg=18.3287m/s (1.5cm)** *(212microns; 200lb/1000bbl)*

Vsl=0.0732m/sVsg=11.6535m/s (2.5cm) *(212microns; 200lb/1000bbl)*	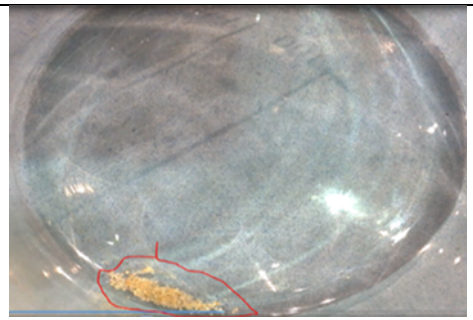 **Vsl=0.0743m/sVsg=13.5431m/s (2.5cm)** *(212microns; 200lb/1000bbl)*	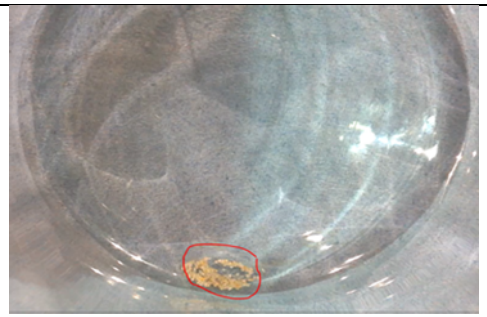 **Vsl=0.0705m/s Vsg=15.2210m/s (2.5cm)** *(212microns; 200lb/1000bbl)*	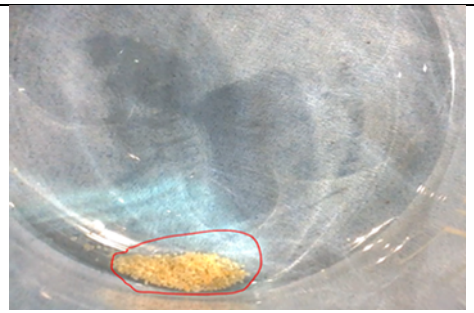 **Vsl=0.0725m/s Vsg=18.3201m/s (2.5cm)** *(212microns; 200lb/1000bbl)*
Vsl=0.0801m/s,Vsg=11.5529m/s (Bottom) *(500microns; 500lb/1000bbl)*	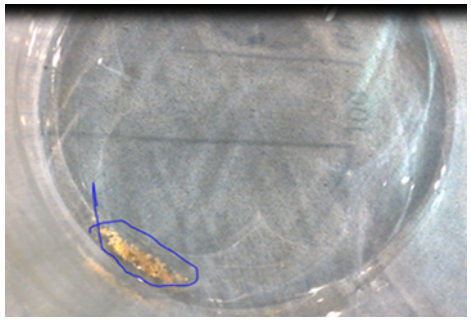 **Vsl=0.0821m/s,Vsg=13.5401m/s (Bottom)** *(500microns; 500lb/1000bbl)*	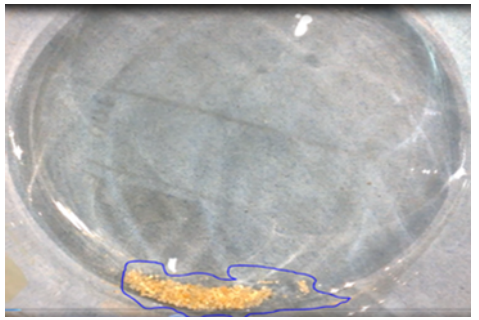 **Vsl=0.0836m/s,Vsg=15.0671m/s (Bottom)** *(500microns; 500lb/1000bbl)*	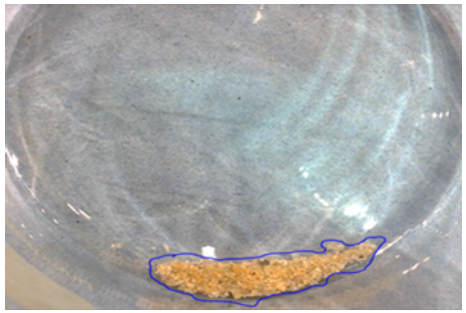 **Vsl=0.0821m/s,Vsg=18.0321m/s (Bottom)** *(500microns; 500lb/1000bbl)*
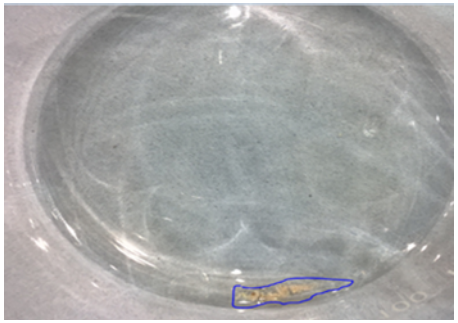 **Vsl=0.0821m/s, Vsg=11.2178m/s (1.5cm)** *(500microns; 500lb/1000bbl)*	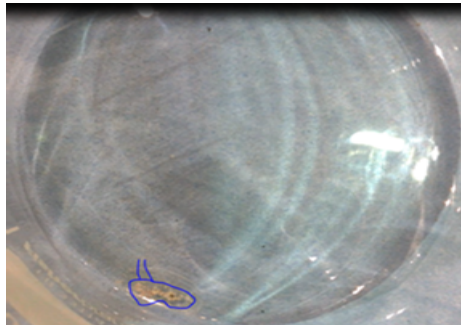 **Vsl=0.0802m/s, Vsg=13.4510m/s, (1.5cm)** *(500microns; 500lb/1000bbl)*	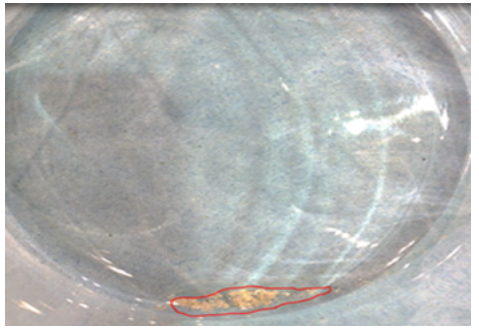 **Vsl=0.0807m/s,Vsg=15.5891m/s (1.5cm)** *(500microns; 500lb/1000bbl)*	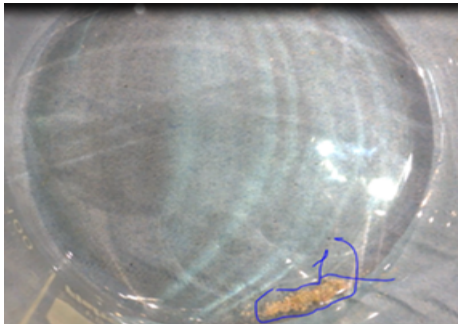 **Vsl=0.0802m/s,Vsg=18.5341m/s (1.5cm)** *(500microns; 500lb/1000bbl)*

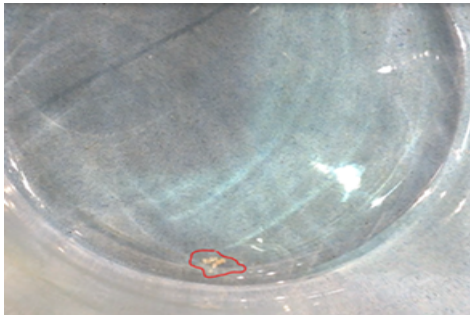 **Vsl=0.0823m/s, Vsg=11.5100m/s (2.5cm)** *(500microns; 500lb/1000bbl)*	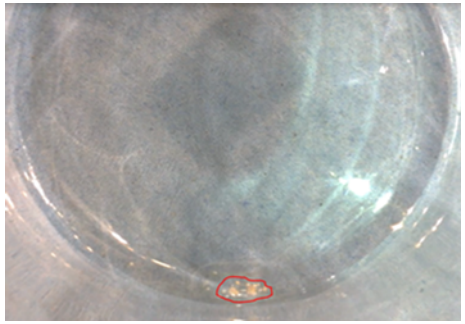 **Vsl=0.0835m/s, Vsg=13.4225m/s (2.5cm)** *(500microns; 500lb/1000bbl)*	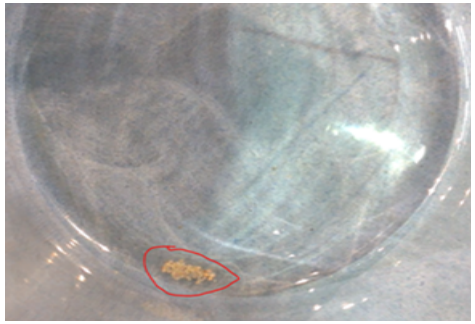 **Vsl=0.0835m/s,Vsg=15.7632m/s (2.5cm)** *(500microns; 500lb/1000bbl)*	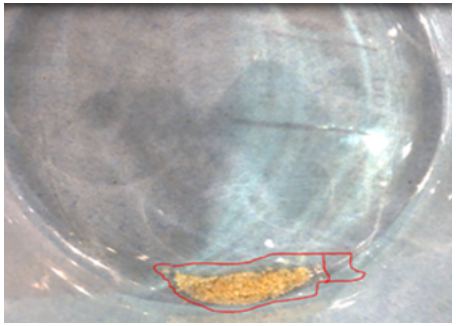 **Vsl=0.0832m/s, Vsg=18.3210m/s (2.5cm)** *(500microns; 500lb/1000bbl)*
Vsl=0.0741m/s,Vsg=18.1130m/s(Top-walls) *(212microns; 200lb/1000bbl)*	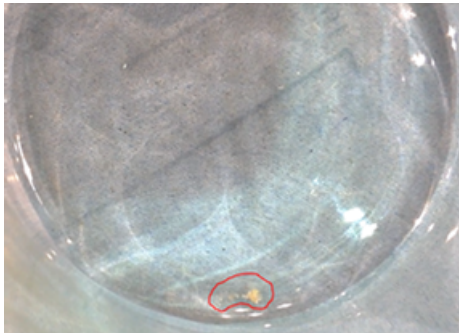 **Vsl=0.0822m/s, Vsg=18.4532m/s (Top wall)** *(500microns; 500lb/1000bbl)*		

Table G-1.6: OLGA Screenshots and Input data for Water/Air/Sand Annular Flow

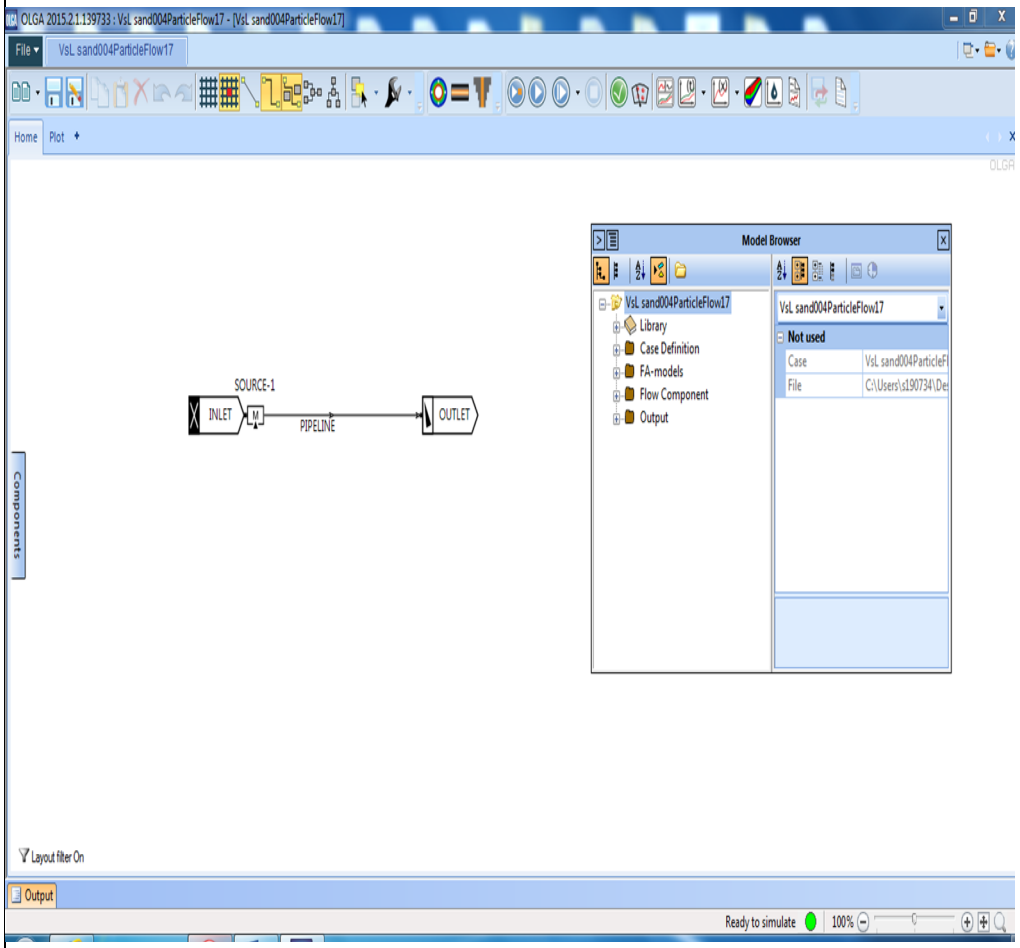

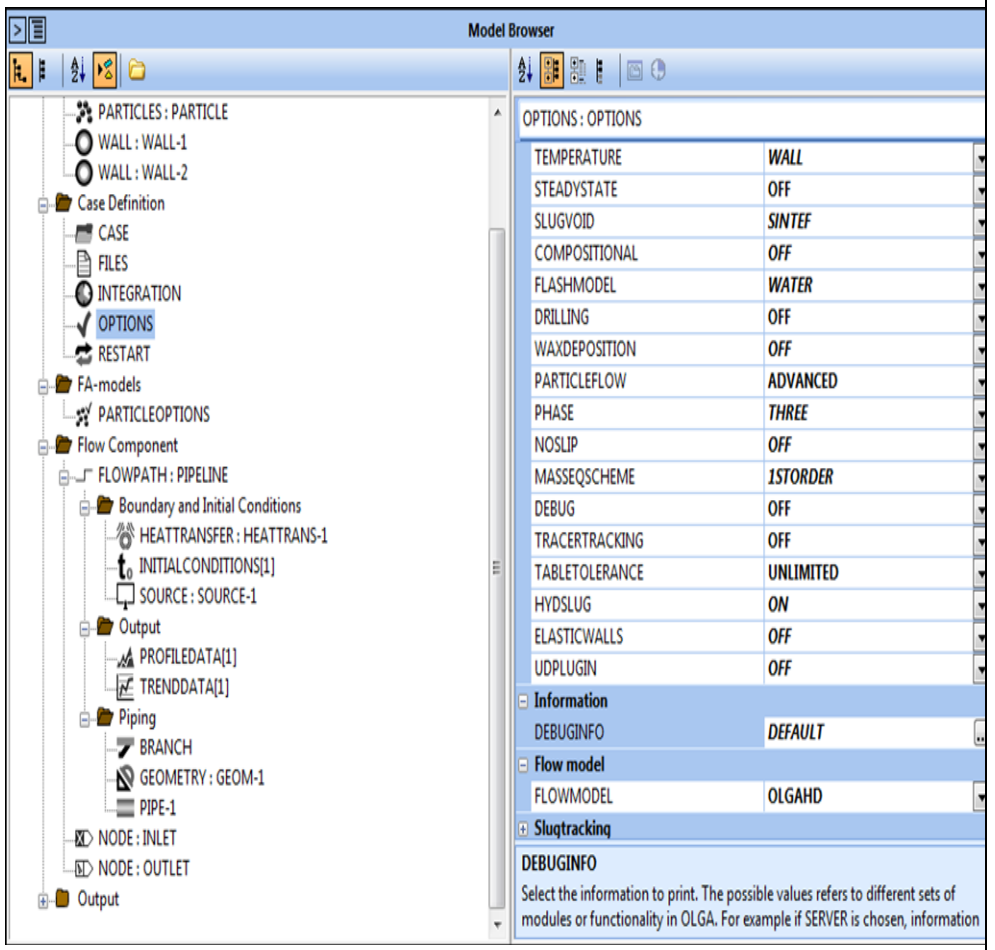

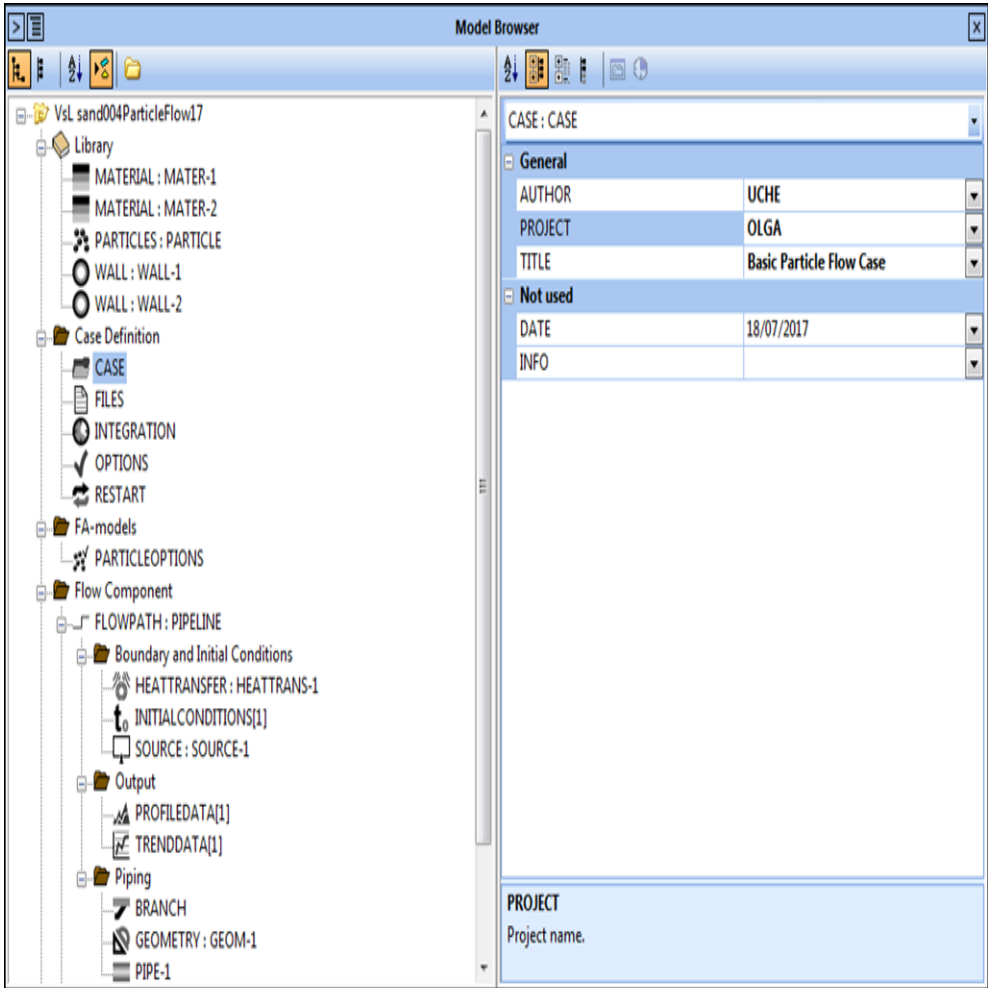
Model Browser
VsL sand004ParticleFlow17
Library
MATERIAL : MATER-1
MATERIAL : MATER-2
PARTICLES : PARTICLE
WALL : WALL-1
WALL : WALL-2
Case Definition
CASE
FILES
INTEGRATION
OPTIONS
RESTART
FA-models
PARTICLEOPTIONS
Flow Component
FLOWPATH : PIPELINE
Boundary and Initial Conditions
HEATTRANSFER : HEATTRANS-1
INITIALCONDITIONS[1]
SOURCE : SOURCE-1
Output
PROFILEDATA[1]
TRENDDATA[1]
Piping
BRANCH
GEOMETRY : GEOM-1
PIPE-1
CASE : CASE
General
AUTHOR
UCHE
PROJECT
OLGA
TITLE
Basic Particle Flow Case
Not used
DATE
18/07/2017
INFO
PROJECT
Project name.

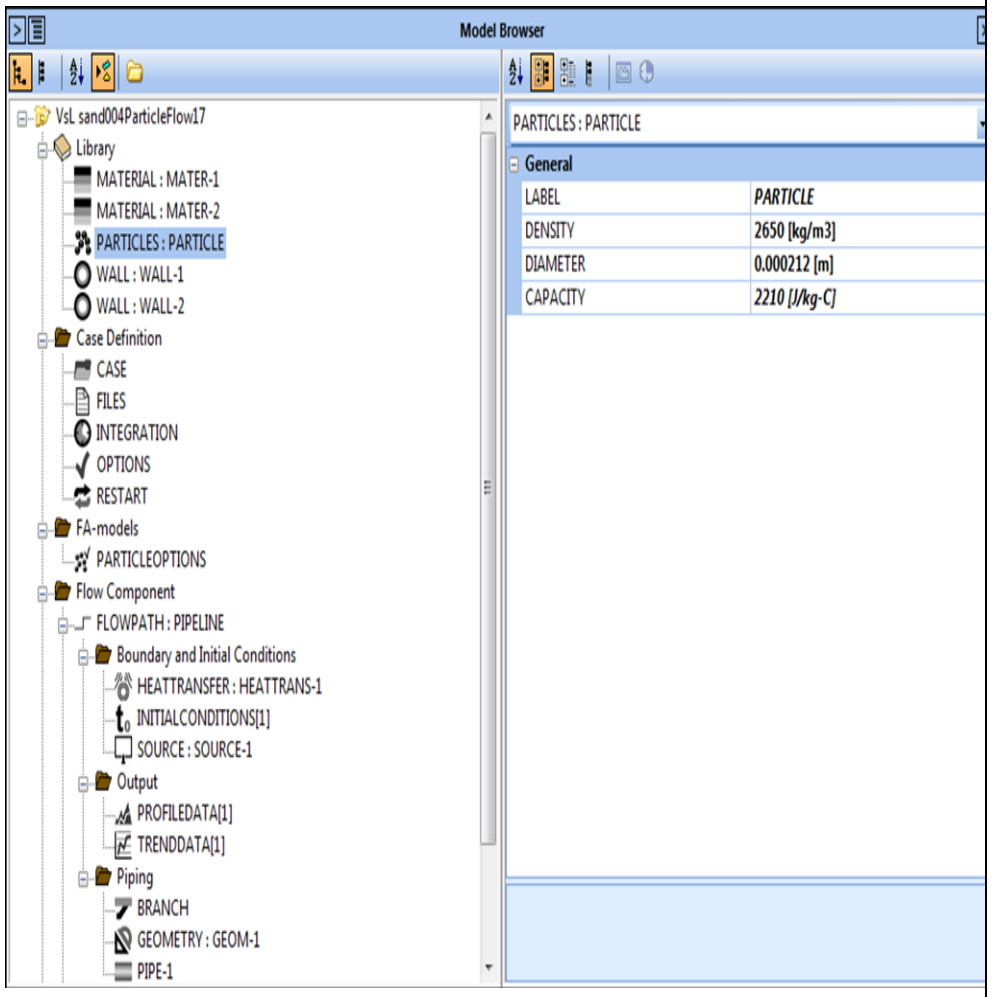
Model Browser
VsL sand004ParticleFlow17
Library
MATERIAL : MATER-1
MATERIAL : MATER-2
PARTICLES : PARTICLE
WALL : WALL-1
WALL : WALL-2
Case Definition
CASE
FILES
INTEGRATION
OPTIONS
RESTART
FA-models
PARTICLEOPTIONS
Flow Component
FLOWPATH : PIPELINE
Boundary and Initial Conditions
HEATTRANSFER : HEATTRANS-1
INITIALCONDITIONS[1]
SOURCE : SOURCE-1
Output
PROFILEDATA[1]
TRENDDATA[1]
Piping
BRANCH
GEOMETRY : GEOM-1
PIPE-1
PARTICLES : PARTICLE
General
LABEL
PARTICLE
DENSITY
2650 [kg/m3]
DIAMETER
0.000212 [m]
CAPACITY
2210 [J/kg-C]

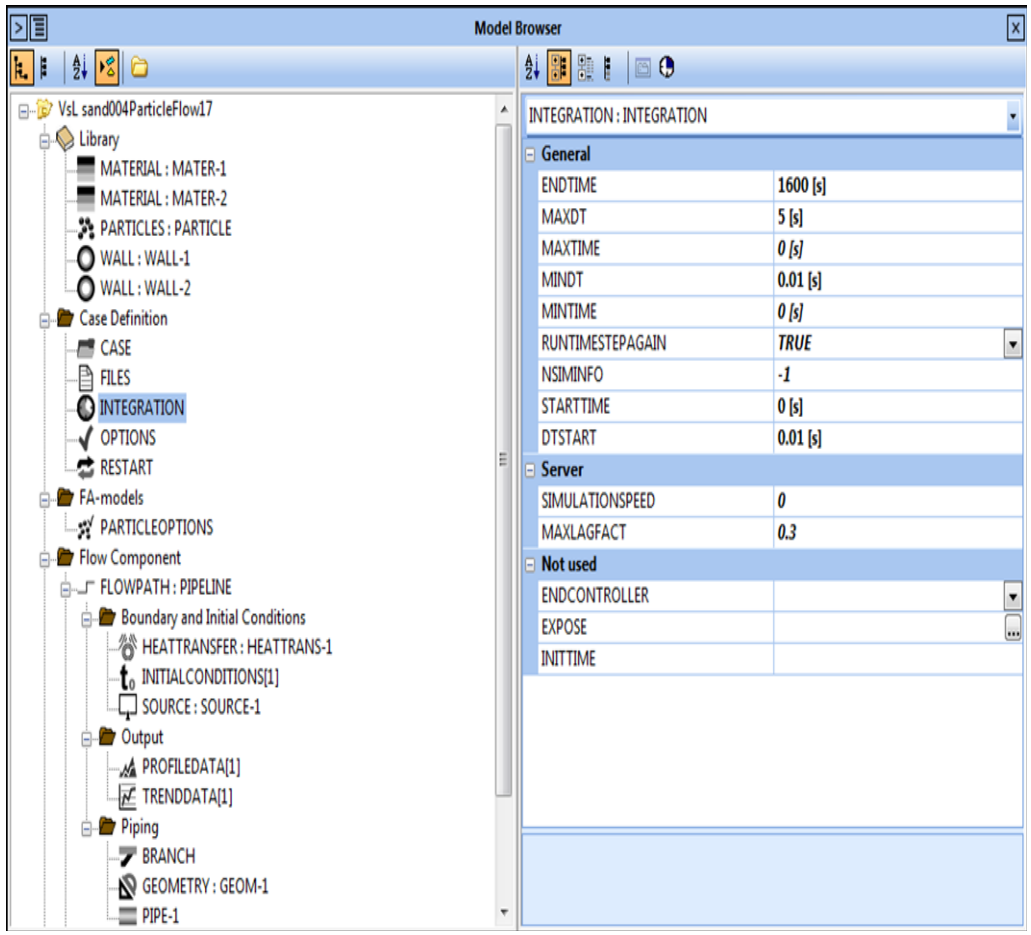
Model Browser
VsL sand004ParticleFlow17
Library
MATERIAL : MATER-1
MATERIAL : MATER-2
PARTICLES : PARTICLE
WALL : WALL-1
WALL : WALL-2
Case Definition
CASE
FILES
INTEGRATION
OPTIONS
RESTART
FA-models
PARTICLEOPTIONS
Flow Component
FLOWPATH : PIPELINE
Boundary and Initial Conditions
HEATTRANSFER : HEATTRANS-1
INITIALCONDITIONS[1]
SOURCE : SOURCE-1
Output
PROFILEDATA[1]
TRENDDATA[1]
Piping
BRANCH
GEOMETRY : GEOM-1
PIPE-1
INTEGRATION : INTEGRATION
General
ENDTIME 1600 [s]
MAXDT 5 [s]
MAXTIME 0 [s]
MINDT 0.01 [s]
MINTIME 0 [s]
RUNTIMESTEPAGAIN TRUE
NSIMINFO -1
STARTTIME 0 [s]
DTSTART 0.01 [s]
Server
SIMULATIONSPEED 0
MAXLAGFACT 0.3
Not used
ENDCONTROLLER
EXPOSE
INITTIME

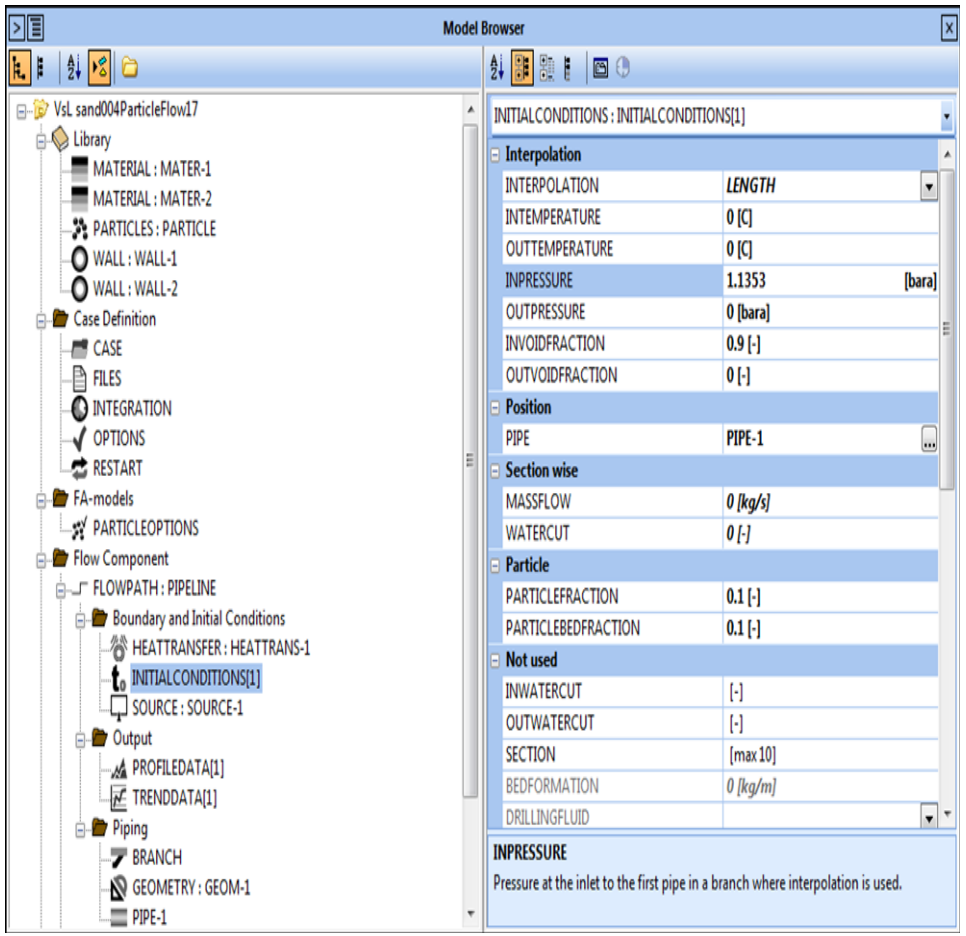
Model Browser
VsL sand004ParticleFlow17
Library
MATERIAL : MATER-1
MATERIAL : MATER-2
PARTICLES : PARTICLE
WALL : WALL-1
WALL : WALL-2
Case Definition
CASE
FILES
INTEGRATION
OPTIONS
RESTART
FA-models
PARTICLEOPTIONS
Flow Component
FLOWPATH : PIPELINE
Boundary and Initial Conditions
HEATTRANSFER : HEATTRANS-1
INITIALCONDITIONS[1]
SOURCE : SOURCE-1
Output
PROFILEDATA[1]
TRENDDATA[1]
Piping
BRANCH
GEOMETRY : GEOM-1
PIPE-1
INITIALCONDITIONS : INITIALCONDITIONS[1]
Interpolation
INTERPOLATION LENGTH
INTEMPERATURE 0 [C]
OUTTEMPERATURE 0 [C]
INPRESSURE 1.1353 [bara]
OUTPRESSURE 0 [bara]
INVOIDFRACTION 0.9 [-]
OUTVOIDFRACTION 0 [-]
Position
PIPE PIPE-1
Section wise
MASSFLOW 0 [kg/s]
WATERCUT 0 [-]
Particle
PARTICLEFRACTION 0.1 [-]
PARTICLEBEDFRACTION 0.1 [-]
Not used
INWATERCUT [-]
OUTWATERCUT [-]
SECTION [max 10]
BEDFORMATION 0 [kg/m]
DRILLINGFLUID
INPRESSURE
Pressure at the inlet to the first pipe in a branch where interpolation is used.

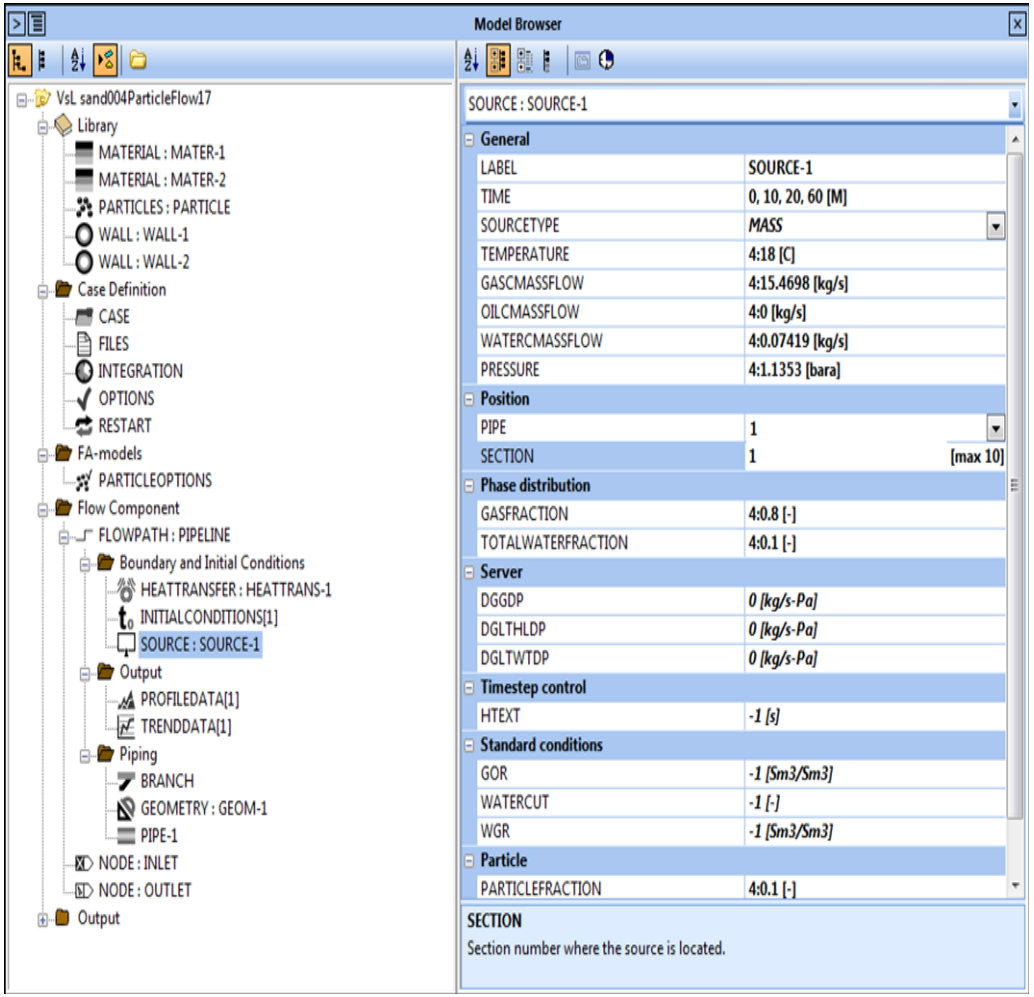
Model Browser
VsL sand004ParticleFlow17
Library
MATERIAL : MATER-1
MATERIAL : MATER-2
PARTICLES : PARTICLE
WALL : WALL-1
WALL : WALL-2
Case Definition
CASE
FILES
INTEGRATION
OPTIONS
RESTART
FA-models
PARTICLEOPTIONS
Flow Component
FLOWPATH : PIPELINE
Boundary and Initial Conditions
HEATTRANSFER : HEATTRANS-1
INITIALCONDITIONS[1]
SOURCE : SOURCE-1
Output
PROFILEDATA[1]
TRENDDATA[1]
Piping
BRANCH
GEOMETRY : GEOM-1
PIPE-1
NODE : INLET
NODE : OUTLET
Output
SOURCE : SOURCE-1
General
LABEL SOURCE-1
TIME 0, 10, 20, 60 [M]
SOURCETYPE MASS
TEMPERATURE 4:18 [C]
GASCMASSFLOW 4:15.4698 [kg/s]
OILCMASSFLOW 4:0 [kg/s]
WATERCMASSFLOW 4:0.07419 [kg/s]
PRESSURE 4:1.1353 [bara]
Position
PIPE 1
SECTION 1 [max 10]
Phase distribution
GASFRACTION 4:0.8 [-]
TOTALWATERFRACTION 4:0.1 [-]
Server
DGGDP 0 [kg/s-Pa]
DGLTHLDP 0 [kg/s-Pa]
DGLTWTDP 0 [kg/s-Pa]
Timestep control
HTEXT -1 [s]
Standard conditions
GOR -1 [Sm3/Sm3]
WATERCUT -1 [-]
WGR -1 [Sm3/Sm3]
Particle
PARTICLEFRACTION 4:0.1 [-]
SECTION
Section number where the source is located.

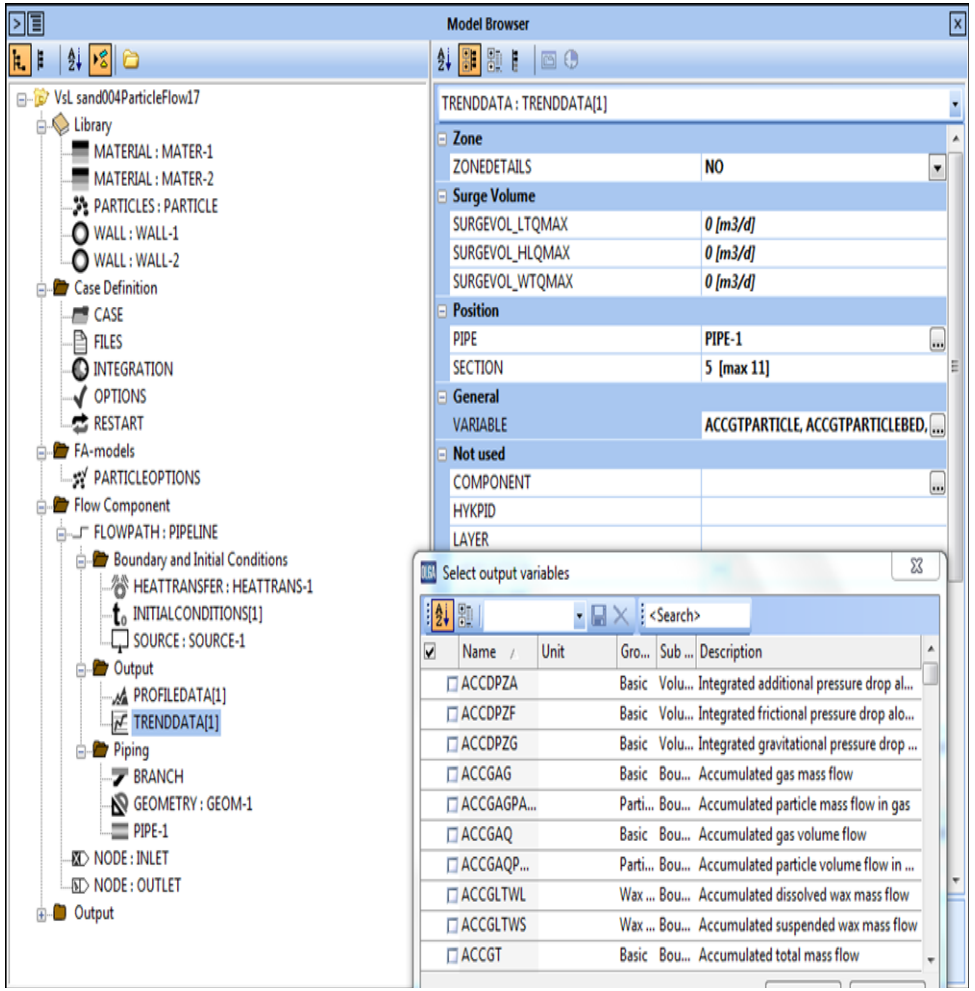
Model Browser
VsL sand004ParticleFlow17
Library
MATERIAL : MATER-1
MATERIAL : MATER-2
PARTICLES : PARTICLE
WALL : WALL-1
WALL : WALL-2
Case Definition
CASE
FILES
INTEGRATION
OPTIONS
RESTART
FA-models
PARTICLEOPTIONS
Flow Component
FLOWPATH : PIPELINE
Boundary and Initial Conditions
HEATTRANSFER : HEATTRANS-1
INITIALCONDITIONS[1]
SOURCE : SOURCE-1
Output
PROFILEDATA[1]
TRENDDATA[1]
Piping
BRANCH
GEOMETRY : GEOM-1
PIPE-1
NODE : INLET
NODE : OUTLET
Output
TRENDDATA : TRENDDATA[1]
Zone
ZONEDETAILS NO
Surge Volume
SURGEVOL_LTQMAX 0 [m3/d]
SURGEVOL_HLQMAX 0 [m3/d]
SURGEVOL_WTQMAX 0 [m3/d]
Position
PIPE PIPE-1
SECTION 5 [max 11]
General
VARIABLE ACCGTPARTICLE, ACCGTPARTICLEBED,
Not used
COMPONENT
HYKPID
LAYER
Select output variables
<Search>
Name Unit Gro... Sub ... Description
ACCDPZA Basic Volu... Integrated additional pressure drop al...
ACCDPZF Basic Volu... Integrated frictional pressure drop alo...
ACCDPZG Basic Volu... Integrated gravitational pressure drop ...
ACCGAG Basic Bou... Accumulated gas mass flow
ACCGAGPA... Parti... Bou... Accumulated particle mass flow in gas
ACCGAQ Basic Bou... Accumulated gas volume flow
ACCGAQP... Parti... Bou... Accumulated particle volume flow in ...
ACCGLTWL Wax ... Bou... Accumulated dissolved wax mass flow
ACCGLTWS Wax ... Bou... Accumulated suspended wax mass flow
ACCGT Basic Bou... Accumulated total mass flow

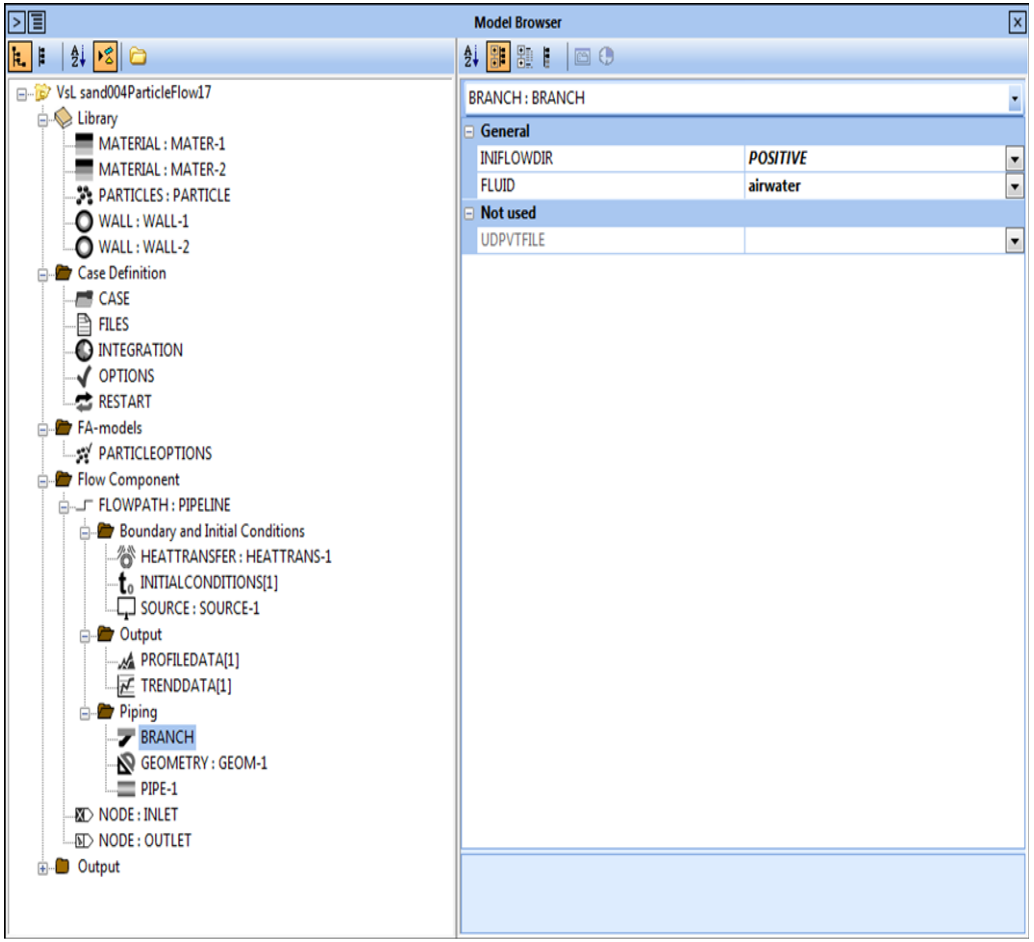
Model Browser
VsL sand004ParticleFlow17
Library
MATERIAL : MATER-1
MATERIAL : MATER-2
PARTICLES : PARTICLE
WALL : WALL-1
WALL : WALL-2
Case Definition
CASE
FILES
INTEGRATION
OPTIONS
RESTART
FA-models
PARTICLEOPTIONS
Flow Component
FLOWPATH : PIPELINE
Boundary and Initial Conditions
HEATTRANSFER : HEATTRANS-1
INITIALCONDITIONS[1]
SOURCE : SOURCE-1
Output
PROFILEDATA[1]
TRENDDATA[1]
Piping
BRANCH
GEOMETRY : GEOM-1
PIPE-1
NODE : INLET
NODE : OUTLET
Output
BRANCH : BRANCH
General
INIFLOWDIR
POSITIVE
FLUID
airwater
Not used
UDPVTFILE

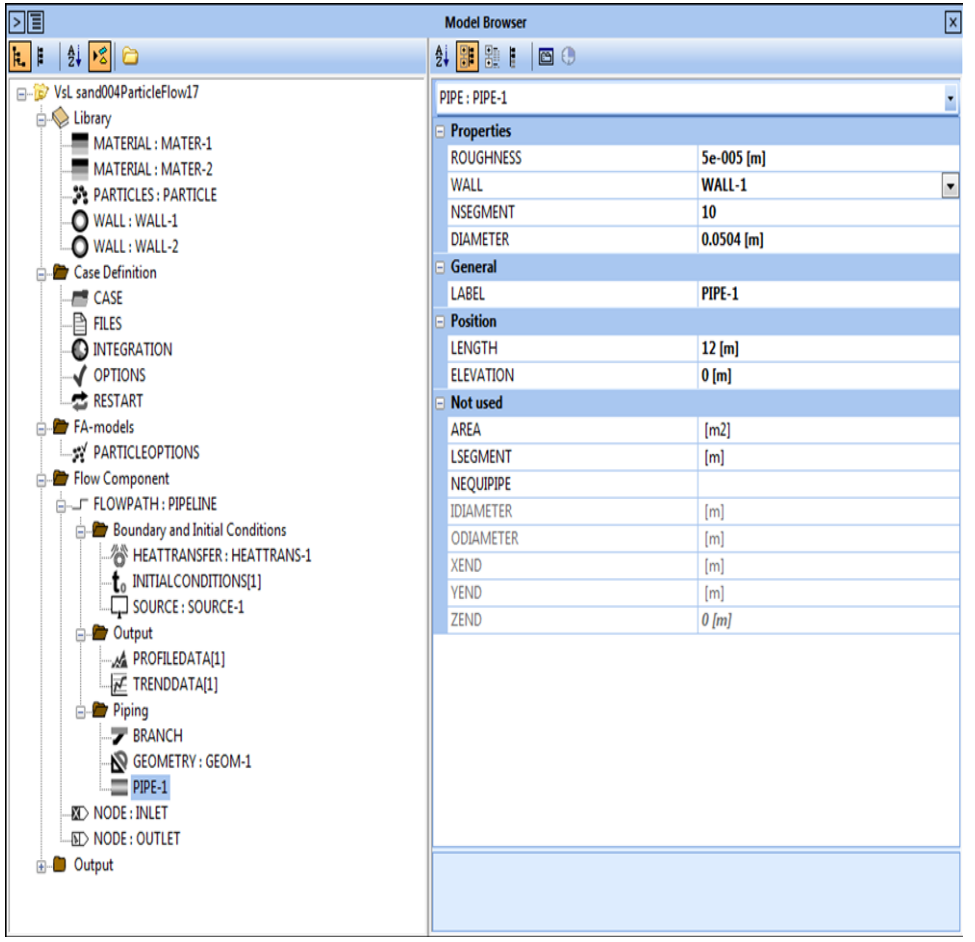
Model Browser
VsL sand004ParticleFlow17
Library
MATERIAL : MATER-1
MATERIAL : MATER-2
PARTICLES : PARTICLE
WALL : WALL-1
WALL : WALL-2
Case Definition
CASE
FILES
INTEGRATION
OPTIONS
RESTART
FA-models
PARTICLEOPTIONS
Flow Component
FLOWPATH : PIPELINE
Boundary and Initial Conditions
HEATTRANSFER : HEATTRANS-1
INITIALCONDITIONS[1]
SOURCE : SOURCE-1
Output
PROFILEDATA[1]
TRENDDATA[1]
Piping
BRANCH
GEOMETRY : GEOM-1
PIPE-1
NODE : INLET
NODE : OUTLET
Output
PIPE : PIPE-1
Properties
ROUGHNESS
5e-005 [m]
WALL
WALL-1
NSEGMENT
10
DIAMETER
0.0504 [m]
General
LABEL
PIPE-1
Position
LENGTH
12 [m]
ELEVATION
0 [m]
Not used
AREA
[m2]
LSEGMENT
[m]
NEQUIPIPE
IDIAMETER
[m]
ODIAMETER
[m]
XEND
[m]
YEND
[m]
ZEND
0 [m]

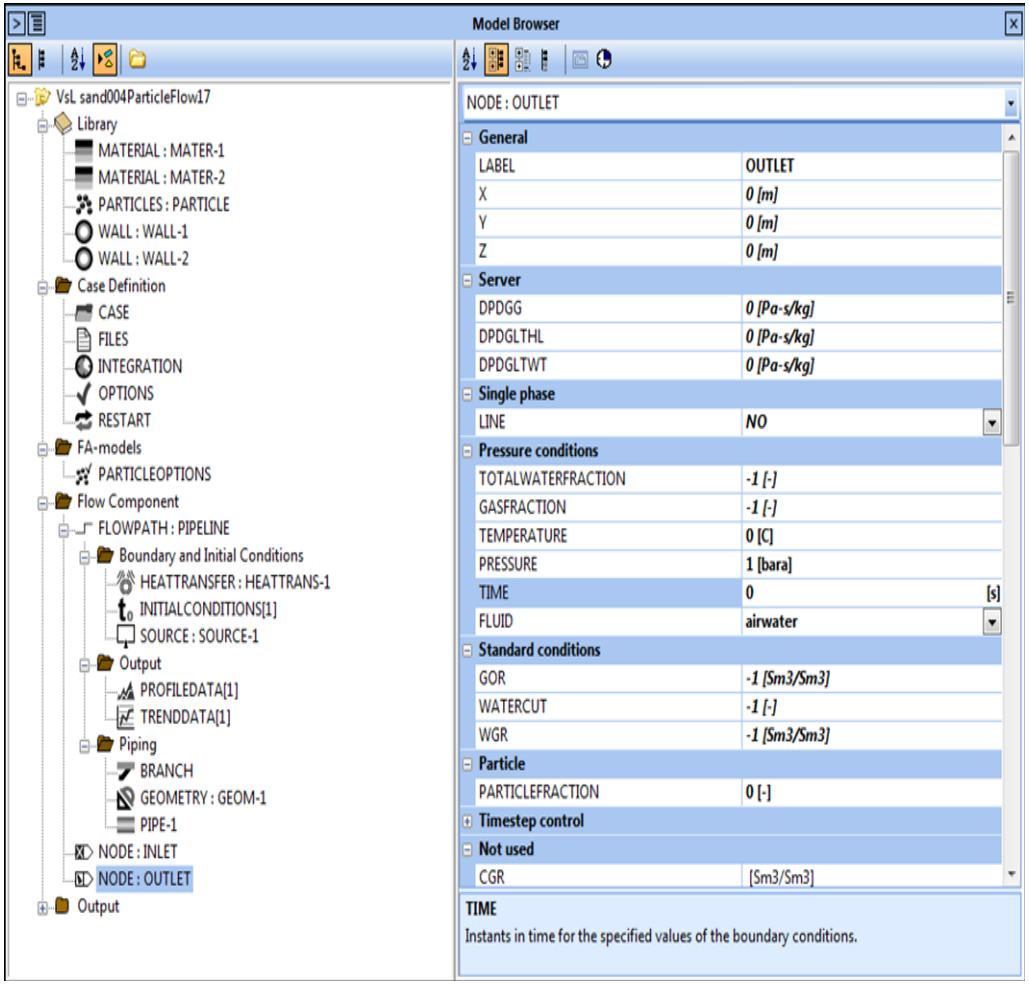
Model Browser
VsL sand004ParticleFlow17
Library
MATERIAL : MATER-1
MATERIAL : MATER-2
PARTICLES : PARTICLE
WALL : WALL-1
WALL : WALL-2
Case Definition
CASE
FILES
INTEGRATION
OPTIONS
RESTART
FA-models
PARTICLEOPTIONS
Flow Component
FLOWPATH : PIPELINE
Boundary and Initial Conditions
HEATTRANSFER : HEATTRANS-1
INITIALCONDITIONS[1]
SOURCE : SOURCE-1
Output
PROFILEDATA[1]
TRENDDATA[1]
Piping
BRANCH
GEOMETRY : GEOM-1
PIPE-1
NODE : INLET
NODE : OUTLET
Output
NODE : OUTLET
General
LABEL OUTLET
X 0 [m]
Y 0 [m]
Z 0 [m]
Server
DPDGG 0 [Pa-s/kg]
DPDGLTHL 0 [Pa-s/kg]
DPDGLTWT 0 [Pa-s/kg]
Single phase
LINE NO
Pressure conditions
TOTALWATERFRACTION -1 [-]
GASFRACTION -1 [-]
TEMPERATURE 0 [C]
PRESSURE 1 [bara]
TIME 0 [s]
FLUID airwater
Standard conditions
GOR -1 [Sm3/Sm3]
WATERCUT -1 [-]
WGR -1 [Sm3/Sm3]
Particle
PARTICLEFRACTION 0 [-]
Timestep control
Not used
CGR [Sm3/Sm3]
TIME
Instants in time for the specified values of the boundary conditions.

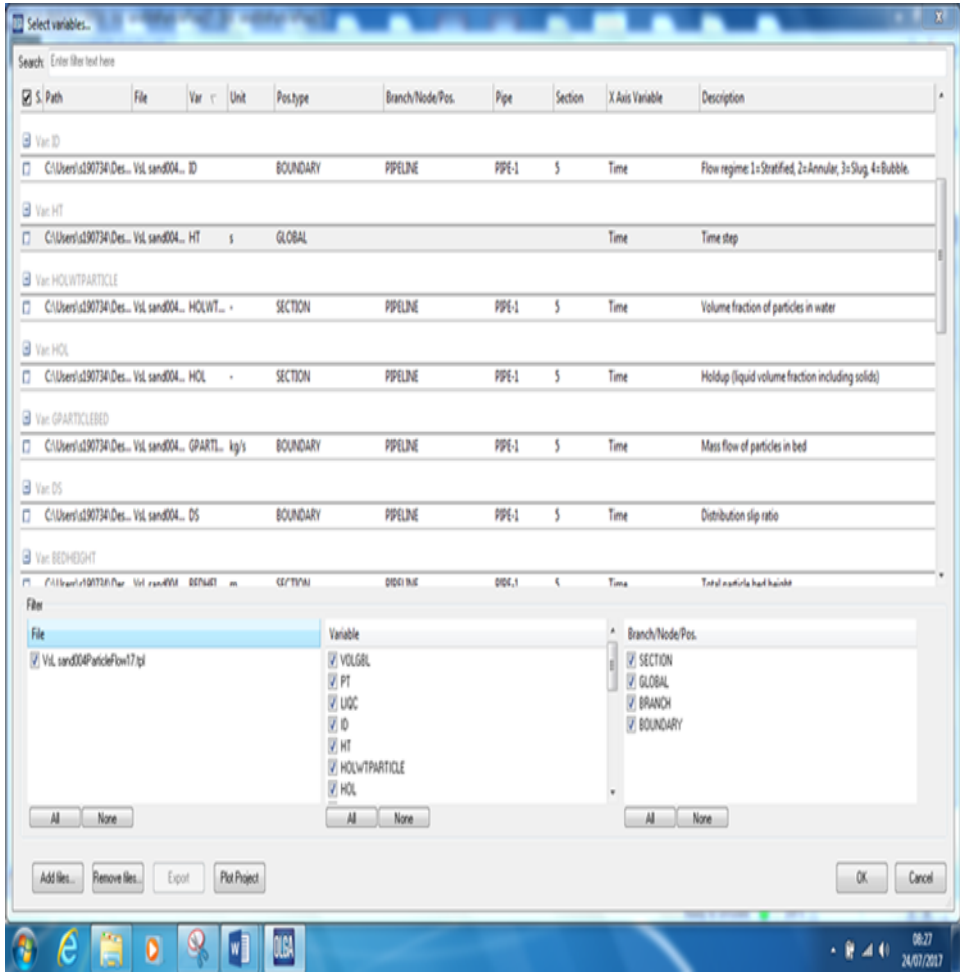
Select variables...
Search:
Path
File
Var
Unit
Pos.type
Branch/Node/Pos.
Pipe
Section
X Axis Variable
Description
Filter
File
Variable
Branch/Node/Pos.
VsL sand004ParticleFlow17.tpl
VOLGBL
PT
UGC
ID
HT
HOLWTPARTICLE
HOL
SECTION
GLOBAL
BRANCH
BOUNDARY
All
None
Add files...
Remove files...
Export
Plot Project
OK
Cancel

The Entire Experimental Data Results Analysed in this study

Table H-1.1: Liquid Hold-up, Film Thickness, Liquid Entrainment and Pressure Gradient Analysis

			Vsl= 0.0505m/s		Rings+ Liq Entrain	Probes (Bottom)	Triangular Relationship				Liquid Entrainment Correlations			
Vsl(m/s)	Vsg(m/s)	Gas Hold-Up	Liquid Hold-Up	HL+Liq Entrain	Film Thickness(mm)	Film Thickness(mm)	Film Thickness	Slip	Slip Ratio	Wave Velocity,m/s	Pan & Hanratty (2002b)	Paleev & Fillippovich (1966)	Mantilla (2008)	dp/dx (kPa/m)
0.0511	8.3179	0.9819	0.0180	0.0181	0.2285	0.1811	0.2540	162.9038	2.9950	0.0175	8.8E-06	0.0116	0.0007	0.3988
0.0509	9.4533	0.9832	0.0168	0.0168	0.2124	0.1762	0.2201	185.7425	3.1708	0.0183	1.3E-05	0.0403	0.0007	0.4587
0.0508	10.0773	0.9839	0.0161	0.0161	0.2034	0.1736	0.2079	198.3132	3.2402	0.0191	1.6E-05	0.0547	0.0007	0.4850
0.0509	10.9194	0.9852	0.0148	0.0148	0.1877	0.1681	0.1795	214.5316	3.2327	0.0200	2.0E-05	0.0728	0.0007	0.5626
0.0506	11.9057	0.9855	0.0145	0.0145	0.1839	0.1650	0.1657	235.4830	3.4749	0.0210	2.6E-05	0.0928	0.0007	0.6053
0.0504	12.8888	0.9858	0.0141	0.0142	0.1793	0.1629	0.1553	255.7960	3.6788	0.0221	3.2E-05	0.1115	0.0007	0.6438
0.0502	14.0307	0.9864	0.0135	0.0136	0.1714	0.1592	0.1420	279.2442	3.8371	0.0221	4.2E-05	0.1315	0.0007	0.7018
0.0503	15.0982	0.9869	0.0130	0.0131	0.1651	0.1562	0.1301	300.0130	3.9712	0.0233	5.2E-05	0.1490	0.0008	0.7677
0.0501	15.5284	0.9872	0.0127	0.0128	0.1616	0.1551	0.1256	310.0378	4.0150	0.0233	5.7E-05	0.1564	0.0008	0.7913
0.0504	17.0857	0.9877	0.0122	0.0123	0.1550	0.1514	0.1130	339.1997	4.2121	0.0247	7.4E-05	0.1788	0.0008	0.8843
0.0503	18.0246	0.9880	0.0119	0.0120	0.1520	0.1501	0.1086	358.5537	4.3662	0.0247	8.7E-05	0.1922	0.0008	0.9183
0.0501	20.0773	0.9880	0.0119	0.0120	0.1522	0.1498	0.1080	400.5432	4.8813	0.0247	1.2E-04	0.2194	0.0008	0.9209
0.0501	23.2796	0.9878	0.0121	0.0122	0.1547	0.1503	0.1077	464.9259	5.7617	0.0247	1.9E-04	0.2575	0.0009	0.9226
0.0505														

Table H-1.2: Liquid Hold-up, Film Thickness, Liquid Entrainment and Pressure Gradient Analysis

			Vsl= 0.0714m/s		Rings+ Liq Entrain	Probes (Bottom)	Triangular Relationship				Liquid Entrainment Correlations			
Vsl(m/s)	Vsg(m/s)	Gas Hold-Up	Liquid Hold-Up	HL+Liq Entrain	Film Thickness(mm)	Film Thickness(mm)	Film Thickness	Slip	Slip Ratio	Wave Velocity,m/s	Pan & Hanratty (2002b)	Paleev & Fillippovich (1966)	Mantilla (2008)	dp/dx (kPa/m)
0.0733	8.0774	0.9775	0.0225	0.0225	0.2853	0.2071	0.2696	110.2320	2.5388	0.0200	8.8E-06	0.0659	0.0007	0.5393
0.0730	8.9605	0.9789	0.0211	0.0211	0.2679	0.2036	0.2391	122.8186	2.6534	0.0210	1.3E-05	0.0913	0.0007	0.6053
0.0721	10.1592	0.9804	0.0196	0.0196	0.2478	0.1993	0.2048	140.9019	2.8125	0.0220	1.7E-05	0.1143	0.0007	0.6984
0.0723	11.0207	0.9811	0.0188	0.0189	0.2387	0.1973	0.1894	152.4562	2.9295	0.0233	2.2E-05	0.1320	0.0007	0.7573
0.0704	11.6847	0.9824	0.0176	0.0176	0.2225	0.1936	0.1741	165.9815	2.9707	0.0233	2.6E-05	0.1443	0.0007	0.8023
0.0716	13.1697	0.9835	0.0165	0.0165	0.2086	0.1910	0.1606	184.0460	3.0859	0.0247	3.6E-05	0.1706	0.0007	0.8839
0.0713	14.3350	0.9846	0.0153	0.0154	0.1945	0.1876	0.1486	200.9900	3.1392	0.0247	4.6E-05	0.1892	0.0007	0.9521
0.0712	15.4484	0.9857	0.0142	0.0143	0.1808	0.1839	0.1404	216.9250	3.1458	0.0262	5.7E-05	0.2058	0.0007	1.0062
0.0708	16.3867	0.9863	0.0137	0.0137	0.1736	0.1815	0.1348	231.4095	3.2220	0.0262	6.8E-05	0.2193	0.0007	1.0423
0.0706	17.3721	0.9867	0.0132	0.0133	0.1680	0.1793	0.1312	246.0523	3.3139	0.0262	8.1E-05	0.2326	0.0007	1.0678
0.0707	18.2912	0.9865	0.0134	0.0135	0.1710	0.1805	0.1329	258.7624	3.5486	0.0262	9.4E-05	0.2450	0.0007	1.0549
0.0707	20.2922	0.9867	0.0132	0.0133	0.1686	0.1794	0.1318	286.8683	3.8785	0.0262	1.3E-04	0.2699	0.0008	1.0651
0.0706	23.5416	0.9863	0.0135	0.0137	0.1730	0.1806	0.1340	333.4386	4.6264	0.0262	2.0E-04	0.3064	0.0008	1.0451
0.0714														

Table H-1.3: Liquid Hold-up, Film Thickness, Liquid Entrainment and Pressure Gradient Analysis

			Vsl= 0.0903m/s		Rings+ Liq Entrain	Probes (Bottom)	Triangular Relationship				Liquid Entrainment Correlations			
Vsl(m/s)	Vsg(m/s)	Gas Hold-Up	Liquid Hold-Up	HL+Liq Entrain	Film Thickness(mm)	Film Thickness(mm)	Film Thickness	Slip	Slip Ratio	Wave Velocity,m/s	Pan & Hanratty (2002b)	Paleev & Fillippovich (1966)	Mantilla (2008)	dp/dx (kPa/m)
0.0923	8.4940	0.9724	0.0275	0.0276	0.3497	0.2126	0.2428	92.0331	2.6083	0.0221	1.1E-05	0.1209	0.0006	0.7540
0.0920	9.1611	0.9736	0.0264	0.0264	0.3350	0.2106	0.2237	99.5674	2.7006	0.0233	1.3E-05	0.1363	0.0006	0.8161
0.0910	10.1754	0.9749	0.0251	0.0251	0.3188	0.2087	0.2070	111.7988	2.8832	0.0233	1.8E-05	0.1579	0.0006	0.8722
0.0902	11.3827	0.9764	0.0235	0.0236	0.2986	0.2067	0.1925	126.2572	3.0464	0.0247	2.4E-05	0.1813	0.0006	0.9294
0.0913	12.3319	0.9776	0.0224	0.0224	0.2836	0.2053	0.1850	134.9973	3.0906	0.0262	3.1E-05	0.1979	0.0006	0.9795
0.0905	13.2463	0.9790	0.0210	0.0210	0.2662	0.2026	0.1746	146.3389	3.1413	0.0262	3.8E-05	0.2129	0.0006	1.0284
0.0900	14.3424	0.9806	0.0194	0.0194	0.2462	0.1992	0.1645	159.3714	3.1601	0.0280	4.7E-05	0.2296	0.0006	1.0857
0.0896	15.3535	0.9815	0.0184	0.0185	0.2340	0.1968	0.1563	171.2993	3.2262	0.0280	5.7E-05	0.2441	0.0006	1.1378
0.0893	16.3559	0.9822	0.0177	0.0178	0.2253	0.1948	0.1516	183.1076	3.3183	0.0280	6.9E-05	0.2580	0.0006	1.1686
0.0893	17.3035	0.9824	0.0176	0.0176	0.2233	0.1943	0.1516	193.8144	3.4808	0.0280	8.1E-05	0.2706	0.0006	1.1683
0.0888	18.3279	0.9822	0.0177	0.0178	0.2257	0.1949	0.1521	206.3837	3.7478	0.0280	9.7E-05	0.2839	0.0006	1.1584
0.0891	20.5905	0.9821	0.0177	0.0179	0.2263	0.1949	0.1515	231.0057	4.2046	0.0280	1.4E-04	0.3110	0.0007	1.1676
0.0901	23.5707	0.9818	0.0179	0.0182	0.2297	0.1956	0.1545	261.4630	4.8335	0.0280	2.1E-04	0.3431	0.0007	1.1576
0.0903														

Table H-1.4: Liquid Hold-up, Film Thickness, Liquid Entrainment and Pressure Gradient Analysis

			Vsl= 0.1355m/s		Rings+ Liq Entrain	Probes (Bottom)	Triangular Relation				Liquid Entrainment Correlations			
Vsl(m/s)	Vsg(m/s)	Gas Hold-Up	Liquid Hold-Up	HL+Liq Entrain	Film Thickness(mm)	Film Thickness(mm)	Film Thickness	Slip	Slip Ratio	Wave Velocity,m/s	Pan & Hanratty (2002b)	Paleev & Fillippovich (1966)	Mantilla (2008)	dp/dx (kPa/m)
0.1336	8.1564	0.9654	0.0346	0.0346	0.4395	0.2163	0.2237	61.0693	2.1871	0.0247	1.0E-05	0.1953	0.0004	1.1847
0.1275	9.3771	0.9688	0.0312	0.0312	0.3960	0.2133	0.2035	73.5648	2.3680	0.0262	1.5E-05	0.2219	0.0004	1.2426
0.1272	10.2753	0.9698	0.0301	0.0302	0.3828	0.2124	0.1972	80.7944	2.5117	0.0280	2.0E-05	0.2402	0.0004	1.2794
0.1266	11.3896	0.9707	0.0293	0.0293	0.3725	0.2117	0.1914	89.9561	2.7195	0.0280	2.6E-05	0.2611	0.0004	1.3123
0.1275	12.0846	0.9713	0.0287	0.0287	0.3646	0.2112	0.1905	94.7972	2.8035	0.0280	3.1E-05	0.2731	0.0005	1.3280
0.1266	13.2336	0.9730	0.0270	0.0270	0.3429	0.2092	0.1820	104.4997	2.9027	0.0300	4.1E-05	0.2912	0.0005	1.3807
0.1270	14.2926	0.9746	0.0254	0.0254	0.3227	0.2070	0.1751	112.5432	2.9387	0.0300	5.0E-05	0.3067	0.0004	1.4393
0.1264	15.1316	0.9753	0.0246	0.0247	0.3125	0.2057	0.1695	119.6863	3.0248	0.0300	5.9E-05	0.3185	0.0005	1.4800
0.1482	16.3562	0.9716	0.0283	0.0284	0.3598	0.2093	0.1728	110.3676	3.2209	0.0323	7.7E-05	0.3376	0.0005	1.7016
0.1482	17.2538	0.9712	0.0287	0.0288	0.3660	0.2098	0.1768	116.3973	3.4561	0.0323	9.1E-05	0.3494	0.0005	1.6636
0.1471	18.1475	0.9713	0.0286	0.0287	0.3643	0.2095	0.1755	123.4041	3.6473	0.0323	1.1E-04	0.3605	0.0005	1.6627
0.1476	20.2508	0.9715	0.0283	0.0285	0.3612	0.2092	0.1750	137.2252	4.0195	0.0323	1.5E-04	0.3844	0.0006	1.6729
0.1480	23.1697	0.9711	0.0287	0.0289	0.3666	0.2096	0.1773	156.5539	4.6569	0.0323	2.2E-04	0.4148	0.0006	1.6559
0.1355														

Table H-1.5: Liquid Hold-up, Film Thickness, Liquid Entrainment and Pressure Gradient Analysis

			Vsl= 0.1851m/s		Rings+ Liq Entrain	Probes (Bottom)	Triangular Relationship				Liquid Entrainment Correlations			
Vsl(m/s)	Vsg(m/s)	Gas Hold-Up	Liquid Hold-Up	HL+Liq Entrain	Film Thickness(mm)	Film Thickness(mm)	Film Thickness	Slip	Slip Ratio	Wave Velocity,m/s	Pan & Hanratty (2002b)	Paleev & Fillippovich (1966)	Mantilla (2008)	dp/dx (kPa/m)
0.1950	8.3042	0.9592	0.0408	0.0408	0.5201	0.2197	0.1907	42.5794	1.8134	0.0280	1.1E-05	0.2641	0.0003	2.0295
0.1920	9.3747	0.9607	0.0393	0.0393	0.5001	0.2187	0.1797	48.8334	1.9977	0.0290	1.6E-05	0.2876	0.0003	2.1195
0.1892	10.3928	0.9617	0.0383	0.0383	0.4876	0.2183	0.1771	54.9331	2.1892	0.0300	2.1E-05	0.3078	0.0004	2.1195
0.1867	11.4133	0.9635	0.0365	0.0365	0.4643	0.2169	0.1715	61.1308	2.3165	0.0320	2.7E-05	0.3258	0.0004	2.1595
0.1852	12.3305	0.9645	0.0355	0.0355	0.4515	0.2163	0.1678	66.5972	2.4522	0.0320	3.4E-05	0.3409	0.0004	2.1895
0.1834	13.3075	0.9652	0.0348	0.0348	0.4429	0.2158	0.1685	72.5659	2.6195	0.0330	4.3E-05	0.3563	0.0004	2.1595
0.1819	14.4407	0.9658	0.0341	0.0342	0.4342	0.2153	0.1679	79.3687	2.8074	0.0350	5.4E-05	0.3728	0.0004	2.1495
0.1823	15.5866	0.9658	0.0341	0.0342	0.4346	0.2152	0.1707	85.4879	3.0267	0.0350	6.8E-05	0.3888	0.0004	2.1195
0.1840	16.5037	0.9654	0.0345	0.0346	0.4400	0.2153	0.1699	89.6819	3.2159	0.0362	8.1E-05	0.4008	0.0004	2.1495
0.1822	17.5280	0.9656	0.0343	0.0344	0.4372	0.2152	0.1681	96.2272	3.4282	0.0362	9.7E-05	0.4134	0.0004	2.1495
0.1832	18.4493	0.9653	0.0345	0.0347	0.4405	0.2152	0.1683	100.7026	3.6155	0.0362	1.1E-04	0.4243	0.0004	2.1595
0.1810	20.7125	0.9651	0.0347	0.0349	0.4432	0.2155	0.1707	114.4408	4.1342	0.0350	1.6E-04	0.4491	0.0005	2.1030
0.1805	23.7260	0.9655	0.0343	0.0345	0.4387	0.2150	0.1674	131.4102	4.6974	0.0350	2.4E-04	0.4782	0.0005	2.1395
0.1851														

Table I-1.1: Wave Frequency Analysis with several Correlations.

		Vsl=0.0505m/s						
Vsl	Vsg		Wave Frequency					
m/s	m/s	Experiment	Ousaka et al (1992)	Schubring & Shedd (2008)	Setyawan et al (2014)	Mantilla (2008)	Al-Sarkhi et al (2012)	Setyawan et al (2016)
0.0511	8.3179	4.4999	1.0022	0.6969	1.3166	2.0240	5.5628	1.1834
0.0509	9.4533	4.6643	1.1662	0.8444	1.4845	2.3691	6.2847	1.3770
0.0508	10.0773	4.8840	1.2579	0.9294	1.5767	2.5627	6.6794	1.4851
0.0509	10.9194	5.2361	1.3825	1.0483	1.7023	2.8163	7.1860	1.6261
0.0506	11.9057	5.2863	1.5328	1.1935	1.8460	3.1494	7.8365	1.8105
0.0504	12.8888	5.4635	1.6843	1.3443	1.9904	3.4782	8.4633	1.9917
0.0502	14.0307	5.7042	1.8627	1.5268	2.1584	3.8642	9.1826	2.2035
0.0503	15.0982	5.9052	2.0304	1.7044	2.3176	4.2116	9.8161	2.3934
0.0501	15.5284	6.0050	2.1007	1.7777	2.3792	4.3811	10.1208	2.4857
0.0504	17.0857	6.3562	2.3491	2.0518	2.6136	4.8801	11.0033	2.7568
0.0503	18.0246	6.3769	2.5030	2.2232	2.7524	5.2161	11.5860	2.9387
0.0501	20.0773	6.3276	2.8442	2.6136	3.0574	5.9575	12.8429	3.3382
0.0501	23.2796	6.4358	3.3876	3.2632	3.5374	7.1243	14.7525	3.9628

Table I-1.2: Wave Frequency Analysis with several Correlations

		Vsl=0.0714m/s						
Vsl	Vsg		Wave Frequency					
m/s	m/s	Experiment	Ousaka et al (1992)	Schubring & Shedd (2008)	Setyawan et al (2014)	Mantilla (2008)	Al-Sarkhi et al (2012)	Setyawan et al (2016)
0.0733	8.0774	3.4712	0.9071	0.6669	1.3941	1.2666	3.8685	0.7533
0.0730	8.9605	3.6274	1.0261	0.7792	1.5340	1.4421	4.2777	0.8537
0.0721	10.1592	3.8550	1.1925	0.9407	1.7202	1.7005	4.8606	1.0007
0.0723	11.0207	4.0853	1.3121	1.0629	1.8579	1.8692	5.2303	1.0962
0.0704	11.6847	4.3663	1.4126	1.1604	1.9511	2.0699	5.6605	1.2093
0.0716	13.1697	4.6206	1.6220	1.3885	2.1925	2.3431	6.2313	1.3625
0.0713	14.3350	4.8251	1.7937	1.5768	2.3743	2.6043	6.7632	1.5083
0.0712	15.4484	4.9892	1.9598	1.7640	2.5485	2.8540	7.2605	1.6470
0.0708	16.3867	5.0240	2.1031	1.9271	2.6927	3.0842	7.7103	1.7745
0.0706	17.3721	5.0857	2.2544	2.1036	2.8456	3.3198	8.1631	1.9045
0.0707	18.2912	5.0518	2.3952	2.2727	2.9906	3.5267	8.5545	2.0184
0.0707	20.2922	4.9792	2.7070	2.6556	3.3054	3.9912	9.4155	2.2730
0.0706	23.5416	5.0580	3.2267	3.3184	3.8156	4.7808	10.8294	2.7030

Table I-1.3: Wave Frequency Analysis with several Correlations

		Vsl=0.0903m/s						
Vsl	Vsg		Wave Frequency					
m/s	m/s	Experiment	Ousaka et al (1992)	Schubring & Shedd (2008)	Setyawan et al (2014)	Mantilla (2008)	Al-Sarkhi et al (2012)	Setyawan et al (2016)
0.0923	8.4940	3.2413	0.9234	0.7192	1.5447	1.0200	3.2709	0.6111
0.0920	9.1611	3.3622	1.0102	0.8056	1.6556	1.1210	3.5192	0.6695
0.0910	10.1754	3.6059	1.1457	0.9430	1.8204	1.2883	3.9196	0.7657
0.0902	11.3827	3.8991	1.3099	1.1157	2.0163	1.4907	4.3890	0.8814
0.0913	12.3319	4.2103	1.4364	1.2581	2.1798	1.6154	4.6709	0.9524
0.0905	13.2463	4.4809	1.5655	1.4006	2.3259	1.7796	5.0348	1.0455
0.0900	14.3424	4.6895	1.7212	1.5780	2.5029	1.9714	5.4505	1.1538
0.0896	15.3535	4.7698	1.8667	1.7478	2.6664	2.1498	5.8290	1.2542
0.0893	16.3559	4.9378	2.0125	1.9217	2.8284	2.3288	6.2018	1.3545
0.0893	17.3035	4.7967	2.1510	2.0911	2.9830	2.4931	6.5383	1.4463
0.0888	18.3279	4.9230	2.3043	2.2795	3.1467	2.6884	6.9318	1.5550
0.0891	20.5905	4.7964	2.6418	2.7144	3.5187	3.0777	7.6978	1.7709
0.0901	23.5707	4.8847	3.0924	3.3246	4.0148	3.5709	8.6375	2.0427

Table I-1.4: Wave Frequency Analysis with several Correlations

		Vsl=0.1355m/s						
Vsl	Vsg		Wave Frequency					
m/s	m/s	Experiment	Ousaka et al (1992)	Schubring & Shedd (2008)	Setyawan et al (2014)	Mantilla (2008)	Al-Sarkhi et al (2012)	Setyawan et al (2016)
0.1336	8.1564	2.9654	0.8236	0.6767	1.6314	0.6235	2.2336	0.3792
0.1275	9.3771	3.3840	0.9792	0.8342	1.8329	0.7796	2.6558	0.4710
0.1272	10.2753	3.5050	1.0912	0.9569	1.9930	0.8725	2.8978	0.5253
0.1266	11.3896	3.8115	1.2332	1.1167	2.1895	0.9925	3.2022	0.5951
0.1275	12.0846	3.9343	1.3208	1.2205	2.3167	1.0569	3.3622	0.6324
0.1266	13.2336	4.2335	1.4720	1.3986	2.5162	1.1880	3.6811	0.7081
0.1270	14.2926	4.3544	1.6111	1.5698	2.7047	1.2986	3.9439	0.7716
0.1264	15.1316	4.4307	1.7247	1.7100	2.8492	1.3981	4.1762	0.8286
0.1482	16.3562	4.2403	1.8373	1.9218	3.1818	1.2685	3.8729	0.7543
0.1482	17.2538	4.2003	1.9568	2.0821	3.3442	1.3521	4.0694	0.8023
0.1471	18.1475	4.0963	2.0799	2.2460	3.4988	1.4504	4.2967	0.8584
0.1476	20.2508	4.2517	2.3657	2.6475	3.8795	1.6474	4.7426	0.9706
0.1480	23.1697	4.1405	2.7717	3.2401	4.4049	1.9297	5.3609	1.1303

Table I-1.5: Wave Frequency Analysis with several Correlations

		Vsl=0.1851m/s						
Vsl	Vsg		Wave Frequency					
m/s	m/s	Experiment	Ousaka et al (1992)	Schubring & Shedd (2008)	Setyawan et al (2014)	Mantilla (200	Al-Sarkhi et al (2012)	Setyawan et al (2016)
0.1950	8.3042	2.7945	0.7858	0.6952	1.8266	0.4045	1.5972	0.2485
0.1920	9.3747	2.9664	0.9093	0.8339	2.0323	0.4768	1.8143	0.2919
0.1892	10.3928	3.2126	1.0296	0.9734	2.2250	0.5491	2.0242	0.3350
0.1867	11.4133	3.2968	1.1527	1.1202	2.4164	0.6243	2.2357	0.3796
0.1852	12.3305	3.4152	1.2647	1.2579	2.5887	0.6919	2.4211	0.4195
0.1834	13.3075	3.5870	1.3862	1.4103	2.7701	0.7669	2.6223	0.4636
0.1819	14.4407	3.6842	1.5287	1.5943	2.9809	0.8540	2.8502	0.5145
0.1823	15.5866	3.5650	1.6722	1.7877	3.2002	0.9336	3.0540	0.5609
0.1840	16.5037	3.6239	1.7859	1.9478	3.3816	0.9888	3.1931	0.5930
0.1822	17.5280	3.5648	1.9209	2.1319	3.5665	1.0761	3.4093	0.6435
0.1832	18.4493	3.5649	2.0385	2.3022	3.7452	1.1364	3.5565	0.6783
0.1810	20.7125	3.6105	2.3419	2.7386	4.1581	1.3249	4.0057	0.7867
0.1805	23.7260	3.5396	2.7502	3.3575	4.7170	1.5640	4.5554	0.9232

J-1.1: Pressure Gradient from the Experiment and other Correlations

	Vsl=0.05m/s						Vsl=0.0714m/s		
Vsl	Vsg	P Beggs and Brill	P dukler	Experiment	Vsl	Vsg	Beggs and Brill 1973	Dukler 1963	Experiment
m/s	m/s	kPa/m	kPa/m	kPa/m	m/s	m/s	kPa/m	kPa/m	kPa/m
0.0511	8.3179	0.3302	0.3667	0.3988	0.0733	8.0774	0.4128	0.4745	0.5393
0.0509	9.4533	0.3825	0.4189	0.4587	0.0730	8.9605	0.4615	0.5246	0.6053
0.0508	10.0773	0.4122	0.4482	0.4850	0.0721	10.1592	0.5270	0.5905	0.6984
0.0509	10.9194	0.4543	0.4896	0.5626	0.0723	11.0207	0.5795	0.6437	0.7573
0.0506	11.9057	0.5025	0.5359	0.6053	0.0704	11.6847	0.6089	0.6704	0.8023
0.0504	12.8888	0.5530	0.5840	0.6438	0.0716	13.1697	0.7085	0.7705	0.8839
0.0502	14.0307	0.6138	0.6414	0.7018	0.0713	14.3350	0.7821	0.8419	0.9521
0.0503	15.0982	0.6741	0.6981	0.7677	0.0712	15.4484	0.8552	0.9122	1.0062
0.0501	15.5284	0.6968	0.7187	0.7913	0.0708	16.3867	0.9158	0.9692	1.0423
0.0504	17.0857	0.7907	0.8058	0.8843	0.0706	17.3721	0.9824	1.0317	1.0678
0.0503	18.0246	0.8469	0.8568	0.9183	0.0707	18.2912	1.0482	1.0938	1.0549
0.0501	20.0773	0.9754	0.9717	0.9209	0.0707	20.2922	1.1952	1.2303	1.0651
0.0501	23.2796	1.1908	1.1609	0.9226	0.0706	23.5416	1.4452	1.4574	1.0451

J-1.2: Pressure Gradient from the Experiment and other Correlations

		Vsl=0.0903m/s					Vsl=0.1355m/s		
Vsl	Vsg	Beggs and Brill 1973	Dukler 1963	Experiment	Vsl	Vsg	Beggs and Brill 1973	Dukler 1963	Experiment
m/s	m/s	kPa/m	kPa/m	kPa/m	m/s	m/s	kPa/m	kPa/m	kPa/m
0.0923	8.4940	0.5185	0.6054	0.7540	0.1336	8.1564	0.6661	0.8072	1.1847
0.0920	9.1611	0.5613	0.6500	0.8161	0.1275	9.3771	0.7408	0.8817	1.2426
0.0910	10.1754	0.6245	0.7146	0.8722	0.1272	10.2753	0.8143	0.9597	1.2794
0.0902	11.3827	0.7026	0.7935	0.9294	0.1266	11.3896	0.9057	1.0554	1.3123
0.0913	12.3319	0.7763	0.8700	0.9795	0.1275	12.0846	0.9706	1.1245	1.3280
0.0905	13.2463	0.8369	0.9295	1.0284	0.1266	13.2336	1.0664	1.2223	1.3807
0.0900	14.3424	0.9137	1.0050	1.0857	0.1270	14.2926	1.1635	1.3223	1.4393
0.0896	15.3535	0.9867	1.0761	1.1378	0.1264	15.1316	1.2358	1.3947	1.4800
0.0893	16.3559	1.0608	1.1478	1.1686	0.1482	16.3562	1.5153	1.7206	1.7016
0.0893	17.3035	1.1342	1.2186	1.1683	0.1482	17.2538	1.6085	1.8150	1.6636
0.0888	18.3279	1.2113	1.2915	1.1584	0.1471	18.1475	1.6926	1.8969	1.6627
0.0891	20.5905	1.3994	1.4706	1.1676	0.1476	20.2508	1.9223	2.1263	1.6729
0.0901	23.5707	1.6672	1.7226	1.1576	0.1480	23.1697	2.2510	2.4486	1.6559

J-1.3: Pressure Gradient from the Experiment and other Correlations

		Vsl=0.1851m/s		
Vsl	Vsg	***Beggs and Brill 1973***	***Dukler 1963***	***Experiment***
m/s	m/s	***kPa/m***	***kPa/m***	***kPa/m***
0.1950	*8.3042*	*0.9322*	*1.1656*	*2.0295*
0.1920	*9.3747*	*1.0368*	*1.2799*	*2.1195*
0.1892	*10.3928*	*1.1359*	*1.3865*	*2.1195*
0.1867	*11.4133*	*1.2362*	*1.4928*	*2.1595*
0.1852	*12.3305*	*1.3299*	*1.5918*	*2.1895*
0.1834	*13.3075*	*1.4292*	*1.6952*	*2.1595*
0.1819	*14.4407*	*1.5485*	*1.8189*	*2.1495*
0.1823	*15.5866*	*1.6831*	*1.9604*	*2.1195*
0.1840	*16.5037*	*1.8031*	*2.0883*	*2.1495*
0.1822	*17.5280*	*1.9101*	*2.1946*	*2.1495*
0.1832	*18.4493*	*2.0294*	*2.3189*	*2.1595*
0.1810	*20.7125*	*2.2866*	*2.5734*	*2.0995*
0.1805	*23.7260*	*2.6618*	*2.9445*	*2.1395*

K-1.1: Liquid Hold-Up Analysis with Proposed Model & several Correlations

	Vsl=0.0505m/s			Experiment,	Proposed Model	& other Models					
Vsl(m/s)	Vsg(m/s)	Qw, L/s	Qg, L/s	HL	HL	Flanigan (1958)	Chen & Spedding (1981)	Beggs & Brill (1973)	Spedding et al (1998)	Minami & Brill (1987)	Abdul-Majeed (1996)
0.0511	8.3179	0.1035	9.5864	0.0181	0.0216	0.9839	0.3125	0.0365	0.1480	0.9244	0.1181
0.0509	9.4533	0.1032	10.5541	0.0168	0.0195	0.9839	0.2937	0.0333	0.1382	0.9277	0.1039
0.0508	10.0773	0.1030	11.0649	0.0161	0.0186	0.9840	0.2845	0.0317	0.1336	0.9293	0.0974
0.0509	10.9194	0.1032	11.7780	0.0148	0.0175	0.9839	0.2742	0.0301	0.1280	0.9313	0.0901
0.0506	11.9057	0.1025	12.5420	0.0145	0.0163	0.9840	0.2613	0.0282	0.1220	0.9334	0.0819
0.0504	12.8888	0.1021	13.2823	0.0142	0.0154	0.9841	0.2504	0.0267	0.1170	0.9352	0.0752
0.0502	14.0307	0.1018	14.1245	0.0136	0.0144	0.9841	0.2393	0.0251	0.1119	0.9371	0.0686
0.0503	15.0982	0.1020	14.9027	0.0131	0.0137	0.9841	0.2309	0.0239	0.1079	0.9387	0.0636
0.0501	15.5284	0.1015	15.2028	0.0128	0.0134	0.9842	0.2266	0.0233	0.1060	0.9393	0.0614
0.0504	17.0857	0.1021	16.3090	0.0123	0.0125	0.9841	0.2168	0.0219	0.1014	0.9413	0.0559
0.0503	18.0246	0.1019	16.9283	0.0120	0.0120	0.9841	0.2104	0.0211	0.0987	0.9424	0.0526
0.0501	20.0773	0.1016	18.1877	0.0120	0.0112	0.9842	0.1981	0.0195	0.0937	0.9445	0.0466
0.0501	23.2796	0.1015	20.0167	0.0122	0.0101	0.9842	0.1827	0.0176	0.0876	0.9472	0.0395

K-1.2: Liquid Hold-Up Analysis with Proposed Model & several Correlations

	Vsl=0.0714m/s			Experiment,	Proposed Model	& other Models					
Vsl(m/s)	Vsg(m/s)	Qw, L/s	Qg, L/s	HL	HL	Flanigan (1958)	Chen & Spedding (1981)	Beggs & Brill (1973)	Spedding et al (1998)	Minami & Brill (1987)	Abdul-Majeed (1996)
0.0733	8.0774	0.1485	9.6567	0.0225	0.0308	0.9770	0.4169	0.0459	0.1890	0.9246	0.1747
0.0730	8.9605	0.1479	10.4651	0.0211	0.0283	0.9771	0.3990	0.0426	0.1783	0.9274	0.1593
0.0721	10.1592	0.1461	11.5416	0.0196	0.0253	0.9774	0.3758	0.0388	0.1653	0.9305	0.1412
0.0723	11.0207	0.1465	12.2924	0.0189	0.0238	0.9773	0.3638	0.0367	0.1585	0.9325	0.1317
0.0704	11.6847	0.1427	12.8496	0.0176	0.0222	0.9779	0.3476	0.0347	0.1509	0.9339	0.1215
0.0716	13.1697	0.1450	14.0806	0.0165	0.0206	0.9775	0.3341	0.0322	0.1433	0.9367	0.1107
0.0713	14.3350	0.1446	15.0136	0.0154	0.0193	0.9776	0.3208	0.0303	0.1367	0.9385	0.1019
0.0712	15.4484	0.1444	15.8775	0.0143	0.0182	0.9776	0.3096	0.0287	0.1314	0.9401	0.0947
0.0708	16.3867	0.1435	16.5637	0.0137	0.0173	0.9778	0.2999	0.0275	0.1271	0.9414	0.0889
0.0706	17.3721	0.1431	17.2608	0.0133	0.0166	0.9778	0.2910	0.0263	0.1233	0.9425	0.0837
0.0707	18.2912	0.1433	17.8234	0.0135	0.0161	0.9778	0.2843	0.0254	0.1206	0.9435	0.0796
0.0707	20.2922	0.1434	19.0901	0.0133	0.0150	0.9778	0.2706	0.0237	0.1151	0.9455	0.0718
0.0706	23.5416	0.1431	20.9560	0.0137	0.0137	0.9778	0.2510	0.0213	0.1077	0.9482	0.0616

K-1.3: Liquid Hold-Up Analysis with Proposed Model & several Correlations

	Vsl=0.0903m/s			Experiment,	Proposed Model	& other Models					
Vsl(m/s)	Vsg(m/s)	Qw, L/s	Qg, L/s	HL	HL	Flanigan (1958)	Chen & Spedding (1981)	Beggs & Brill (1973)	Spedding et al (1998)	Minami & Brill (1987)	Abdul-Majeed (1996)
0.0923	8.4940	0.1871	10.2527	0.0276	0.0365	0.9712	0.4770	0.0508	0.2126	0.9267	0.2037
0.0920	9.1611	0.1865	10.8829	0.0264	0.0343	0.9712	0.4635	0.0481	0.2036	0.9286	0.1916
0.0910	10.1754	0.1845	11.8220	0.0251	0.0312	0.9715	0.4430	0.0445	0.1909	0.9312	0.1746
0.0902	11.3827	0.1827	12.8987	0.0236	0.0283	0.9718	0.4218	0.0409	0.1786	0.9339	0.1580
0.0913	12.3319	0.1852	13.7453	0.0224	0.0269	0.9714	0.4127	0.0390	0.1725	0.9358	0.1495
0.0905	13.2463	0.1835	14.5438	0.0210	0.0252	0.9717	0.3985	0.0369	0.1649	0.9374	0.1395
0.0900	14.3424	0.1824	15.4681	0.0194	0.0236	0.9719	0.3843	0.0348	0.1573	0.9392	0.1295
0.0896	15.3535	0.1817	16.2801	0.0185	0.0223	0.9720	0.3724	0.0331	0.1514	0.9406	0.1215
0.0893	16.3559	0.1811	17.0402	0.0178	0.0213	0.9721	0.3617	0.0316	0.1464	0.9419	0.1144
0.0893	17.3035	0.1810	17.6932	0.0176	0.0205	0.9721	0.3529	0.0304	0.1426	0.9430	0.1087
0.0888	18.3279	0.1800	18.3331	0.0178	0.0196	0.9722	0.3428	0.0291	0.1386	0.9441	0.1025
0.0891	20.5905	0.1807	19.7772	0.0179	0.0183	0.9721	0.3265	0.0269	0.1318	0.9463	0.0924
0.0901	23.5707	0.1827	21.5380	0.0182	0.0170	0.9718	0.3099	0.0246	0.1252	0.9487	0.0823

K-1.4: Liquid Hold-Up Analysis with Proposed Model & several Correlations

	Vsl=0.1355m/s			Experiment,	Proposed Model	& other Models					
Vsl(m/s)	Vsg(m/s)	Qw, L/s	Qg, L/s	HL	HL	Flanigan (1958)	Chen & Spedding (1981)	Beggs & Brill (1973)	Spedding et al (1998)	Minami & Brill (1987)	Abdul-Majeed (1996)
0.1336	8.1564	0.2667	10.3275	0.0346	0.0516	0.9587	0.5935	0.0636	0.2697	0.9270	0.2679
0.1275	9.3771	0.2545	11.5806	0.0312	0.0440	0.9605	0.5571	0.0562	0.2416	0.9305	0.2377
0.1272	10.2753	0.2539	12.4129	0.0302	0.0409	0.9606	0.5414	0.0527	0.2300	0.9327	0.2229
0.1266	11.3896	0.2528	13.4225	0.0293	0.0377	0.9608	0.5230	0.0489	0.2173	0.9351	0.2066
0.1275	12.0846	0.2545	14.0794	0.0287	0.0362	0.9605	0.5151	0.0471	0.2113	0.9365	0.1988
0.1266	13.2336	0.2528	15.1442	0.0270	0.0334	0.9608	0.4980	0.0441	0.2000	0.9385	0.1851
0.1270	14.2926	0.2536	16.1026	0.0254	0.0315	0.9607	0.4860	0.0418	0.1921	0.9402	0.1750
0.1264	15.1316	0.2524	16.8104	0.0247	0.0300	0.9608	0.4752	0.0401	0.1859	0.9414	0.1669
0.1482	16.3562	0.2959	18.1278	0.0284	0.0326	0.9544	0.5099	0.0416	0.1969	0.9433	0.1774
0.1482	17.2538	0.2960	18.6971	0.0288	0.0317	0.9544	0.5010	0.0401	0.1928	0.9443	0.1705
0.1471	18.1475	0.2936	19.3202	0.0287	0.0304	0.9547	0.4902	0.0385	0.1875	0.9453	0.1632
0.1476	20.2508	0.2946	20.7565	0.0285	0.0284	0.9545	0.4730	0.0358	0.1789	0.9473	0.1505
0.1480	23.1697	0.2955	22.5677	0.0289	0.0262	0.9544	0.4516	0.0326	0.1691	0.9496	0.1357

K-1.5: Liquid Hold-Up Analysis with Proposed Model & several Correlations

	Vsl=0.1851m/s			Experiment,	Proposed Model	& other Models					
Vsl(m/s)	Vsg(m/s)	Qw, L/s	Qg, L/s	HL	HL	Flanigan (1958)	Chen & Spedding (1981)	Beggs & Brill (1973)	Spedding et al (1998)	Minami & Brill (1987)	Abdul-Majeed (1996)
0.1950	8.3042	0.3953	11.2538	0.0408	0.0703	0.9407	0.6944	0.0780	0.3325	0.9289	0.3134
0.1920	9.3747	0.3891	12.4198	0.0393	0.0627	0.9416	0.6729	0.0711	0.3077	0.9319	0.2920
0.1892	10.3928	0.3835	13.4849	0.0383	0.0569	0.9424	0.6536	0.0656	0.2881	0.9343	0.2740
0.1867	11.4133	0.3784	14.5112	0.0365	0.0522	0.9431	0.6357	0.0611	0.2716	0.9364	0.2579
0.1852	12.3305	0.3753	15.4511	0.0355	0.0486	0.9436	0.6213	0.0576	0.2587	0.9381	0.2452
0.1834	13.3075	0.3717	16.3692	0.0348	0.0454	0.9441	0.6065	0.0543	0.2470	0.9398	0.2328
0.1819	14.4407	0.3688	17.3772	0.0342	0.0424	0.9445	0.5912	0.0511	0.2359	0.9414	0.2201
0.1823	15.5866	0.3696	18.2564	0.0342	0.0405	0.9444	0.5794	0.0485	0.2283	0.9429	0.2097
0.1840	16.5037	0.3730	18.8810	0.0346	0.0395	0.9439	0.5728	0.0469	0.2246	0.9440	0.2030
0.1822	17.5280	0.3692	19.6341	0.0344	0.0376	0.9444	0.5599	0.0447	0.2171	0.9451	0.1938
0.1832	18.4493	0.3714	20.2767	0.0347	0.0366	0.9441	0.5532	0.0432	0.2132	0.9461	0.1878
0.1810	20.7125	0.3669	21.8066	0.0349	0.0336	0.9448	0.5304	0.0396	0.2011	0.9481	0.1718
0.1805	23.7260	0.3660	23.7582	0.0345	0.0308	0.9449	0.5071	0.0360	0.1892	0.9504	0.1555

Table L 1: Error & Uncertainty – Water/Air in Annular Flow

Table L-1.1: Differential Pressure Measurement (Water/air flow in annular Flow)

Test Matrix		Vsl~0.05m/s	Results		Test Matrix		Vsl~0.07m/s	Results	
Vsl [m/s]	Vsg [m/s]	DP =P₁ - P₂ [bar]	Error [bar]	Uncertantity [±%]	Vsl [m/s]	Vsg [m/s]	DP =P₁ - P₂ [bar]	Error [bar]	Uncertantity [±%]
0.0511	8.3179	0.0446	0.0043	9.7042	0.0733	8.0774	0.0474	0.0043	9.1288
0.0509	9.4533	0.0458	0.0043	9.4500	0.0730	8.9605	0.0487	0.0043	8.8815
0.0508	10.0773	0.0463	0.0043	9.3428	0.0721	10.1592	0.0506	0.0043	8.5543
0.0509	10.9194	0.0479	0.0043	9.0397	0.0723	11.0207	0.0518	0.0043	8.3596
0.0506	11.9057	0.0487	0.0043	8.8813	0.0704	11.6847	0.0527	0.0043	8.2167
0.0504	12.8888	0.0495	0.0043	8.7432	0.0716	13.1697	0.0543	0.0043	7.9697
0.0502	14.0307	0.0506	0.0043	8.5429	0.0713	14.3350	0.0557	0.0043	7.7745
0.0503	15.0982	0.0520	0.0043	8.3262	0.0712	15.4484	0.0567	0.0043	7.6263
0.0501	15.5284	0.0524	0.0043	8.2514	0.0708	16.3867	0.0575	0.0043	7.5303
0.0504	17.0857	0.0543	0.0043	7.9687	0.0706	17.3721	0.0580	0.0043	7.4641
0.0503	18.0246	0.0550	0.0043	7.8701	0.0707	18.2912	0.0577	0.0043	7.4974
0.0501	20.0773	0.0550	0.0043	7.8627	0.0707	20.2922	0.0579	0.0043	7.4710
0.0501	23.2796	0.0551	0.0043	7.8577	0.0706	23.5416	0.0575	0.0043	7.5230
			Avg	8.6031				Avg	7.9998

Table L-1.2: Differential Pressure Measurement (Water/air flow in annular Flow)

Test Matrix		Vsl~0.09m/s	Results		Test Matrix		Vsl~0.14m/s	Results	
Vsl [m/s]	Vsg [m/s]	DP =P₁ - P₂ [bar]	Error [bar]	Uncertantity [±%]	Vsl [m/s]	Vsg [m/s]	DP =P₁ - P₂ [bar]	Error [bar]	Uncertantity [±%]
0.0923	8.4940	0.0517	0.0043	8.3703	0.1336	8.1564	0.0603	0.0043	7.1748
0.0920	9.1611	0.0529	0.0043	8.1740	0.1275	9.3771	0.0615	0.0043	7.0396
0.0910	10.1754	0.0541	0.0043	8.0042	0.1272	10.2753	0.0622	0.0043	6.9562
0.0902	11.3827	0.0552	0.0043	7.8384	0.1266	11.3896	0.0629	0.0043	6.8834
0.0913	12.3319	0.0562	0.0043	7.6988	0.1275	12.0846	0.0632	0.0043	6.8493
0.0905	13.2463	0.0572	0.0043	7.5670	0.1266	13.2336	0.0642	0.0043	6.7369
0.0900	14.3424	0.0583	0.0043	7.4184	0.1270	14.2926	0.0654	0.0043	6.6160
0.0896	15.3535	0.0594	0.0043	7.2880	0.1264	15.1316	0.0662	0.0043	6.5348
0.0893	16.3559	0.0600	0.0043	7.2132	0.1482	16.3562	0.0706	0.0043	6.1248
0.0893	17.3035	0.0600	0.0043	7.2141	0.1482	17.2538	0.0699	0.0043	6.1913
0.0888	18.3279	0.0598	0.0043	7.2379	0.1471	18.1475	0.0699	0.0043	6.1930
0.0891	20.5905	0.0600	0.0043	7.2156	0.1476	20.2508	0.0701	0.0043	6.1749
0.0901	23.5707	0.0598	0.0043	7.2397	0.1480	23.1697	0.0697	0.0043	6.2051
			Avg	7.5753				Avg	6.5908

Table L-1.3: Differential Pressure Measurement (Water/air flow in annular Flow)

Test Matrix		Vsl~0.20m/s	Results	
Vsl [m/s]	Vsg [m/s]	DP =P_1 - P_2 [bar]	Error [bar]	Uncertantity [±%]
0.1950	8.3042	0.0772	0.0043	5.6036
0.1920	9.3747	0.0791	0.0043	5.4702
0.1892	10.3928	0.0789	0.0043	5.4829
0.1867	11.4133	0.0797	0.0043	5.4279
0.1852	12.3305	0.0803	0.0043	5.3853
0.1834	13.3075	0.0797	0.0043	5.4282
0.1819	14.4407	0.0796	0.0043	5.4372
0.1823	15.5866	0.0791	0.0043	5.4700
0.1840	16.5037	0.0796	0.0043	5.4362
0.1822	17.5280	0.0796	0.0043	5.4325
0.1832	18.4493	0.0798	0.0043	5.4250
0.1810	20.7125	0.0787	0.0043	5.4998
0.1805	23.7260	0.0794	0.0043	5.4459
			Avg	5.4573

Table L-2.1: Liquid (Water) Flow Rate (Flow Meter) for Water/Air in Annular Flow

Test Matrix	Vsl~0.05m/s	FM(Liquid)	Results			Test Matrix	Vsl~0.07m/s	FM(Liquid)	Results	
Vsl [m/s]	Vsg [m/s]	QL[L/s]	Error [L/s]	Uncertantity [±%]		Vsl [m/s]	Vsg [m/s]	QL[L/s]	Error [L/s]	Uncertantity [±%]
0.0511	8.3179	0.1035	0.0444	42.9421		0.0733	8.0774	0.1485	0.0444	29.9228
0.0509	9.4533	0.1032	0.0444	43.0817		0.0730	8.9605	0.1479	0.0444	30.0538
0.0508	10.0773	0.1030	0.0444	43.1494		0.0721	10.1592	0.1461	0.0444	30.4105
0.0509	10.9194	0.1032	0.0444	43.0783		0.0723	11.0207	0.1465	0.0444	30.3322
0.0506	11.9057	0.1025	0.0444	43.3683		0.0704	11.6847	0.1427	0.0444	31.1466
0.0504	12.8888	0.1021	0.0444	43.5159		0.0716	13.1697	0.1450	0.0444	30.6420
0.0502	14.0307	0.1018	0.0444	43.6387		0.0713	14.3350	0.1446	0.0444	30.7429
0.0503	15.0982	0.1020	0.0444	43.5696		0.0712	15.4484	0.1444	0.0444	30.7889
0.0501	15.5284	0.1015	0.0444	43.7778		0.0708	16.3867	0.1435	0.0444	30.9639
0.0504	17.0857	0.1021	0.0444	43.5301		0.0706	17.3721	0.1431	0.0444	31.0557
0.0503	18.0246	0.1019	0.0444	43.6171		0.0707	18.2912	0.1433	0.0444	31.0189
0.0501	20.0773	0.1016	0.0444	43.7433		0.0707	20.2922	0.1434	0.0444	30.9971
0.0501	23.2796	0.1015	0.0444	43.7901		0.0706	23.5416	0.1431	0.0444	31.0561
			Avg	43.4464					Avg	30.7024

Table L-2.2: Liquid (Water) Flow Rate (Flow Meter) for Water/Air in Annular Flow

Test Matrix	Vsl~0.09m/s	FM(Liquid)	Results			Test Matrix	Vsl~0.14m/s	FM(Liquid)	Results	
Vsl [m/s]	Vsg [m/s]	QL[L/s]	Error [L/s]	Uncertantity [±%]		Vsl [m/s]	Vsg [m/s]	QL[L/s]	Error [L/s]	Uncertantity [±%]
0.0923	8.4940	0.1871	0.0444	23.7575		0.1336	8.1564	0.2667	0.0444	16.6669
0.0920	9.1611	0.1865	0.0444	23.8307		0.1275	9.3771	0.2545	0.0444	17.4637
0.0910	10.1754	0.1845	0.0444	24.0909		0.1272	10.2753	0.2539	0.0444	17.5027
0.0902	11.3827	0.1827	0.0444	24.3209		0.1266	11.3896	0.2528	0.0444	17.5809
0.0913	12.3319	0.1852	0.0444	24.0028		0.1275	12.0846	0.2545	0.0444	17.4622
0.0905	13.2463	0.1835	0.0444	24.2232		0.1266	13.2336	0.2528	0.0444	17.5779
0.0900	14.3424	0.1824	0.0444	24.3644		0.1270	14.2926	0.2536	0.0444	17.5281
0.0896	15.3535	0.1817	0.0444	24.4633		0.1264	15.1316	0.2524	0.0444	17.6072
0.0893	16.3559	0.1811	0.0444	24.5471		0.1482	16.3562	0.2959	0.0444	15.0204
0.0893	17.3035	0.1810	0.0444	24.5595		0.1482	17.2538	0.2960	0.0444	15.0170
0.0888	18.3279	0.1800	0.0444	24.6905		0.1471	18.1475	0.2936	0.0444	15.1370
0.0891	20.5905	0.1807	0.0444	24.5993		0.1476	20.2508	0.2946	0.0444	15.0841
0.0901	23.5707	0.1827	0.0444	24.3223		0.1480	23.1697	0.2955	0.0444	15.0406
			Avg	24.2902					Avg	16.5145

Table L-2.3: Liquid (Water) Flow Rate (Flow Meter) for Water/Air in Annular Flow

Test Matrix	Vsl~0.20m/s	FM(Liquid)	Results	
Vsl [m/s]	Vsg [m/s]	QL[L/s]	Error [L/s]	Uncertantity [±%]
0.1950	8.3042	0.3953	0.0444	11.2427
0.1920	9.3747	0.3891	0.0444	11.4215
0.1892	10.3928	0.3835	0.0444	11.5897
0.1867	11.4133	0.3784	0.0444	11.7440
0.1852	12.3305	0.3753	0.0444	11.8425
0.1834	13.3075	0.3717	0.0444	11.9565
0.1819	14.4407	0.3688	0.0444	12.0511
0.1823	15.5866	0.3696	0.0444	12.0260
0.1840	16.5037	0.3730	0.0444	11.9149
0.1822	17.5280	0.3692	0.0444	12.0374
0.1832	18.4493	0.3714	0.0444	11.9682
0.1810	20.7125	0.3669	0.0444	12.1147
0.1805	23.7260	0.3660	0.0444	12.1443
			Avg	11.8503

Table L-3.1: Gas (Air) Flow Rate (Flow Meter) for Water/Air in Annular Flow

Test Matrix	Vsl~0.05m/s	FM(Gas)	Results			Test Matrix	Vsl~0.07m/s	FM(Gas)	Results	
Vsl [m/s]	Vsg [m/s]	Qg[L/s]	Error [L/s]	Uncertantity [±%]		Vsl [m/s]	Vsg [m/s]	Qg[L/s]	Error [L/s]	Uncertantity [±%]
0.0511	8.3179	9.5864	0.1556	1.6227		0.0733	8.0774	9.6567	0.1556	1.6109
0.0509	9.4533	10.5541	0.1556	1.4739		0.0730	8.9605	10.4651	0.1556	1.4864
0.0508	10.0773	11.0649	0.1556	1.4059		0.0721	10.1592	11.5416	0.1556	1.3478
0.0509	10.9194	11.7780	0.1556	1.3207		0.0723	11.0207	12.2924	0.1556	1.2655
0.0506	11.9057	12.5420	0.1556	1.2403		0.0704	11.6847	12.8496	0.1556	1.2106
0.0504	12.8888	13.2823	0.1556	1.1712		0.0716	13.1697	14.0806	0.1556	1.1048
0.0502	14.0307	14.1245	0.1556	1.1013		0.0713	14.3350	15.0136	0.1556	1.0361
0.0503	15.0982	14.9027	0.1556	1.0438		0.0712	15.4484	15.8775	0.1556	0.9797
0.0501	15.5284	15.2028	0.1556	1.0232		0.0708	16.3867	16.5637	0.1556	0.9391
0.0504	17.0857	16.3090	0.1556	0.9538		0.0706	17.3721	17.2608	0.1556	0.9012
0.0503	18.0246	16.9283	0.1556	0.9189		0.0707	18.2912	17.8234	0.1556	0.8728
0.0501	20.0773	18.1877	0.1556	0.8553		0.0707	20.2922	19.0901	0.1556	0.8149
0.0501	23.2796	20.0167	0.1556	0.7771		0.0706	23.5416	20.9560	0.1556	0.7423
			Avg	1.1468					Avg	1.1009

Table L-3.2: Gas (Air) Flow Rate (Flow Meter) for Water/Air in Annular Flow

Test Matrix	Vsl~0.09m/s	FM(Gas)	Results			Test Matrix	Vsl~0.14m/s	FM(Gas)	Results	
Vsl [m/s]	Vsg [m/s]	Qg[L/s]	Error [L/s]	Uncertantity [±%]		Vsl [m/s]	Vsg [m/s]	Qg[L/s]	Error [L/s]	Uncertantity [±%]
0.0923	8.4940	10.2527	0.1556	1.5172		0.1336	8.1564	10.3275	0.1556	1.5062
0.0920	9.1611	10.8829	0.1556	1.4294		0.1275	9.3771	11.5806	0.1556	1.3433
0.0910	10.1754	11.8220	0.1556	1.3158		0.1272	10.2753	12.4129	0.1556	1.2532
0.0902	11.3827	12.8987	0.1556	1.2060		0.1266	11.3896	13.4225	0.1556	1.1589
0.0913	12.3319	13.7453	0.1556	1.1317		0.1275	12.0846	14.0794	0.1556	1.1049
0.0905	13.2463	14.5438	0.1556	1.0696		0.1266	13.2336	15.1442	0.1556	1.0272
0.0900	14.3424	15.4681	0.1556	1.0057		0.1270	14.2926	16.1026	0.1556	0.9660
0.0896	15.3535	16.2801	0.1556	0.9555		0.1264	15.1316	16.8104	0.1556	0.9254
0.0893	16.3559	17.0402	0.1556	0.9129		0.1482	16.3562	18.1278	0.1556	0.8581
0.0893	17.3035	17.6932	0.1556	0.8792		0.1482	17.2538	18.6971	0.1556	0.8320
0.0888	18.3279	18.3331	0.1556	0.8485		0.1471	18.1475	19.3202	0.1556	0.8052
0.0891	20.5905	19.7772	0.1556	0.7865		0.1476	20.2508	20.7565	0.1556	0.7494
0.0901	23.5707	21.5380	0.1556	0.7222		0.1480	23.1697	22.5677	0.1556	0.6893
			Avg	1.0600					Avg	1.0168

Table L-3.3: Gas (Air) Flow Rate (Flow Meter) for Water/Air in Annular Flow

Test Matrix	Vsl~0.20m/s	FM(Gas)	Results	
Vsl [m/s]	Vsg [m/s]	Qg[L/s]	Error [L/s]	Uncertantity [±%]
0.1950	8.3042	11.2538	0.1556	1.3823
0.1920	9.3747	12.4198	0.1556	1.2525
0.1892	10.3928	13.4849	0.1556	1.1536
0.1867	11.4133	14.5112	0.1556	1.0720
0.1852	12.3305	15.4511	0.1556	1.0068
0.1834	13.3075	16.3692	0.1556	0.9503
0.1819	14.4407	17.3772	0.1556	0.8952
0.1823	15.5866	18.2564	0.1556	0.8521
0.1840	16.5037	18.8810	0.1556	0.8239
0.1822	17.5280	19.6341	0.1556	0.7923
0.1832	18.4493	20.2767	0.1556	0.7672
0.1810	20.7125	21.8066	0.1556	0.7133
0.1805	23.7260	23.7582	0.1556	0.6548
			Avg	0.9474

Table L-4.1: Error Propagation on Conductivity Ring Sensors (Water/Air in Annular Flow) - Liquid Hold-Up

Test Matrix		Vsl~0.05m/s		Results		Error Propagation			Test Matrix		Vsl~0.07m/s		Results		Error Propagation	
Vsl [m/s]	Vsg [m/s]	HL	C2-C1	Error [V]	Uncertantity [±%]	[±]	HL		Vsl [m/s]	Vsg [m/s]	HL	C2-C1	Error [V]	Uncertantity [±%]	[±]	HL
0.0511	8.3179	0.0181	0.0579	0.0283	48.8718	0.0088	0.0181 ±0.0088		0.0733	8.0774	0.0225	0.1003	0.0283	28.2072	0.0064	0.0225 ±0.0063
0.0509	9.4533	0.0168	0.0546	0.0283	51.7799	0.0087	0.0168 ±0.0086		0.0730	8.9605	0.0211	0.0953	0.0283	29.6825	0.0063	0.0211 ±0.0062
0.0508	10.0773	0.0161	0.0525	0.0283	53.8505	0.0087	0.0161 ±0.0086		0.0721	10.1592	0.0196	0.0893	0.0283	31.6624	0.0062	0.0196 ±0.0061
0.0509	10.9194	0.0148	0.0490	0.0283	57.7287	0.0086	0.0148 ±0.0085		0.0723	11.0207	0.0189	0.0867	0.0283	32.6217	0.0062	0.0189 ±0.0061
0.0506	11.9057	0.0145	0.0485	0.0283	58.3247	0.0085	0.0145 ±0.0084		0.0704	11.6847	0.0176	0.0816	0.0283	34.6634	0.0061	0.0176 ±0.0060
0.0504	12.8888	0.0142	0.0477	0.0283	59.3567	0.0084	0.0142 ±0.0084		0.0716	13.1697	0.0165	0.0772	0.0283	36.6431	0.0060	0.0165 ±0.0060
0.0502	14.0307	0.0136	0.0462	0.0283	61.2537	0.0083	0.0136 ±0.0083		0.0713	14.3350	0.0154	0.0724	0.0283	39.0402	0.0060	0.0154 ±0.0060
0.0503	15.0982	0.0131	0.0450	0.0283	62.9067	0.0082	0.0131 ±0.0082		0.0712	15.4484	0.0143	0.0681	0.0283	41.5587	0.0059	0.0143 ±0.0059
0.0501	15.5284	0.0128	0.0443	0.0283	63.8453	0.0082	0.0128 ±0.0081		0.0708	16.3867	0.0137	0.0658	0.0283	43.0126	0.0059	0.0137 ±0.0059
0.0504	17.0857	0.0123	0.0430	0.0283	65.8093	0.0081	0.0123 ±0.0080		0.0706	17.3721	0.0133	0.0640	0.0283	44.2008	0.0059	0.0133 ±0.0058
0.0503	18.0246	0.0120	0.0423	0.0283	66.8135	0.0080	0.0120 ±0.0080		0.0707	18.2912	0.0135	0.0648	0.0283	43.6175	0.0059	0.0135 ±0.0059
0.0501	20.0773	0.0120	0.0423	0.0283	66.8166	0.0080	0.0120 ±0.0080		0.0707	20.2922	0.0133	0.0638	0.0283	44.3026	0.0059	0.0133 ±0.0059
0.0501	23.2796	0.0122	0.0427	0.0283	66.1681	0.0081	0.0122 ±0.0081		0.0706	23.5416	0.0137	0.0650	0.0283	43.5106	0.0060	0.0137 ±0.0059
				Avg	60.2712								Avg	37.9018		

Table L-4.2: Error Propagation on Conductivity Ring Sensors (Water/Air in Annular Flow) - Liquid Hold-Up

Test Matrix		Vsl~0.09m/s		Results		Error Propagation			Test Matrix		Vsl~0.14m/s		Results		Error Propagation	
Vsl [m/s]	Vsg [m/s]	HL	C2-C1	Error [V]	Uncertantity [±%]	[±]	HL		Vsl [m/s]	Vsg [m/s]	HL	C2-C1	Error [V]	Uncertantity [±%]	[±]	HL
0.0923	8.4940	0.0276	0.1201	0.0283	23.5495	0.0065	0.0276 ±0.0064		0.1336	8.1564	0.0346	0.1456	0.0283	19.4315	0.0067	0.0346 ±0.0067
0.0920	9.1611	0.0264	0.1159	0.0283	24.4113	0.0064	0.02641 ±0.0064		0.1275	9.3771	0.0312	0.1327	0.0283	21.3106	0.0066	0.0312 ±0.0066
0.0910	10.1754	0.0251	0.1111	0.0283	25.4668	0.0064	0.0251 ±0.0064		0.1272	10.2753	0.0302	0.1287	0.0283	21.9771	0.0066	0.0302 ±0.0066
0.0902	11.3827	0.0236	0.1047	0.0283	27.0268	0.0064	0.0236 ±0.0063		0.1266	11.3896	0.0293	0.1252	0.0283	22.5848	0.0066	0.0293 ±0.0066
0.0913	12.3319	0.0224	0.0996	0.0283	28.4039	0.0064	0.0223 ±0.0063		0.1275	12.0846	0.0287	0.1226	0.0283	23.0706	0.0066	0.0287 ±0.0066
0.0905	13.2463	0.0210	0.0940	0.0283	30.1020	0.0063	0.0210 ±0.0063		0.1266	13.2336	0.0270	0.1155	0.0283	24.4808	0.0066	0.0270 ±0.0066
0.0900	14.3424	0.0194	0.0874	0.0283	32.3635	0.0063	0.0194 ±0.0062		0.1270	14.2926	0.0254	0.1094	0.0283	25.8573	0.0066	0.0254 ±0.0065
0.0896	15.3535	0.0185	0.0835	0.0283	33.8584	0.0063	0.0185 ±0.0062		0.1264	15.1316	0.0247	0.1062	0.0283	26.6416	0.0066	0.0247 ±0.0065
0.0893	16.3559	0.0178	0.0806	0.0283	35.0707	0.0062	0.0178 ±0.0062		0.1482	16.3562	0.0284	0.1212	0.0283	23.3442	0.0066	0.0284 ±0.0066
0.0893	17.3035	0.0176	0.0800	0.0283	35.3700	0.0062	0.0176 ±0.0062		0.1482	17.2538	0.0288	0.1229	0.0283	23.0192	0.0066	0.0288 ±0.0066
0.0888	18.3279	0.0178	0.0809	0.0283	34.9821	0.0062	0.0178 ±0.0062		0.1471	18.1475	0.0287	0.1224	0.0283	23.1100	0.0066	0.0287 ±0.0066
0.0891	20.5905	0.0179	0.0809	0.0283	34.9818	0.0063	0.0179 ±0.0062		0.1476	20.2508	0.0285	0.1212	0.0283	23.3448	0.0066	0.0285 ±0.0066
0.0901	23.5707	0.0182	0.0816	0.0283	34.6754	0.0063	0.0182 ±0.0062		0.1480	23.1697	0.0289	0.1225	0.0283	23.0863	0.0067	0.0289 ±0.0066
				Avg	30.7894								Avg	23.1738		

Table L-4.3: Error Propagation on Conductivity Ring Sensors (Water/Air in Annular Flow) - Liquid Hold-Up

Test Matrix		Vsl~0.20m/s		Results		Error Propagation	
Vsl [m/s]	Vsg [m/s]	HL	C2-C1	Error [V]	Uncertantity [±%]	[±]	HL
0.1950	8.3042	0.0408	0.1717	0.0283	16.4761	0.0067	0.0408±0.0067
0.1920	9.3747	0.0393	0.1654	0.0283	17.1010	0.0067	0.0393±0.0067
0.1892	10.3928	0.0383	0.1616	0.0283	17.5018	0.0067	0.0383±0.0067
0.1867	11.4133	0.0365	0.1551	0.0283	18.2376	0.0067	0.0365±0.0066
0.1852	12.3305	0.0355	0.1511	0.0283	18.7237	0.0066	0.0355±0.0066
0.1834	13.3075	0.0348	0.1484	0.0283	19.0643	0.0066	0.0348±0.0066
0.1819	14.4407	0.0342	0.1459	0.0283	19.3863	0.0066	0.0342±0.0066
0.1823	15.5866	0.0342	0.1458	0.0283	19.3945	0.0066	0.0342±0.0066
0.1840	16.5037	0.0346	0.1474	0.0283	19.1831	0.0066	0.0346±0.0066
0.1822	17.5280	0.0344	0.1466	0.0283	19.2870	0.0066	0.0344±0.0066
0.1832	18.4493	0.0347	0.1478	0.0283	19.1340	0.0066	0.0347±0.0066
0.1810	20.7125	0.0349	0.1480	0.0283	19.1081	0.0067	0.0347±0.0066
0.1805	23.7260	0.0345	0.1466	0.0283	19.2895	0.0067	0.0345±0.0066
				Avg	18.6067		

Table L-5.1: Superficial Liquid Velocity Error Propagation

Test Matrix	Vsl~0.05m/s	FM(Liquid)	Results		Error Propagation			Test Matrix	Vsl~0.07m/s	FM(Liquid)	Results		Error Propagation	
Vsl [m/s]	Vsg [m/s]	QL[L/s]	Error [L/s]	Uncertantity [±%]		[± m/s]		Vsl [m/s]	Vsg [m/s]	QL[L/s]	Error [L/s]	Uncertantity [±%]		[± m/s]
0.0511	8.3179	0.1035	0.0444	42.9421	0.4294	0.0219		0.0733	8.0774	0.1485	0.0444	29.9228	0.2992	0.0219
0.0509	9.4533	0.1032	0.0444	43.0817	0.4308	0.0219		0.0730	8.9605	0.1479	0.0444	30.0538	0.3005	0.0219
0.0508	10.0773	0.1030	0.0444	43.1494	0.4315	0.0219		0.0721	10.1592	0.1461	0.0444	30.4105	0.3041	0.0219
0.0509	10.9194	0.1032	0.0444	43.0783	0.4308	0.0219		0.0723	11.0207	0.1465	0.0444	30.3322	0.3033	0.0219
0.0506	11.9057	0.1025	0.0444	43.3683	0.4337	0.0219		0.0704	11.6847	0.1427	0.0444	31.1466	0.3115	0.0219
0.0504	12.8888	0.1021	0.0444	43.5159	0.4352	0.0219		0.0716	13.1697	0.1450	0.0444	30.6420	0.3064	0.0219
0.0502	14.0307	0.1018	0.0444	43.6387	0.4364	0.0219		0.0713	14.3350	0.1446	0.0444	30.7429	0.3074	0.0219
0.0503	15.0982	0.1020	0.0444	43.5696	0.4357	0.0219		0.0712	15.4484	0.1444	0.0444	30.7889	0.3079	0.0219
0.0501	15.5284	0.1015	0.0444	43.7778	0.4378	0.0219		0.0708	16.3867	0.1435	0.0444	30.9639	0.3096	0.0219
0.0504	17.0857	0.1021	0.0444	43.5301	0.4353	0.0219		0.0706	17.3721	0.1431	0.0444	31.0557	0.3106	0.0219
0.0503	18.0246	0.1019	0.0444	43.6171	0.4362	0.0219		0.0707	18.2912	0.1433	0.0444	31.0189	0.3102	0.0219
0.0501	20.0773	0.1016	0.0444	43.7433	0.4374	0.0219		0.0707	20.2922	0.1434	0.0444	30.9971	0.3100	0.0219
0.0501	23.2796	0.1015	0.0444	43.7901	0.4379	0.0219		0.0706	23.5416	0.1431	0.0444	31.0561	0.3106	0.0219
			Avg	43.4464							Avg	30.7024		

Table L-5.2: Superficial Liquid Velocity Error Propagation

Test Matrix	Vsl~0.09m/s	FM(Liquid)	Results		Error Propagation			Test Matrix	Vsl~0.14m/s	FM(Liquid)	Results		Error Propagation	
Vsl [m/s]	Vsg [m/s]	QL[L/s]	Error [L/s]	Uncertantity [±%]		[± m/s]		Vsl [m/s]	Vsg [m/s]	QL[L/s]	Error [L/s]	Uncertantity [±%]		[± m/s]
0.0923	8.4940	0.1871	0.0444	23.7575	0.2376	0.0219		0.1336	8.1564	0.2667	0.0444	16.6669	0.1667	0.0223
0.0920	9.1611	0.1865	0.0444	23.8307	0.2383	0.0219		0.1275	9.3771	0.2545	0.0444	17.4637	0.1746	0.0223
0.0910	10.1754	0.1845	0.0444	24.0909	0.2409	0.0219		0.1272	10.2753	0.2539	0.0444	17.5027	0.1750	0.0223
0.0902	11.3827	0.1827	0.0444	24.3209	0.2432	0.0219		0.1266	11.3896	0.2528	0.0444	17.5809	0.1758	0.0223
0.0913	12.3319	0.1852	0.0444	24.0028	0.2400	0.0219		0.1275	12.0846	0.2545	0.0444	17.4622	0.1746	0.0223
0.0905	13.2463	0.1835	0.0444	24.2232	0.2422	0.0219		0.1266	13.2336	0.2528	0.0444	17.5779	0.1758	0.0223
0.0900	14.3424	0.1824	0.0444	24.3644	0.2436	0.0219		0.1270	14.2926	0.2536	0.0444	17.5281	0.1753	0.0223
0.0896	15.3535	0.1817	0.0444	24.4633	0.2446	0.0219		0.1264	15.1316	0.2524	0.0444	17.6072	0.1761	0.0223
0.0893	16.3559	0.1811	0.0444	24.5471	0.2455	0.0219		0.1482	16.3562	0.2959	0.0444	15.0204	0.1502	0.0223
0.0893	17.3035	0.1810	0.0444	24.5595	0.2456	0.0219		0.1482	17.2538	0.2960	0.0444	15.0170	0.1502	0.0223
0.0888	18.3279	0.1800	0.0444	24.6905	0.2469	0.0219		0.1471	18.1475	0.2936	0.0444	15.1370	0.1514	0.0223
0.0891	20.5905	0.1807	0.0444	24.5993	0.2460	0.0219		0.1476	20.2508	0.2946	0.0444	15.0841	0.1508	0.0223
0.0901	23.5707	0.1827	0.0444	24.3223	0.2432	0.0219		0.1480	23.1697	0.2955	0.0444	15.0406	0.1504	0.0223
			Avg	24.2902							Avg	16.5145		

Table L-5.3: Superficial Liquid Velocity Error Propagation

Test Matrix	Vsl~0.20m/s	FM(Liquid)	Results		Error Propagation	
Vsl [m/s]	Vsg [m/s]	QL[L/s]	Error [L/s]	Uncertantity [±%]		[± m/s]
0.1950	8.3042	0.3953	0.0444	11.2427	0.1124	0.0219
0.1920	9.3747	0.3891	0.0444	11.4215	0.1142	0.0219
0.1892	10.3928	0.3835	0.0444	11.5897	0.1159	0.0219
0.1867	11.4133	0.3784	0.0444	11.7440	0.1174	0.0219
0.1852	12.3305	0.3753	0.0444	11.8425	0.1184	0.0219
0.1834	13.3075	0.3717	0.0444	11.9565	0.1196	0.0219
0.1819	14.4407	0.3688	0.0444	12.0511	0.1205	0.0219
0.1823	15.5866	0.3696	0.0444	12.0260	0.1203	0.0219
0.1840	16.5037	0.3730	0.0444	11.9149	0.1191	0.0219
0.1822	17.5280	0.3692	0.0444	12.0374	0.1204	0.0219
0.1832	18.4493	0.3714	0.0444	11.9682	0.1197	0.0219
0.1810	20.7125	0.3669	0.0444	12.1147	0.1211	0.0219
0.1805	23.7260	0.3660	0.0444	12.1443	0.1214	0.0219
			Avg	11.8503		

Table L-6.1: Superficial Gas Velocity Error Propagation

Test Matrix	*Error Propagation for Vsg*	
Vsg [m/s]	[± m/s]	*Vsg [* ± m/s]
8.3179	*0.0008*	*8.318 ±0.0008*
9.4533	*0.0007*	*9.4534 ±0.0007*
10.0773	*0.0006*	*10.0773 ±0.0006*
10.9194	*0.0005*	*10.9195 ±0.0005*
11.9057	*0.0005*	*11.9057 ±0.0005*
12.8888	*0.0004*	*12.8889 ±0.0004*
14.0307	*0.0003*	*14.0308 ±0.0003*
15.0982	*0.0003*	*15.0982 ±0.0003*
15.5284	*0.0003*	*15.5285 ±0.0003*
17.0857	*0.0002*	*17.0858 ±0.0002*
18.0246	*0.0002*	*18.0246 ±0.0002*
20.0773	*0.0002*	*20.0773 ±0.0002*
23.2796	*0.0002*	*23.2796 ±0.0002*
	0.0004	

Table M-4.1: Error & Uncertainty – Water/Air/Sand in Annular Flow - Differential Pressure Measurement.

	200lb/1000bbl of 212microns							200lb/1000bbl of 500microns						
Test Matrix			Results		Error Propagation			Test Matrix			Results		Error Propagation	
Vsl [m/s]	Vsg [m/s]	Qw[L/s]	Error [L/s]	Uncertantity [±%]		[± m/s]		Vsl [m/s]	Vsg [m/s]	Qw[L/s]	Error [L/s]	Uncertantity [±%]		[± m/s]
0.0372	10.4769	0.0742	0.0444	59.9051	0.5991	0.0223		0.0349	9.0558	0.0697	0.0444	63.7632	0.6376	0.0223
0.0371	14.9132	0.0741	0.0444	59.9677	0.5997	0.0223		0.0345	15.2251	0.0690	0.0444	64.4491	0.6445	0.0223
0.0499	9.3775	0.1002	0.0444	44.3603	0.4436	0.0221		0.0470	9.0497	0.0939	0.0444	47.3437	0.4734	0.0223
0.0497	14.9179	0.0993	0.0444	44.7618	0.4476	0.0223		0.0469	14.8023	0.0936	0.0444	47.4946	0.4749	0.0223
0.0502	9.3775	0.1002	0.0444	44.3603	0.4436	0.0223		0.0494	9.1572	0.0987	0.0444	45.0501	0.4505	0.0223
0.0500	14.9179	0.0993	0.0444	44.7618	0.4476	0.0224		0.0487	14.5038	0.0972	0.0444	45.7222	0.4572	0.0223
0.0580	8.9792	0.1158	0.0444	38.3967	0.3840	0.0223		0.0601	14.4386	0.1201	0.0444	37.0212	0.3702	0.0223
0.0568	14.9517	0.1135	0.0444	39.1633	0.3916	0.0223					Avg	50.1206		

Table M-4.2: Error & Uncertainty – Water/Air/Sand in Annular Flow - Differential Pressure Measurement.

	500lb/1000bbl of 212microns							500lb/1000bbl of 500microns						
Test Matrix			Results		Error Propagation			Test Matrix			Results		Error Propagation	
Vsl [m/s]	Vsg [m/s]	Qw[L/s]	Error [L/s]	Uncertantity [±%]		[± m/s]		Vsl [m/s]	Vsg [m/s]	Qw[L/s]	Error [L/s]	Uncertantity [±%]		[± m/s]
0.0372	8.9650	0.0742	0.0444	59.9035	0.5990	0.0223		0.0350	8.4750	0.0700	0.0444	63.5256	0.6353	0.0223
0.0374	14.4564	0.0747	0.0444	59.5253	0.5953	0.0223		0.0321	15.2296	0.0641	0.0444	69.3055	0.6931	0.0223
0.0484	8.8011	0.0967	0.0444	45.9736	0.4597	0.0223		0.0488	8.7086	0.0974	0.0444	45.6255	0.4563	0.0223
0.0480	14.9606	0.0958	0.0444	46.3747	0.4637	0.0223		0.0481	15.3296	0.0961	0.0444	46.2417	0.4624	0.0223
0.0539	8.9535	0.1075	0.0444	41.3369	0.4134	0.0223		0.0518	8.7601	0.1034	0.0444	42.9634	0.4296	0.0223
0.0535	14.5936	0.1069	0.0444	41.5778	0.4158	0.0223		0.0514	14.4325	0.1026	0.0444	43.3246	0.4332	0.0223
0.0623	8.9811	0.1243	0.0444	35.7533	0.3575	0.0223		0.0567	9.2246	0.1131	0.0444	39.2861	0.3929	0.0223
0.0613	14.8428	0.1225	0.0444	36.2844	0.3628	0.0223		0.0563	14.6875	0.1124	0.0444	39.5582	0.3956	0.0223
			Avg	45.8412							Avg	48.7288		

Table M-4.3: Error & Uncertainty – Water/Air/Sand in Annular Flow - Differential Pressure Measurement.

	200lb/1000bbl of 800microns							500lb/1000bbl of 800microns						
Test Matrix			Results		Error Propagation			Test Matrix			Results		Error Propagation	
Vsl [m/s]	Vsg [m/s]	Qw[L/s]	Error [L/s]	Uncertantity [±%]		[± m/s]		Vsl [m/s]	Vsg [m/s]	Qw[L/s]	Error [L/s]	Uncertantity [±%]		[± m/s]
0.0345	8.8898	0.0689	0.0444	64.4710	0.6447	0.0223		0.0374	9.2332	0.0748	0.0444	59.4483	0.5945	0.0223
0.0354	14.9812	0.0706	0.0444	62.9460	0.6295	0.0223		0.0373	14.5006	0.0745	0.0444	59.6964	0.5970	0.0223
0.0490	8.0960	0.0979	0.0444	45.3967	0.4540	0.0223		0.0480	8.7924	0.0958	0.0444	46.4156	0.4642	0.0223
0.0354	14.9812	0.0706	0.0444	62.9460	0.6295	0.0223		0.0474	14.8215	0.0946	0.0444	46.9570	0.4696	0.0223
0.0496	9.0353	0.0990	0.0444	44.8806	0.4488	0.0223		0.0480	9.0533	0.0958	0.0444	46.3986	0.4640	0.0223
0.0493	15.1954	0.0984	0.0444	45.1884	0.4519	0.0223		0.0475	15.1651	0.0949	0.0444	46.8467	0.4685	0.0223
0.0618	8.7283	0.1234	0.0444	36.0293	0.3603	0.0223		0.0561	8.9115	0.1121	0.0444	39.6620	0.3966	0.0223
0.0605	15.1237	0.1209	0.0444	36.7751	0.3678	0.0223		0.0563	15.0489	0.1125	0.0444	39.5239	0.3952	0.0223
			Avg	49.8291							Avg	48.1186		

Table M-5.1: Liquid Flow Rate (Water) from Flow Meter

200lb/1000bbl of 212microns					200lb/1000bbl of 500microns					500lb/1000bbl of 212microns				
Test Matrix			Results		Test Matrix			Results		Test Matrix			Results	
Vsl [m/s]	Vsg [m/s]	Qw[L/s]	Error [L/s]	Uncertantity [±%]	Vsl [m/s]	Vsg [m/s]	Qw[L/s]	Error [L/s]	Uncertantity [±%]	Vsl [m/s]	Vsg [m/s]	Qw[L/s]	Error [L/s]	Uncertantity [±%]
0.0372	10.4769	0.0742	0.0444	59.9051	0.0349	9.0558	0.0697	0.0444	63.7632	0.0372	8.9650	0.0742	0.0444	59.9035
0.0371	14.9132	0.0741	0.0444	59.9677	0.0345	15.2251	0.0690	0.0444	64.4491	0.0374	14.4564	0.0747	0.0444	59.5253
0.0499	9.3775	0.1002	0.0444	44.3603	0.0470	9.0497	0.0939	0.0444	47.3437	0.0484	8.8011	0.0967	0.0444	45.9736
0.0497	14.9179	0.0993	0.0444	44.7618	0.0469	14.8023	0.0936	0.0444	47.4946	0.0480	14.9606	0.0958	0.0444	46.3747
0.0502	9.3775	0.1002	0.0444	44.3603	0.0494	9.1572	0.0987	0.0444	45.0501	0.0539	8.9535	0.1075	0.0444	41.3369
0.0500	14.9179	0.0993	0.0444	44.7618	0.0487	14.5038	0.0972	0.0444	45.7222	0.0535	14.5936	0.1069	0.0444	41.5778
0.0580	8.9792	0.1158	0.0444	38.3967	0.0601	14.4386	0.1201	0.0444	37.0212	0.0623	8.9811	0.1243	0.0444	35.7533
0.0568	14.9517	0.1135	0.0444	39.1633				Avg	50.1206	0.0613	14.8428	0.1225	0.0444	36.2844
			Avg	46.9596									Avg	45.8412

Table M-5.2: Liquid Flow Rate (Water) from Flow Meter

500lb/1000bbl of 500microns					200lb/1000bbl of 800microns					500lb/1000bbl of 800microns				
Test Matrix			Results		Test Matrix			Results		Test Matrix			Results	
Vsl [m/s]	Vsg [m/s]	Qw[L/s]	Error [L/s]	Uncertantity [±%]	Vsl [m/s]	Vsg [m/s]	Qw[L/s]	Error [L/s]	Uncertantity [±%]	Vsl [m/s]	Vsg [m/s]	Qw[L/s]	Error [L/s]	Uncertantity [±%]
0.0350	8.4750	0.0700	0.0444	63.5256	0.0345	8.8898	0.0689	0.0444	64.4710	0.0374	9.2332	0.0748	0.0444	59.4483
0.0321	15.2296	0.0641	0.0444	69.3055	0.0354	14.9812	0.0706	0.0444	62.9460	0.0373	14.5006	0.0745	0.0444	59.6964
0.0488	8.7086	0.0974	0.0444	45.6255	0.0490	8.0960	0.0979	0.0444	45.3967	0.0480	8.7924	0.0958	0.0444	46.4156
0.0481	15.3296	0.0961	0.0444	46.2417	0.0354	14.9812	0.0706	0.0444	62.9460	0.0474	14.8215	0.0946	0.0444	46.9570
0.0518	8.7601	0.1034	0.0444	42.9634	0.0496	9.0353	0.0990	0.0444	44.8806	0.0480	9.0533	0.0958	0.0444	46.3986
0.0514	14.4325	0.1026	0.0444	43.3246	0.0493	15.1954	0.0984	0.0444	45.1884	0.0475	15.1651	0.0949	0.0444	46.8467
0.0567	9.2246	0.1131	0.0444	39.2861	0.0618	8.7283	0.1234	0.0444	36.0293	0.0561	8.9115	0.1121	0.0444	39.6620
0.0563	14.6875	0.1124	0.0444	39.5582	0.0605	15.1237	0.1209	0.0444	36.7751	0.0563	15.0489	0.1125	0.0444	39.5239
			Avg	48.7288				Avg	49.8291				Avg	48.1186

Table M-6.1: Gas Flow Rate (Air) from Flow Meter

200lb/1000bbl of 212microns					200lb/1000bbl of 500microns					500lb/1000bbl of 212microns				
Test Matrix			Results		Test Matrix			Results		Test Matrix			Results	
Vsl [m/s]	Vsg [m/s]	Qg[L/s]	Error [L/s]	Uncertantity [±%]	Vsl [m/s]	Vsg [m/s]	Qg[L/s]	Error [L/s]	Uncertantity [±%]	Vsl [m/s]	Vsg [m/s]	Qg[L/s]	Error [L/s]	Uncertantity [±%]
0.0372	10.4769	11.4698	0.1556	1.3562	0.0349	9.0558	10.3105	0.1556	1.5087	0.0372	8.9650	10.2489	0.1556	1.5178
0.0371	14.9132	14.9398	0.1556	1.0412	0.0345	15.2251	15.2026	0.1556	1.0232	0.0374	14.4564	14.6741	0.1556	1.0601
0.0499	9.3775	10.7077	0.1556	1.4528	0.0470	9.0497	10.4383	0.1556	1.4902	0.0484	8.8011	10.2724	0.1556	1.5143
0.0497	14.9179	15.2676	0.1556	1.0189	0.0469	14.8023	15.1214	0.1556	1.0287	0.0480	14.9606	15.4202	0.1556	1.0088
0.0502	9.3775	10.7077	0.1556	1.4528	0.0494	9.1572	10.5363	0.1556	1.4764	0.0539	8.9535	10.4868	0.1556	1.4834
0.0500	14.9179	15.2676	0.1556	1.0189	0.0487	14.5038	14.9565	0.1556	1.0401	0.0535	14.5936	15.2839	0.1556	1.0178
0.0580	8.9792	10.5085	0.1556	1.4803	0.0601	14.4386	15.2978	0.1556	1.0169	0.0623	8.9811	10.6415	0.1556	1.4618
0.0568	14.9517	15.5961	0.1556	0.9974				Avg	1.2263	0.0613	14.8428	15.7403	0.1556	0.9883
			Avg	1.2273									Avg	1.2565

Table M-6.2: Gas Flow Rate (Air) from Flow Meter

500lb/1000bbl of 500microns					200lb/1000bbl of 800microns					500lb/1000bbl of 800microns				
Test Matrix			Results		Test Matrix			Results		Test Matrix			Results	
Vsl [m/s]	Vsg [m/s]	Qg[L/s]	Error [L/s]	Uncertantity [±%]	Vsl [m/s]	Vsg [m/s]	Qg[L/s]	Error [L/s]	Uncertantity [±%]	Vsl [m/s]	Vsg [m/s]	Qg[L/s]	Error [L/s]	Uncertantity [±%]
0.0350	8.4750	9.8283	0.1556	1.5827	0.0345	8.8898	10.1437	0.1556	1.5335	0.0374	9.2332	10.4341	0.1556	1.4908
0.0321	15.2296	15.2445	0.1556	1.0204	0.0354	14.9812	15.0107	0.1556	1.0363	0.0373	14.5006	14.6397	0.1556	1.0626
0.0488	8.7086	10.1836	0.1556	1.5275	0.0490	8.0960	9.5876	0.1556	1.6225	0.0480	8.7924	10.1919	0.1556	1.5263
0.0481	15.3296	15.5898	0.1556	0.9978	0.0354	14.9812	15.0107	0.1556	1.0363	0.0474	14.8215	15.1955	0.1556	1.0237
0.0518	8.7601	10.2462	0.1556	1.5182	0.0496	9.0353	10.4388	0.1556	1.4902	0.0480	9.0533	10.4226	0.1556	1.4925
0.0514	14.4325	15.0254	0.1556	1.0353	0.0493	15.1954	15.5565	0.1556	0.9999	0.0475	15.1651	15.4425	0.1556	1.0073
0.0567	9.2246	10.7128	0.1556	1.4521	0.0618	8.7283	10.4005	0.1556	1.4957	0.0561	8.9115	10.4426	0.1556	1.4896
0.0563	14.6875	15.3699	0.1556	1.0121	0.0605	15.1237	15.9312	0.1556	0.9764	0.0563	15.0489	15.6679	0.1556	0.9928
			Avg	1.2683				Avg	1.2739				Avg	1.2607

Table M-7.1: Mixture of Sand & Water Flow Rate (from Hopper) on Flow Meter

200lb/1000bbl of 212microns					200lb/1000bbl of 500microns					500lb/1000bbl of 212microns				
Test Matrix			Results		Test Matrix			Results		Test Matrix			Results	
Vsl [m/s]	Vsg [m/s]	Qs[L/s]	Error [L/s]	Uncertantity [±%]	Vsl [m/s]	Vsg [m/s]	Qs[L/s]	Error [L/s]	Uncertantity [±%]	Vsl [m/s]	Vsg [m/s]	Qs[L/s]	Error [L/s]	Uncertantity [±%]
0.0372	10.4769	0.1174	0.0117	9.9345	0.0349	9.0558	0.1331	0.0117	8.7621	0.0372	8.9650	0.1219	0.0117	9.5739
0.0371	14.9132	0.1157	0.0117	10.0859	0.0345	15.2251	0.1311	0.0117	8.8984	0.0374	14.4564	0.1297	0.0117	8.9969
0.0499	9.3775	0.1245	0.0117	9.3688	0.0470	9.0497	0.1461	0.0117	7.9876	0.0484	8.8011	0.1446	0.0117	8.0706
0.0497	14.9179	0.1291	0.0117	9.0403	0.0469	14.8023	0.1418	0.0117	8.2295	0.0480	14.9606	0.1404	0.0117	8.3124
0.0502	9.3775	0.1245	0.0117	9.3688	0.0494	9.1572	0.1312	0.0117	8.8927	0.0539	8.9535	0.1423	0.0117	8.1975
0.0500	14.9179	0.1291	0.0117	9.0403	0.0487	14.5038	0.1389	0.0117	8.3977	0.0535	14.5936	0.1421	0.0117	8.2129
0.0580	8.9792	0.1365	0.0117	8.5501	0.0601	14.4386	0.1370	0.0117	8.5146	0.0623	8.9811	0.1436	0.0117	8.1257
0.0568	14.9517	0.1277	0.0117	9.1387				Avg	8.5261	0.0613	14.8428	0.1377	0.0117	8.4723
			Avg	9.3159									Avg	8.4953

Table M-7.2: Mixture of Sand & Water Flow Rate (from Hopper) on Flow Meter

500lb/1000bbl of 500microns					200lb/1000bbl of 800microns					500lb/1000bbl of 800microns				
Test Matrix			Results		Test Matrix			Results		Test Matrix			Results	
Vsl [m/s]	Vsg [m/s]	Qs[L/s]	Error [L/s]	Uncertantity [±%]	Vsl [m/s]	Vsg [m/s]	Qs[L/s]	Error [L/s]	Uncertantity [±%]	Vsl [m/s]	Vsg [m/s]	Qs[L/s]	Error [L/s]	Uncertantity [±%]
0.0350	8.4750	0.1470	0.0117	7.9385	0.0345	8.8898	0.1350	0.0117	8.6447	0.0374	9.2332	0.1276	0.0117	9.1459
0.0321	15.2296	0.1441	0.0117	8.0964	0.0354	14.9812	0.1309	0.0117	8.9104	0.0373	14.5006	0.1329	0.0117	8.7753
0.0488	8.7086	0.1465	0.0117	7.9641	0.0490	8.0960	0.1346	0.0117	8.6670	0.0480	8.7924	0.1461	0.0117	7.9863
0.0481	15.3296	0.1433	0.0117	8.1413	0.0354	14.9812	0.1309	0.0117	8.9104	0.0474	14.8215	0.1408	0.0117	8.2887
0.0518	8.7601	0.1472	0.0117	7.9278	0.0496	9.0353	0.1361	0.0117	8.5747	0.0480	9.0533	0.1455	0.0117	8.0180
0.0514	14.4325	0.1439	0.0117	8.1051	0.0493	15.1954	0.1321	0.0117	8.8287	0.0475	15.1651	0.1403	0.0117	8.3157
0.0567	9.2246	0.1438	0.0117	8.1124	0.0618	8.7283	0.1285	0.0117	9.0763	0.0561	8.9115	0.1452	0.0117	8.0340
0.0563	14.6875	0.1401	0.0117	8.3269	0.0605	15.1237	0.1263	0.0117	9.2399	0.0563	15.0489	0.1384	0.0117	8.4300
			Avg	8.0766				Avg	8.8565				Avg	8.3742

Table N-1.1 Error Propagation on Conductivity Ring Sensors (Water/Air/Sand in Annular Flow) - Superficial Liquid Velocity

	200lb/1000bbl of 212microns							200lb/1000bbl of 500microns							500lb/1000bbl of 212microns						
Test Matrix			Results		Error Propagation			Test Matrix			Results		Error Propagation			Test Matrix			Results		Error Propagation	
Vsl [m/s]	Vsg [m/s]	Qw[L/s]	Error [L/s]	Uncertantity [±%]		[± m/s]		Vsl [m/s]	Vsg [m/s]	Qw[L/s]	Error [L/s]	Uncertantity [±%]		[± m/s]		Vsl [m/s]	Vsg [m/s]	Qw[L/s]	Error [L/s]	Uncertantity [±%]		[± m/s]
0.0372	10.4769	0.0742	0.0444	59.9051	0.5991	0.0223		0.0349	9.0558	0.0697	0.0444	63.7632	0.6376	0.0223		0.0372	8.9650	0.0742	0.0444	59.9035	0.5990	0.0223
0.0371	14.9132	0.0741	0.0444	59.9677	0.5997	0.0223		0.0345	15.2251	0.0690	0.0444	64.4491	0.6445	0.0223		0.0374	14.4564	0.0747	0.0444	59.5253	0.5953	0.0223
0.0499	9.3775	0.1002	0.0444	44.3603	0.4436	0.0221		0.0470	9.0497	0.0939	0.0444	47.3437	0.4734	0.0223		0.0484	8.8011	0.0967	0.0444	45.9736	0.4597	0.0223
0.0497	14.9179	0.0993	0.0444	44.7618	0.4476	0.0223		0.0469	14.8023	0.0936	0.0444	47.4946	0.4749	0.0223		0.0480	14.9606	0.0958	0.0444	46.3747	0.4637	0.0223
0.0502	9.3775	0.1002	0.0444	44.3603	0.4436	0.0223		0.0494	9.1572	0.0987	0.0444	45.0501	0.4505	0.0223		0.0539	8.9535	0.1075	0.0444	41.3369	0.4134	0.0223
0.0500	14.9179	0.0993	0.0444	44.7618	0.4476	0.0224		0.0487	14.5038	0.0972	0.0444	45.7222	0.4572	0.0223		0.0535	14.5936	0.1069	0.0444	41.5778	0.4158	0.0223
0.0580	8.9792	0.1158	0.0444	38.3967	0.3840	0.0223		0.0601	14.4386	0.1201	0.0444	37.0212	0.3702	0.0223		0.0623	8.9811	0.1243	0.0444	35.7533	0.3575	0.0223
0.0568	14.9517	0.1135	0.0444	39.1633	0.3916	0.0223					Avg	50.1206				0.0613	14.8428	0.1225	0.0444	36.2844	0.3628	0.0223
			Avg	46.9596															Avg	45.8412		

Table N-1.2: Error Propagation on Conductivity Ring Sensors (Water/Air/Sand in Annular Flow) - Superficial Liquid Velocity

0	500lb/1000bbl of 500microns							200lb/1000bbl of 800microns							500lb/1000bbl of 800microns						
Test Matrix			Results		Error Propagation			Test Matrix			Results		Error Propagation			Test Matrix			Results		Error Propagation	
Vsl [m/s]	Vsg [m/s]	Qw[L/s]	Error [L/s]	Uncertantity [±%]		[± m/s]		Vsl [m/s]	Vsg [m/s]	Qw[L/s]	Error [L/s]	Uncertantity [±%]		[± m/s]		Vsl [m/s]	Vsg [m/s]	Qw[L/s]	Error [L/s]	Uncertantity [±%]		[± m/s]
0.0350	8.4750	0.0700	0.0444	63.5256	0.6353	0.0223		0.0345	8.8898	0.0689	0.0444	64.4710	0.6447	0.0223		0.0374	9.2332	0.0748	0.0444	59.4483	0.5945	0.0223
0.0321	15.2296	0.0641	0.0444	69.3055	0.6931	0.0223		0.0354	14.9812	0.0706	0.0444	62.9460	0.6295	0.0223		0.0373	14.5006	0.0745	0.0444	59.6964	0.5970	0.0223
0.0488	8.7086	0.0974	0.0444	45.6255	0.4563	0.0223		0.0490	8.0960	0.0979	0.0444	45.3967	0.4540	0.0223		0.0480	8.7924	0.0958	0.0444	46.4156	0.4642	0.0223
0.0481	15.3296	0.0961	0.0444	46.2417	0.4624	0.0223		0.0354	14.9812	0.0706	0.0444	62.9460	0.6295	0.0223		0.0474	14.8215	0.0946	0.0444	46.9570	0.4696	0.0223
0.0518	8.7601	0.1034	0.0444	42.9634	0.4296	0.0223		0.0496	9.0353	0.0990	0.0444	44.8806	0.4488	0.0223		0.0480	9.0533	0.0958	0.0444	46.3986	0.4640	0.0223
0.0514	14.4325	0.1026	0.0444	43.3246	0.4332	0.0223		0.0493	15.1954	0.0984	0.0444	45.1884	0.4519	0.0223		0.0475	15.1651	0.0949	0.0444	46.8467	0.4685	0.0223
0.0567	9.2246	0.1131	0.0444	39.2861	0.3929	0.0223		0.0618	8.7283	0.1234	0.0444	36.0293	0.3603	0.0223		0.0561	8.9115	0.1121	0.0444	39.6620	0.3966	0.0223
0.0563	14.6875	0.1124	0.0444	39.5582	0.3956	0.0223		0.0605	15.1237	0.1209	0.0444	36.7751	0.3678	0.0223		0.0563	15.0489	0.1125	0.0444	39.5239	0.3952	0.0223
			Avg	48.7288							Avg	49.8291							Avg	48.1186		

E. Table O-1.1: Water/Sand Flow - Differential-Pressure Measurement (Water/Sand Flow)

200lb/1000bbl of 212microns						200lb/1000bbl of 500microns						500lb/1000bbl of 500microns					
Test Matrix				Results		Test Matrix				Results		Test Matrix				Results	
Vsl [m/s]	Sand Flow [L/s]	Qw [L/s]	DP =P_1 - P_2 [bar]	Error [bar]	Uncertantity [±%]	Vsl [m/s]	Sand Flow [L/s]	Qw [L/s]	DP =P_1 - P_2 [bar]	Error [bar]	Uncertantity [±%]	Vsl [m/s]	Sand Flow [L/s]	Qw [L/s]	DP =P_1 - P_2 [bar]	Error [bar]	Uncertantity [±%]
0.1504	0.1403	0.3004	0.0398	0.0043	10.8682	0.1526	0.1152	0.3048	0.0378	0.0043	11.4504	0.1481	0.1431	0.2957	0.0380	0.0043	11.3803
0.1775	0.1292	0.3544	0.0400	0.0043	10.8079	0.1783	0.1167	0.3561	0.0382	0.0043	11.3340	0.1772	0.1482	0.3538	0.0384	0.0043	11.2565
0.1968	0.1226	0.3929	0.0403	0.0043	10.7273	0.1950	0.1238	0.3893	0.0385	0.0043	11.2430	0.1931	0.1374	0.3856	0.0376	0.0043	11.4970
0.2426	0.1234	0.4845	0.0404	0.0043	10.6975	0.2486	0.1251	0.4964	0.0393	0.0043	11.0193	0.2466	0.1367	0.4923	0.0384	0.0043	11.2687
0.2983	0.1235	0.5955	0.0415	0.0043	10.4217	0.2945	0.1176	0.5880	0.0402	0.0043	10.7660	0.2958	0.1397	0.5906	0.0402	0.0043	10.7593
				Avg	10.7045					Avg	11.1625					Avg	11.2323

Table O-1.2: Water/Sand Flow - Differential-Pressure Measurement (Water/Sand Flow) - Liquid Flow Rate (Water/Sand Flow)

200lb/1000bbl of 212microns				200lb/1000bbl of 500microns				500lb/1000bbl of 500microns			
Test Matrix		Results		Test Matrix		Results		Test Matrix	Results		
Vsl [m/s]	Qw [L/s]	Error [L/s]	Uncertantity [±%]	Vsl [m/s]	Qw [L/s]	Error [L/s]	Uncertantity [±%]	Vsl [m/s]	Qw [L/s]	Error [L/s]	Uncertantity [±%]
0.1504	0.3004	0.0444	14.7959	0.1526	0.3048	0.0444	14.5826	0.1481	0.2957	0.0444	15.0288
0.1775	0.3544	0.0444	12.5391	0.1783	0.3561	0.0444	12.4818	0.1772	0.3538	0.0444	12.5626
0.1968	0.3929	0.0444	11.3125	0.1950	0.3893	0.0444	11.4158	0.1931	0.3856	0.0444	11.5263
0.2426	0.4845	0.0444	9.1739	0.2486	0.4964	0.0444	8.9532	0.2466	0.4923	0.0444	9.0278
0.2983	0.5955	0.0444	7.4634	0.2945	0.5880	0.0444	7.5589	0.2958	0.5906	0.0444	7.5254
		Avg	11.0570			Avg	10.9985			Avg	11.1342

Table O-1.3: Liquid/Sand Mixture Flow Rate (from Hopper) for Water/Sand Flow

200lb/1000bbl of 212microns				200lb/1000bbl of 500microns				500lb/1000bbl of 500microns			
Test Matrix		Results		Test Matrix		Results		Test Matrix			Results
Vsl [m/s]	Qs [L/s]	Error [L/s]	Uncertantity [±%]	Vsl [m/s]	Qs [L/s]	Error [L/s]	Uncertantity [±%]	Vsl [m/s]	Qs [L/s]	Error [L/s]	Uncertantity [±%]
0.1504	0.1403	0.0117	8.3140	0.1526	0.1152	0.0117	10.1232	0.1481	0.1431	0.0117	8.1505
0.1775	0.1292	0.0117	9.0266	0.1783	0.1167	0.0117	9.9963	0.1772	0.1482	0.0117	7.8745
0.1968	0.1226	0.0117	9.5175	0.1950	0.1238	0.0117	9.4220	0.1931	0.1374	0.0117	8.4917
0.2426	0.1234	0.0117	9.4534	0.2486	0.1251	0.0117	9.3236	0.2466	0.1367	0.0117	8.5377
0.2983	0.1235	0.0117	9.4454	0.2945	0.1176	0.0117	9.9191	0.2958	0.1397	0.0117	8.3505
		Avg	9.1514			Avg	9.7568			Avg	8.2810

Table P-1.1: Re-Calibration for Annular Flow showing the Old and New Liquid Hold-up Results.

		OLD						NEW			
		Vsl= 0.0505m/s						Vsl= 0.0505m/s			
Vsl(m/s)	Vsg(m/s)	Gas Hold-Up	Liquid Hold-Up	HL+Liq Entrain	Vsl(m/s)	Vsg(m/s)	Gas Hold-Up	Liquid Hold-Up	HL+Liq Entrain	Actual Error	Relative Error
0.0511	8.3179	0.9819	0.0180	0.0181	0.0511	8.3179	0.9605	0.0395	0.0395	0.0214	54.2837
0.0509	9.4533	0.9832	0.0168	0.0168	0.0509	9.4533	0.9625	0.0375	0.0375	0.0208	55.2938
0.0508	10.0773	0.9839	0.0161	0.0161	0.0508	10.0773	0.9637	0.0363	0.0363	0.0203	55.7716
0.0509	10.9194	0.9852	0.0148	0.0148	0.0509	10.9194	0.9658	0.0342	0.0342	0.0194	56.6382
0.0506	11.9057	0.9855	0.0145	0.0145	0.0506	11.9057	0.9663	0.0337	0.0337	0.0192	56.8685
0.0504	12.8888	0.9858	0.0141	0.0142	0.0504	12.8888	0.9669	0.0330	0.0331	0.0189	57.1430
0.0502	14.0307	0.9864	0.0135	0.0136	0.0502	14.0307	0.9680	0.0319	0.0320	0.0184	57.6289
0.0503	15.0982	0.9869	0.0130	0.0131	0.0503	15.0982	0.9689	0.0311	0.0311	0.0181	58.0237
0.0501	15.5284	0.9872	0.0127	0.0128	0.0501	15.5284	0.9694	0.0306	0.0306	0.0178	58.2492
0.0504	17.0857	0.9877	0.0122	0.0123	0.0504	17.0857	0.9703	0.0296	0.0297	0.0174	58.6849
0.0503	18.0246	0.9880	0.0119	0.0120	0.0503	18.0246	0.9707	0.0292	0.0293	0.0172	58.8774
0.0501	20.0773	0.9880	0.0119	0.0120	0.0501	20.0773	0.9708	0.0291	0.0292	0.0172	58.8311
0.0501	23.2796	0.9878	0.0121	0.0122	0.0501	23.2796	0.9704	0.0294	0.0296	0.0173	58.5829
									mean	0.0187	57.2982
									Total	0.2434	744.8768
									Avg.Std Dev	=	7.5696
								Mean or	Avg Actual	Error =	0.0187

Table P-1.2: Re-Calibration for Annular Flow showing the Old and New Liquid Hold-up Results.

			OLD						NEW			
			Vsl= 0.0714m/s						Vsl= 0.0714m/s			
Vsl(m/s)	Vsg(m/s)	Gas Hold-Up	Liquid Hold-Up	HL+Liq Entrain	Vsl(m/s)	Vsg(m/s)	Gas Hold-Up	Liquid Hold-Up	HL+Liq Entrain	Actual Error	Relative Error
0.0733	8.0774	0.9775	0.0225	0.0225	0.0733	8.0774	0.9359	0.0641	0.0641	0.0416	64.8815
0.0730	8.9605	0.9789	0.0211	0.0211	0.0730	8.9605	0.9389	0.0611	0.0611	0.0399	65.3863
0.0721	10.1592	0.9804	0.0196	0.0196	0.0721	10.1592	0.9425	0.0575	0.0575	0.0380	65.9997
0.0723	11.0207	0.9811	0.0188	0.0189	0.0723	11.0207	0.9441	0.0559	0.0559	0.0371	66.3157
0.0704	11.6847	0.9824	0.0176	0.0176	0.0704	11.6847	0.9470	0.0529	0.0530	0.0354	66.8269
0.0716	13.1697	0.9835	0.0165	0.0165	0.0716	13.1697	0.9496	0.0503	0.0504	0.0339	67.3159
0.0713	14.3350	0.9846	0.0153	0.0154	0.0713	14.3350	0.9523	0.0476	0.0477	0.0323	67.8111
0.0712	15.4484	0.9857	0.0142	0.0143	0.0712	15.4484	0.9550	0.0450	0.0450	0.0308	68.3535
0.0708	16.3867	0.9863	0.0137	0.0137	0.0708	16.3867	0.9563	0.0436	0.0437	0.0299	68.6548
0.0706	17.3721	0.9867	0.0132	0.0133	0.0706	17.3721	0.9574	0.0425	0.0426	0.0293	68.9113
0.0707	18.2912	0.9865	0.0134	0.0135	0.0707	18.2912	0.9569	0.0430	0.0431	0.0296	68.7807
0.0707	20.2922	0.9867	0.0132	0.0133	0.0707	20.2922	0.9574	0.0425	0.0426	0.0292	68.8843
0.0706	23.5416	0.9863	0.0135	0.0137	0.0706	23.5416	0.9567	0.0431	0.0433	0.0297	68.7466
									mean	0.0336	67.4514
									Total	0.4365	876.8683
									Avg.Std Dev	=	8.2129

Table P-1.3: Re-Calibration for Annular Flow showing the Old and New Liquid Hold-up Results.

		OLD						NEW				
			Vsl= 0.0903m/s					Vsl= 0.0903m/s				
Vsl(m/s)	Vsg(m/s)	Gas Hold-Up	Liquid Hold-Up	HL+Liq Entrain		Vsl(m/s)	Vsg(m/s)	Gas Hold-Up	Liquid Hold-Up	HL+Liq Entrain	Actual Error	Relative Error
0.0923	8.4940	0.9724	0.0275	0.0276		0.0923	8.4940	0.9248	0.0752	0.0752	0.0477	63.3567
0.0920	9.1611	0.9736	0.0264	0.0264		0.0920	9.1611	0.9273	0.0727	0.0727	0.0463	63.6955
0.0910	10.1754	0.9749	0.0251	0.0251		0.0910	10.1754	0.9300	0.0700	0.0700	0.0449	64.1076
0.0902	11.3827	0.9764	0.0235	0.0236		0.0902	11.3827	0.9335	0.0665	0.0665	0.0430	64.5954
0.0913	12.3319	0.9776	0.0224	0.0224		0.0913	12.3319	0.9361	0.0638	0.0639	0.0415	64.9593
0.0905	13.2463	0.9790	0.0210	0.0210		0.0905	13.2463	0.9393	0.0607	0.0607	0.0397	65.3906
0.0900	14.3424	0.9806	0.0194	0.0194		0.0900	14.3424	0.9430	0.0570	0.0570	0.0376	65.9121
0.0896	15.3535	0.9815	0.0184	0.0185		0.0896	15.3535	0.9452	0.0548	0.0548	0.0363	66.2720
0.0893	16.3559	0.9822	0.0177	0.0178		0.0893	16.3559	0.9468	0.0531	0.0532	0.0354	66.5193
0.0893	17.3035	0.9824	0.0176	0.0176		0.0893	17.3035	0.9472	0.0527	0.0528	0.0351	66.5617
0.0888	18.3279	0.9822	0.0177	0.0178		0.0888	18.3279	0.9468	0.0531	0.0532	0.0354	66.4972
0.0891	20.5905	0.9821	0.0177	0.0179		0.0891	20.5905	0.9467	0.0531	0.0533	0.0354	66.4483
0.0901	23.5707	0.9818	0.0179	0.0182		0.0901	23.5707	0.9462	0.0536	0.0538	0.0357	66.2717
										mean	0.0395	65.4298
										Total	0.5139	850.5874
										Avg.Std Dev	=	8.0889

Table P-1.4: Re-Calibration for Annular Flow showing the Old and New Liquid Hold-up Results.

			OLD					NEW				
			Vsl= 0.1355m/s					Vsl= 0.1355m/s				
Vsl(m/s)	Vsg(m/s)	Gas Hold-Up	Liquid Hold-Up	HL+Liq Entrain		Vsl(m/s)	Vsg(m/s)	Gas Hold-Up	Liquid Hold-Up	HL+Liq Entrain	Actual Error	Relative Error
0.1336	8.1564	0.9654	0.0346	0.0346		0.1336	8.1564	0.9101	0.0899	0.0899	0.0554	61.5615
0.1275	9.3771	0.9688	0.0312	0.0312		0.1275	9.3771	0.9171	0.0829	0.0829	0.0517	62.3999
0.1272	10.2753	0.9698	0.0301	0.0302		0.1272	10.2753	0.9193	0.0807	0.0807	0.0506	62.6643
0.1266	11.3896	0.9707	0.0293	0.0293		0.1266	11.3896	0.9210	0.0790	0.0790	0.0496	62.8674
0.1275	12.0846	0.9713	0.0287	0.0287		0.1275	12.0846	0.9224	0.0776	0.0776	0.0489	63.0229
0.1266	13.2336	0.9730	0.0270	0.0270		0.1266	13.2336	0.9261	0.0738	0.0739	0.0468	63.4480
0.1270	14.2926	0.9746	0.0254	0.0254		0.1270	14.2926	0.9296	0.0703	0.0704	0.0449	63.8951
0.1264	15.1316	0.9753	0.0246	0.0247		0.1264	15.1316	0.9314	0.0685	0.0686	0.0440	64.1253
0.1482	16.3562	0.9716	0.0283	0.0284		0.1482	16.3562	0.9231	0.0768	0.0769	0.0486	63.1949
0.1482	17.2538	0.9712	0.0287	0.0288		0.1482	17.2538	0.9221	0.0778	0.0779	0.0491	63.0646
0.1471	18.1475	0.9713	0.0286	0.0287		0.1471	18.1475	0.9224	0.0775	0.0776	0.0489	63.1039
0.1476	20.2508	0.9715	0.0283	0.0285		0.1476	20.2508	0.9230	0.0769	0.0770	0.0486	63.1702
0.1480	23.1697	0.9711	0.0287	0.0289		0.1480	23.1697	0.9221	0.0776	0.0779	0.0490	63.0781
										mean	0.0489	63.0459
										Total	0.6360	819.5962
										Avg.Std Dev	=	7.9401

Table P-1.5: Re-Calibration for Annular Flow showing the Old and New Liquid Hold-up Results.

		OLD							NEW			
			Vsl= 0.1851m/s						Vsl= 0.1851m/s			
Vsl(m/s)	Vsg(m/s)	Gas Hold-Up	Liquid Hold-Up	HL+Liq Entrain		Vsl(m/s)	Vsg(m/s)	Gas Hold-Up	Liquid Hold-Up	HL+Liq Entrain	Actual Error	Relative Error
0.1950	8.3042	0.9592	0.0408	0.0408		0.1950	8.3042	0.8967	0.1033	0.1033	0.0625	60.4678
0.1920	9.3747	0.9607	0.0393	0.0393		0.1920	9.3747	0.8999	0.1001	0.1001	0.0608	60.7542
0.1892	10.3928	0.9617	0.0383	0.0383		0.1892	10.3928	0.9018	0.0982	0.0982	0.0598	60.9608
0.1867	11.4133	0.9635	0.0365	0.0365		0.1867	11.4133	0.9054	0.0945	0.0946	0.0580	61.3849
0.1852	12.3305	0.9645	0.0355	0.0355		0.1852	12.3305	0.9075	0.0924	0.0925	0.0570	61.5992
0.1834	13.3075	0.9652	0.0348	0.0348		0.1834	13.3075	0.9089	0.0910	0.0911	0.0562	61.7377
0.1819	14.4407	0.9658	0.0341	0.0342		0.1819	14.4407	0.9103	0.0897	0.0897	0.0555	61.9166
0.1823	15.5866	0.9658	0.0341	0.0342		0.1823	15.5866	0.9102	0.0897	0.0898	0.0556	61.9041
0.1840	16.5037	0.9654	0.0345	0.0346		0.1840	16.5037	0.9094	0.0905	0.0906	0.0560	61.7873
0.1822	17.5280	0.9656	0.0343	0.0344		0.1822	17.5280	0.9098	0.0901	0.0902	0.0558	61.8455
0.1832	18.4493	0.9653	0.0345	0.0347		0.1832	18.4493	0.9093	0.0906	0.0907	0.0561	61.7989
0.1810	20.7125	0.9651	0.0347	0.0349		0.1810	20.7125	0.9090	0.0909	0.0910	0.0562	61.7011
0.1805	23.7260	0.9655	0.0343	0.0345		0.1805	23.7260	0.9098	0.0900	0.0902	0.0557	61.7567
										mean	0.0573	61.5088
										Total	0.7452	799.6149
										Avg.Std Dev	=	7.8428

Table Q-1.1: Re-Calibration for Annular Flow showing the Old and New Liquid Film Thickness Results.

			Vsl= 0.0505m/s		Rings+ Liq Entrain	Probes (Bottom)	Probes (Bottom)		
Vsl(m/s)	Vsg(m/s)	Gas Hold-Up	Liquid Hold-Up	HL+Liq Entrain	Film Thickness(mm)	Film Thickness(mm)	Film Thickness(mm)	Actual Error	Relative Error
0.0511	8.3179	0.9087	0.0180	0.0913	1.1782	0.1811	0.1500	0.0311	17.1724
0.0509	9.4533	0.9103	0.0168	0.0897	1.1571	0.1762	0.1408	0.0354	20.0810
0.0508	10.0773	0.9118	0.0161	0.0882	1.1365	0.1736	0.1360	0.0376	21.6712
0.0509	10.9194	0.9129	0.0148	0.0871	1.1226	0.1681	0.1256	0.0425	25.2626
0.0506	11.9057	0.9151	0.0145	0.0849	1.0936	0.1650	0.1198	0.0452	27.4057
0.0504	12.8888	0.9143	0.0141	0.0857	1.1040	0.1629	0.1157	0.0472	28.9729
0.0502	14.0307	0.9152	0.0135	0.0848	1.0926	0.1592	0.1087	0.0505	31.7063
0.0503	15.0982	0.9158	0.0130	0.0842	1.0846	0.1562	0.1030	0.0532	34.0594
0.0501	15.5284	0.9165	0.0127	0.0835	1.0756	0.1551	0.1008	0.0543	35.0055
0.0504	17.0857	0.9172	0.0122	0.0828	1.0658	0.1514	0.0937	0.0577	38.1125
0.0503	18.0246	0.9174	0.0119	0.0826	1.0636	0.1501	0.0911	0.0589	39.2667
0.0501	20.0773	0.9173	0.0119	0.0827	1.0639	0.1498	0.0907	0.0591	39.4460
0.0501	23.2796	0.9173	0.0121	0.0827	1.0639	0.1503	0.0916	0.0587	39.0499
0.0505							**mean**	**0.0486**	**30.5548**
							Total		397.2121
							Avg.Std Dev	=	**5.5276**

Table Q-1.2: Re-Calibration for Annular Flow showing the Old and New Liquid Film Thickness Results.

						Old	New		
			Vsl= 0.0714m/s		Rings+ Liq Entrain	Probes (Bottom)	Probes (Bottom)		
Vsl(m/s)	Vsg(m/s)	Gas Hold-Up	Liquid Hold-Up	HL+Liq Entrain	Film Thickness(mm)	Film Thickness(mm)	Film Thickness(mm)	Actual Error	Relative Error
0.0733	8.0774	0.9775	0.0225	0.0225	0.2852	0.2071	0.1977	0.0094	4.5441
0.0730	8.9605	0.9789	0.0211	0.0211	0.2677	0.2036	0.1913	0.0123	6.0242
0.0721	10.1592	0.9804	0.0196	0.0196	0.2476	0.1993	0.1835	0.0158	7.9141
0.0723	11.0207	0.9812	0.0188	0.0188	0.2384	0.1973	0.1798	0.0175	8.8535
0.0704	11.6847	0.9824	0.0176	0.0176	0.2222	0.1936	0.1732	0.0205	10.5678
0.0716	13.1697	0.9835	0.0165	0.0165	0.2082	0.1910	0.1683	0.0227	11.8865
0.0713	14.3350	0.9847	0.0153	0.0153	0.1939	0.1876	0.1621	0.0255	13.5923
0.0712	15.4484	0.9858	0.0142	0.0142	0.1800	0.1839	0.1553	0.0287	15.5854
0.0708	16.3867	0.9863	0.0137	0.0137	0.1728	0.1815	0.1507	0.0308	16.9497
0.0706	17.3721	0.9868	0.0132	0.0132	0.1670	0.1793	0.1466	0.0326	18.2100
0.0707	18.2912	0.9866	0.0134	0.0134	0.1698	0.1805	0.1488	0.0316	17.5314
0.0707	20.2922	0.9868	0.0132	0.0132	0.1670	0.1794	0.1468	0.0326	18.1739
0.0706	23.5416	0.9865	0.0135	0.0135	0.1705	0.1806	0.1491	0.0315	17.4346
0.0714							**mean**	**0.0240**	**12.8667**
							Total		167.2675
							Avg.Std Dev	=	**3.5870**

Table Q-1.3: Re-Calibration for Annular Flow showing the Old and New Liquid Film Thickness Results.

						Old	New		
			Vsl= 0.0903m/s		Rings+ Liq Entrain	Probes (Bottom)	Probes (Bottom)		
Vsl(m/s)	Vsg(m/s)	Gas Hold-Up	Liquid Hold-Up	HL+Liq Entrain	Film Thickness(mm)	Film Thickness(mm)	Film Thickness(mm)	Actual Error	Relative Error
0.0923	8.4940	0.8450	0.0275	0.1550	2.0354	0.2126	0.2075	0.0051	2.3800
0.0920	9.1611	0.8464	0.0264	0.1536	2.0156	0.2106	0.2039	0.0067	3.1699
0.0910	10.1754	0.8483	0.0251	0.1517	1.9905	0.2087	0.2005	0.0082	3.9163
0.0902	11.3827	0.8490	0.0235	0.1510	1.9806	0.2067	0.1970	0.0097	4.7087
0.0913	12.3319	0.8510	0.0224	0.1490	1.9529	0.2053	0.1943	0.0109	5.3167
0.0905	13.2463	0.8520	0.0210	0.1480	1.9391	0.2026	0.1896	0.0130	6.4335
0.0900	14.3424	0.8542	0.0194	0.1458	1.9097	0.1992	0.1834	0.0158	7.9452
0.0896	15.3535	0.8334	0.0184	0.1666	2.1951	0.1968	0.1789	0.0179	9.0781
0.0893	16.3559	0.8340	0.0177	0.1660	2.1859	0.1948	0.1754	0.0194	9.9814
0.0893	17.3035	0.8354	0.0176	0.1646	2.1674	0.1943	0.1744	0.0199	10.2402
0.0888	18.3279	0.8347	0.0177	0.1653	2.1770	0.1949	0.1755	0.0194	9.9500
0.0891	20.5905	0.8343	0.0177	0.1657	2.1828	0.1949	0.1755	0.0194	9.9678
0.0901	23.5707	0.8466	0.0179	0.1534	2.0138	0.1956	0.1767	0.0188	9.6317
0.0903							mean	0.0142	7.1323
							Total		92.7195
							Avg.Std Dev	=	2.6706

Table Q-1.4: Re-Calibration for Annular Flow showing the Old and New Liquid Film Thickness Results.

						Old	New		
			Vsl= 0.1355m/s		Rings+ Liq Entrain	Probes (Bottom)	Probes (Bottom)		
Vsl(m/s)	Vsg(m/s)	Gas Hold-Up	Liquid Hold-Up	HL+Liq Entrain	Film Thickness(mm)	Film Thickness(mm)	Film Thickness(mm)	Actual Error	Relative Error
0.1336	8.1564	0.9654	0.0346	0.0346	0.4393	0.2163	0.2141	0.0021	0.9909
0.1275	9.3771	0.9688	0.0312	0.0312	0.3959	0.2133	0.2089	0.0044	2.0761
0.1272	10.2753	0.9699	0.0301	0.0301	0.3826	0.2124	0.2073	0.0051	2.4229
0.1266	11.3896	0.9707	0.0293	0.0293	0.3722	0.2117	0.2061	0.0057	2.6850
0.1275	12.0846	0.9713	0.0287	0.0287	0.3642	0.2112	0.2051	0.0061	2.8981
0.1266	13.2336	0.9730	0.0270	0.0270	0.3423	0.2092	0.2015	0.0077	3.6752
0.1270	14.2926	0.9746	0.0254	0.0254	0.3221	0.2070	0.1974	0.0095	4.5965
0.1264	15.1316	0.9754	0.0246	0.0246	0.3118	0.2057	0.1951	0.0106	5.1350
0.1482	16.3562	0.9717	0.0283	0.0283	0.3589	0.2093	0.2017	0.0076	3.6453
0.1482	17.2538	0.9713	0.0287	0.0287	0.3648	0.2098	0.2026	0.0072	3.4451
0.1471	18.1475	0.9714	0.0286	0.0286	0.3630	0.2095	0.2021	0.0074	3.5510
0.1476	20.2508	0.9717	0.0283	0.0283	0.3593	0.2092	0.2014	0.0077	3.6914
0.1480	23.1697	0.9713	0.0287	0.0287	0.3638	0.2096	0.2023	0.0073	3.5055
0.1355							mean	0.0068	3.2552
							Total		42.3178
							Avg.Std Dev	=	1.8042

Table Q-1.5: Re-Calibration for Annular Flow showing the Old and New Liquid Film Thickness Results.

						Old	New		
			Vsl= 0.1851m/s		Rings+ Liq Entrain	Probes (Bottom)	Probes (Bottom)		
Vsl(m/s)	Vsg(m/s)	Gas Hold-Up	Liquid Hold-Up	HL+Liq Entrain	Film Thickness(mm)	Film Thickness(mm)	Film Thickness(mm)	Actual Error	Relative Error
0.1950	8.3042	0.9592	0.0408	0.0408	0.5199	0.2197	0.2192	0.0005	0.2261
0.1920	9.3747	0.9607	0.0393	0.0393	0.4999	0.2187	0.2185	0.0002	0.1138
0.1892	10.3928	0.9617	0.0383	0.0383	0.4873	0.2183	0.2178	0.0006	0.2520
0.1867	11.4133	0.9635	0.0365	0.0365	0.4640	0.2169	0.2153	0.0016	0.7586
0.1852	12.3305	0.9645	0.0355	0.0355	0.4511	0.2163	0.2142	0.0021	0.9735
0.1834	13.3075	0.9652	0.0348	0.0348	0.4423	0.2158	0.2133	0.0025	1.1610
0.1819	14.4407	0.9659	0.0341	0.0341	0.4335	0.2153	0.2124	0.0029	1.3457
0.1823	15.5866	0.9659	0.0341	0.0341	0.4337	0.2152	0.2123	0.0029	1.3620
0.1840	16.5037	0.9655	0.0345	0.0345	0.4390	0.2153	0.2125	0.0029	1.3251
0.1822	17.5280	0.9657	0.0343	0.0343	0.4360	0.2152	0.2123	0.0029	1.3698
0.1832	18.4493	0.9655	0.0345	0.0345	0.4391	0.2152	0.2122	0.0030	1.3905
0.1810	20.7125	0.9653	0.0347	0.0347	0.4412	0.2155	0.2129	0.0027	1.2469
0.1805	23.7260	0.9657	0.0343	0.0343	0.4356	0.2150	0.2119	0.0031	1.4393
0.1851							mean	**0.0022**	**0.9972**
							Total		12.9642
							Avg.Std Dev	=	**0.9986**

Table R-1.1: Summary of Water/Air/Sand Annular Flow

								Assume				
		(212microns 200lb/1000bbl)						Vp = VL	Liquid Entrainment Correlations			
Vsl (m/s)	Vsg (m/s)	Void Fraction	Sand Hold-Up	Liq.Hold-Up	Liq.Hold-Up+Liq. Ent	Film Thickness (mm)	Wave velocity (m/s)	Actual Liquid Velocity(m/s)	Pan & Hanratty (2002b)	Mantilla (2008)	dp/dx (kPa/m)	Wall shear stress[kPa]
0.0961	10.4769	0.9642	0.0005	0.0352	0.0352	0.1791	0.0191	2.7265	1.8E-05	0.0001	0.6285	0.0079
0.1126	9.3775	0.9449	0.0005	0.0545	0.0545	0.2033	0.0200	2.0651	1.4E-05	0.0002	0.6531	0.0082
0.1264	8.9792	0.9292	0.0005	0.0702	0.0702	0.2111	0.0210	1.7995	1.3E-05	0.0002	0.6217	0.0078
		(212microns 200lb/1000bbl)							Liquid Entrainment Correlations			
Vsl (m/s)	Vsg (m/s)	Void Fraction	Sand Hold-Up	Liq.Hold-Up	Liq.Hold-Up+Liq. Ent	Film Thickness (mm)	Wave velocity (m/s)	Actual Liquid Velocity(m/s)	Pan & Hanratty (2002b)	Mantilla (2008)	dp/dx (kPa/m)	Wall shear stress[kPa]
0.0951	14.9132	0.9700	0.0005	0.0294	0.0295	0.1596	0.0221	3.2270	5.1E-05	0.0001	0.7727	0.0097
0.1145	14.9179	0.9535	0.0005	0.0459	0.0459	0.1799	0.0233	2.4931	5.3E-05	0.0002	0.9088	0.0115
0.1209	14.9517	0.9524	0.0005	0.0470	0.0470	0.1858	0.0262	2.5717	5.3E-05	0.0002	1.0198	0.0128
		(212microns 500lb/1000bbl)							Liquid Entrainment Correlations			
Vsl (m/s)	Vsg (m/s)	Void Fraction	Sand Hold-Up	Liq.Hold-Up	Liq.Hold-Up+Liq. Ent	Film Thickness (mm)	Wave velocity (m/s)	Actual Liquid Velocity(m/s)	Pan & Hanratty (2002b)	Mantilla (2008)	dp/dx (kPa/m)	Wall shear stress[kPa]
0.0983	8.9651	0.9537	0.0005	0.0457	0.0458	0.1871	0.0175	2.1486	1.1E-05	0.0001	0.4639	0.0058
0.1252	8.9535	0.9413	0.0005	0.0582	0.0582	0.2052	0.0200	2.1509	1.2E-05	0.0002	0.6231	0.0079
0.1343	8.9811	0.9344	0.0005	0.0651	0.0651	0.2094	0.0210	2.0640	1.2E-05	0.0002	0.6717	0.0085
		(212microns 500lb/1000bbl)							Liquid Entrainment Correlations			
Vsl (m/s)	Vsg (m/s)	Void Fraction	Sand Hold-Up	Liq.Hold-Up	Liq.Hold-Up+Liq. Ent	Film Thickness (mm)	Wave velocity (m/s)	Actual Liquid Velocity(m/s)	Pan & Hanratty (2002b)	Mantilla (2008)	dp/dx (kPa/m)	Wall shear stress[kPa]
0.1024	14.4564	0.9674	0.0005	0.0320	0.0321	0.1618	0.0221	3.1920	4.6E-05	0.0001	0.7658	0.0096
0.1248	14.5936	0.9584	0.0005	0.0410	0.0411	0.1819	0.0247	3.0394	4.8E-05	0.0002	0.9856	0.0124
0.1304	14.8428	0.9540	0.0005	0.0454	0.0454	0.1871	0.0262	2.8706	5.2E-05	0.0002	1.0995	0.0139
		(500microns 500lb/1000bbl)							Liquid Entrainment Correlations			
Vsl (m/s)	Vsg (m/s)	Void Fraction	Sand Hold-Up	Liq.Hold-Up	Liq.Hold-Up+Liq. Ent	Film Thickness (mm)	Wave velocity (m/s)	Actual Liquid Velocity(m/s)	Pan & Hanratty (2002b)	Mantilla (2008)	dp/dx (kPa/m)	Wall shear stress[kPa]
0.1087	8.4749	0.9526	0.0005	0.0468	0.0468	0.1867	0.0168	2.3202	9.6E-06	0.0001	0.4760	0.0060
0.1256	8.7601	0.9408	0.0005	0.0586	0.0586	0.2029	0.0191	2.1429	1.1E-05	0.0002	0.6260	0.0079
0.1288	9.2246	0.9353	0.0005	0.0641	0.0641	0.2053	0.0200	2.0081	1.3E-05	0.0002	0.6589	0.0083
		(500microns 500lb/1000bbl)							Liquid Entrainment Correlations			
Vsl (m/s)	Vsg (m/s)	Void Fraction	Sand Hold-Up	Liq.Hold-Up	Liq.Hold-Up+Liq. Ent	Film Thickness (mm)	Wave velocity (m/s)	Actual Liquid Velocity(m/s)	Pan & Hanratty (2002b)	Mantilla (2008)	dp/dx (kPa/m)	Wall shear stress[kPa]
0.1003	15.2296	0.9707	0.0005	0.0287	0.0287	0.1559	0.0233	3.4900	5.3E-05	0.00011	0.86057	0.01084
0.1236	14.4325	0.9600	0.0005	0.0394	0.0394	0.1796	0.0247	3.1335	4.6E-05	0.00016	0.97757	0.01232
0.1265	14.6875	0.9524	0.0005	0.0470	0.0471	0.1829	0.0248	2.6875	5.0E-05	0.00019	1.02287	0.01289

Table S-1.1: Statistical Error for the Difference between OLGA and Measured Liquid Hold-Up

	Vsl~0.0505m/s							Vsl~0.0714m/s						
Vsl(m/s)	Vsg(m/s)	Liquid Hold-Up	HL+Liq Entrain	OLGA (HL)	Actual Error	Relative Error		Vsl(m/s)	Vsg(m/s)	Liquid Hold-Up	HL+Liq Entrain	OLGA (HL)	Actual Error	Relative Error
0.0511	8.3179	0.0180	0.0181	0.0170	0.0010	5.7832		0.0733	8.0774	0.0225	0.0225	0.0185	0.0040	17.7571
0.0509	9.4533	0.0168	0.0168	0.0153	0.0015	9.0217		0.0730	8.9605	0.0211	0.0211	0.0169	0.0043	20.2406
0.0508	10.0773	0.0161	0.0161	0.0146	0.0015	9.2381		0.0721	10.1592	0.0196	0.0196	0.0153	0.0043	21.8268
0.0509	10.9194	0.0148	0.0148	0.0137	0.0011	7.4846		0.0723	11.0207	0.0188	0.0189	0.0143	0.0046	24.2115
0.0506	11.9057	0.0145	0.0145	0.0129	0.0016	10.9513		0.0704	11.6847	0.0176	0.0176	0.0136	0.0039	22.4905
0.0504	12.8888	0.0141	0.0142	0.0122	0.0019	13.6584		0.0716	13.1697	0.0165	0.0165	0.0130	0.0034	20.7599
0.0502	14.0307	0.0135	0.0136	0.0112	0.0023	16.8447		0.0713	14.3350	0.0153	0.0154	0.0116	0.0038	24.6144
0.0503	15.0982	0.0130	0.0131	0.0110	0.0020	15.3519		0.0712	15.4484	0.0142	0.0143	0.0109	0.0033	23.2131
0.0501	15.5284	0.0127	0.0128	0.0109	0.0018	14.0765		0.0708	16.3867	0.0137	0.0137	0.0105	0.0032	23.2344
0.0504	17.0857	0.0122	0.0123	0.0105	0.0017	13.7737		0.0706	17.3721	0.0132	0.0133	0.0102	0.0030	22.5336
0.0503	18.0246	0.0119	0.0120	0.0102	0.0017	14.5779		0.0707	18.2912	0.0134	0.0135	0.0101	0.0034	25.0206
0.0501	20.0773	0.0119	0.0120	0.0097	0.0022	18.7017		0.0707	20.2922	0.0132	0.0133	0.0097	0.0036	26.8727
0.0501	23.2796	0.0121	0.0122	0.0093	0.0028	22.9299		0.0706	23.5416	0.0135	0.0137	0.0090	0.0044	32.8970
				Mean	0.0018	13.2610		0.0714				Mean	0.0038	23.5132
				Total		172.3934						Total		305.6722
				Avg.Std Dev		3.6416						Avg.Std Dev		4.8490

Table S-1.2: Statistical Error for the Difference between OLGA and Measured Liquid Hold-Up

	Vsl~0.0903m/s							Vsl~0.1355m/s						
Vsl(m/s)	Vsg(m/s)	Liquid Hold-Up	HL+Liq Entrain	OLGA (HL)	Actual Error	Relative Error		Vsl(m/s)	Vsg(m/s)	Liquid Hold-Up	HL+Liq Entrain	OLGA (HL)	Actual Error	Relative Error
0.0923	8.4940	0.0275	0.0276	0.0206	0.0069	25.1270		0.1336	8.1564	0.0346	0.0346	0.0278	0.0067	19.4808
0.0920	9.1611	0.0264	0.0264	0.0193	0.0071	26.9790		0.1275	9.3771	0.0312	0.0312	0.0255	0.0057	18.1558
0.0910	10.1754	0.0251	0.0251	0.0182	0.0070	27.6843		0.1272	10.2753	0.0301	0.0302	0.0228	0.0073	24.2904
0.0902	11.3827	0.0235	0.0236	0.0172	0.0063	26.7195		0.1266	11.3896	0.0293	0.0293	0.0213	0.0081	27.4976
0.0913	12.3319	0.0224	0.0224	0.0158	0.0066	29.3774		0.1275	12.0846	0.0287	0.0287	0.0196	0.0091	31.6418
0.0905	13.2463	0.0210	0.0210	0.0149	0.0060	28.7556		0.1266	13.2336	0.0270	0.0270	0.0186	0.0084	31.1386
0.0900	14.3424	0.0194	0.0194	0.0141	0.0053	27.2929		0.1270	14.2926	0.0254	0.0254	0.0170	0.0084	33.0808
0.0896	15.3535	0.0184	0.0185	0.0132	0.0052	28.2030		0.1264	15.1316	0.0246	0.0247	0.0157	0.0088	35.9786
0.0893	16.3559	0.0177	0.0178	0.0126	0.0051	28.9891		0.1482	16.3562	0.0283	0.0284	0.0150	0.0132	46.8389
0.0893	17.3035	0.0176	0.0176	0.0120	0.0055	31.5754		0.1482	17.2538	0.0287	0.0288	0.0139	0.0148	51.5157
0.0888	18.3279	0.0177	0.0178	0.0116	0.0062	34.8567		0.1471	18.1475	0.0286	0.0287	0.0135	0.0151	52.6731
0.0891	20.5905	0.0177	0.0179	0.0111	0.0066	37.2434		0.1476	20.2508	0.0283	0.0285	0.0131	0.0152	53.8161
0.0901	23.5707	0.0179	0.0182	0.0104	0.0076	42.2426		0.1480	23.1697	0.0287	0.0289	0.0122	0.0164	57.3247
0.0903				Mean	0.0063	30.3882		0.1355				Mean	0.0106	37.1871
				Total		395.0460						Total		483.4329
				Avg.Std Dev		5.5125						Avg.Std Dev		6.0981

Table S-1.3: Statistical Error of OLGA variance from Experiment on Water/Air/Sand Annular Flow

			M[kg]		Cv [m3]	
Vsl[m/s]	Vsg[m/s]	Sand Particles[microns]	Actual Error	Relative Error[%]	Actual Error	Relative Error[%]
0.1145	14.9179	212(200lb/1000bbl)	0.1073	20.2403	0.00002	9.8068
0.1236	14.4325	500(500lb/1000bbl)	0.8684	65.5368	0.0003	62.6159
0.1257	15.0489	800(500lb/1000bbl)	1.0135	76.4903	0.0003	63.8437